



HAL
open science

Generation and selection of photoreceptor precursors from human-induced pluripotent stem cells for cell therapy

Giuliana Gagliardi

► **To cite this version:**

Giuliana Gagliardi. Generation and selection of photoreceptor precursors from human-induced pluripotent stem cells for cell therapy. *Neurons and Cognition [q-bio.NC]*. Sorbonne Université, 2018. English. NNT : 2018SORUS082 . tel-02505074

HAL Id: tel-02505074

<https://theses.hal.science/tel-02505074>

Submitted on 11 Mar 2020

HAL is a multi-disciplinary open access archive for the deposit and dissemination of scientific research documents, whether they are published or not. The documents may come from teaching and research institutions in France or abroad, or from public or private research centers.

L'archive ouverte pluridisciplinaire **HAL**, est destinée au dépôt et à la diffusion de documents scientifiques de niveau recherche, publiés ou non, émanant des établissements d'enseignement et de recherche français ou étrangers, des laboratoires publics ou privés.

Sorbonne Université

Ecole doctorale Cerveau Cognition Comportement (ED158)

Institut de la Vision

Generation and selection of photoreceptor precursors from human-induced pluripotent stem cells for cell therapy

Par **Giuliana GAGLIARDI**

Thèse de doctorat de Neurosciences

Dirigée par **Olivier GOUREAU**

Présentée et soutenue publiquement le 21 septembre 2018

Devant un jury composé de :

Pr. Marius ADER, Rapporteur

Dr. Anselme PERRIER, Rapporteur

Dr. Deniz DALKARA, Examineur

Dr. Vasiliki KALATZIS, Examineur

Pr. Ann LOHOF, Examineur

Dr. Olivier GOUREAU, Directeur de thèse

First of all, I would like to thank all the members of the jury for having accepted to be part of the thesis committee and for the time spent reviewing my work.

Je vais poursuivre ces remerciements dans les trois langues qui désormais forment un grand *miscuglio* dans ma tête (et dans mon cahier de manips) : ils n'auront pas une grammaire et syntaxe parfaites, mais ils seront sûrement sincères et authentiques.

Je vais d'abord remercier mon équipe, l'équipe S2. Je vous remercie tous pour ce véritable esprit communautaire, pour lequel on prend soin du travail des autres, on partage les tâches les plus dures et on fait face aux problèmes ensemble.

Olivier, je vais toujours te remercier pour la confiance que tu m'as donnée en moi-même et en mon propre travail, et que d'ailleurs tu m'as accordée même avant de me rencontrer du moment que tu m'as embauchée sans me rencontrer avant. De ma part, je suis consciente que j'ai bien eu de la chance ! T'as su m'accorder la juste autonomie tout en laissant la porte de ton bureau toujours ouverte à la discussion et à l'aide en cas de besoin. Je suis extrêmement reconnaissante pour ta générosité et sur un niveau professionnel, pour toutes les opportunités que tu m'as encouragées à saisir, que sur le niveau humain, pour la juste considération du travail que t'as par rapport à tout le reste. Merci pour les bonnes bouteilles, j'espère de ma part de t'avoir ouvert la porte au vin et à la gastronomie italienne.

Sacha, merci pour toute les fois que tu m'as remonté la morale. Ton optimisme et ton enthousiasme sont un pilastre de l'équipe. Merci pour tout le savoir-faire que tu m'as transmis non seulement pour les cellules mais aussi pour la vie.

Gaël, merci d'avoir toujours répondu à mes questions les plus variées et de m'avoir patiemment appris les stats. Ton point de vue m'a toujours été très utile pour apporter de la clarté et remettre les focus sur les points les plus importantes.

Les filles, Amélie « la grande », Céline, Oriane et Amélie « la petite », merci pour vos mots d'encouragement et votre énorme travail. Merci aussi à Angélique, une guide à suivre lors de mes premiers pas dans le L2, et à Sarah pour ton travail à mes côtés.

Un énorme merci à Karim, ç'a été un véritable plaisir de travailler avec toi, surtout pour ta gentillesse et ta précision. Merci aussi pour les intéressantes discussions scientifiques et non scientifiques.

Je remercie toutes les gens à l'institut avec lesquelles j'ai collaboré et qui ont rendu possible mon travail. En particulier, un énorme merci à Manu, Julie, Quenol et Mylène pour leur aide avec toutes les expériences avec les rats. Julie et Manu merci pour votre disponibilité à explorer toutes les pistes, même quand les résultats n'étaient pas très encourageants. Merci à Jean-Baptiste pour avoir accepté le défi des injections sur les rats et pour m'avoir formée aux injections intravitréennes.

Toute ma reconnaissance à Antoine, le maître du bi-photon : merci de m'avoir réservé une petite place dans ton planning super blindé.

Merci à Corentin, Gregory et Romain pour m'avoir dédié leur temps et leur expertise lors de plusieurs manips test.

Merci à Stéphane pour toutes les fois qui est venu à mon secours tout au long de ma relation difficile avec les confocaux. Merci à Anaïs pour les analyses et le re-analyses à l'arrayscan et merci à Luisa de m'avoir fait découvrir les joies de la cytométrie.

Marcela, mother of dragons, thank you for the interesting discussions about stem cells and for all the time you have proof-read my work. The dancing in the L2 will stay with me as one of the highest moment of this PhD.

Thank you to my office and lunch group mates – current and past- for the good time and the good food we shared together: this PhD would have been so much boring - and so much healthier-without you.

To my friends, à mes amis, ai miei amici e amiche *grazie di cuore* for being there for the good and for the bad, despite the distance. You are my source of inspiration and my best excuse for travelling. Of course, you are all welcome to discover the beauty of Nijmegen.

Matteo, grazie di essere il mio punto fermo e razionale. Anche se quando ti parlo di quello che faccio in laboratorio per te è incomprensibile, sei quello che più mi capisce.

Infine grazie alla mia famiglia, per il sostegno che ha dato alle mie scelte, anche quando ho deciso di andare lontano da casa, e per il calore che mi fa sentire quando rientro. Grazie per avermi trasmesso l'amore per il lavoro ben fatto. Sono orgogliosa che per le Gagliarde le difficoltà, anche quelle più dure, non sono una scusa per tirarsi indietro. Per questo papà ti dedico questo lavoro, ora che è finito.

Table of contents

Introduction	9
1. Retina and photoreceptors.....	11
1.1 The eye	11
1.2 Overview of the anatomy and functionality of the retina.....	13
1.3 Photoreceptors	16
1.4 Phototransduction and visual cycle	22
1.5 Retinal development	24
2. Outer retinal dystrophies	31
2.1 Age-related macular degeneration	31
2.2 Inherited retinal dystrophies.....	31
2.3 Animal models of inherited retinal diseases	36
2.4 Therapeutic approaches for photoreceptor degenerative diseases.....	43
2.5 Photoreceptor replacement by cell therapy	46
3. Human-induced pluripotent stem cells	53
3.1 Stem cells and differentiation potentials	53
3.2 Embryonic stem cells	55
3.3 Human-induced pluripotent stem cells.....	56
3.4 Progress and challenges in iPSC-based cell therapy	58
4. Generation of photoreceptors from ESCs and iPSCs.....	63
4.1 Differentiation protocols	63
4.2 Future optimization.....	71
4.3 Clinical utility of iPSC-derived photoreceptors.....	74
5. Transplantation of PSC-derivatives	77
5.1 Historical transplantation studies using PSCs derivatives.....	77
5.2 Change of perspective on donor photoreceptor integration	82
5.3 Transplantation of PSC-derived retinal sheets	89
5.4 Isolation and transplantation of photoreceptors derived from PSCs	93
Aims	97
Results	99
1. Generation of photoreceptor precursors from human iPSCs in near GMP conditions: identification of a photoreceptor marker and development of a cryopreservation strategy (Paper 1).....	101

2. Separation and characterization of photoreceptor precursors from human retinal organoids by targeting of a cell surface antigen (Paper 2).....	137
3. Additional results.....	183
3.1 Characterization of human transplants by fluorescence in situ hybridization	183
3.2 Evaluation of the visual function in P23H rats by full field ERG recording	185
Discussion and Perspectives	191
1. <i>In vitro</i> photoreceptor differentiation, maturation and isolation.....	193
2. <i>In vivo</i> cell integration, maturation and functionality	198
Conclusions	207
Bibliography	209

List of Tables

Table 1 Comparison of anatomical features in human, mouse and rat eye.	12
Table 2 Mouse models of inherited retinal diseases used in principal transplantation studies.	39
Table 3 Rat models of inherited retinal diseases most used in principal transplantation studies.	40
Table 4 Principal protocols for the differentiation of human PSCs to retinal cells.	67
Table 5 Models of photoreceptor diseases established using iPSCs.	76
Table 6 Transplantation studies with retinal cells derived from mouse PSCs.	80
Table 7 Summary of studies describing material exchange.	83
Table 8 Transplantation studies with retinal cells derived from human PSCs.	88

List of Figure

Figure 1 Anatomical structure of the human and rodent eye.	12
Figure 2 Structure of mammalian retina and its major cell types.	14
Figure 3 Schematic representations of cones and rods.	17
Figure 4 Different opsins in mouse and primate cones.	19
Figure 5 Distribution of rods and cones in human retina.	21
Figure 6 Phototransduction and visual cycle.	23
Figure 7 Early eye development.	25
Figure 8 Comparison of mouse/ human <i>in vivo</i> versus <i>in vitro</i> development.	27
Figure 9 Factors involved in the specification of different types of photoreceptors.	29
Figure 10 Photoreceptor loss and functional alterations in dystrophic retina.	33
Figure 11 Examples of proteins associated with retinal dystrophies classified according to their function and localization in photoreceptors and retinal pigment epithelium.	35
Figure 12 Summary of pros and cons of the most common animal species used in inherited retinal degeneration studies.	37
Figure 13 Phenotypic characterization of heterozygous P23H line 1 (P23H-1) rats.	42
Figure 14 Potential therapeutic strategies to treat photoreceptor degenerative diseases.	44
Figure 15 Alternative strategies for the delivery of cells to the retina.	48
Figure 16 Increased integration of mouse donor photoreceptor precursors.	50
Figure 17 Stem cells and differentiation potentials in organism development.	54
Figure 18 Genomic and epigenetic alterations in PSC lines.	59
Figure 19 Overview of differentiating cells and 3D structures obtained with five examples of retinal differentiation protocols.	64
Figure 20 Improving lamination in PSC-derived retinal organoids.	73
Figure 21 Investigation of donor/host material exchange by two-color fluorescence and Y chromosome FISH.	84
Figure 22 Transplantation of human PSC-derivatives as cell suspension versus retinal sheet.	90
Figure 23: Identification of transplanted human cells by FISH and immunolabeling.	184
Figure 24 ERG recordings and SD-OCT images from P23H rats after trans-vitreous injection.	186
Figure 25: ERG recordings and SD-OCT images from P23H rats after trans-scleral injection.	188
Figure 26 Different strategies for the implementation of production and delivery of cell therapy products for the treatment of outer retinal dystrophies.	205

Introduction

1. Retina and photoreceptors

1.1 The eye

The eye is an organ with the function of detecting light stimuli, adjusting light intensity, in order to convert it into electric signals that are sent from the retina to the brain (**Figure 1**).

The light first penetrates into the eye by passing through the cornea, a transparent tissue at the front of the eye that acts not only as a shield to pathogens and UV rays, but also as a powerful lens, allowing together with the crystalline lens the production of a sharp image at the retinal level. The crystalline lens is composed of a transparent epithelial tissue characterized by a soft structure, so that the shape of the lens can be modified accordingly to the distance of an object. This process, known as accommodation, is ensured by the muscular part of the ciliary body. The epithelial part of the ciliary body produces the aqueous humor filling the space between the cornea and the crystalline lens.

A pigmented circular muscle, the iris, responsible for the external color of the eye, borders the crystalline lens. This muscular ring controls the size of the pupil, a hole at the center of the iris, so that the appropriate amount of light, depending on conditions, is allowed to enter the eye. Once the light has passed through the lens, it arrives into the posterior segment of the eyeball, filled with a transparent viscous fluid, the vitreous humor, before being finally focused on the retina, the innermost of the three different layers forming eye. The retina is composed by a retinal pigmented epithelium (RPE) and a neural retina, the sensory part of the eye. The inner part of the retina receives its blood supply from capillaries originating from the central retinal artery. The outer retina is nourished by the choroid, a highly vascularized conjunctive tissue that lies just behind the RPE. The outmost layer of the eye is the sclera, which is in continuity with the cornea but it corresponds to the peculiar white part of the eye visible from the outside. It provides the eye with structural and mechanical support, contributing to the maintenance of the intraocular pressure.

The different anatomical parts described above are common to all mammals, including human and rat eye, which constitute the two models on which this study is focused. However, several differences exist and a few of them will be detailed below (**Table 1**), as they have an impact on the problematics of this study. First of all, rat and human eyes differ in their sizes and subsequently in their volume: human eye axial length is four times bigger than in rat eye and the depth of human vitreous chamber is more than ten times bigger than in rats (Deering, 2004; Massof and Chang, 1972). This means that the distance between ocular surface and internal

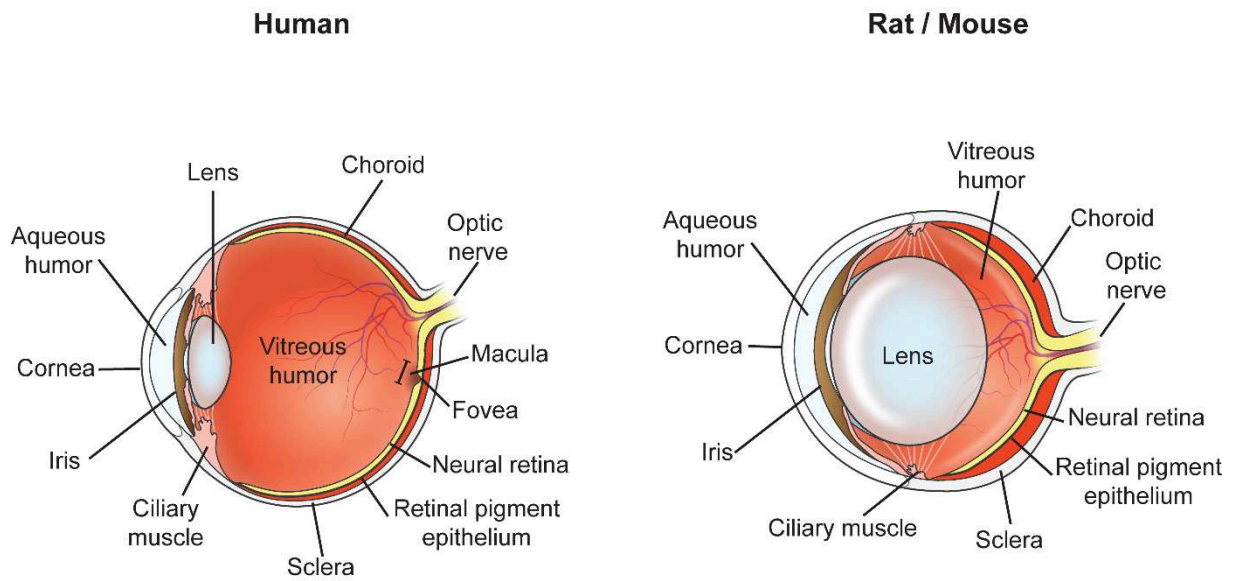


Figure 1 Anatomical structure of the human and rodent eye. Adapted from Veleri et al., 2015.

	Human	Mouse	Rat
Antero-posterior axial length	24mm	3,37 mm	6,29 mm
Aqueous volume	260 μ l	4,4 μ l	13,6 μ l
Vitreous volume	5200 μ l	5,3 μ l	54,4 μ l
Retinal area	1024 \pm 184 mm ²	15,6 mm ²	52 mm ²
References	<i>Howland et al., 2004; Panda-Jonas et al., 1994</i>	<i>Remtulla and Hallett, 1985</i>	<i>Hughes, 1979</i>

Table 1 Comparison of anatomical features in human, mouse and rat eye.

ocular tissues is shorter in rodents than in large animals. At the same time, rat crystalline lens is bigger than human lens, making the vitreous space of difficult access in rats. These anatomical features have to be taken in consideration when designing the strategy for the delivery of a therapeutic product into the eye. Importantly, primate and rodent retinas also present some substantial differences, beside their different sizes, which will be explained in the following paragraphs, dedicated to an extensive description of this tissue and its different cell populations.

1.2 Overview of the anatomy and functionality of the retina

As mentioned, the retina is composed of two separate parts: a neural retina, consisting of five major neuronal cell classes and one type of glial cells arranged in a highly laminated structure, and the RPE, formed by a monolayer of pigmented epithelial cells. Both parts have a common developmental origin, as detailed in paragraph 1.5.

The cells of RPE not only absorb the excess of light with their pigmented granules, but they are also essential for maintaining the functionality of photoreceptors, the photosensitive cell population within the retina. The presence of tight-junctions between RPE cells ensures a hermetic barrier between the choroid and the retina, known as blood-retinal barrier, so that all the exchanges (of nutrients, ions and metabolites) between the blood flow in the choroid vessels and photoreceptors are regulated, in both directions, by the RPE. This efficient isolation of the retina from systemic influences at the choroidal side is equally important for the immune privilege of the eye.

Within the neural retina, three nuclear strata and two synaptic layers are distinguishable from a histological perspective (**Figure 2**). In the outmost layer, the outer nuclear layer (ONL) contains the high-densely packed cell bodies of photoreceptors. Photoreceptors are broadly divided in rods and cones that differ in their sensitivity and in their kinetics of response to light. As a general definition, rods are responsible for vision in dim light conditions, whereas cones function in daylight allowing color vision. Following the direction of light information processing through the retina, the electric signal generated in photoreceptors is transmitted to bipolar cells residing within the inner cell layer (INL). The synaptic connections between photoreceptor and bipolar cells occur at the outer plexiform layer (OPL), the neuropil localized between ONL and INL. In mouse 12 types of bipolar cells have been identified (Wassle et al., 2009), one type driven by rods and 11 types that are stimulated mostly from cones. Bipolar cell types can be further distinguished on the basis of their functional responses, depolarization versus hyperpolarization (known respectively as ON and OFF bipolar cells), as well as sustained versus transient.

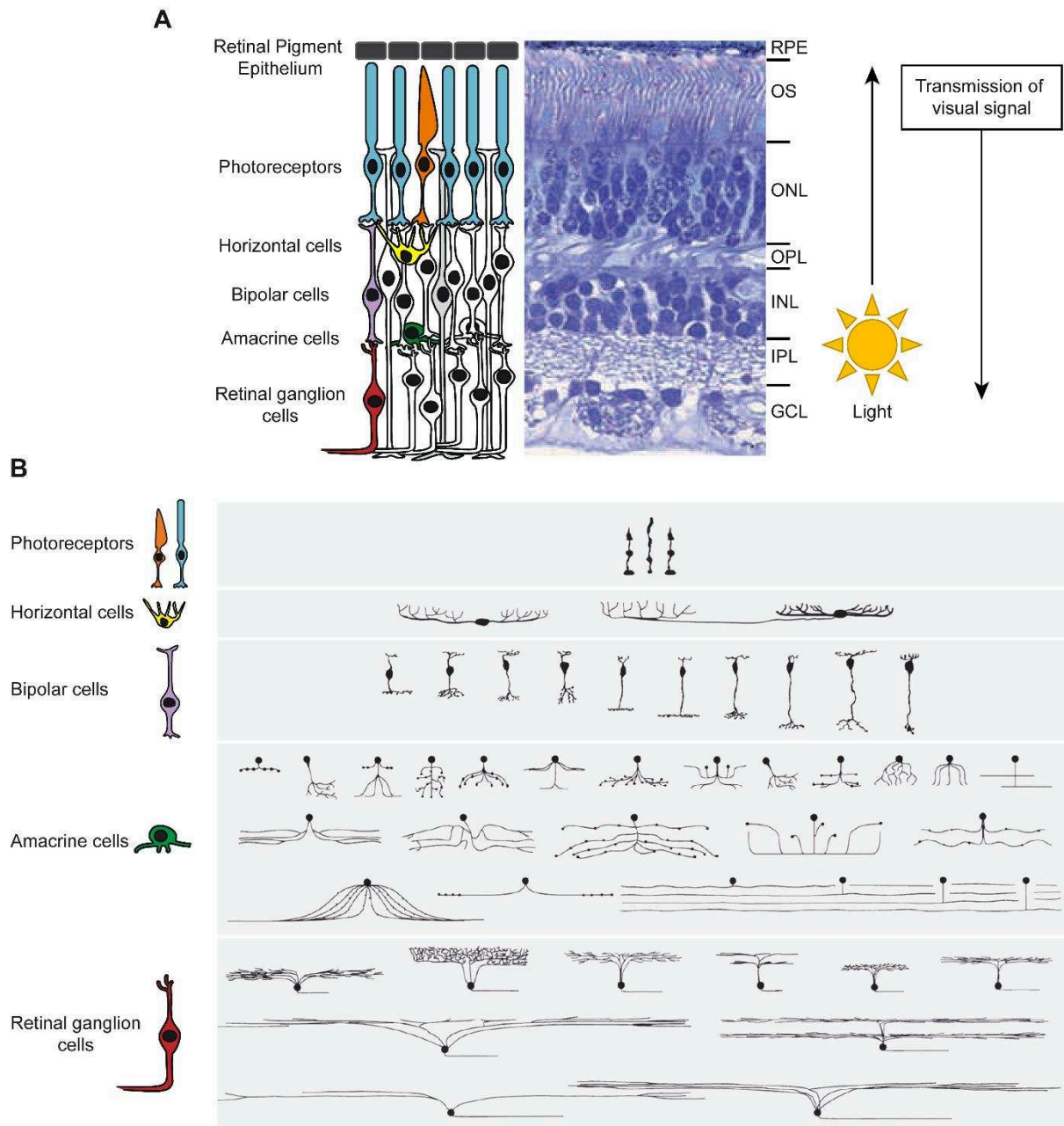


Figure 2 Structure of mammalian retina and its major cell types.

A) Schematic representation of the retina. Arrows indicate the opposite directions of light path and of visual message processing through the retina. Cross-section of human retina extracted from Wright et al., 2010. **B)** Illustration of cell variety within each major neural cell type of the retina. Adapted from Masland, 2001

RPE, Retinal Pigment Epithelium; OS, Outer Segment; ONL, Outer Nuclear Layer; OPL, Outer Plexiform Layer; INL, Inner Nuclear Layer; IPL, Inner Plexiform Layer; GCL, Ganglion Cell Layer.

Cones are wired to multiple individual bipolar cells of different types, each having characteristic molecular signatures, so that the information can diverge into distinct parallel pathways, each communicating a different version of the cone's output to the inner retina. The signaling between photoreceptors and bipolar cells is modulated at the level of the OPL by the horizontal cells. Their cell bodies are included in the INL, where they represent only the 5% of the total population; two types are present in most mammals (with the exception of rats and mice, which have only one type). At their opposite extremities facing the inner part of the retina, bipolar cells contact retinal ganglion cells (RGCs) and amacrine cells. The synaptic processes are arranged within the inner plexiform layer (IPL), delimited by the INL and ganglion cell layer (GCL), where RGCs and some of the amacrine cell bodies are aligned. Most of the amacrine cell bodies are found within the INL, but the vast varieties of amacrine cells can be classified accordingly not only to their stratification pattern, but also to their shapes and sizes, with 40 different morphological subtypes. Their role is to modulate and integrate the visual message presented to the RGCs, either via direct contact with the RGCs, or indirectly, by providing feedback inhibition onto axon terminals of bipolar cells. Interestingly, the synaptic connections occurring in the IPL are spatially restricted to distinct levels, so that bipolar cells can contact only the dendritic processes of amacrine cells and RGCs confined in the same spatial level (Masland, 2012).

Situated in the innermost layer of the retina, RGCs are the final and only output neurons of the retina. Their axons fasciculate to form the optic nerve and project to the brain visual centers. The information from bipolar and amacrine cells is integrated by RGCs and travels along the length of their axons in the form of nerve spikes, a time-coded digital form of electrical signaling. There are no less than 10-15 different morphological types of RGCs, of which only a small fraction have been functionally characterized in rat, mouse or monkey retinas (Masland, 2001, 2012). As a simplification, individual ganglion cells selectively detect precise 'features' of a visual stimulus, as color, size, and direction and speed of motion, but they all operate simultaneously, so that each aspect of the stimulus is transmitted to the brain at the same moment by at least 15 independent filters.

Altogether, the mammalian retina contains more than 60 distinct types of neuron, each with a specific function in processing of visual information (Masland, 2012). To this mastered neural complexity, we have to add the principal glial population of the retina, the Müller Glial Cells, having their nuclei within the INL but with their extensions spanning almost the entire thickness of the retina. They actually constitute two barriers delimitating the retina at its internal interface with the vitreous humor, the inner limiting membrane, and at the external interface between the ONL and the subretinal space, known as outer limiting membrane. In addition, Müller cells are involved in the structural organization of the blood-retina barrier (Reichenbach et al., 1995). Müller cells are important for retinal neuron metabolism and modulate neuronal activity

by regulating the extracellular concentration of neuroactive substances (Newman and Reichenbach, 1996). As another important class of glial cells, astrocytes, Müller Glial Cells are immunoreactive to the glial fibrillary acidic protein (GFAP), although in normal conditions GFAP is detected exclusively in the inner part of Müller cells. Perturbation of the retina, such as retinal detachment, lead to glial cells activation and massively upregulation of GFAP in the entire cell (Guerin et al., 1990). Müller cell reactivity can finally result into formation of glial scars.

The human retina structure as described here is not homogenous throughout its surface, some differences distinguish the periphery from the its center. In humans, the central retina is enriched in cones and the INL is thicker due to a greater density of cone bipolar cells. Most important, human central retina, as well as other primates but also other vertebrates, presents a specialized region of high acuity, the fovea, containing exclusively cones at high spatial density. In contrast, rodents have a rod-dominated retina, do not have a fovea, and the thickness of the ONL decreases from the center to the periphery. Structural retinal differences reflect adaptation to different habitat and functional needs. Further differences have evolved at the cellular level, so that distinct cone photoreceptor subtypes can be distinguished in rodents and primates.

1.3 Photoreceptors

The common morphological features characterizing photoreceptors are: 1) an outer segment, composed of membrane discs containing the photopigment molecules; 2) an inner segment, where mitochondria and ribosomes and the rest of the cell machinery are localized; 3) a cell body, containing the nucleus of the photoreceptors and 4) synaptic terminals, where neurotransmission to inner retinal neurons occurs (**Figure 3**).

The morphologies of the two major types of photoreceptors, rods and cones, are distinguished by the architecture of their outer segment, as well as the type of photopigment contained in it, and by the pattern of their synaptic connections. (Mustafi et al., 2009). Outer segment in rods is longer and composed of a tile of individual discs unconnected to the ciliary plasma membrane. On the contrary, cone have a shorter outer segment, formed by invaginations of the membrane that is continuous with the plasma membrane of the cilium, spanning the entire outer segment length. In photoreceptors, the cilium is the major cytoskeletal element providing the only cytoplasmic connection between the outer and the inner segment, and is also the route for the transport of materials to the outer segment. Once arrived in the cone outer segment, proteins can freely diffuse, even if slowly, and are randomly distributed throughout the continuous plasma membrane of the outer segment. Terminal tips of cone outer segment discs are phagocytized by RPE. In rods, newly synthesized protein is trapped in the new discs

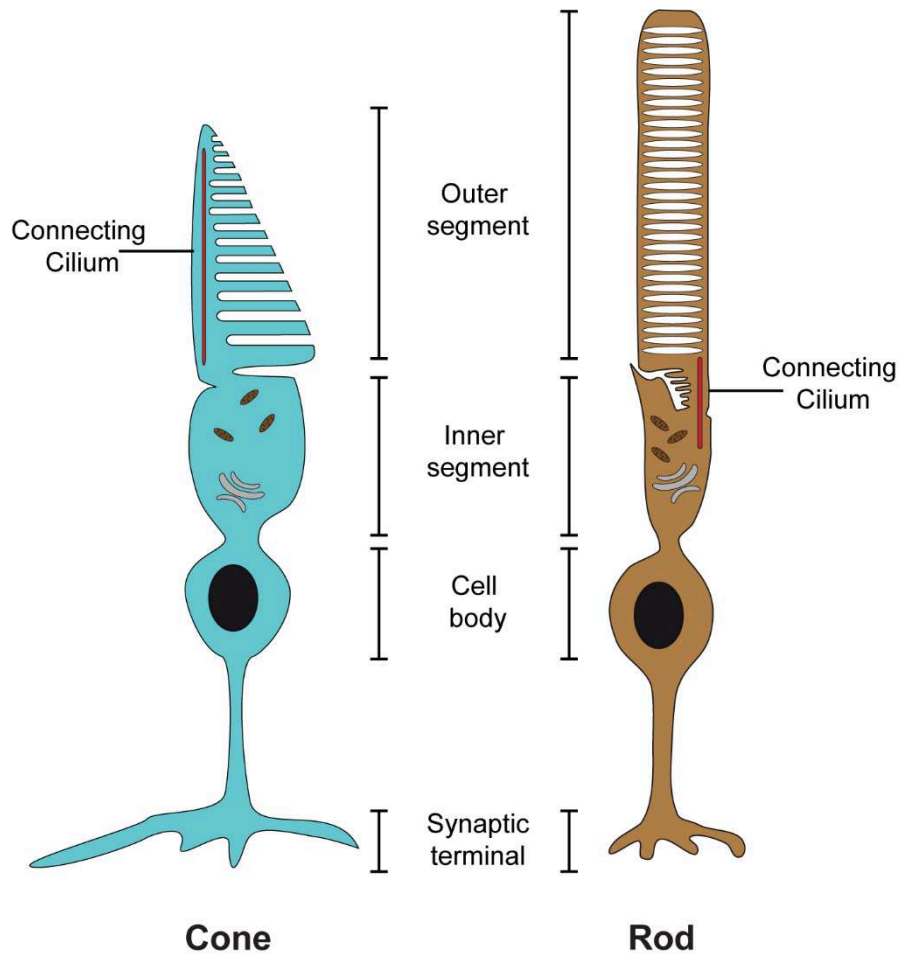


Figure 3 Schematic representations of cones and rods.

The main morphological features of photoreceptors are indicated: outer segment, where discs are localized; inner segment, containing cellular organelles such as mitochondria and Golgi apparatus; cell body, bearing cell nucleus, and synaptic terminals. Note that rods are characterized by longer outer segments but smaller synaptic terminals than cones.

and slowly displaces those formed earlier along the length of the outer segment toward its tip, over a period of weeks. The older discs are ejected and phagocytized by the apical processes of RPE cells (Young, 1976). Thus, the functioning of photoreceptors is based on a continuous renewal of membranes and proteins, including photopigment molecules. Rod and cones visual pigments are composed of a protein moiety, opsin, linked to retinal, a derivative of vitamin A. Opsins are a subclass of G-protein-linked membrane receptors (GPCRs) defined by their ability to bind a retinal-based chromophore to form a light-sensitive photopigment. The rod and cone opsins are divided into classes based on amino acid sequence similarity and spectral tuning properties, each class distinguishable by range of the light spectrum to which is maximally sensitive. These classes consist of two rhodopsin-like classes (RH1 and RH2), two short-wavelength-sensitive classes (SWS1 and SWS2), and a medium/long-wavelength-sensitive class (M/LWS). Phylogenetic analysis shows that the ancestral visual opsin class is the M/LWS class, from which SWS and rhodopsin-like classes have evolved. In most mammals, two of these classes, the RH2 and SWS2 class, have been lost, leaving only the RH1, contained in rods, and SWS1 and M/LWS classes, localized to cones respectively of S type and L/M type (Nickle and Robinson, 2007). Among mammals, only primates have evolved trichromatic vision, by gene duplication and divergence of the cone opsin gene on the X-chromosome, with three cone pigments: an SWS1 pigment and two variants of the LWS pigments (**Figure 4**). These variants show close identity with each other and encode L and M pigments with λ_{\max} values of around 563 nm and 532 nm, respectively (Bowmaker and Hunt, 2006). In humans, there are twice as many L-cones than M-cones, randomly intermixed and highly concentrated in the fovea, where they are determinant for image production. On the contrary, S-cones are excluded from the center of the human fovea. They are distributed more peripherally and constitute only 5% of the total cone population (Roorda et al., 2001).

Rodents further differ in their mechanism of color vision: they show two peaks of sensitivity, one around 500 nm, due to cones coexpressing both M and S opsins, and another at 360 nm, into the UV range (Jacobs et al., 1991). Indeed, the absorbance of rodent S opsin is shifted to the UV range, so that rodent cones are not particularly sensitive to visible light. With the exception of 5% of cones purely expressing S opsin, homogeneously distributed across the retina (Haverkamp, 2005), all the cones in the mouse retina coexpress M and S opsin. However, coexpression occurs in a gradient along the dorsal-ventral axis of the retina: M/S opsin ratio is higher in the superior retina, whereas the inferior retina contains cones expressing almost exclusively the S opsin (Applebury et al., 2000). If opsins account for the sensitivity to different wavelengths, the ability to respond to different light intensities mediated by rods and cones is due to their differences in transduction mechanisms and the circuitry mediating the transmission of the visual information through the inner retina. Rods are able to elicit a response to a single photon of light and they are saturated in photopic conditions,

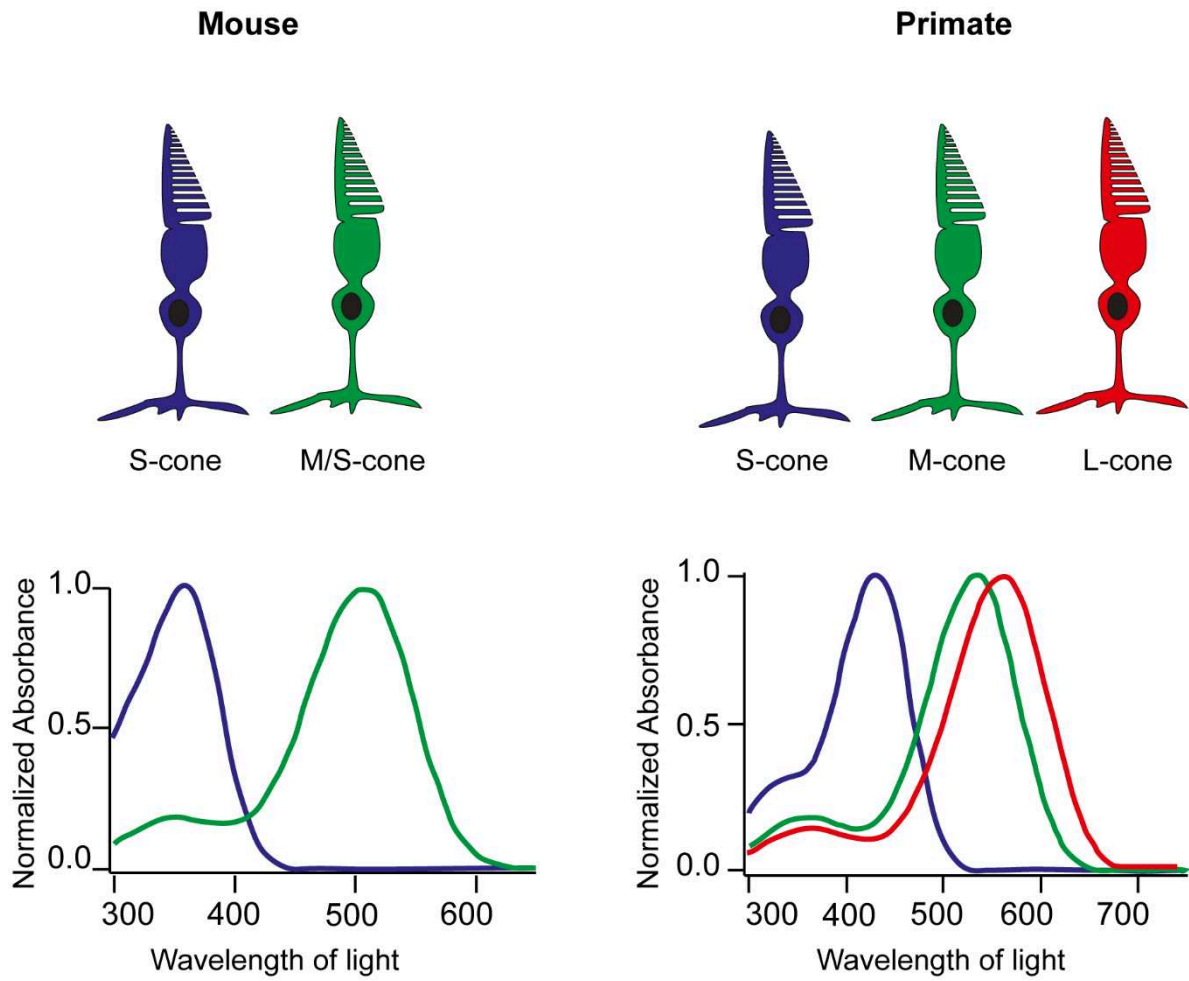


Figure 4 Different opsins in mouse and primate cones.

Absorption spectra for each cone pigment are shown in the graphs. Adapted from Hoon et al., 2014.

enabling nocturnal vision. Conversely, cones do not saturate at high levels of illumination: more than 100 photons are required to produce a comparable response to rods. The entire rod system is a better detector of light, because small signals generated from many rods converge onto a rod bipolar cell to produce a bigger signal. This system provides maximal light sensitivity, but reduces spatial resolution. The cone system, made to optimize visual acuity, is much less convergent, especially in the central retina (Mustafi et al., 2009).

Since rods are active during night vision, also indicated as scotopic vision, and cones are active during daylight (photopic) vision, it would be tempting to conclude that nocturnal animals have a rod-dominated retina, whereas diurnal animal retinas are cone-enriched. However, in mammals, even if it is true that nocturnal animals have a smaller cone proportion than diurnal animals, retinas are almost all rod-dominated. For example, there is a small difference in the cone proportion between mouse and human retina – representing respectively 3% versus 5% of the total photoreceptor population.

The real difference is that in primates about 75% of the light entering the eye converges on the fovea, the region that possesses the maximal density of cone photoreceptors (**Figure 5**). Rods are absent from the fovea. The foveal pit, the center of the fovea, lacks of S cones, as well as RGCs and inner retinal cells, allowing light to reach directly photoreceptors without being scattered. The fovea is actually the center of a larger cone-enriched area, denominated macula, where cones and rods are present in equal ratio (as a comparison, in the peripheral retina rods outnumber cones 1 to 13). This locally cone-dominant pattern provides an optimized solution for high acuity vision.

It is worthy to note that also in nocturnal retinas some structural adaptations have evolved to maximize light detection. By comparing nuclear architecture (i.e. euchromatin and heterochromatin domains in the nucleus) of nocturnal and diurnal mammals, it has emerged that rods within nocturnal mammal retinas adopt an inverted nuclear architecture, with heterochromatin condensed at the center of the nucleus and the euchromatin domains localized at its periphery. Cone nuclei, however, always possess a conventional pattern, with a rim of condensed chromatin along the border. The inverted conformation not only reduces the size of rod cell bodies, but, most important, it reduces the scattering of light in the ONL, limiting the loss of photons, a notable advantage in low light conditions (Solovei et al., 2009). Also for this reason, mouse and rat photoreceptors are smaller than human photoreceptors. Therefore, when describing photoreceptor contribution to vision, we should keep in consideration that, not only their specific pigment absorption spectrum and their characterizing morphological features, but also their size, packing density and relative position have an impact to the highly specialization of photoreceptor task.

1.4 Phototransduction and visual cycle

Photoreceptor outer segments are the site of phototransduction that have the same molecular basis in rods and cones. Phototransduction is the biochemical process converting one or more photons absorbed by the visual pigment into an electric signal, corresponding to a variation of the membrane potential (**Figure 6A**). Specifically, light causes hyperpolarization of photoreceptors, whereas darkness leads to depolarization. Depolarization in dark conditions is due to a constant influx, known as dark current, of sodium and calcium, with a minor contribution magnesium, through the cGMP-gated channels located in the plasma membrane of the outer segment. This cGMP-dependent conductance can be maintained, as long as intracellular concentration of cGMP is high in the dark. In this dark-depolarization status, there is a continuous release of the glutamate neurotransmitter at photoreceptor synaptic terminals. The first step of phototransduction is the change of conformation of the chromophore attached to the opsin protein induced by photons: 11-*cis*-retinal, the same in rods and cones, is photoisomerized to all-*trans*-retinal, inducing a conformational change in the structure of the opsin protein molecule. In this way the opsin protein, or the meta-rhodopsin in the case of rods, is catalytically activated and can bind to transducin, a G protein. Activation of transducin results in the dissociation of its α subunit, which in turn can activate the membrane-associated phosphodiesterase (PDE). cGMP hydrolysis by PDE makes intracellular cGMP levels drop, leading to the closure of the cGMP-gated channels. Consequently, hyperpolarization occurs, inhibiting neurotransmitter release. In this way the signal is transmitted to the adjacent neurons of the inner retina (Mustafi et al., 2009). The re-establishment of the initial status is due to guanylate cyclase, which, following its activation by the decrease in calcium, ensures the production of cGMP and the re-opening of the cGMP-gated channels. Inactivation of each activated component and recovery from light is essential to guarantee a rapid response. An exception is constituted by all-*trans*-retinal, which cannot be regenerated to its *cis* isomer, due to the lack of *cis-trans* isomerases in photoreceptors (**Figure 6B**). In rods, all-*trans*-retinal is transferred from disc membrane to the cytoplasm of rod outer segment by transporter ABCA4 (ATP-binding cassette, subfamily A, member 4), where it is transformed into all-*trans*-retinol by a retinol dehydrogenase (RDH12). Bound to IRBP (Interstitial Retinal Binding Protein), all-*trans*-retinol is transported to the RPE, where it is transformed to 11-*cis*-retinal thanks to the multiple actions of an enzymatic complex. CRALB (Cellular Retinaldehyde Binding Protein) binds to 11-*cis*-retinal to carry it back to photoreceptors, where it is relocated by IRBP into the disc membrane in contact with opsin protein.

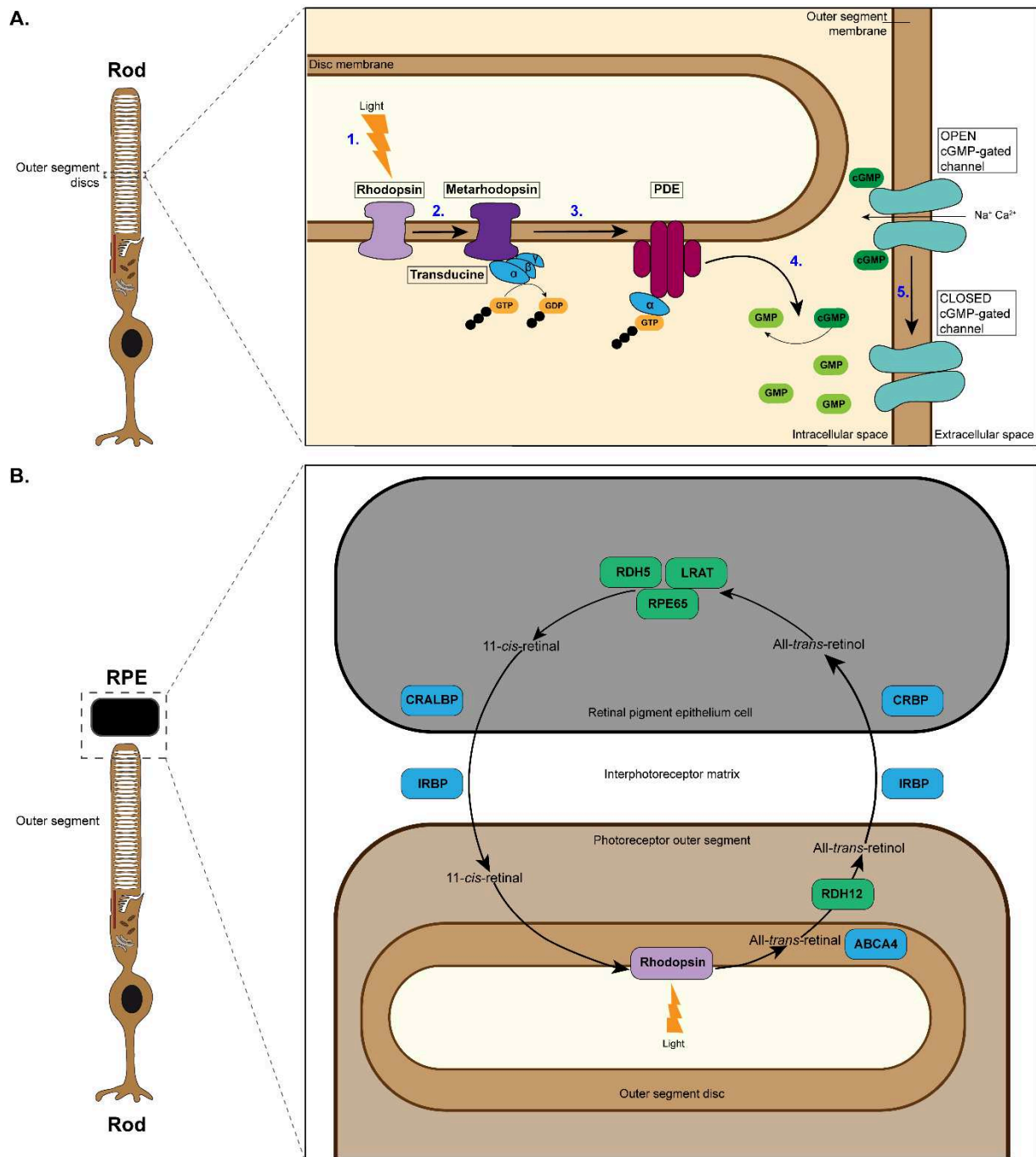


Figure 6 Phototransduction and visual cycle

A) Schematic representation of the main steps of phototransduction occurring in the outer segment discs within rod outer segment. First Rhodopsin is activated by light (1.). Activated Rhodopsin (Metarhodopsin) can bind to Transducin, activating its α subunit (2.). Phosphodiesterase (PDE) is activated by Transducin (3.) and hydrolyzes cGMP into GMP (4.). cGMP is no longer available to cGMP-gated channels, which close causing photoreceptor hyperpolarization (5.).

B) Principal steps of visual cycle taking place in photoreceptor outer segment and RPE. 11-cis-retinal bound to Rhodopsin is converted to all-trans-retinal following photon absorption. All-trans-retinal is carried from photoreceptor outer segment to the RPE, where it is re-isomerized to 11-cis-retinal.

Transporters (in blue): ABCA4, ATP-binding cassette subfamily A member 4; IRBP, Interstitial Retinal Binding Protein; CRBP, Cellular Retinol Binding Protein; CRALBP, Cellular Retinaldehyde Binding Protein.

Enzymes (in green): RDH12, retinol dehydrogenase 12; LRAT, Lecithin Retinol Acyltransferase; RPE65, RPE 65 isomerase; RDH5, retinol dehydrogenase 5.

1.5 Retinal development

During embryogenesis, the eye of vertebrates is derived from three types of tissue: the retina and RPE arise from the neural ectoderm, the cornea and the lens from the surface ectoderm, and the sclera from the mesoderm. Eye formation initiates during gastrulation in connection with the induction and patterning of the neuroepithelium. A series of patterning events governed by specific signals leads to the eye specification of a group of neuroepithelial cells within the midline of the anterior neural plate. Fundamental experiments from the last decades in different species (Graw, 2010; Zuber, 2010) demonstrated that the delimitation of the eye field territory is promoted by fibroblast growth factor (FGF) and insulin-like growth factor (IGF) signals and by repression of the transforming growth factor β (TGF β)/bone morphogenetic protein (BMP) and Wingless-Int (Wnt) pathways (**Figure 7**). Secretion of endogenous antagonists such as Noggin/Chordin and Dickkopf lead respectively to the inhibition of the TGF β /BMP and Wnt pathways, at the level of the presumptive eye field. This territory is characterized at the molecular level by the coordinated expression of specific intrinsic determinants, called “eye-field transcription factors” (EFTFs). These specific transcription factors coded for five different homeobox proteins (see below), one nuclear receptor (Nr2e1, also known as Tlx), and one T-box protein (Tbx3), whose expression temporally and spatially overlapped. These homeobox transcription factors, LIM homeobox protein 2 (Lhx2), orthodenticle homeobox 2 (Otx2), paired box 6 (Pax6), Retina and anterior neural fold homeobox (Rax), sine oculis-related homeobox 3 (Six3), sine oculis-related homeobox 6 (Six6), act synergistically to form and maintain the eye field territory in a self-regulating feedback highly conserved between species (Zuber, 2010). Interestingly, pluripotent cells isolated from the xenopus pole of blastula stage embryos misexpressing the EFTFs were able to generate eyes that are molecularly and functionally similar to the normal eye (Vicgian et al., 2009).

During midline formation, the single eye field separates giving rise to two optic areas. Following eye field formation in each of these two areas, the neuroepithelium of the ventral forebrain (diencephalon) evaginates, resulting in the formation of the optic vesicle. In the early optic vesicle all the cells co-express the EFTFs and are competent to form the neural retina, the RPE or the optic stalk. The specification of the neural retina and RPE domains takes place during the evagination process, with signaling molecules that coordinate the expression of intrinsic factors, allowing the differentiation of the cells in a specific lineage depending on their initial regionalization. The lens placode (that originate from the surface ectoderm after contacting the distal portion of the optic vesicle) invaginates into the optic vesicle resulting in the formation of the lens vesicle and the optic cup. The inner surface of the optic cup

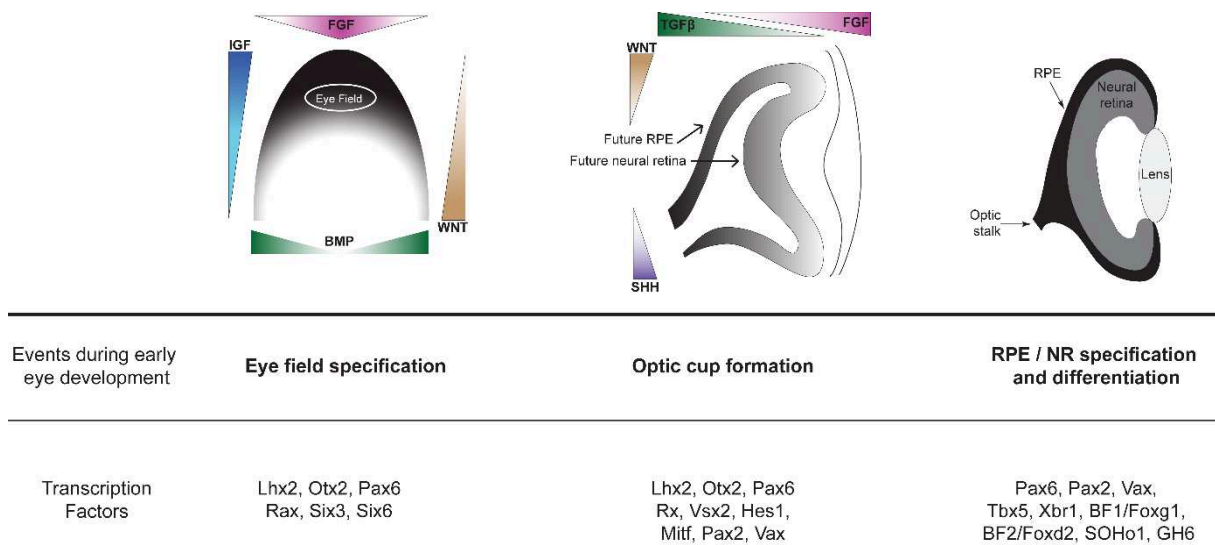


Figure 7 Early eye development.

Schematic representation of delimitation of optic vesicle, optic cup invagination and specification of neural retina and RPE. For each phase are indicated the gradient of signaling molecules and transcription factors involved.

corresponds to the future neural retina, while the RPE emerges from the outer part of the optic cup. Exogenous signals coming from adjacent tissues influence the early specification of the optic vesicle into neural retina and RPE. FGF signal from the overlying lens ectoderm normally inhibits RPE specification and promotes neural retina lineage, while specification of the RPE requires input from the surrounding extra-ocular mesenchyme by members of the TGF β /BMP superfamily (Fuhrmann, 2010; Fuhrmann et al., 2014). These extrinsic cues regulate the expression of a specific set of transcription factors that are important for the development of the cell type in which they are expressed: the expression of the transcription factor, Visual system homeobox 2 (Vsx2), also named Chx10, delineates the future neural retina, while the future RPE expresses the transcription factor, Microphthalmia-associated transcription factor (Mitf) and the optic stalk expresses the paired box protein 2 (Pax2) (Adler and Canto-Soler, 2007; Fuhrmann et al., 2014). Reciprocal transcriptional repression between these transcription factors contributes to the establishment of the boundaries between these developing territories.

Within the optic vesicle / cup, the neural retina is generated from common multipotent retinal progenitor cells (RPCs), expressing Vsx2 and Pax6, which give rise to all types of cells in an orderly manner that is generally conserved among many species (**Figure 8**). RGCs, amacrine and horizontal cells and cone photoreceptors are generated at relatively early stages, while rod photoreceptors, bipolar and Müller cells differentiate mainly at later stages (Turner and Cepko, 1987; Young, 1985). The widely accepted competence model of retinal histogenesis hypothesizes that RPCs progress through a competence window of time during which they can generate specific cell types (Cepko, 2014). Recent live imaging studies consistent with a stochastic model (Gomes et al., 2011; He et al., 2012), suggest that RPCs could choose from multiple cell fate at any time, even though the transition of competence occurs in a unidirectional way (Boije et al., 2014). Several lines of evidence demonstrate that transcription factors, such as bHLH-type and homeobox-type factors, expressed in RPCs, are required for the correct specification of retinal cell types (Bassett and Wallace, 2012; Livesey and Cepko, 2001; Ohsawa and Kageyama, 2008). A core transcriptional hierarchy is at the basis of the molecular decisions made by the RPCs to acquire specific retinal fates. As nicely reviewed by Boije et al. (2014), expression of Vsx2 in proliferative RPCs, allows the inhibition of transcription factors influencing specific cell fate such as Atonal bHLH transcription factor 7 (Atoh7; also known as Math5), Forkhead box N4 (FoxN4), Pancreas specific transcription factor 1a (Ptf1a) and Visual system homeobox 1 (Vsx1). As the development progress this inhibition is abolished and depending on the level of Atoh7 (promoting RGC lineage) and the presence or not of FoxN4 and Ptf1a (promoters of amacrine and horizontal cells lineages), each RPC follows different paths giving rise to different cell fates. Loss of Atoh7 in RPCs

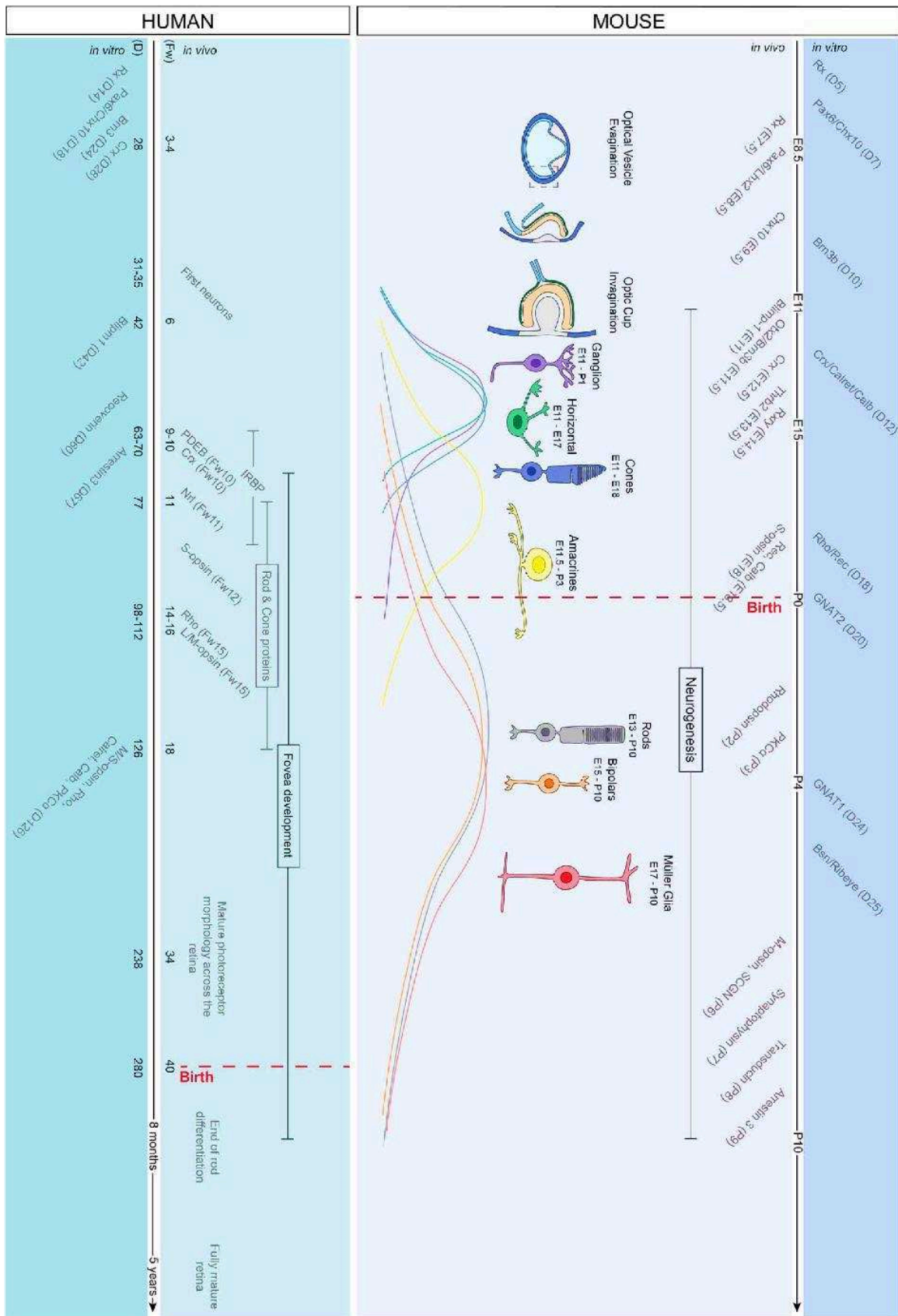


Figure 8 Comparison of mouse/ human *in vivo* versus *in vitro* development. Extracted from Llonch et al., 2018.

provides a permissive environment in absence of FoxN4 and Ptf1a for a photoreceptor fate (Bassett and Wallace, 2012; Boije et al., 2014).

The process of photoreceptor development can be divided into different successive steps. First specification and commitment of RPCs towards a photoreceptor cell fate, after final mitosis; secondly the choice of cone or rod cell fate, and finally the selection of a sub-type of cones, corresponding to the maturation of photoreceptors with the expression of photoreceptor-specific genes and outer segments biogenesis (**Figure 9**). Several intrinsic factors have been identified together with their gene regulation network, leading to a model in which differentiation into type S cones would be the default pathway (Brzezinski and Reh, 2015; Swaroop et al., 2010). The down regulation of Notch signaling and the implication of proneural genes, such as achaete-scute homologue 1 (ASCL1; also known as Mash1) and Neuronal differentiation 1 (NeuroD1) could be the earliest molecular mechanisms that prompt RPCs to adopt a photoreceptor fate over other cell fates (Hatakeyama and Kageyama, 2004; Jadhav et al., 2006).

The coordinated action of six major transcription factors is required for the RPC commitment to a rod or cone photoreceptor cell fate (Brzezinski and Reh, 2015; Swaroop et al., 2010): Cone-Rod homeobox (Crx), Otx2, neural retina leucine zipper (Nrl), orphan nuclear receptor Nr2e3, Retinoid-related orphan nuclear receptor β (Ror β) and the Thyroid hormone receptor β 2 (TR β 2).

Otx2 is expressed in RPCs undergoing their final mitotic division and in early photoreceptor precursors, while Crx starts to be expressed in these post-mitotic committed precursors and its presence is important for the terminal differentiation of photoreceptors (Chen et al., 1997; Furukawa et al., 1997; Koike et al., 2007; Nishida et al., 2003). Otx2 biases the RPC to a photoreceptor precursor fate and activates the expression of Crx and the combination of these two transcription factors is necessary and sufficient to induce the photoreceptor cell fate (Hennig et al., 2008; Nishida et al., 2003). Recent studies in mice have reported the role of photoreceptor domain zinc finger protein 1 (Prdm1), also known as Blimp1 in maintaining RPCs expressing Otx2 in the photoreceptor lineage (Brzezinski et al., 2013; Katoh et al., 2010). Prdm1 had the ability to repress genes involved in the specification of bipolar cells within Otx2-positive RPCs, stabilizing the commitment of these Otx2-expressing precursors to a photoreceptor fate. The retinoid-related orphan nuclear receptor β (Ror β), also plays a role in the specification of photoreceptors downstream Otx2 and Onecut1 (OC1) and upstream of Nrl and Nr2e3. Ror β participates in the induction of Nrl expression and the loss of function of Ror β in the retina leads to a drastic decrease of rod number and to an increase in the population of cones, mainly non-functional since they lack of outer segments (Jia et al., 2009).

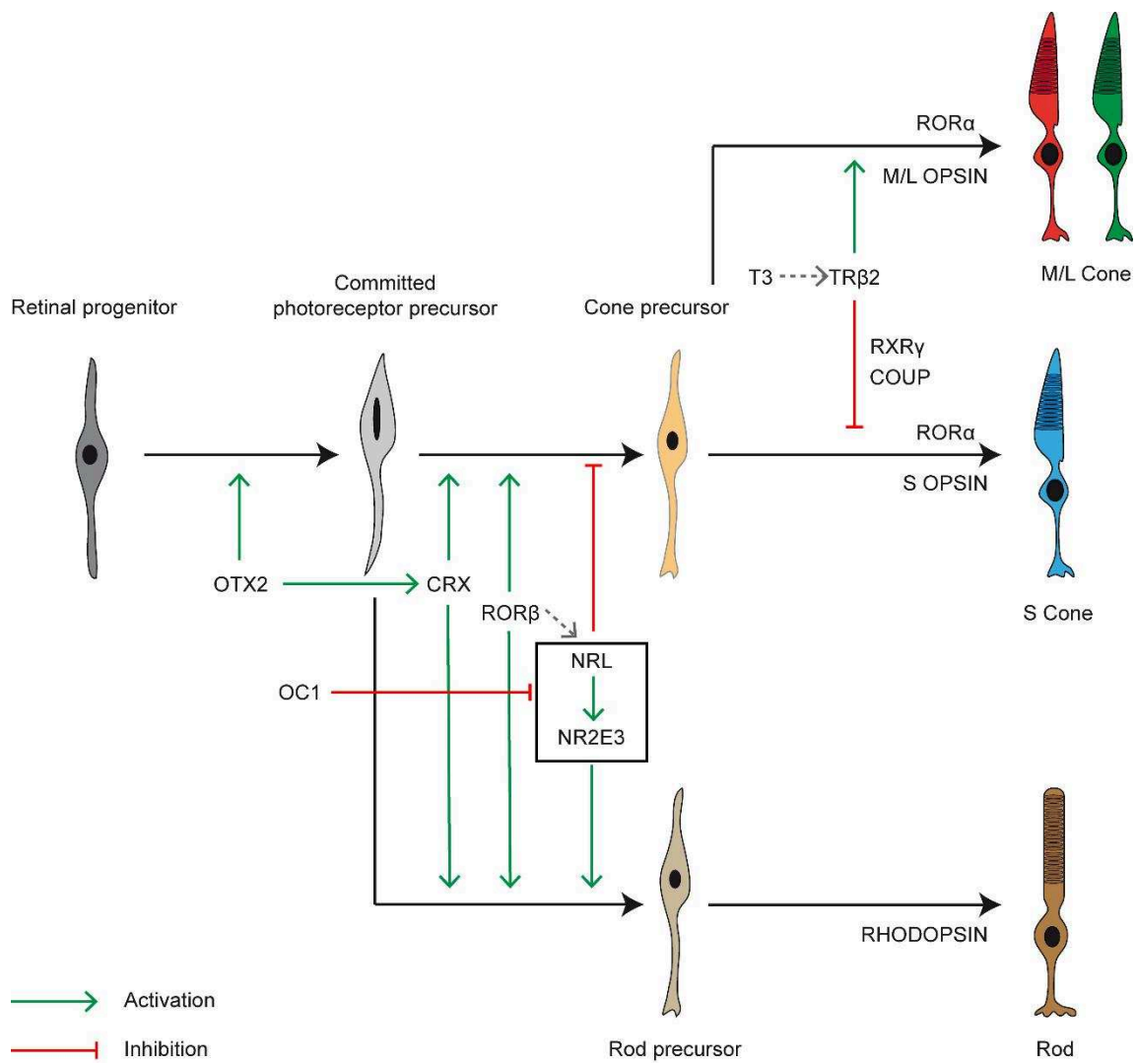


Figure 9 Factors involved in the specification of different types of photoreceptors.
Adapted from Swaroop et al., 2010.

The transcription factor Nrl is a key player in the choice of a RPC to become a rod or a cone. Nrl can interact with Crx leading to a rod differentiation program (Akimoto et al., 2006; Mears et al., 2001). One of the direct transcriptional targets of Nrl is the nuclear receptor Nr2e3, expressed in post-mitotic rod precursors (Oh et al., 2008). The Nrl-Nr2e3 complex can suppress the expression of cone-specific genes, which consolidate the rod fate directed by Nrl (Chen et al., 2005; Cheng et al., 2006; Peng et al., 2005). The photoreceptor precursors can differentiate as a cone only when Nrl and Nr2e3 fail to act, corresponding to low level of Nrl expression. In the mouse and chicken retina, OC1 has been shown to act, together with Otx2, upstream Nrl as a repressor of early rod photoreceptor gene expression (Emerson et al., 2013). In these committed cone precursors, TR β 2 and its ligand triiodothyronine T3 induce M opsin and suppress S opsin expression (Ng et al., 2001). Other factors have been reported to be involved in S and M opsin patterning, including retinoid X receptor γ (RXR γ), Retinoid-related orphan nuclear receptor α (ROR α) and Chicken ovalbumin upstream promoter (COUP) transcription factors (Fujieda et al., 2009; Roberts et al., 2005; Satoh et al., 2009).

Thanks to the advent of next-generation sequencing, we have gained deeper and, at the same time, more global look at the transcriptional changes guiding development of mouse and human retina (Aldiri et al., 2017; Hoshino et al., 2017). These studies confirmed that human retinal development basically occurs in three phases, each dominated by the emergence of specific cell types and the expression of specific genes: first progenitor cells and RGC production, then horizontal and amacrine cells and finally photoreceptors, bipolar cells and Müller glia. However, for all the cell types the morphological differentiation in the fovea is completed much earlier than in other region of the retina. The differences in the timing of gene expression between central and peripheral retina should be considered when correlating temporal gene expression between human and mouse retina. The accelerated developmental timing in foveal development may explain why rods are excluded from this region, as rods are among the last cell types to be generated (Hoshino et al., 2017). This type of study should provide significant help in dissecting and controlling gene networks associated with functional maturations of specific retinal cell types in human retina.

2. Outer retinal dystrophies

Outer retinal dystrophies are caused by the progressive loss of the light sensitive photoreceptor cells, and accounts for averaging half of the blindness cases of in the developed countries. These conditions can be caused genetically or acquired later in life. Complex diseases are caused by a combination of both genetic and environmental factors. Inherited retinal degenerations, on the other hand, are entirely linked to mutations in genes expressed in photoreceptors and RPE.

2.1 Age-related macular degeneration

The most common form of multifactorial outer retinal diseases is age-related macular degeneration (AMD), the prevalent cause of vision loss in the elderly. Nearly 10% of the worldwide population has AMD, and the number of people with the disease is expected to grow to 196 million in 2020 (Wong et al., 2014). A combination of genetic and environmental factors, such as aging, lifestyle factors such as smoking, nutrition and sunlight exposure, are important risk factors for the disease. A major pathological hallmark of AMD is the presence of drusen in the macula, deposits of lipids between the RPE and an adjacent basement membrane complex known as Bruch's membrane, accompanied by loss of sharp and central vision with advancing disease. Late age-related macular degeneration has "dry", or atrophic, and "wet" forms, with approximately 10% – 15% of all AMD patients eventually developing the wet form. Wet age-related macular degeneration implies that fluid, exudates and/or blood causes the neuroretina or the RPE to detach from Bruch's membrane. The fluid originates from ectopic development of a subretinal neovascular membrane (de Jong, 2006). Irreversible cell loss and functional impairment initially of RPE cells, and subsequently of neuroretinal and choroidal cell, occur in late AMD.

2.2 Inherited retinal dystrophies

Monogenic diseases of the retina affect more than 2 million people worldwide (Haider et al., 2014; Hartong et al., 2006) and depending on the affected photoreceptor cell type, it is possible to discriminate cone-dominated diseases, rod-dominated diseases and generalized photoreceptor diseases, where both cell types were implicated. For each group of diseases, the ocular phenotype can be associated with symptoms affecting other tissues, corresponding to syndromic forms and the mode of inheritance can be dominant, recessive, or X-linked (Berger et al., 2010; Hamel, 2006; Hartong et al., 2006).

Cone-dominated diseases

Cone-dominated diseases, such as macular degenerations, cone and cone-rod dystrophies lead to severe visual impairment. Macular dystrophies are characterized by a restricted disease to the macula whereas pure cone and cone-rod dystrophies are defined by a generalized cone dystrophy affecting both macular and peripheral cones, and a characteristic decrease in both cone or cone and rod responses at the full field electroretinogram (ERG) (**Figure 10**). Currently about 20 and 10 different genes have been shown to be responsible of non-syndromic progressive cone-rod dystrophies and monogenic macular dystrophies respectively (Berger et al., 2010; Haider et al., 2014). Stargardt disease (with its phenotypic variant fundus flavimaculatus), which has autosomal recessive inheritance, is the most common form of inherited juvenile macular degeneration (1 in 8,000 to 10,000 individuals) that is due to mutations in the ATP-binding cassette transporter (*ABCA4*) gene (Allikmets et al., 1997). Rare cases of Stargardt-like disease, inherited as a dominant trait, are due to mutations in the Elongation Of Very Long Chain Fatty Acids 4 (*ELOVL4*) gene (Haji Abdollahi and Hirose, 2013). Cones can also be affected in stationary disorders as part of cone dysfunction syndromes, the most common form of which is achromatopsia (complete and incomplete) (Zeitze et al., 2015).

Rod-dominated diseases

The most common form of rod-dominated diseases is retinitis pigmentosa (RP) also known as rod-cone dystrophy. RP is a term given to a set of clinically similar phenotypes associated with genetically heterogeneous causes. Even though the onset and the progression of the disease vary between patients, typical symptoms include night blindness followed by constriction of visual fields, which results in tunnel vision and leading in many cases to complete blindness with the secondary loss of cones in later stages (Hamel, 2006; Hartong et al., 2006). The worldwide prevalence of RP is about 1 in 4000 for a total of 1.2 million affected individuals (Hartong et al., 2006). RP is either affecting only the retina or be part of a syndrome in 25% cases. Among the most frequent syndromic forms of RP, the Usher syndrome in which hearing impairment, and in some forms vestibular imbalance, is associated to the RP, account for about 20% of all cases of RP (Mathur and Yang, 2015). Bardet-Biedl syndrome is RP with hexadactyly, obesity, mental retardation and in some cases kidney disease. Currently, mutations in 12 and 17 genes are known to cause respectively Usher syndrome and Bardet-Biedl syndrome (Mathur and Yang, 2015; Mockel et al., 2011). Disease-causing mutations can be inherited autosomal recessive (50 to 60%), autosomal dominant (30 to 40%) and X-linked (5 to 15%) and mutations in several genes can be either dominant or recessive. High-throughput “next-generation sequencing” approaches have allowed to identify novel RP genes

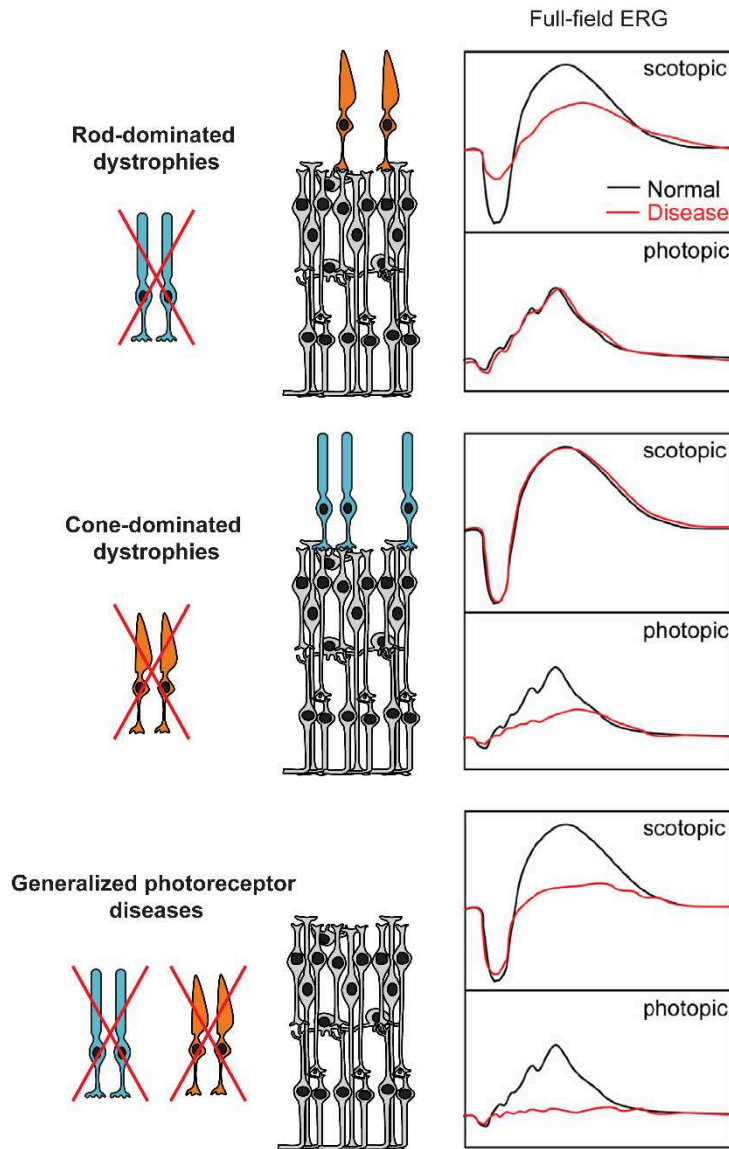


Figure 10 Photoreceptor loss and functional alterations in dystrophic retina.

Scotopic and photopic electroretinograms (ERGs) of normal animals (black) and of animals afflicted by disease (red). Loss of photoreceptor functionality may be caused by mutations or cell death. Adapted from Hoon et al., 2014.

and new mutations; nearly 60 genes were involved in non-syndromic RP and more than 3000 mutations have been reported in these genes (Berger et al., 2010; Daiger et al., 2013). According to the presumed function of the encoded protein, the different RP-associated genes have been categorized into four major groups: phototransduction, retinal metabolism, cellular structure and splicing (Berger et al., 2010; Daiger et al., 2013) (**Figure 11**). The majority of causal mutations affect genes specifically expressed in photoreceptors, such as Rhodopsin, which is the most commonly mutated RP gene (25% of the autosomal dominant cases). Few genes are specifically expressed in the RPE, such as genes coding for the MER Proto-Oncogene Tyrosine Kinase (*MERTK*), the Lecithin Retinol Acyltransferase (*LRAT*) or the Retinol Dehydrogenase 5 (*RDH5*). As expected mutations in one of these genes lead to a dysfunctional RPE (absence of photoreceptor outer segments phagocytosis, absence of re-isomerization of the retinal,...) and subsequently to the death of photoreceptors. Interestingly, the genes coding for the pre-mRNA processing factor 3 (*PRPF3*), *PRPF8* and *PRPF31*, implicated in around 10% of the autosomal dominant cases, are ubiquitously expressed although the phenotype of patients is restricted to the retina (Liu and Zack, 2013). Since the splicing activity is essential in almost all cell types, it is not clear why mutations in *PRPF* genes cause only a retinal specific disease and which is the specific retinal cell type(s) firstly affected by these mutations. Although the functional properties of several RP-associated genes have been largely studied, the correlations between the phenotype and the genotype is not fully understood and is the next critical step in the diagnosis of RP.

Generalized photoreceptor diseases

In the group of generalized photoreceptor diseases, the Leber congenital amaurosis (LCA) is one of the most common causes of blindness in children and the frequency is about 2 to 3 per 100.000 newborns (Haider et al., 2014; den Hollander et al., 2008). Currently more than 15 genes were identified to carry mutations in LCA patients, with a mode of inheritance mostly autosomal recessive. Among these genes, between 30 and 50 mutations have been reported to cause LCA in each of these four major genes coding for Centrosomal protein 290kDa (*CEP290*), Crumbs Family Member 1 (*CRB1*), Guanylate cyclase 2D (*GUCY2D*) and the RPE-Specific Protein 65kDa (*RPE65*) (den Hollander et al., 2008). Choroideremia (causal mutation in *CHM* gene) and Gyrate atrophy (causal mutation in *OAT* gene) are the two other major forms of non-syndromic generalized photoreceptor diseases with an estimated incidence rate of 1:50.000 (Berger et al., 2010; Haider et al., 2014).

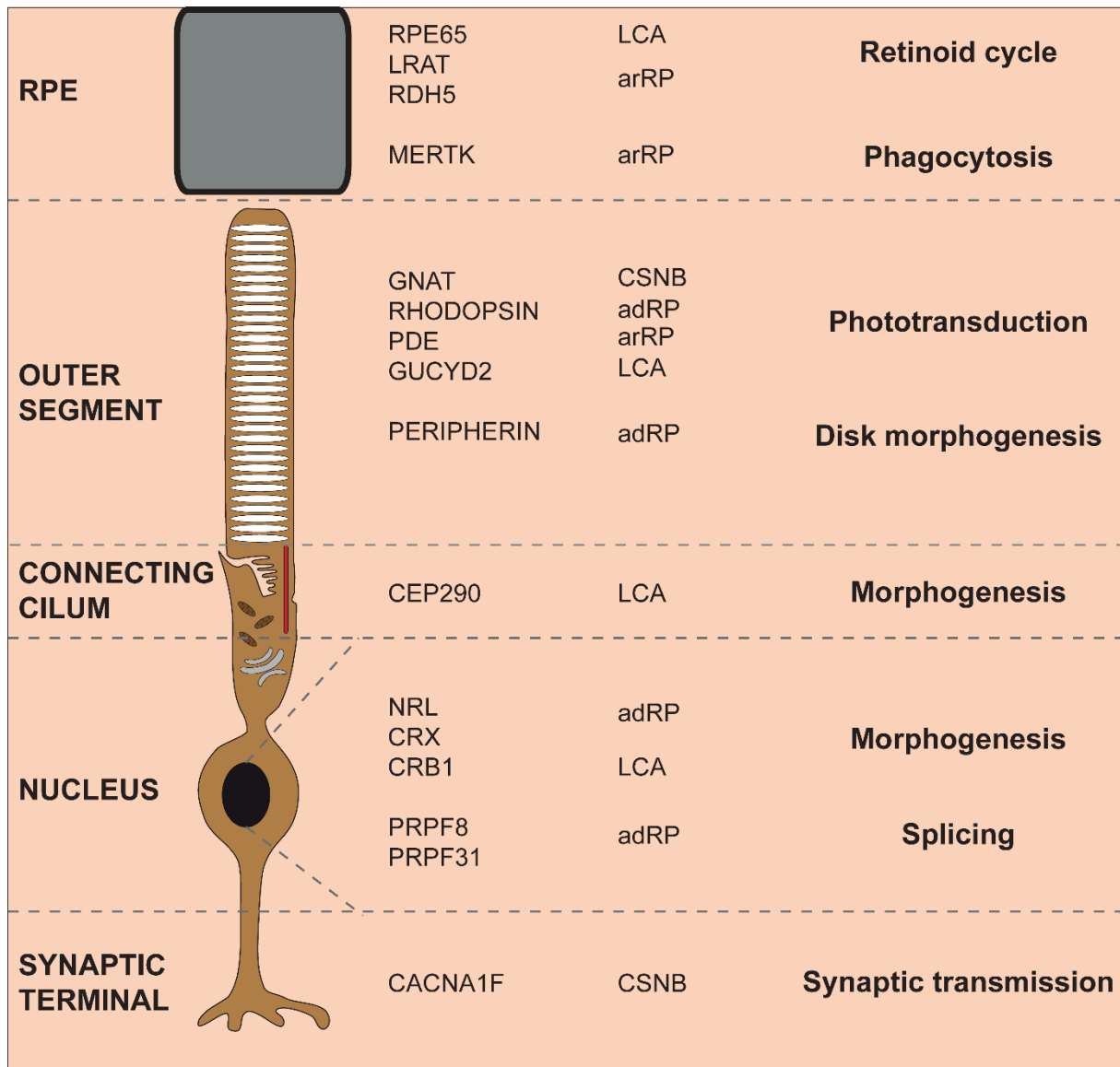


Figure 11 Examples of proteins associated with retinal dystrophies classified according to their function and localization in photoreceptors and retinal pigment epithelium.

adRP, autosomal dominant retinitis pigmentosa; arRP, autosomal recessive retinitis pigmentosa; CSNB, congenital stationary night blindness; ESCS, enhanced S-cone syndrome; LCA, Leber Congenital Amaurosis; RP, Retinitis Pigmentosa.

2.3 Animal models of inherited retinal diseases

The use of mutant animal models, either naturally occurring or generated by genetic modification, have contributed greatly to our understanding of the physiological processes that regulate vision and of the pathophysiological mechanisms that underlie retinal dystrophies.

Macaque, mouse, rat, dog, cat, pig, sheep, chicken and zebrafish are the most commonly used vertebrate animal model models to study retinal function, the mechanisms underlying inherited retinal dystrophies, and/or the development of novel treatments. These mutant animal models do not always mimic the retinal phenotype that is observed in humans with mutations in the orthologous gene, often due to specie-specific characteristics of the retina, and/or diverse functions of the gene products in different species (Slijkerman et al., 2015).

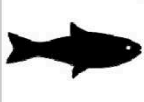
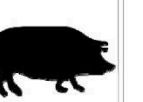
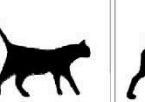
Besides detailed genetic, functional and anatomical characteristics of the retina, other aspects, including duration of embryonic development, ethical restrictions, housing requirements and cost need to be considered when selecting the ideal animal model (**Figure 12**). Historically, chicken and zebrafish have been used to investigate retinal development, transdifferentiation and innate regenerative capacities; mammal models are preferred for therapeutic research.

Non-human primates resemble the most to human in their eye anatomy and the frontal position in the skull (binocular vision). Like humans, they see with three different cone subtypes (trichromatic) and have a macula with cone-only foveal pit in its center, making this model crucial for developing treatment strategies. However, there are no inherited retinal dystrophies so far described in nonhuman primates; photoreceptor degeneration must be induced mechanically or by the injection of cytotoxic compounds that cannot recapitulate the pathogenesis of the disease (Shirai et al., 2016).

Due to the large size of its eyes, the cone-rich nature of the retina and the presence of an *area centralis*, the porcine retina is considered to be an ideal model for testing new surgical procedures and studying inherited retinal dystrophies, especially cone-dominated disorders. Two mutant rhodopsin transgenic pigs, carrying P347L and P347S mutations, have been created as models for autosomal dominant RP research (Kraft et al., 2005; Petters et al., 1997). More recently, transgenic P23H pigs and minipigs have been established (Scott et al., 2014, 2017), which will be useful for the study rod-cone dystrophies in cone-enriched retina.

Dog models have been frequently used because of the large diversity of naturally occurring mutations similar to human. The most famous RPE65^{-/-} mutation is found in the Swedish Briard Beagle dog, which is a naturally occurring model for Leber congenital amaurosis that has been used for pre-clinical testing of gene augmentation therapy (Acland et al., 2001).

Pros

<ul style="list-style-type: none"> - Genetic modification - Housing - Lots of offspring - Generation time - Animal laws (55 dpf) - <i>Ex utero</i> development 	<ul style="list-style-type: none"> - Generation time - Lots of offspring - Egg incubation into any desired stage - <i>Ex utero</i> development 	<ul style="list-style-type: none"> - Human eye size - Area centralis - Genetic modification 	<ul style="list-style-type: none"> - Human eye size - Cone-dominated retina - Area centralis - Genetic modification 	<ul style="list-style-type: none"> - Human eye size - Area centralis - Mutations similar to humans 	<ul style="list-style-type: none"> - Many naturally occurring models - Human eye size - Area centralis - Mutations similar to humans 	<ul style="list-style-type: none"> - Many naturally occurring models - Genetic modification - Lots of offspring - Generation time 	<ul style="list-style-type: none"> - Human eye size - Anatomically similar to humans
							
Zebrafish	Chick	Sheep	Pig	Cat	Dog	Rat/Mouse	Macaque
<ul style="list-style-type: none"> - Evolutionary distant from human - Many duplicated genes in genome - Retinal regeneration capacity - Ectothermic 	<ul style="list-style-type: none"> - Evolutionary distant from human - Photoreceptor anatomy (oil droplets) - Poorly annotated genome 	<ul style="list-style-type: none"> - Housing - Regeneration time - Tapetal structure complicates imaging - Moderately annotated genome 	<ul style="list-style-type: none"> - Housing - Regeneration time - Poorly annotated genome 	<ul style="list-style-type: none"> - Housing - Regeneration time - Tapetal structure complicates imaging - Moderately annotated genome 	<ul style="list-style-type: none"> - Housing - Regeneration time - Tapetal structure complicates imaging - Moderately annotated genome 	<ul style="list-style-type: none"> - Nocturnal - Photoreceptor anatomy (calyceal processes) 	<ul style="list-style-type: none"> - No IRD model existing - Moderately annotated genome - Ethical restrictions

Cons

Figure 12 Summary of pros and cons of the most common animal species used in inherited retinal degeneration studies.

General maintenance factors as well as specific anatomical features of the retina are considered. Extracted from Slijkerman et al., 2015.

Rodent models are the most used and the most thoroughly characterized, especially mouse (**Table 2** and **Table 3**). Housing and breeding for rodents are convenient and well mastered; their genome is extensively annotated and amenable to genomic modifications. Several natural heritable degeneration models have been identified, including *rd1* mouse and RCS rat (refer to Naash et al., 1993 for complete review). *Rd1* mice carry a mutation in the β subunit of the PDE, involved in the phototransductive pathway in rods (*cf.* 1.4). The mutated PDE is inactive and unable to regulate cytoplasmic cGMP levels that peak to a cytotoxic concentration, causing a rapid degeneration of photoreceptors starting as early as P10. Given the loss of ONL, *rd1* mice are useful to recapitulate advanced stages of retinal dystrophies.

Cone photoreceptor function loss 1 (*cpfl1*) mutant mouse is a spontaneously arising mutant that carries an 116-bp cDNA insertion and a 1-bp deletion in the catalytic subunit of the cone photoreceptor phosphodiesterase gene (*Pde6c*) (Chang et al., 2009). Analogous molecular defect human PDE6C causes autosomal recessive achromatopsia or early-onset progressive cone dystrophy (Chang et al., 2009; Thiadens et al., 2009). The mutant is characterized by an early and rapid loss of cones leading to the absence of cone-elicited photoresponse already at P21, as assessed by ERG measurements (Chang et al., 2002).

RCS rat is largely used as a model to study the replacement of RPE cells. A genetic defect in *Mertk*, has been identified as the causative gene defect (D'Cruz et al., 2000), resulting in an inability of RPE to correctly phagocytize photoreceptor outer segments. RPE dysfunction lead to gradual photoreceptor loss.

Several rodent models of photoreceptor degenerative diseases have been established either by transgenic approaches, including insertion of mutation or of transgenes carrying the mutation, or by gene knockouts (Baehr and Frederick, 2006).

In addition to recapitulate human photoreceptor dystrophies, knockout models have been a valuable method to dissect the role of a gene product in phototransduction or during development. For example, knockout of *Nrl*, a key transcription factor for the acquisition of rod identity, results in a rod-less retina, where rods undergo a default fate switch to hybrid cone-like cells, expressing only S opsin (Mears et al., 2001). Because of their differences with wild-type cones, including expression of rod arrestin, synaptic connections with rod bipolar cells and reduced flicker response in ERG recording (Daniele et al., 2005; Mears et al., 2001; Strettoi et al., 2004), hybrid cone-like cells in *Nrl*^{-/-} mice have also been referred to as cods (Mears et al., 2001). In *Nrl*^{-/-} mice, even if ONL is not completely structurally preserved, S-cones are partially functional. The loss of gene product can result in rapid, slow or very slow photoreceptor loss. In some cases, the ONL is structurally preserved but is completely or partially dysfunctional. For example, *Gnat1*^{-/-} mice are a model for stationary night-blindness, where rods are conserved for long time but they are not functional.

	Mutant animal	Reference	Phenotype	Transplantation studies
<i>Naturally occurring mouse models</i>	<i>Cpfl1</i>	(Chang et al., 2002, 2009)	Achromatopsia, cone functionally impaired and reduced in number from P21; normal rods.	(Santos-Ferreira et al., 2015)
	<i>Crb1</i> ^(rd8/rd8)	(Chang et al., 2002)	LCA, slow ONL degeneration.	(Barber et al., 2013; Lakowski et al., 2011)
	<i>PDE6β</i> ^(rd1/rd1)	(Keeler, 1966; Pittler et al., 1993)	RP, very fast ONL degeneration, severe PR loss within P21-P28.	(Assawachananont et al., 2014; Barber et al., 2013; Barnea-Cramer et al., 2016; Lakowski et al., 2018; Mandai et al., 2017a; Singh et al., 2013)
	<i>Prph2</i> ^(rd2/rd2)	(van Nie et al., 1978)	RP, slow ONL degeneration, PR complete loss by 9 months.	(Barber et al., 2013; Gonzalez-Cordero et al., 2013; Lakowski et al., 2011; Waldron et al., 2017)
<i>Knockout mouse models</i>	<i>Aip1</i> ^(-/-)	(Ramamurthy et al., 2004)	LCA, fast ONL degeneration with complete PR loss at P30.	(Gonzalez-Cordero et al., 2017; Kruczek et al., 2017)
	<i>Cpfl1:Rho</i> ^(-/-)	(Santos-Ferreira et al., 2016a)	RP, moderate ONL degeneration, severe PR loss within 2,5-3 months.	(Santos-Ferreira et al., 2016a)
	<i>Crx</i> ^(-/-)	(Furukawa et al., 1999)	LCA, slow ONL degeneration but not functional; severe PR loss by 6 months.	(Homma et al., 2013; Lamba et al., 2009; Ortin-Martinez et al., 2017; Smiley et al., 2016)
	<i>Crx</i> ^{ivrm65}	(Won et al., 2011)	LCA, faster degeneration than in <i>Crx</i> ^(-/-) with severe PR loss by 3 months.	(Zhu et al., 2017a)
	<i>Gnat1</i> ^(-/-)	(Calvert et al., 2000)	Stationary night-blindness, very slow ONL degeneration but functionally impaired rods.	(Barber et al., 2013; Gonzalez-Cordero et al., 2013; Lakowski et al., 2015; Pearson et al., 2012)
	<i>Nrl</i> ^(-/-)	(Mears et al., 2001)	Rodless retina, enhanced S cone function. Disturbed ONL cytoarchitecture.	(Gonzalez-Cordero et al., 2017; Ortin-Martinez et al., 2017; Santos-Ferreira et al., 2015; Waldron et al., 2017)
	<i>Prom1</i> ^(-/-)	(Yang et al., 2008)	Slow cone-rod degeneration, with complete PR loss by 7 months.	(Santos-Ferreira et al., 2016a)
	<i>Rho</i> ^(-/-)	(Humphries et al., 1997)	RP, moderate ONL, with PR loss by ~3 months.	(Barber et al., 2013; Gonzalez-Cordero et al., 2013; MacLaren et al., 2006; Tucker et al., 2011a)
<i>Immune-compromised mouse models</i>	<i>NOD/SCID</i>	(Shultz et al., 1995)	Decreased natural killer cell activity and innate immunity.	(Decembrini et al., 2014)
	<i>IL2γ</i> ^(-/-)	(DiSanto et al., 1995)	Decreased numbers of B and T cells, lack of natural killer cells.	(Zhu et al., 2017a)
	<i>Crx</i> ^{ivrm65} / <i>IL2γ</i> ^(-/-)	(Zhu et al., 2017a)	PR degeneration as in <i>Crx</i> ^{ivrm65} on <i>IL2γ</i> ^(-/-) background.	(Zhu et al., 2017a)
	<i>NOG-PDE6β</i> ^(rd1/rd1)	(Iraha et al., 2018)	NOG background results in lack of T,B and natural killer cells, reduced innate immunity. PR degeneration as in rd1 mice.	(Iraha et al., 2018)

Table 2 Mouse models of inherited retinal diseases used in principal transplantation studies. LCA, Leber Congenital Amaurosis; ONL, outer nuclear layer; PR, photoreceptor; RP, retinitis pigmentosa. Adapted from Nickerson et al., 2018.

	Mutant animal	Reference	Phenotype	Transplantation studies
<i>Naturally occurring rat model</i>	RCS (Mertk)	(Bourne et al., 1938; D'Cruz et al., 2000)	RP and AMD-like, moderate ONL degeneration with almost complete PR loss at 6 weeks.	(Tsai et al., 2015)
<i>Transgenic rat models</i>	P23H (Rhodopsin) (SD-Tg(P23H)Lav1)	(LaVail et al., 2018)	RP, moderate ONL degeneration with severe PR loss by 3 months.	(Yang et al., 2010)
	S334ter-3 (Rhodopsin)	(LaVail et al., 2018)	RP, fast ONL degeneration, with complete PR loss by P60.	(Seiler et al., 2010)
<i>Immune-compromised rat models</i>	NUDE (SD Foxn 1)	(Segre et al., 1995)	Athymic, lack of T cells.	(Shirai et al., 2016)
	SD-Foxn1 Tg(S334ter)3LavRrrc	(Seiler et al., 2014)	PR degeneration as in S334ter-3 on NUDE background.	(Lin et al., 2018; Mclelland et al., 2018; Seiler et al., 2014, 2017; Shirai et al., 2016)

Table 3 Rat models of inherited retinal diseases most used in principal transplantation studies. AMD, age-related macular degeneration; ONL, outer nuclear layer; PR, photoreceptor; RP, retinitis pigmentosa. Adapted from Nickerson et al., 2018.

Knockout of genes regulating the immune-competence have also been generated, with the aim of obtaining immune-privileged models to use in xeno-transplantation studies or to evaluate tumorigenic risk. Examples are the rat and mouse NUDE strains (*Foxn1*^{-/-}) that have a deteriorated or removed thymus resulting in a great reduction of functional T cell and lack of hair. NOD-scid *IL2Rg*^{-/-} mice, or NOG mice, obtained by deletion of multiple genes, are characterized by lack of B and T cells, as well as natural killer cells (Ito et al., 2002). Introduction of photoreceptor degenerative causing mutations onto these backgrounds has allowed generating immunodeficient retinal degeneration models (Iraha et al., 2018; Seiler et al., 2014; Zhu et al., 2017a). These models allow avoiding the side effects associated with the use of immunosuppressant drugs, especially with long-term use, while recapitulating the photoreceptor degeneration occurring in dystrophic models, even if some differences may arise in the immunodeficient and retinal-degenerated strain compared to the immunocompetent retinal-degenerated strain. For example, in the mouse strain obtained by crossing of NOG mice with *rd10* mice, carrying a missense point mutation in the Pde6 β leading to a slower photoreceptor degeneration than in *rd1* mouse, thinning of ONL was accelerated compared to *rd10* mice (Iraha et al., 2018). Since NOG strain is albino, the faster rate of degeneration of NOG-*rd10* mice could be due to an increased susceptibility to light damage compared to dark-reared *rd10* mice.

The P23H rat, a transgenic model of RP

Mutations in the Rhodopsin gene have been used to generate a large proportion of transgenic rodent models. Rhodopsin was the first gene identified to cause RP when mutated (Dryja et al., 1990a). Since that moment, more than 100 different *RHO* mutations have been reported, accounting for 30–40% of autosomal dominant RP cases in United States (Hartong et al., 2006) and 16% in France (Audo et al., 2010).

One of the best studied *RHO* mutations, as well as the most common mutation affecting those with autosomal dominant RP in the USA, is a substitution of proline for histidine in codon 23 near the N-terminus of Rhodopsin, within the intradiscal space (Dryja et al., 1990b). Accordingly to the classification proposed to distinguish Rhodopsin mutants (Mendes et al., 2005), the Pro23His mutation belongs to the class II with toxic gain-of-function and dominant negative effect, as it results in protein misfolding, impaired ER trafficking and inability to bind 11-*cis*-retinal. Indeed, the misfolded mutant Rhodopsin can aggregate into cytosolic ubiquitinated protein inclusions that disrupt the processing of wild-type Rhodopsin; consequently wild-type Rhodopsin is also aggregated in the cytosolic inclusions and targeted for proteasome mediated degradation (Illing et al., 2002; Saliba et al., 2002).

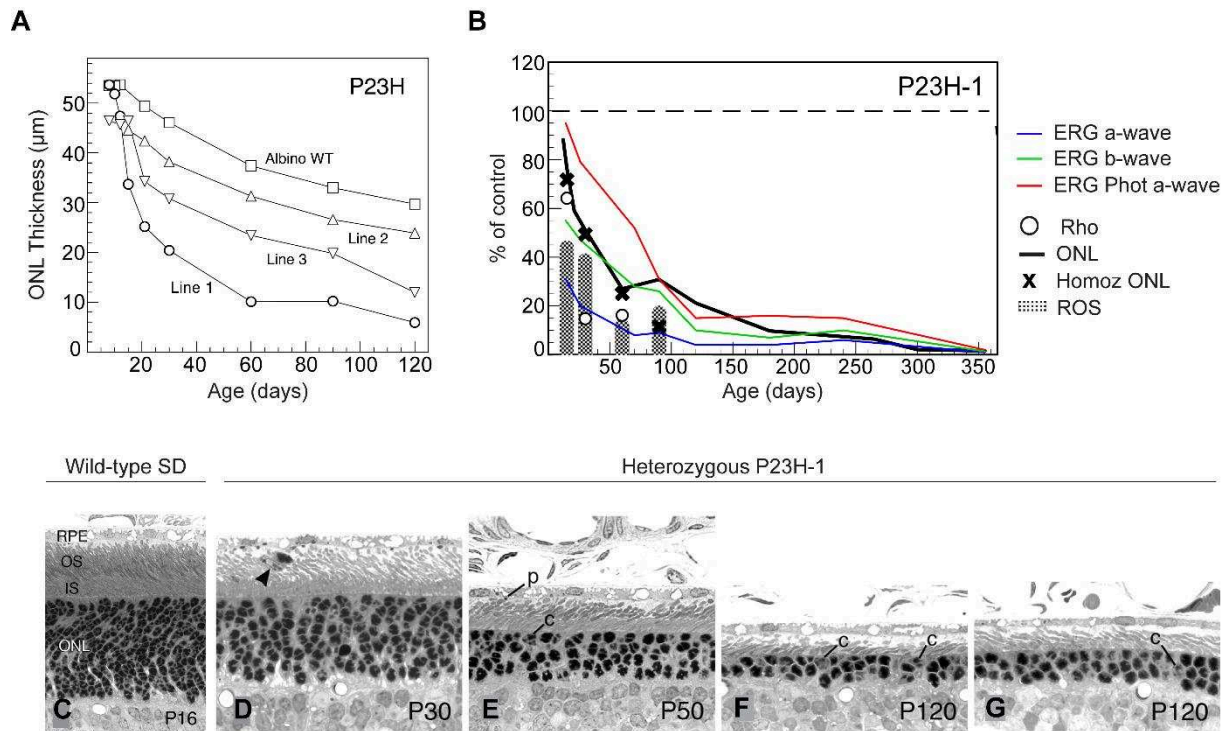


Figure 13 Phenotypic characterization of heterozygous P23H line 1 (P23H-1) rats.

A) Outer nuclear layer thickness in albino controls and different P23H lines. **B)** Different phenotypic characteristics of P23H-1 rats, including scotopic (blue line and green line) and photopic (red line) ERG responses, ONL thickness in heterozygous (black line) and homozygous animals (black cross), whole-eye rhodopsin (circle) and length of rod outer segments (bars). **C-G)** Light micrographs of the outer retina at different ages in control (wild type Sprague Dawley rat) and heterozygous P23H line 1 rat. Residual cones (c) are detectable in degenerated retinas (E-G). Phagosomes (p) in the RPE and the RPE processes are indicative of OS disc shedding (E) Arrowhead indicates invading presumptive microglia (D). Adapted from (LaVail et al., 2018).

WT, Wild-type; ONL, Outer Nuclear Layer, ERG, electroretinogram; Phot, photopic; Rho, Rhodopsin; Homoz, Homozygous; ROS, Rod Outer Segment; SD, Sprague Dawley rat; RPE, Retinal Pigment Epithelium, OS, Outer Segment, IS, Inner Segment; P, postnatal day.

Several transgenic mice have been established that express mutant human Pro23His or mouse Pro23His rhodopsin, developing progressive retinal degeneration similarly to human RP patients (Naash et al., 1993; Olsson et al., 1992; Sakami et al., 2011). In reason of the bigger size of rat eye, more amenable for surgical practices, three transgenic rat lines have been developed carrying multiple copies of mutated mouse Rhodopsin transgene. The transgenic lines differ in the levels of transgene expression and the in rate of photoreceptor degeneration (LaVail et al., 2018; Steinberg et al., 1996). Line 1, or P23H-1, is characterized by fast degeneration (the most used for therapeutic studies with neuroprotective agents), Line 3 by a slower degeneration and Line 2 displays the slowest degeneration (**Figure 13**). Usually, hemizygous are preferred over homozygous animals, as they present a slower degeneration and they better recapitulate the human autosomal dominant genetic condition. In all the three lines, rods degenerate first, followed by cone loss. P23H-1 retina reveals gradual thinning of the ONL thickness, detectable as early as P12 compared to ONL thickness in wild-type retina (LaVail et al., 2018), reaching 86% at 6 months of age (Orhan et al., 2015). The loss of photoreceptors is reflected by a reduction of synaptic contacts in the OPL as well as of numbers of bipolar and horizontal cells (Cuenca et al., 2014), and is consistent with a progressive deterioration of full field electroretinogram (ERG) response in scotopic conditions (Orhan et al., 2015).

The extensive histological and functional characterization of P23H rat make it a good tool for research in retinal degeneration and provide good basis for the development therapeutic interventions.

2.4 Therapeutic approaches for photoreceptor degenerative diseases

Despite different initiating causes, all photoreceptor degenerative diseases result in an irreversible loss of the retinal photosensitive cell population and permanent vision impairment. Nonetheless, the inner neurons of the retina are not severely affected even after significant photoreceptor cell loss. At this stage, a progressive retinal remodeling, consisting of gradual morphological, functional, and molecular reprogramming, do occur in all retinal components, comprising neurons, glial cells and blood vessels (Jones and Marc, 2005). Different therapeutic approaches have been attempted to try to halt photoreceptor degeneration or to replace lost photoreceptors (**Figure 14**).

Notably, the eye represents an ideal target for the development of cutting-edge treatments: it is easily accessible, small and highly compartmentalized (permitting to target different ocular tissues such as vitreous or subretinal space). Its separation from the rest of the body by the blood-retinal barrier ensures ocular immune privilege and minimal systemic dissemination. In addition, the development of non-invasive imaging approaches, such as optical coherence

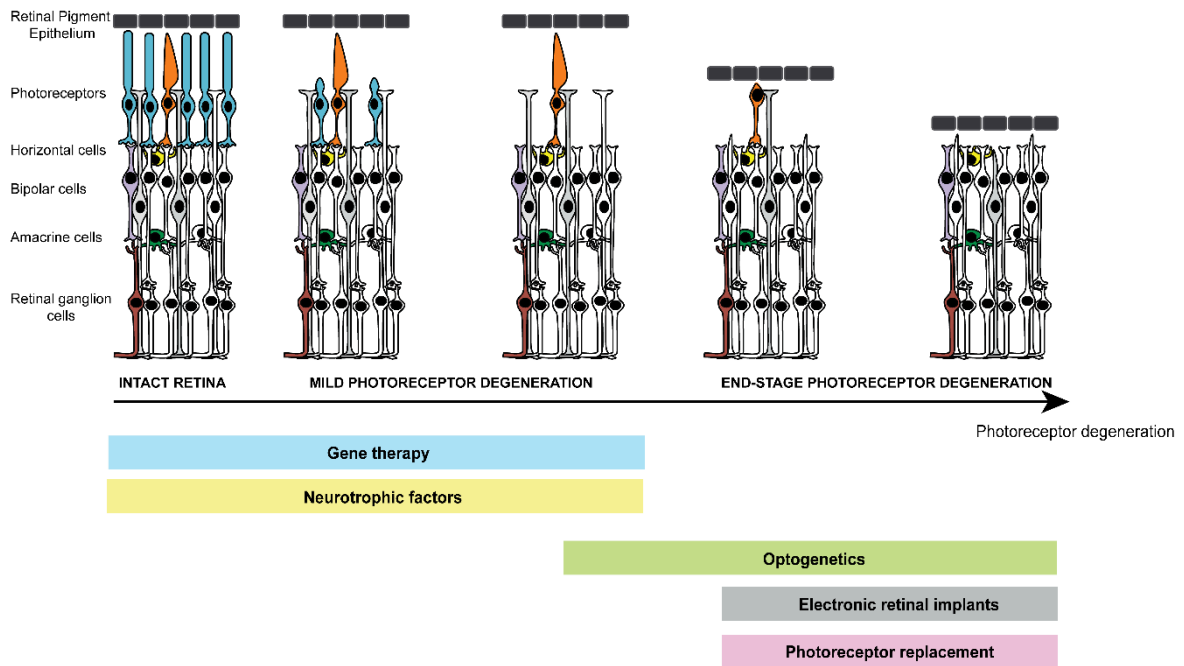


Figure 14 Potential therapeutic strategies to treat photoreceptor degenerative diseases.

The most appropriate therapeutic option depends on the severity of photoreceptor loss. Gene therapy and neuroprotective strategies are suitable when photoreceptors are still at least partially present and can also be used as preventive approaches, before the onset of photoreceptor degeneration. For severe photoreceptor degenerations optogenetics, retinal prostheses and cell therapy should be more appropriate.

tomography and adaptive optics, is of great value in both diagnostics and follow-up after treatment. Lastly, being a paired organ, one eye can be treated individually and the contralateral eye can be used as a control. In this way, any adverse effects potentially caused by treatment can be readily detected, treated locally and the trial can be immediately halted, preventing further harm. For all of these reasons, the eye has been at the forefront in the development of new therapeutic approaches.

In the treatment of wet AMD, antiangiogenic agents, such as VEGF inhibitors, are now currently use to slow disease progression. Neurotrophic factors, such as ciliary neurotrophic factor (CNTF) or rod-derived cone viability factor (RdCVF), could provide solutions to prevent photoreceptor death, independently from the cause driving degeneration.

Their major drawback is that, to be effective, they require a sustained and continuous secretion, so that their delivery must be mediated either by implanted devices or by viral vectors (Byrne et al., 2015; Sieving et al., 2006).

Gene therapy has been extensively developed, especially gene augmentation, in which a corrected copy of a mutated gene is introduced in the cells using viral vectors. Several clinical trials have been completed or are ongoing for different inherited diseases using mostly adeno-associated viral vectors (AAVs) (Dalkara et al., 2016). While ensuring high safety and long-lasting gene expression, AAVs present limitation concerning the size of genetic material they can contain. As a consequence, a large fraction of inherited retinal diseases, including dominant monogenic disease, cannot be treated with vectors currently available. An alternative strategy is to directly correct the gene mutation, particularly since CRISPR system is proving to be a more and more precise, easy and effective way to obtain gene editing in mammalian cells. Clustered Regularly Interspaced Short Palindromic Repeats (CRISPR) and CRISPR-associated nucleases such as Cas9 have been shown that they can mediate *in vivo* phenotype rescue, by ablating the allele disease specifically in two models of RP dominant forms (Bakondi et al., 2016; Burnight et al., 2017). Despite these encouraging but preliminary results, many obstacles need to be overcome before considering any clinical application. First, editing efficiency is far below any therapeutic threshold. Both delivery method and CRISPR activity *in situ* will have to be improved, avoiding at the same time off-targets events, which constitute a major concern. Although AAVs would represent an ideal delivery system, as CRISPR-Cas9 constructions can fit into an AAV vector, the persistence of AAVs in post-mitotic cell after delivery could increase exponentially the potential for off-target cleavage events (Burnight et al., 2018).

No matter the technology used, gene therapy implies the knowledge of the pathogenic gene mutation. In 2013, Daiger et al. reported that for RP the underlying mutation were known in 20–30% of autosomal recessive RP cases, 60–70% of autosomal-dominant cases and 80–

85% of X-linked cases (Daiger et al., 2013). The complexity in RP genetics and its pathological phenotypes represent a challenging point. In addition, gene therapy is suitable as a treatment only in early stages of photoreceptor degeneration, since cells need to be still alive at the moment of gene correction.

To restore visual function in late-stages of photoreceptor degenerative diseases, when most of photoreceptors have already been lost and only some quiescent cones are left, alternative strategies have been developed: optogenetics, electronic retinal implants and cell transplantation. Both optogenetics and retinal prostheses attempt at bypassing photoreceptor activity by inserting artificial photosensors and coupling them to the remaining neurons of the retina. Optogenetic approaches consist in inserting into light-insensitive cells of the retina genes encoding a light-sensitive protein, such as channelrhodopsin and halorhodopsin, so that they can induce a light-response activity. This strategy has already proved to be successful in preclinical studies and its translation to the clinic is currently developed by several companies (Dalkara et al., 2016). Electronic retinal prostheses comprehend different types of light detecting devices designed to generate and transmit electrical responses to the surviving inner retinal neurons. Retinal prostheses have already entered the clinic with promising results (Ho et al., 2015; Stingl et al., 2013); they are limited by the technology in use (e.g. limit in spatial resolution of the devices).

Cell therapy consists in replacing the degenerated cells with new healthy cells, in the attempt of recreating the preexisting functional retinal system. As nicely summarized by Seiler and Amarant, to be successful, transplants should (1) replace lost photoreceptors with new, functional and morphologically differentiated cells, (2) make appropriate synaptic connections with the host retina, and (3) restore visual function to an objectively degree, measurable by different functional tests (electrophysiology, behavior, etc.). In addition, transplants should not form tumors or in any other way be harmful to recipients (Seiler and Aramant, 2012).

One of the main advantages of cell therapies is that they are mutation-independent and can be used in a wide range of retinal degenerative conditions. Due to the limited capacity of endogenous repair in mammalian retina, cell therapy requires the transplantation of donor cells.

2.5 Photoreceptor replacement by cell therapy

A wide range of cell type has been evaluated for its ability to restore vision after transplantation: neural stem cells (NSCs), mesenchymal stem cells derived from bone marrow (BMSC), adipose tissues stem cells (ADSC) and dental pulp stem cells (DPSC), retinal stem cells, retinal progenitors and pluripotent stem cells. Improvement of visual function obtained by transplantation of derivatives from BMSC, ADSC and DPSC seems to be mediated more by the release of neurotrophic and anti-inflammatory factors, than by the capacity of these stem

cells to actually replace photoreceptors. Different cell therapy products are currently tested in different clinical trials, mostly for AMD treatment (reviewed in Mead et al., 2015).

NSCs and neural precursors have also been investigated as a potential source of photoreceptors following transplantation. However, these cells fail to differentiate in mature retinal cells, even in the rare case of integration into the recipient retina (Klassen et al., 2007; Sakaguchi et al., 2004; Takahashi et al., 1998; Young et al., 2000).

Two independent groups reported the isolation and the expansion *in vitro* of retinal stem cells from rodent ciliary epithelium (Ahmad et al., 2000; Tropepe et al., 2000), but their ability to generate new retinal neurons appear limited both *in vitro* and *in vivo* (reviewed in Jayakody et al., 2015).

Donor retinal cells have the advantage of being already committed to a retinal fate. Identifying an integration-competent cell source and developing an efficient delivery strategy preserving both donor and host cells have been two major challenges. Many retinal transplantation studies from 1980s to 1990s, comparing different rat or human donor ages, indicated that fetal cells, in a progressive scale from dissociated cells to intact sheets, were more suitable for photoreceptor replacement than adult or early embryonic retinal cells (reviewed in Seiler and Aramant, 2012). The work of Aramant and others has focused on the transplantation of full-thickness fetal retinal sheets (with or without RPE), showing that a large continuous layer of transplant photoreceptors with outer segments can be achieved with this approach (Aramant and Seiler, 2002; Aramant et al., 1999; Seiler and Aramant, 1998). In their opinion, transplantation of intact fetal retinal sheets would preserve the environment of the developing donor retina, including the Müller cells that are responsible for the organization and nourishment of the retinal neurons. These results led to clinical trials of transplantation of fetal human retinal sheets together with its RPE, in five RP and AMD patients. No adverse effects were reported; seven out of ten patients showed visual improvement, with one patient showing long-term improvements (6 years) (Radtke et al., 2008). However, as intraocular lenses were implanted before transplantation, it is difficult to evaluate the benefits deriving actually from donor cell transplantation and those deriving from cataract treatment. Even if some connectivity with the recipient retina has been demonstrated (Lin et al., 2018; Seiler et al., 2010), the presence of donor inner retinal neurons within the transplants represent a major obstacle to the establishment of synaptic connections between new photoreceptors and the endogenous retinal circuitry. In addition, delivery of the donor retinal sheet into the host subretinal space, while maintaining the appropriate polarity, required the development of an adequate sample preparation (slicing, matrix embedding), as well as delicate surgical practice (specific injector and retinal detachment prior to injection).

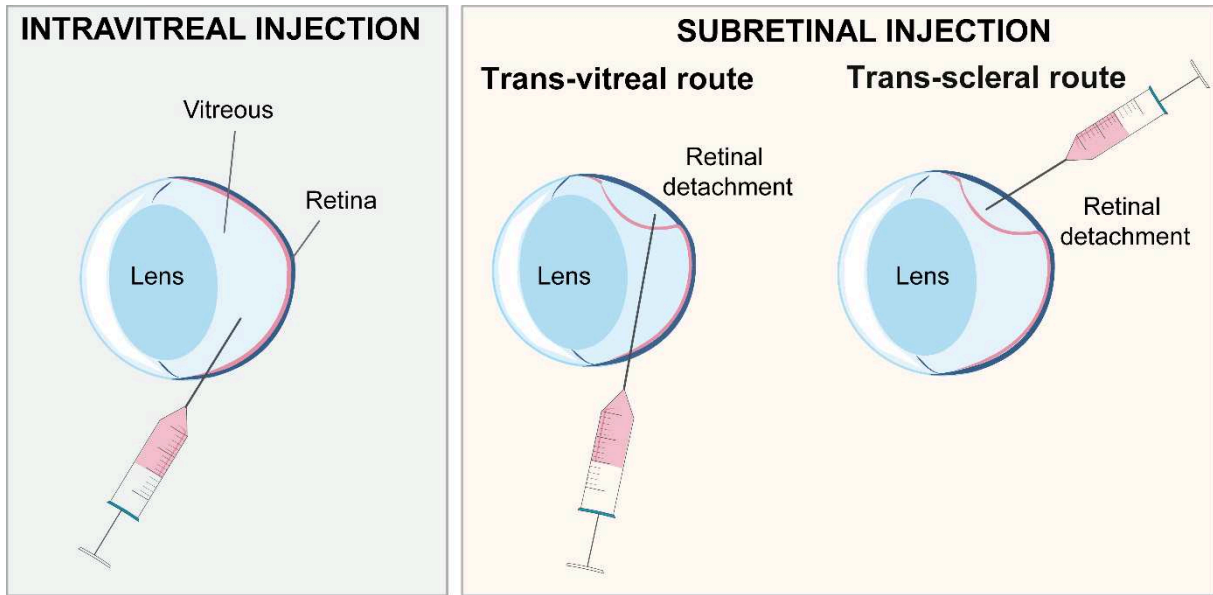


Figure 15 Alternative strategies for the delivery of cells to the retina.

Transplantation of dissociated cells has the advantage that only a small, self-sealing incision is necessary to deliver the cells. Historically two routes have been attempted: injection into the vitreous cavity and injection into the subretinal space (**Figure 15**). The vitreous cavity has the advantage of being more easily accessible than subretinal space, whereas the latter has the advantage of being immediately adjacent to the host ONL.

Several studies have aimed at replacing photoreceptors by using *in vitro* expansion of embryonic RPCs followed by differentiation accordingly to different protocols. Subretinal transplantation of mouse or human RPCs generally resulted in limited photoreceptor differentiation and poor integration (Aftab et al., 2009; Klassen et al., 2004; Luo et al., 2014). Nevertheless, a clinical trial using human RPCs has started in June 2015, in which fetal-tissue derived cells are injected in the vitreous cavity of RP patients (ClinicaTrials.gov identifier NCT02464436)

Major efforts have been dedicated to determine the optimal photoreceptor cell population for transplantation, focusing specifically on photoreceptor development. By using a mouse reporter line, with ubiquitous green fluorescent protein (GFP) expression, and collecting GFP-positive (+) retinal cells at different stage of development, MacLaren et al. first showed that transplantation of cells from retina at postnatal days (P) 3 to 5 led to the highest number of GFP+ cells within the host ONL (MacLaren et al., 2006) (**Figure 16A**). Importantly, they and others (Bartsch et al., 2008) could demonstrate that transplantation success is dependent upon the ontogenetic stage of the donor cells, and not of the host, as transplantation in both adult and P1 wild-type mouse retina led to equivalent results. In mouse retinal development, P1-P7 correspond to the peak of rod generation. To confirm whether the integrated GFP+ cells were actually constituted by immature post-mitotic rod precursors, similar transplantation experiments were performed by using the *Nrl*.GFP transgenic mouse line, in which GFP expression is restricted to photoreceptor precursors committed to the rod fate (as well as mature adult rods, see paragraph 1.4). Results from the transplantation of *Nrl*-GFP+ cells, isolated by fluorescence-activated cell sorting (FACS), provided the final confirmation that only cells at a specific ontogenetic stage, defined by activation of the transcription factor *Nrl*, and corresponding to photoreceptor precursors, have the ability to integrate into a host retina. In addition, integrated donor cells had morphological features of mature rods, such as outer segments and synaptic terminals (Bartsch et al., 2008; Eberle et al., 2012; MacLaren et al., 2006). Despite this major breakthrough, the number of integrated cells with the host ONL was still extremely low, around 1000 cells out of 200 000 transplanted cells. Injection into the vitreous cavity led to no detectable donor cells in the ONL (MacLaren et al., 2006). In rodents, delivery of donor cells into the subretinal space is currently performed either via trans-vitreous or via trans-scleral injection. In the trans-vitreous approach, the needle pierces twice through the

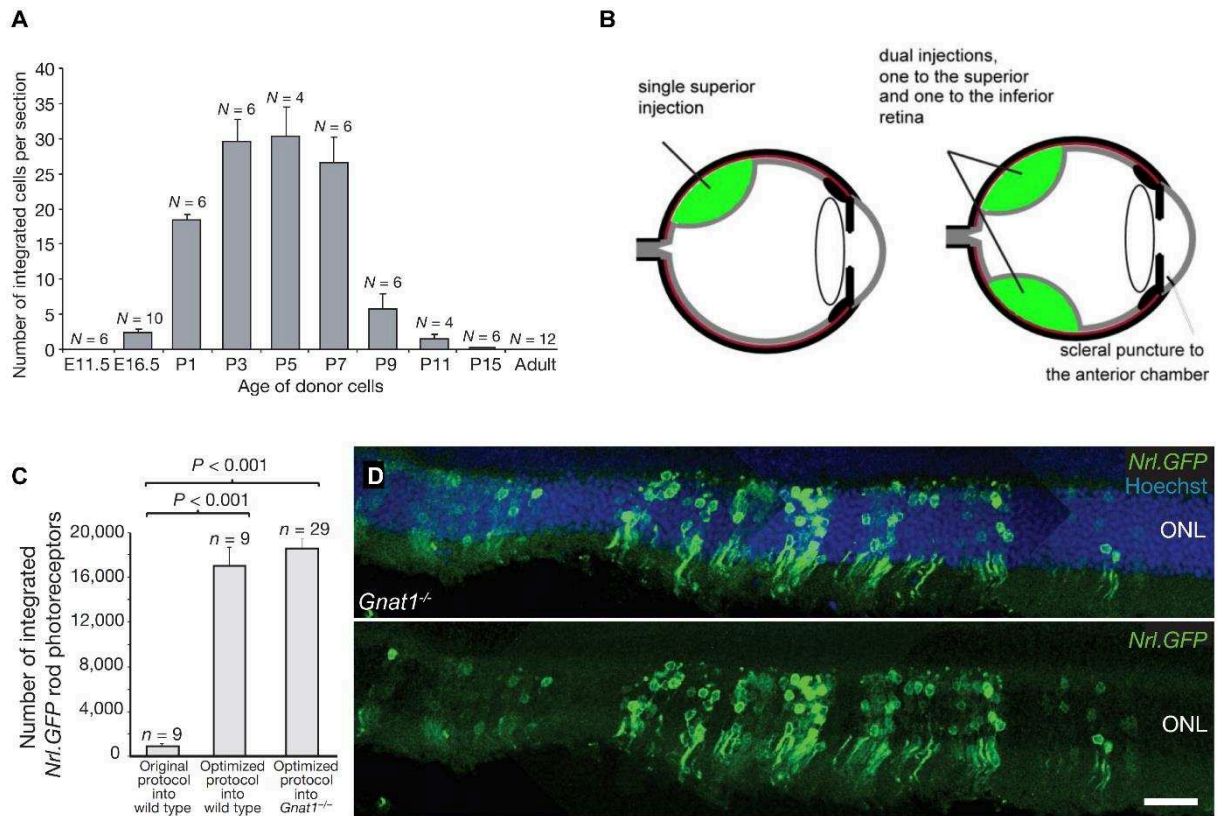


Figure 16 Increased integration of mouse donor photoreceptor precursors.

A) Comparison of the number of integrated cells as a function of donor age (mean \pm s.e.m.) after subretinal injection into adult wild-type recipients, indicating post-mitotic photoreceptor precursor as optimal ontogenetic stage of donor cells. **B-C)** Optimized injection strategy led to increased delivery and integration donor cells into recipient retinas. **D)** Integrated *Nrl*-GFP⁺ rods in *Gnat1*^{-/-} recipient retinas. Extracted from MacLaren et al., 2006 (A) and Pearson et al., 2012 (B-D).

Scale bar 50 μ m (D). E, embryonic day; P, postnatal day; ONL, Outer Nuclear Layer.

retina, once at the entrance into the eye and again at the injection site, after having passed through the vitreous cavity. In the trans-scleral injection, the needle passes through the sclera and the choroid before arriving directly into the subretinal space. These two methods will be further discussed later in this manuscript, as both can affect the transplantation outcome, even if in different ways.

Pearson et al. implemented the trans-scleral approach and, by performing a double injection, they could considerably increase the number of integrated cells (**Figure 16B-D**). For the first time they demonstrated a rescue of the visual function after transplantation of donor Nrl.GFP+ cells into a model of congenital stationary blindness, *Gnat1*^{-/-} mice. They showed a correlation between the number of integrated GFP+ cells and the visual restoration; the number of integrated cells were insufficient to drive a detectable ERG response, but they could register specific activity in the visual cortex, as well as visual-guided response in behavioral tests (Pearson et al., 2012).

Gust and Reh reported that adult photoreceptors were still able to integrate into a recipient retina, even if in reduced number (Gust and Reh, 2011). Therefore, integration competence of donor post-mitotic photoreceptors declines with maturation, without being completely lost.

Extensive studies in different models of retinal degeneration highlighted how the different pathological context can affect transplantation outcomes. Namely, transplantation in mouse models recapitulating late stages of photoreceptor degeneration, lacking a structured ONL, resulted in donor cells rarely developing mature outer segments or synaptic processes, even if it was still possible to achieve some restoration of the visual function (Barber et al., 2013; Singh et al., 2013).

All the findings described so far have been accomplished using post-natal rod precursors from mouse retina, also due to the abundance of rods in the murine retina. A relative small bulk of work has focused on transplantation of cones (Santos-Ferreira et al., 2015; Smiley et al., 2016), with the purpose of proving that cone replacement is also feasible, in a therapeutic perspective more pertinent with human daylight vision. Santos-Ferreira and colleagues used the mouse *Nrl*^{-/-} retina as a source of cone-like cells. Nrl mutant mice were crossed with actin-GFP transgenic mice in order to trace postnatally derived cone-like cells after transplantation in the CPFL1 mouse, a model of cone degeneration (see 2.3) (Chang et al., 2009). GFP+ cells in the host ONL showed morphological resemblance to rod and cone cells, even if only a subset of GFP+ cells stained for the cone marker cone arrestin. Importantly, transplanted cells could specifically mediate RGC responses under daylight conditions recorded by micro-electrode arrays (MEA) (Santos-Ferreira et al., 2015). In order to investigate the integration competence of true cones, the group led by Valerie Wallace generated a new mouse reporter line, where GFP is trapped in the coiled-coil domain containing 136 (*Ccdc136*) locus (Smiley

et al., 2016). The expression of *Ccdc136* gene marks S cones in ONL and rod bipolar cells in the INL. The expression of the GFP reporter from the trapped allele faithfully recapitulated the endogenous *Ccdc136* gene expression. Transplanted GFP+ cells in adult wild type recipients lacked cone-specific markers. As only 10 000 GFP+ cells could be obtained for injection from *Ccdc136*^{GFP} reporter line they also performed transplantation of GFP+ cods, obtained by crossing *Ccdc136*^{GFP} mice with *Nrl*^{-/-} mice. Again, GFP+ cods integrated in wild-type host retina did not expressed mature cone markers and displayed rod-like nuclear morphology (Smiley et al., 2016).

At the same time, strategies aiming at the separation and the enrichment of the photoreceptor precursors before transplantation without the use of fluorescent reporter lines have started to be developed, with the identification of surface antigens specifically expressed in the mouse photoreceptors (Eberle et al., 2011; Koso et al., 2009; Lakowski et al., 2011).

The ontogenetic equivalent of mouse photoreceptor precursors are found in human fetuses in the second trimester of development. In addition to ethic concerns, human material from fetal origin cannot satisfies the supply needed for a generalized treatment of photoreceptor degenerative disease. The recent advancements in pluripotent stem cell technologies represent a promising solution to obtain a potential unlimited source of cells for regenerative medicine, not only in the retinal field. The challenge is to obtain *in vitro* a cell population recapitulating the same properties of human photoreceptor precursors *in vivo*. In the following chapters, we discuss pluripotent stem cell properties and the protocols allowing retinal differentiation.

3. Human-induced pluripotent stem cells

3.1 Stem cells and differentiation potentials

A stem cell possesses two fundamental properties: 1) self-renewal, or the ability to divide while retaining an undifferentiated character; and 2) differentiation, defined as a process of acquisition of specialized molecular and functional phenotype. Stem cells are able to renew themselves at each division while also producing a daughter cell that can undergo one or more paths of differentiation. Stem cells can be classified accordingly to their potential of generate numerous different cell types, or potency, and their origin (**Figure 17**).

Totipotent stem cells have the highest potency, as they are able to form every cell type in the embryo as well as the trophoblast cells of the chorion, the embryonic portion of the placenta. Totipotent cells are found exclusively in developmental stages immediately following fertilization, from the zygote until the 4-8 blastomere before compaction. Pluripotent stem cells (PSCs) can give rise to any cell type, including germ line cells, with the only exception of trophoblast cells. Embryonic stem cells are pluripotent stem cells that can be isolated from the inner cell mass of the mammalian blastocyst. Multipotent stem cells can generate a restricted subset of cell types of the body (e.g. retinal progenitor cells, hematopoietic stem cells, etc.) and they are present in both developing and differentiated tissues. Finally, unipotent stem cells can produce only a specific type of cell. Multipotent and unipotent stem cells residing in specialized tissue after completion of maturation are also known as adult stem cells. They are usually located in specialized compartments, called stem cell niches, and they ensure tissue homeostasis and repair.

Given the clinical success, for example, with bone marrow transplantation, allowing for reconstitution of blood tissue from donor hematopoietic stem cells contained in the bone marrow, much effort have been devoted to the isolation and expansion of adult stem cells for therapeutic applications. However, adult stem cells are not very easy to isolate and manipulate, as they are rare and naturally divide at very low rate. On the contrary, pluripotent stem cells proliferate very rapidly, they are relatively easy to maintain in culture (nowadays more easily than in the past), and they can be used as source to obtain any cell type, if correctly instructed. For these reasons, since the first isolation of human embryonic stem cells (ESCs) in 1998, PSCs have elicit great expectations about the development of innovative treatments. Now, twenty years later, several type of cells derived from PSCs are under clinical trials; PSCs can be obtained not only from embryonic blastocysts, but also from somatic cells by different methods, namely reprogramming and nuclear transfer – or, more commonly, cloning. Considered as two major breakthroughs in stem cell research and regenerative medicine, both

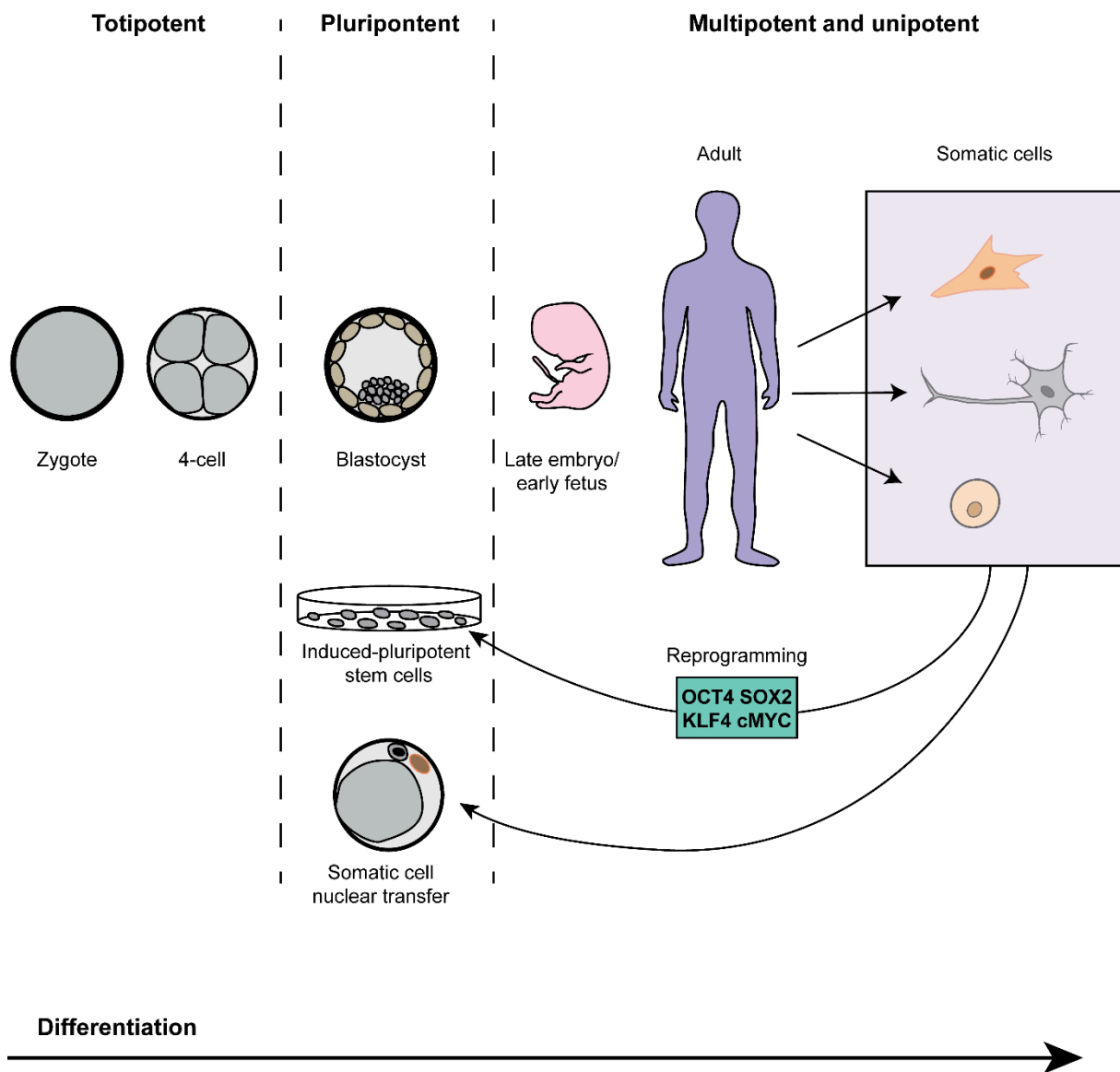


Figure 17 Stem cells and differentiation potentials in organism development.

Zygote up to 4-cell blastomere are totipotent, with the differentiation potential of creating a whole new organism. With the progression of differentiation during embryonic development, differentiation potential is reduced to pluripotency, multipotency and unipotency. Terminally differentiated cells, or somatic cells, can be reprogrammed to pluripotent stem cells by expression of specific transcription factors or nuclear transfer.

these techniques are based on the principle of genome equivalence. In 1975, Gurdon et al. demonstrated that the nucleus in all cells within an organism, from the zygote to each somatic cell, contain the same genome, whereas specialization of different cell types relies on differential gene expression. Thus, each cell nucleus should be able to direct the development of an entire new organism, if correctly manipulated. Three groups have independently reported the derivation of human PSC lines by transferring somatic cell nucleus into a human oocytes (Noggle et al., 2011; Tachibana et al., 2013; Yamada et al., 2014). The necessity for human oocytes, the technical complexity as well as ethical constraints, are among the factors that have strongly limited the diffusion of somatic cell nuclear transfer, also because in the meantime another method was experiencing an escalating success: the induction of pluripotency in differentiated cells by manipulating expression of transcription factors involved in the pluripotency of ESCs (Takahashi and Yamanaka, 2006). Such cells are called induced pluripotent stem cells (iPSCs).

Below we will focus on the description and comparison of the two most diffused types of PSCs, ESCs and iPSCs.

3.2 Embryonic stem cells

As we have seen, each cell within the inner cell mass of the mammalian blastocyst is pluripotent, as they are able to generate the entire embryo. *In vivo*, pluripotency is not a permanent state; pluripotent stem cells are rapidly lost with the progression of development. However, when inner cell mass blastomeres are isolated and cultured *in vitro* under defined conditions, they can be artificially maintained in a pluripotent state, where they are capable of unlimited, undifferentiated proliferation. The identification of the extrinsic factors required for the maintenance of pluripotency, either added to the growth medium or provided by growth on a feeder layer of differentiated cells, led to the isolation of the first ESC line from mouse blastocyst in 1981 (Evans and Kaufman, 1981). The requisite factor for self-renewal of mouse ESCs was subsequently determined to be leukemia inhibitory factor (LIF) (Williams et al., 1988). Serum is also important for mouse ESC cell maintenance, although bone morphogenic protein 4 (BMP4) is able to replace this requirement (Qi et al., 2004; Ying et al., 2003). These extrinsic factors are responsible for the maintenance of a network of key transcription factors within the cell that controls pluripotency. This network includes the octamer-binding transcription factor 4 (Oct4) (Nichols et al., 1998; Niwa et al., 2000), the variant homeodomain transcription factor Nanog (Chambers et al., 2003; Mitsui et al., 2003) and the sex-determining region Y –box 2 (Sox2) (Avilion et al., 2003).

The expression of this core of transcription factors characterizes also human ESCs. However, the extrinsic factors required for maintenance and self-renewal are different between mouse

and human ESCs. Determining cell culture conditions allowing the isolation of human ESCs has required almost 20 years, with the establishment of the first human ESC lines in 1998 by Thomson and collaborators (Thomson, 1998). Unlike from mouse ESCs, BMP4 has been shown to negatively regulate pluripotency and induce trophoblast-like cell formation (Xu et al., 2002) in human ESCs. The growth factors capable of promoting pluripotency are FGF2 together with IGF, secreted by human ESCs, which setup interdependent paracrine loops (Bendall et al., 2007).

In addition to specific genetic and epigenetic profile, human ESCs are characterized by the expression of specific surface markers, such as the stage-specific embryonic antigen-4 (SSEA-4) and the keratan sulfate-related antigens TRA-1-60 and TRA-1-81 (Thomson, 1998). Human ESCs show both high telomerase and alkaline phosphatase activity. From a functional perspective, by definition human ESCs are characterized by their ability to differentiate in any cell type belonging to any of the three germ layer, namely ectoderm, mesoderm and endoderm. Spontaneous differentiation potential can be assessed both *in vitro* and *in vivo*. In the first case, ESCs are cultured as cell aggregates in suspension in the absence of FGF2, denoted as embryoid bodies (EB). In the second case, human ESCs are injected into an immunodeficient mouse or rat model where they form a teratoma containing cell types of all three germ layers (Thomson, 1998).

Human ESCs are considered as the “golden standard” to refer to when studying PSCs features and they have provided researchers with a fundamental tool to investigate human embryonic developments. Additionally, many protocols allowing for the differentiation of human ESCs have been reported, with important implications for both cell therapies and new drug development. Of notice, human ESC-derived RPE cells have been among the first PSC-derived cell types to be tested in a clinical trial, started in 2011 (ClinicaTrials.gov identifiers NCT01345006 and NCT01344993).

Nevertheless, their use is still object of ethical, religious and political controversies about the exploitation and the destruction of human embryos. Generation of new ESC lines and, more in general, research with human ESCs is strictly regulated in most countries. To overcome to ethical and administrative obstacles limiting the research with human ESCs, researchers have looked for alternative sources of PSCs.

3.3 Human-induced pluripotent stem cells

The newfound knowledge of the transcription factors needed to maintain pluripotency in ESCs has open the way to the development of a new possibility to obtain PSCs, bypassing the ethical issues concerning the use of human ESCs.

In 2006, Kazutoshi Takahashi and Shinya Yamanaka reported the discovery that the over-expression of four transcription factors is necessary and sufficient to reprogram almost any somatic cell to a state highly similar to that of a pluripotent ESC (Takahashi and Yamanaka, 2006). A pool of 24 candidate genes was tested for their ability to activate the *Fbx15* locus, specifically expressed in mouse ESCs and early embryos, together with the knocked-in β geo cassette, a fusion of the β -galactosidase and neomycin resistance genes, resulting in the selection of ESC-like colonies. Thanks to this assay system, they identified *Oct4*, *Sox2*, *Klf4*, and *c-Myc* as the core set of transcription factors necessary to generate iPSCs in mouse. Like ESCs, iPSCs are able to self-renew and to differentiate into the three embryonic germ layer derivatives, including germ line (Okita et al., 2007). Upon injection into a host blastocyst, mouse iPSCs contribute to the fetus development and entirely iPSC-derived viable mice were generated by tetraploid complementation (Boland et al., 2009; Zhao et al., 2009), which is considered as the most stringent pluripotency assay. In 2007, the technology was successfully transposed to human cells (Takahashi et al., 2007). The group of James Thomson reported the reprogramming of human fibroblasts by using LIN28 instead of the oncogene c-MYC (Yu et al., 2007). Human iPSCs can be maintained in culture under the same conditions of human ESCs; also in terms of cell morphology, surface antigens and pluripotency gene expression, iPSCs closely resemble ESCs. At the same time, many comparative studies have debated over their transcriptional and epigenetic differences (reviewed in Puri and Nagy, 2012). Epigenetic memory, resulting from the incomplete removal of somatic cell-specific DNA methylation during reprogramming, has been shown persist in some iPSC lines, conferring to iPSCs an increased facility to differentiate into their cell type of origin (Kim et al., 2010; Polo et al., 2010).

In order to systemically establish the nature and magnitude of epigenetic variation existing among human PSC lines, a study from Bock et al. performed extensive genomic assays, including DNA methylation mapping and gene expression profiling using microarrays, onto 20 established ESC and 12 iPSC lines (Bock et al., 2011). All cell lines were maintained under the same standardized culture conditions. First, the authors used the epigenetic and transcriptional statuses of different ESC lines to calculate an “ESC reference”, a measure of the expected gene expression and DNA methylation level for each gene in a pluripotent cell line, against which each ESC or iPSC line was compared individually. They found that epigenetic and transcriptional variation is common among human PSC lines, and that these differences can have significant impact on a cell line utility, with a considerable variability in the efficiency of generating different cell lineages among independent human ESC and iPSC lines. The gene expression and methylation of many iPSC lines fall within the deviation observed among ESC lines, but overall there were more differences between the two types than among the cell lines in each class. The conclusion is that each cell line, from both ESC

and iPSC lines, needs to be carefully characterized, regardless of how it is derived, in order to exclude those that could be problematic for an intended application.

The deepness of this characterization should depend on the final use of the human iPSC line, especially the characterization of novel mutations and chromosome abnormalities.

During expansion and prolonged passage, human ESC and human iPSC lines can accumulate karyotypic abnormalities and copy number variants and lose heterozygosity (**Figure 18**) (Lund et al., 2012). In addition to that, genomic alterations arising from cellular reprogramming can occur in human iPSCs, leading to somatic mutations, copy number variations and aberrant epigenomic reprogramming (Gore et al., 2011; Hussein et al., 2011; Lister et al., 2011). Interestingly, these anomalies seemed to be “erased” with the increase of cell passaging.

The generation of reliable and qualitatively homogenous human iPSC lines, together with the development of robust and reproducible differentiation protocols are of crucial importance for a successful application of iPSC technology. The major interest of human iPSCs is their potential as unlimited patient-specific source of cells for cell therapy, disease modeling and drug screening. In this regard, iPSC technology is particularly attractive for the study of diseases for which animal models are either not available or do not accurately represent the human disease etiology. Many disease-specific cell types have already been derived, recapitulating the disorder’s pathogenesis (Shi et al., 2017). However, clinical utility of human iPSC derivatives necessitates their expansion and efficient differentiation in large-scale under well-defined conditions, as well as a rigorous assessment of their tumorigenicity risk.

3.4 Progress and challenges in iPSC-based cell therapy

The clinical translation of human iPSCs derivatives has taken less than a decade: in 2017, the Japanese group led by Masayo Takahashi has reported the transplantation of one individual affected by wet AMD with a sheet of iPSC-derived RPE. The patient’s vision is apparently progressing satisfactorily, and her vision has stopped deteriorating (Mandai et al., 2017b).

Trials of therapies for Parkinson disease are under consideration and iPSC-derived platelets should also enter a clinical trial in Japan soon (communication from S.Yamanaka, Keystone Symposia Conference *iPSCs: A Decade of Progress and Beyond*, 2018). However, the large-scale availability of treatments involving PSCs remains some years away, because of the long and demanding regulatory pathway that is needed to ensure their safety. Much progress has been made toward this direction since the first discovery of iPSC technology.

Human fibroblast were first used as source of somatic cells for reprogramming (Takahashi et al., 2007). Today, fibroblasts are still the most common source (80%), followed by peripheral blood cells, thanks to the accessibility for sample collection.

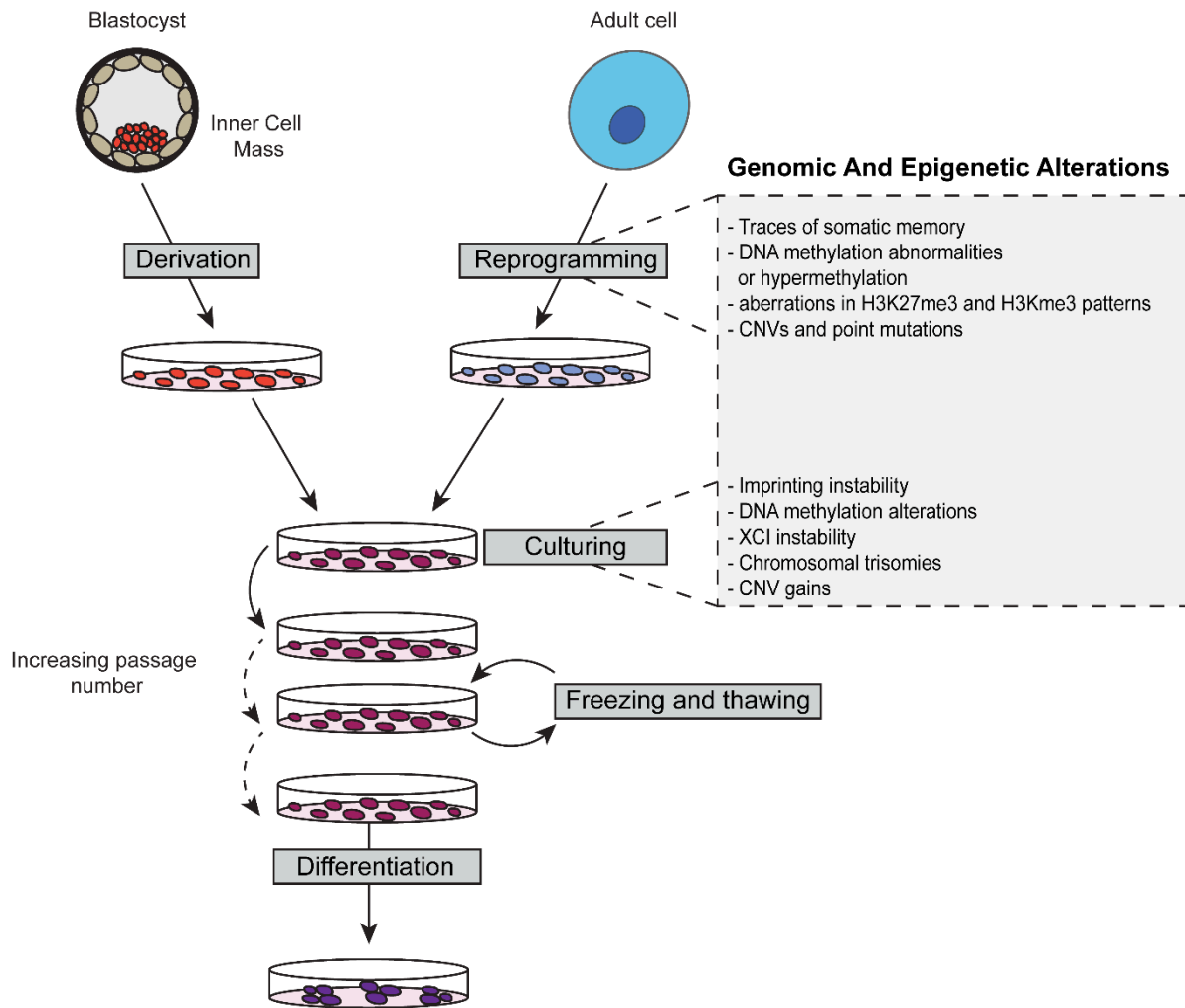


Figure 18 Genomic and epigenetic alterations in PSC lines.

Establishment and culturing of ESCs and iPSC is susceptible to enrichment for genomic and epigenetic changes. Adapted from Lund et al., 2012.

CNV, Copy Number Variants; XCI, X-Chromosome Inactivation.

Historically iPSCs were generated by introducing reprogramming factors via integrating viral vectors, such as retroviral or lentiviral vectors. Potential insertional mutagenesis and genetic alterations caused by integration of transgenes into the genome of host cells represented a concern for iPSC clinical application (Yamanaka, 2012).

To circumvent this risk and make iPSCs more clinically applicable, various non-viral methods or non-integrating viruses have been developed. These non-integrating methods include reprogramming using episomal DNAs (Junying et al., 2009; Okita et al., 2011), Sendai virus (Fusaki et al., 2009), adenovirus (Stadtfield et al., 2008), synthesized RNAs (Warren et al., 2010), proteins (Kim et al., 2009) and small molecules (Hou et al., 2013), although the small-molecule approach is not yet applicable to human iPSC derivation.

Among these approaches, episomal DNAs, synthetic mRNAs and Sendai virus are commonly applied to derive integration-free iPSCs owing to their relative simplicity and high efficiency. The use of nonviral methods or non-integrating viruses could avoid genomic insertions, thus reducing associated risks when human iPSCs are used for clinical applications. At present, there is little agreement on what standards should be used for testing genetic mutations in therapeutic cell lines, since genetic changes, arising during reprogramming or maintenance in cell culture, do not necessarily represent a safety risk for human iPSC-derived cells. Whole-genome sequencing and whole-genome methylation profiling were recently used to characterize human iPSC lines in the first clinical trial with human iPSC-derived RPE. The detection of three aberrations in DNA copy number (deletions) in one iPSC line generated from a second patient halted transplantation of autologous cells (Mandai et al., 2017b).

A second security-check during the development of a cell-therapy product should be performed on the differentiated iPSC derivative, to ensure that the final product does not contain undifferentiated cells that have the potential to generate teratomas. Stem cell-derived clinical products may consist of a heterogeneous population of cells, caused by the product being contaminated with undifferentiated cells. In addition, cell product might dedifferentiate into cells capable of producing neoplasms. Normally, risk of tumorigenicity is tested in animal models during pre-clinical studies. Following cell transplantation, distribution and tumorigenicity of these cells can be monitored by histologic assessment or human Alu quantitative PCR analysis (Neofytou et al., 2015).

A common solution is to sort iPSC-derived cells before transplantation through positive selection for desired cell types and negative selection against human PSC markers using FACS or magnetic-activated cell sorting (MACS). Following a different approach, several small molecules have been identified to eliminate undifferentiated human PSCs and prevent teratoma formation, without affecting their differentiated derivatives (Ben-David et al., 2013; Lee et al., 2013). Treatment of the iPSC-derived cellular product with these inhibitors may

reduce the potential tumorigenicity. Ultimately, only long-term studies of cell products after transplantation will be able to accurately assess the tumorigenesis risk associated with such therapies.

Compliance with good manufacturing practice (GMP) is mandatory before translation of cell therapies to human. This means that cell products must be consistently manufactured and meet all necessary criteria in terms of viability, function, purity, and sterility during the entire iPSC generation and differentiation process. Chemically undefined media or materials of animal origin, such as fetal bovine serum and mouse embryonic fibroblasts, as support systems should be avoided, because they carry a risk of transmitting xenopathogens to the recipient patients. Several chemically defined media are now available for human PSC culture, as well as different substrata, based on human extracellular matrix proteins (such as laminin or vitronectin), bypassing the need for feeder layers. The following step is the development of xeno-free scalable systems for stem cell products, allowing automated large-scale production of human iPSC derivatives. Scalable systems require first to adapt human iPSCs cultures from adherent colonies to floating aggregates in stirring bioreactors. Floating PSCs could be cultured also on microcarriers or following scaffold encapsulation (Fan et al., 2015). Overcoming such technical challenges will be instrumental in the design and development of bioprocesses for the standardized and cost-effective production of stem cell products.

The application of cells derived from individual patients' own iPSCs or iPSCs from matched donors may become a cornerstone of precision medicine and has the important advantage of not requiring long-term immune suppression to preserve the transplanted cells. Indeed, the first iPSC clinical trial used RPEs from autologous iPSCs derived from the patient. However, autologous iPSC therapy involves extremely high costs (approximately \$800,000 to generate an iPSC-derived tissue product suitable for clinical use (Bravery, 2015)) and a period of time for careful validation of each cell line. For these reasons, the second phase of the iPSC RPE trial in Japan makes use of allogeneic products (Eggan et al., 2016). Unlikely autologous cells, allogeneic cells could be banked as a single product to treat multiple patients, bringing down the cost for iPSC-based cell therapy. Also, cell therapy products would be more consistent, as the inter-cell line variability would be reduced. However, the genetic complexity required of a HLA-matched bank in order to be useful across ethnic barriers is an important aspect to understand before undertaking such development. The number of cell lines theoretically required is highly dependent on the demographics and genetic heterogeneity of a region. For a relatively homogenous population such as the Japanese population, it has been shown that 50 homozygous cell lines would provide a haplotype match for 90.7% of the Japanese population (Nakatsuji et al., 2008) and to date 19 iPSC lines from HLA homozygous donors have already been banked (data S. Yamanaka, Keystone Keystone Symposia Conference

iPSCs: A Decade of Progress and Beyond, 2018). The establishment of a similar bank in countries with different and intermixed ethnic groups would require more lines and would be pricier. Incorporating recent advances in genome editing strategies to create universally accepted donor cells could be another alternative approach (Swijnenburg et al., 2008).

Allogeneic approach would also bypass the need to correct the disease causing mutation in iPSCs before the production of the cell therapy product. Actually, combination of human iPSC technology with the recently developed gene editing is already happening and could make human iPSCs an even more powerful cellular resource for the development of stem cell-based therapies. As a proof of principle, mouse iPSCs corrected through gene editing have been used to generate haematopoietic progenitors to successfully treat sickle cell anaemia in a mouse model (Hanna et al., 2007). Regarding human iPSC models of inherited retinal diseases, there have been several recent studies showing that correction of the disease-causing gene can be accomplished via CRISPR-based genome editing (revised in Burnight et al., 2018). However, there are still challenges to overcome for such approaches to become applicable in human cell therapy, for example, the potential off-target effects, as described in section 2.4.

To conclude, iPSC-based cell therapies are likely to become major tools in the future of regenerative medicine. The combination of iPSC technology with tissue engineering and 3D bio-printing will open new scenarios in regenerative medicine, shifting the ultimate goal from cell to whole organ replacement. Expectations in both scientific and general community is high. This hype should be exploited for positive development, to secure more funding, make rigorous stem cell science and advance sound clinical studies. It is essential that scientists are proactive in expressing their concern at this proliferation of untested and potentially dangerous procedures being offered to vulnerable patient populations throughout the world.

Advancements in PSC research, as well as results from both ESC and iPSC-based clinical trials will contribute to the development of new standards and to design increasingly effective and safe strategies for future cell therapies.

4. Generation of photoreceptors from ESCs and iPSCs

The knowledge of eye development is the basis of regenerative medicine for retinal diseases. Protocols guiding human PSC differentiation have been developed during the last decade by trying to mimic the successive developmental steps *in vitro*. The simple concept was to determine the culture conditions that allowed ESCs or iPSCs to first adopt a neuroectodermal identity, followed by eye field identity and their succeeding directions towards a neural retina lineage or a RPE lineage (section 1.5).

4.1 Differentiation protocols

One of the first efficient protocols for generating neuroretinal cells has been developed from mouse ESCs by using factors normally required during anterior neural and retinal induction *in vivo* (Ikeda et al., 2005). They used a serum-free floating culture of embryoid bodies (called SFEB system) with addition of specific inducers, Lefty-A, a nodal antagonist and Dickkopf-1 (Dkk-1), a Wnt antagonist that allowed the generation of ESC-derived rostral neuronal progenitors. The presence of serum and Activin-A in SFEB system, just before plating the cells, induced significant generation (25-30%) of retinal progenitors co-expressing Pax6 and Rax. These cells did not efficiently differentiate into photoreceptor precursors unless they were cultured with embryonic retinal cells. Using this concept of sequential specification (anterior neuroectoderm and eye field territory), Tom Reh's group reported the first production of retinal cells from human ESCs (Lamba et al., 2006) (**Figure 19**). Neural induction was stimulated in SFEB system by addition of Dkk-1, Noggin (BMP antagonist) and Insulin growth factor 1 (IGF-1), and cells were plated on poly-D-lysine and Matrigel for further differentiation with the same combination of neural inducers in presence of fibroblast growth factor 2 (FGF-2) and proneural medium supplements (B27 and N2). Under these conditions, the authors reported that almost 80% of the differentiated cells express the EFTFs after three weeks, with 10% average of photoreceptor precursors expressing CRX, and less than 0.01% expressing mature markers of photoreceptors, S-OPSIN and RHODOPSIN (Lamba et al., 2006).

Based on the so-called "Lamba protocol", combining a suspension cultures (SFEB system) and adherent cultures (plating on different specific coating) in presence of specific morphogens, a number of other groups have made some changes to improve the generation of both retinal progenitors and precursors or matures photoreceptors (**Table 4**). Osaka et al. confirmed the importance of preventing BMP/TGF β and WNT pathways for "neuronal-retinal commitment" by inhibition of the respective downstream signaling pathways, SMAD and β -Catenin pathways, using the chemicals compounds SB431542 and CKI-7 (Osakada et al., 2008). The use of small molecules (SB431542 and CKI-7) in replacement of morphogens (Lefty-A and DKK1) is of great importance for the development of retinal differentiation protocol

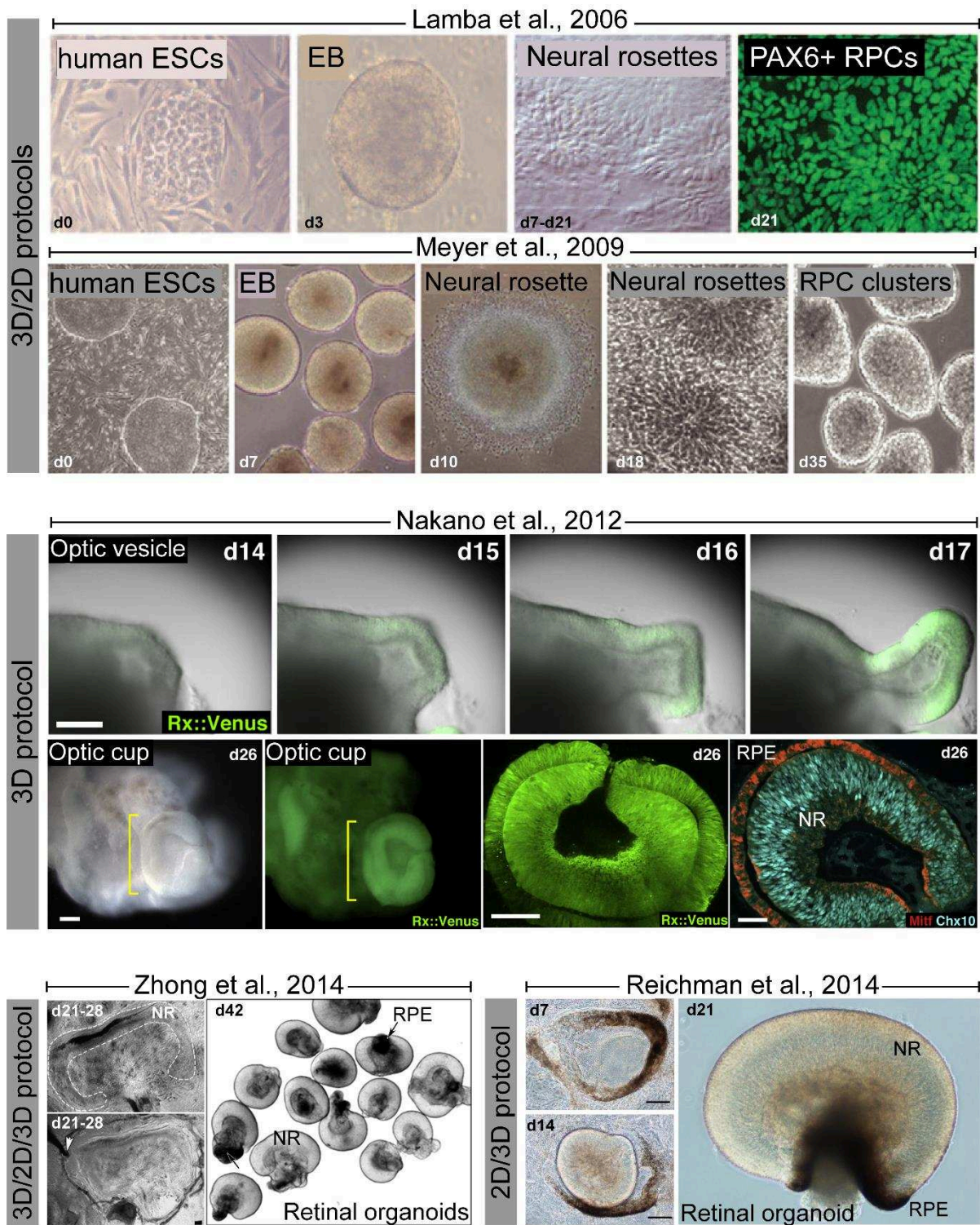


Figure 19 Overview of differentiating cells and 3D structures obtained with five examples of retinal differentiation protocols.

ESC, Embryonic Stem Cells; EB, Embryoid Bodies; RPCs, Retinal Progenitor cells; NR, Neural Retina; RPE, Retinal Pigment Epithelium; d, days; D, dimensions.

used in the future clinical setting. Small molecules such as Dorsomorphin and XAV939 have been also used instead of NOGGIN and DKK-1 to differentiate human iPSCs into retinal progenitors (Meyer et al., 2009). In the stepwise 3D/2D protocol (Lamba et al., 2006; Osakada et al., 2008), addition of factors known to be involved in photoreceptor differentiation during development has been evaluated after plating EBs in order to improve the generation of photoreceptors. The presence of taurine, and retinoic acid (RA) after 90 days of culture increased the number of CRX- and RHODOPSIN-positive photoreceptors observed in cultures after 130 days (Osakada et al., 2009).

In agreement with these pioneers protocols, a variety of retinal differentiation protocols for human ESCs and iPSCs (Amirpour et al., 2012; Boucherie et al., 2013; Hiramani et al., 2009; Krohne et al., 2012; Lamba et al., 2010; Mellough et al., 2012; Tucker et al., 2013; Yanai et al., 2013; Zhou et al., 2015) demonstrated the requirement of preventing the endogenous activation of BMP/TGF β and WNT pathways as well as the presence of IGF-1 or Insulin (a key compound of the N2 and B27 supplements) at early 3D stage of cultures. In some of these protocols, the differentiation of retinal progenitors into photoreceptors has been favored by the addition of specific factors, such as FGF1 and/or FGF2, triiodothyronine (also known as thyroid hormone T3) and Shh (Amirpour et al., 2012; Mellough et al., 2012; Tucker et al., 2013; Yanai et al., 2013). Each of these compounds has been added in specific time windows during the 2D step of the process, when plated EB were cultured in presence of taurine and RA with B27 and N2 supplements. Preferential differentiation toward S-cone photoreceptors was reported with the addition of Coco (Dand5), a member of the Cerberus gene family, acting in synergy with IGF-1 (Zhou et al., 2015). In the presence of Coco, 60-80% of the cells corresponded to S-cone photoreceptors, while addition of thyroid hormone resulted in a mixed M/S-cone population. Another approach described as capable of improving the generation of photoreceptors in the stepwise 3D/2D protocol of differentiation was the calibration of the size of the EBs in the 3D step (Yanai et al., 2013). Using size-controlled EBs (200 μ m diameter and 1000 cells) followed by the addition of Taurine, FGF2 and T3 after EB plating on Matrigel, Yanai et al. have been able to generate more than 80% of CRX+ cells after 17 days of culture (Yanai et al., 2013).

The stepwise 3D/2D method has been elegantly modified by David Gamm's group (Meyer et al., 2011) who added a third step of culture that allowed the selective sorting of self-forming neuroepithelial structures. Following differentiation of EBs in cell suspension, cells were plated on laminin-coated plates, and neuroepithelial structures were then manually picked and further grown as suspension cultures again. They found that these human ESC and iPSC-derived neuroepithelial structures expressed all EFTFs and that the gene and protein expression profiles of the progenitors forming the vesicular structures reflected a differentiation state of

Type of pluripotent stem cells (source)	Method of differentiation	Media supplementation/ Factors added	Markers of photoreceptor lineage and time for detection (immunohistochemistry)	References
hESCs hiPSCs (fibroblasts)	Floating cultures (EB or small clumps of cells), followed by plating (Matrigel coating)	N2 and B27 / IGF-1, Dkk1, Noggin and FGF2	CRX, NRL (D20) RECOVERIN, RHODOPSIN, S-OPSIN (D60)	Lamba et al. 2006 (Lamba et al. 2010; Yoshida et al. 2014)
hESCs hiPSCs (fibroblasts)	Floating cultures (EB-like aggregates), followed by plating (poly-Lysine /laminin/ fibronectin coating)	N2 / Dkk1 (or CKI-7), Lefty (or SB431542), RA and taurine	CRX, RECOVERIN (D50) NRL, RHODOPSIN, OPSIN (D120)	Osakada et al. 2008. (Osakada et al. 2009; Hirami et al. 2009; Jin et al. 2011)
hESCs hiPSCs (fibroblasts, T cells)	Floating cultures (small clumps of cells), followed by plating (laminin coating) and isolation (D 20-25) of self forming optic vesicle-like structures (culture in suspension)	N2 and B27 / <i>Optional: Noggin (or Dorsomorphin) and Dkk1 (or XAV939)</i>	CRX, NRL, RECOVERIN (D40-D70) RHODOPSIN, S-OPSIN (D80-D100)	Meyer et al. 2011 (Meyer et al. 2009; Phillips et al. 2012; Phillips et al. 2014)
hESCs	Adherent cell cultures followed by isolation of "Neural tube-like structures" (day 16) and by plating (Laminin /Poly-ornithin coating)	N2 and B27 / IGF-1, Dkk1, Noggin, FGF2 Shh (optional)	RHODOPSIN, S-OPSIN (D40-50)	Amirpour et al. 2011
hESCs hiPSCs (fibroblasts)	Floating cultures (clumps of cells), followed by isolation (day 30) and plating (Poly-ornithin / laminin coating)	N2 and B27 / IGF-1, Dkk1, Noggin, Lefty, Shh, T3, FGF2, RA and taurine	RHODOPSIN, S-OPSIN (D45-60)	Mellough et al. 2012.
hESCs	Floating cultures (EB-like aggregates) in 1% Matrigel: self-formation of optic cup structures	KSR, FBS, N2 / IWR1e (Wnt inhibitor), SAG (Shh mimetic), CHIR99021 (GSK3 inhibitor), RA and taurine,	CRX, RECOVERIN (D35 -40) NRL, RHODOPSIN, S- OPSIN (D120)	Nakano et al. 2012 (Kaewkhaw et al. 2015)
hESCs	Floating cultures (clumps of cells) in presence of Matrigel followed by isolation (day 5) and plating (Matrigel coating)	N2 and B27 /	CRX (D20-40)	Zhu et al., 2013
hESCs hiPSCs	Floating cultures (clumps of cells) in presence of Matrigel	N2 and B27 / Shh, T3, FGF1, FGF2, RA and taurine	CRX (D10) RHODOPSIN (D30)	Boucherie et al. 2013
hiPSCs (fibroblasts, keratinocytes)	Floating cultures (EBs) followed by isolation (day 5) and plating (synthemax culture plates): self formation of eye cup structures	N2 and B27 / IGF-1, Dkk1, Noggin, FGF2, DAPT and FGF1	RECOVERIN (D90) RHODOPSIN (D120)	Tucker et al. 2013
hESCs	Floating cultures (Size-calibrated EBs) followed by isolation (day 4) and plating (Matrigel coating)	N2 and B27 / Noggin, DKK1, IGF1, FGF2, taurine and T3	CRX (D20)	Yanai et al. 2013
hiPSCs (fibroblasts)	Adherent cell cultures followed by isolation (day 24) of self forming neural-retina structures (culture in suspension)	N2 /	CRX (D25-30) RECOVERIN, CD73 (D35-50) RHODOPSIN, L/M-OPSIN (D90-D120)	Reichman et al. 2014
hiPSCs (fibroblasts)	Floating cultures (small clumps of cells), followed by plating (Matrigel coating) and isolation (D21-28) of self forming retinal structures (culture in suspension)	N2 and B27 and FBS / Heparin, RA and taurine	RECOVERIN (D100) TRANSDUCIN, RHODOPSIN, S-OPSIN, L/M-OPSIN (D120-150)	Zhong et al. 2014

hESCs	Adherent cell cultures followed by isolation (D16) of self-forming neuro-epithelial structures (culture in suspension)	N2 and KSR / FGF2, Nicotinamide	CRX (D40-45)	Wang et al. 2015
hESCs	Floating cultures (EB-like aggregates) in 1% Matrigel: self-formation of laminated retinal structures	KSR, FBS, N2 / BMP4, SU5402 (FGF antagonist), CHIR99021 (GSK3 inhibitor), RA and taurine	CRX, RECOVERIN (D90) NRL, RHODOPSIN, S-OPSIN (D150)	Kuwahara et al. 2015
hESCs	Floating cultures (clumps of cells)	KSR, N2 and B27 / IGF-1, Dkk1, Noggin, Lefty, Shh, T3, FGF2, RA and taurine	S-OPSIN (D30) CRX, RECOVERIN and RHODOPSIN (D90)	Mellough et al. 2015
hESCs	Adherent cells cultures (Matrigel coating)	N2 and B27 / IGF-1, Dkk1, Noggin, FGF2, and FGF9	CRX (D40-45) RECOVERIN PNA	Singh et al., 2015
hESCs	Floating cultures (EBs), followed by plating (Matrigel coating)	N2 and B27 / IGF-1, Dkk1, Noggin, FGF2, and COCO	CRX and S-OPSIN (D21) No NRL and RHODOPSIN	Zhou et al. 2015
hESCs hiPSCs	Adherent cells cultures (Matrigel coating), followed by culture of neural spheres (D19-23) and re-plating on Matrigel coating	N2, B27 / Insulin, Noggin, BDNF, CTNF, DAPT and RA	CRX, NRL, NR2E3 (D90-D100)	Barnea-Cramer et al. 2016
hESCs	Floating cultures (EB-like aggregates) in 2% Matrigel: self-formation of optic cup structures , followed by (D18) manually dissection of retinal organoids in 3-5 parts (floating culture)	KSR, FBS, N2 / IWR1e, SAG, EC23 (synthetic retinoid)	Not reported	Völkner et al. 2016
hESCs hiPSCs	Adherent cell cultures followed by isolation (D28-49) of neuroretinal vesicles (culture in suspension)	N2 and B27 and FBS / RA and taurine	RECOVERIN (D70), RHODOPSIN (D105), S-OPSIN (D84), L/M-OPSIN (D120)	Gonzalez-Cordero et al. 2017
hESCs hiPSCs	Floating cultures (EB-like aggregates) in 1% Matrigel: self-formation of optic cup structures	B27 FBS / IWR1, SAG, RA, DAPT and taurine	RECOVERIN (D45), RHODOPSIN, L/M-OPSIN (D160)	Wahlin et al. 2017

Table 4 Principal protocols for the differentiation of human PSCs to retinal cells.

For human (h) iPSCs, somatic cells used for reprogramming are indicated between brackets.

retinal progenitors closed to the optic vesicle (OV) stage of retinal development (Meyer et al., 2011). In this study, authors found that early endogenous expression of DKK1 and NOGGIN in some PSC lines is sufficient to induce the formation of OV-like structures without addition of small molecules antagonizing the BMP/TGF β and Wnt pathways. Following isolation, floating OV-like structures continued to differentiate towards the photoreceptor lineage, with the expression of CRX and RECOVERIN, between days 45-60 of culture, and more mature photoreceptors expressing RHODOPSIN or S-OPSIN after 100 days in culture (Meyer et al., 2011; Phillips et al., 2012). Recently, adaptation of this stepwise 3D/2D/3D (SFEB floating / plating / isolated OV-like structures in suspension) protocol of differentiation demonstrated that human iPSC lines could efficiently generate retinal structures (Zhong et al., 2014). First, initial SFEBs cultured with N2 supplement have been plated in matrigel-coated dishes, instead of laminin coating. Secondly, they demonstrated that presence of serum, taurine and RA boost in specific time windows during the floating cultures allowed the formation of 3D retinal cups that seemed properly laminated, with the presence after 180 days of culture of mature photoreceptors forming outer segment discs. This study demonstrated for the first time that these iPS cell-derived photoreceptors could be functional, because performed patch-clamp recording showed that some of them were able to response to light stimuli (Zhong et al., 2014).

Over the same period, a couple of very interesting papers from the Sasai's group reported the formation of a bi-layered optic cup using re-aggregated mouse (Eiraku et al., 2011) or human (Kawahara et al., 2015; Nakano et al., 2012) ESCs cultured as SFEB in presence of Matrigel and under high oxygen conditions (40%). Using RX-reporter ESC lines, they demonstrated that these conditions permitted to replicate the first step of retinal morphogenesis, with the evagination of the RX-expressing areas, forming structures similar to optic placode, followed by the invagination of these structures leading to the generation of a bilayered optic cup-like structures, also generally denoted as retinal organoids (Nakano et al., 2012). Like in the eye, the inner part of the invaginated epithelium differentiated to neural retina and the outer layer towards the RPE lineage. In contrast to mouse ESCs, the presence of WNT inhibitor (IWR1e) is required to counter-balance the undesired effect of caudalisation due to the high concentration (20%) of knockout serum (KSR) necessary for human ESC differentiation. Furthermore, the formation of optic cup structures is less frequent (10% of SFEB) than in mouse ESC culture and efficient induction in human ESCs required the presence in a specific time window of serum and a smoothened agonist (SAG), that mimicked the effect of SHH (Nakano et al., 2012). In these conditions, photoreceptors can be identified within neural rosettes formed in the 3D structures by expression of CRX (by day 35), RECOVERIN (by day 60) and NRL and RHODOPSIN (by day 120). Using this 3D culture technique, the same group recently established new culture conditions, called "stepwise induction reversal method" that

enabled the adjacent formation of RPE and neural retina (Kuwahara et al., 2015). SFEB cultured with 10% KSR were primed (day 6 to 18) with low concentrations of BMP4, and transferred in medium with N2 supplement and successively treated with first an inhibitor of FGF receptor and GSK3 inhibitor (day 18 to 24) and secondarily (after day 24) with serum, RA and taurine (Kuwahara et al., 2015). This stepwise protocol in 3D permitted the self-formation of well-laminated neural retina but did not modify the rate and the yield of photoreceptor generation in comparison to their previous protocol (Nakano et al., 2012).

This protocol was further improved by Völkner et al., who noticed that only a part of the neuroepithelium evaginated to form identifiable optic cups, leading to an underestimation and a waste of useful retinal material. By tri-sectioning the neuroepithelium, the efficiency of retinal organoid generation was highly increased, without affecting differentiation of retinal cells (Völkner et al., 2016). A similar approach has been proposed by Wahlin et al., in which each single optic vesicle is manually isolated and cultured separately (Wahlin et al., 2017). They also optimized the neural induction from SFEBs by replacing KSR with E6 supplemented with B27 (without vitamin A). Isolated 3D retinal structures become organized into laminated structures with photoreceptors localized at the outer side. Consistently with the work by Zhong et al., photoreceptors developed outer segment-like structures.

As previously mentioned, moving towards future clinical applications requires the development of simple, robust and reliable retinal differentiation process, which also should reduce the need for exogenous factors (particularly Matrigel with unspecified content) and serum. In this context, Reichman et al. in the laboratory recently developed a retinal differentiation protocol, which bypass the step of EBs formation and subsequent plating on adherent substrates (Reichman et al., 2014). They demonstrated that leaving human iPSCs to overgrow in absence of the pluripotency factor FGF2 allowed the endogenous production of DKK1 and NOGGIN and that in presence of N2 supplement the overgrowing iPSCs could simultaneously generate RPE cells and self-forming neural retinal (NR)-like structures within 2 weeks. Early generated structures containing retinal progenitors presented an OV phenotype revealed by co-expression of the two transcription factors PAX6 and RAX, and an opposite gradient of VSX2 and MITF transcription factors between the neuroepithelium and the RPE (Reichman et al., 2014). Floating cultures of isolated NR-like structures allowed the differentiation of the retinal progenitors into all the retinal cell types, in a sequential manner consistent with the *in vivo* vertebrate retinogenesis. In terms of timing, the detection of photoreceptor precursors expressing CRX and RECOVERIN is observed between day 30 and 40 whereas mature photoreceptors, identified by expression of OPSIN or RHODOPSIN, were obtained after 80 days of culture (Reichman et al., 2014). Successively, other protocols have been developed starting from human ESCs or iPSCs in adherent conditions. Wang et al. reported the

generation of self-forming retinal spheres comprising photoreceptors expressing CRX only in presence of KSR and N2 supplement (Wang et al., 2015). Other authors proposed an exclusively 2D protocol, where 3D retinal tissue is generated and maintained on Matrigel, by using Neurobasal medium, N2 and B27 supplements with the addition of NOGGIN for neural induction, replaced after four weeks by DKK-1 and IGF-1 (Singh et al., 2015). The major drawback of this method is that retinal tissue could not be cultivated for more than 10-12 weeks, which limits the possibility of retinal maturation (no marker for mature photoreceptor were reported). Also, the emergence of retinal tissues was reported to be not homogenous, requiring a purification of retinal cells for downstream applications. With the aim of generating a homogenous population of photoreceptor precursors for transplantation, a four-step protocol has been recently reported (Barnea-Cramer et al., 2016). Adherent ESCs or iPSCs, cultured on Matrigel, are directly switched into retinal induction medium, containing the same components already described for retinal induction starting from EBs (N2, B27 supplements, INSULIN and NOGGIN). After PSCs differentiation into eye field progenitors, in around 20 days, cells are collected to form neural spheres in suspension culture and then plated again on Matrigel to allow expansion and differentiation of RPCs. After four passages, corresponding to three months of culture, more than 90% of cultured cells were reported to stain positively for photoreceptor markers (CRX, NRL and NR2E3), with less than 10% of cells expressing the cell proliferation marker Ki67. Further differentiation of these cells in the presence of RA, brain derived neurotrophic factor (BDNF), CNTF and DAPT, an inhibitor of the γ -secretase, led to the generation of rod-like photoreceptors, expressing RHODOPSIN, RECOVERIN and PHOSPHODIESTERASE-6- α (PDE6 α), but lacking outer segment. These results are surprising, especially because the activation of the CNTF/LIF pathway has been largely described as an inhibitor of photoreceptor differentiation (Ozawa et al., 2004; Rhee et al., 2004).

Finally, a 2D/3D differentiation protocol, based on a combination of the protocols by Goureau and Canto-Soler groups (Reichman et al., 2014; Zhong et al., 2014) has been developed very recently by the group of Robin Ali (Gonzalez-Cordero et al., 2017). As described in Reichman et al., confluent PSC are cultured in absence of FGF2 for the first two days to induce differentiation, and then switched into a N2-supplemented medium to guide differentiation toward a neural fate. Self-forming neuroretinal vesicles as well as RPE appeared between weeks 4 and 7 of differentiation. Retinal differentiation medium consist of the same elements reported by Zhong et al., with the difference that after the boost with RA between week 10 and 12, a small concentration of RA was maintained in the medium with the addition of N2 supplement. The protocol efficiently generated photoreceptors bearing nascent outer segments and developing pre-synaptic structures. Interestingly, the proportion of cone was

quite high, corresponding to 17.8% of cells within the retinal organoid at 20 weeks of differentiation and including both S and L/M cones.

4.2 Future optimization

Additional studies are required for further optimization of retinal cell generation, particularly in the following areas: 1) increasing efficiency and reproducibility of differentiation protocols; 2) accelerating and enhancing full maturation of photoreceptors; 3) adaptation to GMP-compliant conditions, 4) developing storage methods.

Improvement of differentiation protocols will benefit from the identification of the most appropriate cell source and reprogramming method to generate iPSC lines. Most of the protocols published so far use iPSC lines derived from fibroblasts, because reprogramming methods are well established on this type of cells and they represent a convenient source of cells from patients. Deeper understanding of the reprogramming process and of epigenetic memory in particular may contribute to identify cell lines not suitable for retinal differentiation. At the same time, efficiency in generation of retinal neurons has been shown to benefit from epigenetic memory, when retinal cells retaining retinal epigenetic hallmarks, such as rod, has been used as a source for mouse iPSCs (Hiler et al., 2015). There is still no generalized standards to compare robustness of different protocols. In this respect, the development of fluorescent reporter lines specific for different retinal lineages has already proved to be a valuable tool with both mouse and human iPSC lines (Hiler et al., 2015; Kaewkhaw et al., 2015; Phillips et al., 2017; Vergara et al., 2017). Coupling transgenic approaches with automated high-throughput screening will be a valuable tool not only for protocol optimization, but also for phenotypic screening in disease modelling and drug testing (Vergara et al., 2017). Reporter lines will be also useful to deeper dissect the developmental networks regulating commitment into photoreceptor lineage, the choice of cone versus rod identity and the acquisition of mature photoreceptor features (Kaewkhaw et al., 2015).

While the recapitulation of human development *in vitro* is a key element in many differentiation protocols, especially with retinal organoids, the extended time of culture (on average more than 100 days) required to obtain human iPSC-derived photoreceptors represent a limit to the scalability of a potential cell therapy product. In regard of a transplantable cell population, *i.e* photoreceptors precursors, preliminaries strategies have been deployed in order to accelerate their differentiation and increase their number. The Notch signaling pathway has been shown to inhibit photoreceptor production in developing retina (Jadhav et al., 2006). Accordingly, addition of DAPT was able to promote photoreceptor development in mouse ESCs using the SFEB system (Osakada et al., 2008). Blocking Notch pathway during retinal differentiation of

human ESCs or iPSCs led also to an increase of photoreceptor precursors in the “3D retinal structures” generated using the previously described stepwise differentiation protocols (Kawahara et al., 2015; Reichman et al., 2014; Tucker et al., 2013). Addition of DAPT at early stage of differentiation, when retinal progenitors were still dividing, was sufficient to efficiently induce cell cycle exit for a large majority of the progenitors, allowing the generation of about 40% of photoreceptor precursors expressing CRX, after only 35 days of culture (Reichman et al., 2014). Although accelerated differentiation would be desirable, it remains to be determined whether full functionality would still be obtained under such conditions.

Phenotypic features characterizing mature photoreceptors have been achieved, mostly with retinal organoids, but with rare reports of photosensitive activity (Zhong et al., 2014) or dark inward currents (Mellough et al., 2015; Reichman et al., 2017). Interestingly, light-responsive cells were identified in human brain organoids between 7 and 9 months of differentiation containing a broad spectrum of cell types, including cells expressing markers of mature photoreceptors (Quadrato et al., 2017). Molecular mechanism underlying outer segment formation and maintenance are still under investigation. Two miRNAs, miR-182 and miR-183, have been identified to be involved in cone outer segment maintenance *in vivo*, and necessary for its functional formation *in vitro*, using mouse ESC-derived retinal organoids (Buskamp et al., 2014).

Genesis and maturation of retinal cells within organoids may be improved with enhanced nutrient absorption and improved general culture condition in spinning bioreactors (DiStefano et al., 2017; Ovando-Roche et al., 2018). This area of research will benefit from the quick developments related to cerebral organoid culture (Kelava and Lancaster, 2016). Effective transport of oxygen and nutrients are major hurdles shared by the whole organoid field, representing a limit to cell aggregate size, homogenous differentiation and cell survival. Biomaterials might be helpful in providing biomimetic scaffolds and supporting long-term culture of retinal organoids, possibly within bioreactors. Since interactions with extracellular matrix play a role during retinal development and homeostasis, the use of appropriate scaffolds could have a relevant impact. A first study compared the effect of alginate hydrogels and hyaluronic acid-based hydrogels on retinal tissue development from PSCs, showing that the generation could be enhanced by using alginate hydrogels, even if with limited improvement was reported (Hunt et al., 2017). This kind of matrix may enable co-culturing PSC-derived neural retina with RPE, which could provide the critical micro-environmental cues needed for efficient differentiation of photoreceptors to fully laminated neural retina (**Figure 20**).

Important for future clinical application are the continuous efforts to achieve GMP-compliant protocols for all the processes involved: cell line generation, differentiation, storage and distribution. Nowadays human iPSCs are routinely cultured in feeder-free condition; nevertheless, adaptation of retinal differentiation protocols, largely relying on undefined

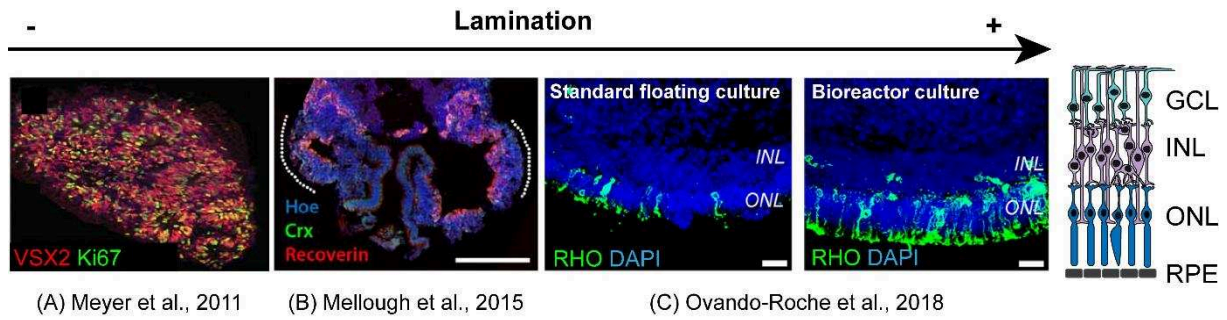


Figure 20 Improving lamination in PSC-derived retinal organoids.

In vivo, cells in the retina are arranged in a multilayered structure that is hardly achieved in PSC-derived retinal organoids. For example, culture conditions described in Meyer et al. (2011) do not support the maintenance of lamination, resulting in the formation of neural rosettes. Some protocols, as in Mellough et al. (2015), achieve a partial lamination restricted to a region within the organoid (indicated by dotted lines). Organoid culture in bioreactors may be useful to improve laminar organization and maturation of retinal cells compared to standard floating culture, as shown by Ovando Roche et al. (2018).

Scale bars: not specified in (A); 200 μm (B), 25 μm (C). RHO, Rhodopsin; ONL, Outer Nuclear Layer; INL, Inner Nuclear Layer, GCL, Ganglion Cell Layer; RPE, Retinal Pigment Epithelium.

compounds and xenogeneic molecules, will require some substantial adjustments. For example, the group of Deepak A. Lamba described the differentiation of retinal and RPE cells from a GMP-compliant human iPSC-line, but still using Matrigel and Fetal Bovine Serum (Zhu et al., 2017b). To this date, the only full adaptation to GMP has been reported by Wiley et al. in 2016. They established 35 human iPSC lines under full GMP condition, from adult fibroblasts of patients affected by different inherited retinal degenerations. Patient-specific iPSCs were differentiated to post-mitotic photoreceptor precursor cells by using a stepwise cGMP-compliant 3D differentiation protocol, modified from Nakano et al. (Wiley et al., 2016a). They demonstrated that they were still able to generate retinal organoids, following the replacement of xenogeneic components with GMP-grade human serum and human proteins of the extracellular matrix. Unexpectedly, the commercially available GMP-compatible cell culture media evaluated were inadequate for isolation and expansion of fibroblast from biopsies of donors over 55 years of age, and new GMP-compliant reagents had to be developed to this purpose. The ability to generate photoreceptor precursor cells from any individual regardless of age is essential to the development of iPSC-based treatments, as advanced stages of retinal degeneration occur mostly in patients with more than 55 years of age.

Despite being a GMP-compliant protocol, the process for the generation of photoreceptor precursors for transplantation requires multiple time-consuming steps (EB formation, manual repacking) and very complex formulation (human serum may present batch to batch differences in its composition) that are an obstacle for an immediate adaptation to large scale-production. Also, cryopreservation of the cell therapy product was not mentioned in the study by Wiley et al.

The development of appropriate cryopreservation methods suitable for photoreceptor precursors is important so that cells at the right stage of development can be obtained at any time. A protocol for the cryopreservation of organoids as whole structures was developed by Sasai's group (Nakano et al., 2012). An alternative approach would consist in banking the population of photoreceptors after its isolation. This implies the development of a selection strategy to separate human ESC- and iPSC-derived photoreceptor precursors from the heterogeneous mixture of cells generated during the differentiation of PSCs. An essential point towards future cell transplantation involving photoreceptor precursor isolation and purification is the identification of specific cell surface antigens.

4.3 Clinical utility of iPSC-derived photoreceptors

iPSC technology is a powerful tool for the development of future therapeutic application. In respect to retinal disease treatment, iPSC are already unleashing their potential, with RPE replacement therapy currently tested in Japan (*cf.* 3.4). In addition to offering a source for the

generation of new photoreceptors for cell therapy, which will be discussed in the following part, the advent of retinal differentiation protocols leading to retinal organoids with similar properties to retina *in vivo* provided researchers with a platform to understand retinal diseases and evaluate new therapeutic molecules. Despite the limitations currently affecting iPSC technology (*cf.* 4.2), retinal cells derived from patient-specific iPSC lines not only possess the precise gene mutation(s) of interest, but also harbor known and unknown genetic modifications that might contribute to that particular individual's disease course and phenotype. Because of their complex genetic heterogeneity, iPSC models of inherited retinal dystrophies are of tremendous importance when animal models do not exist or do not show all the aspects of the human pathology. A number of studies recapitulating different photoreceptor degenerative disease have been reported (reviewed in Sinha et al., 2016 and Yvon et al., 2015) allowing for a deeper understanding of disease etiology and pathobiology (**Table 5**). For example, it was possible to elucidate the pathological mechanism connected with mutations in the *RPGR* gene, accounting for 16% of RP patients, by generating retinal organoids from hiPSCs established from three patients. Mutant iPSC-derived photoreceptors displayed aberrant morphology, localization, transcriptional profiling, and electrophysiological activity. In addition, ciliation defects were observed in patient iPSCs, shortened cilia in RPE cells, and 3D retinae. Described defects were consistent with the clinical phenotype. Importantly, diseased photoreceptor could be restored via CRISPR-Cas9-mediated gene correction (Deng et al., 2018).

Disease modelling proved also to be a tool to uncover new genetic mutations causing photoreceptor degeneration (Tucker et al., 2013). Patient iPSC lines can be used to test different pharmaceutical compounds to rescue the disease phenotype or, on the contrary, to investigate potential toxic effects. For example, α -tocopherol was shown to have a positive effect on rod survival in a single RP line (Jin et al., 2011).

In addition to pharmacologic testing, iPSC-based retinal disease models offer a convenient and informative platform to test gene therapy strategies directly into a human context, which is of extreme importance when assessing the tropism of viral vectors (Gonzalez Cordero et al., 2018; Khabou et al., 2018). Gene therapy mediated by the CRISPR-Cas9 system has already been shown to promise exciting therapeutic opportunities for inherited retinal disease, such as RP (Burnight et al., 2017). The generation of iPSC lines where the disease causing gene is corrected using CRISPR-Cas9 is important not only for therapeutic reasons, but also to generate isogenic control lines for disease modeling. Indeed, generation of patient-specific hiPSCs, along with unaffected sibling and/or gene-corrected control lines, currently is the optimal approach to obtain controls in disease modeling. The inversed strategy, which is inserting the mutation into a wild-type line, can be pursued to obtain a cause-effect demonstration.

Disease	Gene	Mutation	Differentiated cell type /structure	Drug discovery	Gene introduction	Gene discovery	Ref.
RP	<i>RHO</i>	G188R	Rods				(Jin et al., 2011)
	<i>RHO</i>	E181K	PRs	x	x		(Yoshida et al., 2014)
	<i>RP9</i>	H137L	Rods	x			(Jin et al., 2011)
	<i>RP1</i>	721Lfs722X	Rods				(Jin et al., 2011)
	<i>RDS/PRPH2</i>	W316G	Rods				(Jin et al., 2011)
	<i>RPGR</i>	c.1685_1686delAT, c.2234_2235delGA and c.2403_2404delAG	3D retinal organoid and RPE			x	
Sporadic RP	<i>MAK</i>	Alu Insert Ex9	Retinal neurons			x	(Tucker et al., 2011b)
Usher	<i>USH2A</i>	R4192H	Retinal neurons, PRs and RPE			x	(Tucker et al., 2013)
LCA	<i>CEP290</i>	IVS26+1655 A>G	Photoreceptors	x	x		(Burnight et al., 2014)
	<i>CEP290</i>	c.2991+1665A>G	PRs and RPE	x			(Parfitt et al., 2016)
Microphthalmia	<i>VSX2</i>	R200Q	3D Optique vesicles				(Phillips et al., 2014)
JNCL	<i>CLN3</i>	deletions	Retinal neurons		x		(Wiley et al., 2016b)
Macular dystrophy	<i>MCDR1 and MCDR3 loci</i>	Mutation in PRDM13 gene	3D eye cups			x	(Small et al., 2016)

Table 5 Models of photoreceptor diseases established using iPSCs.

Summary of the principal studies that have been identified and examined disease causing mutations using iPSCs, and whether these disease models have led to discovery of the causing gene (gene discovery), drug screening (drug discovery) and rescue of the mutation (gene introduction). Adapted from Yvon et al., 2015.

5. Transplantation of PSC-derivatives

5.1 Historical transplantation studies using PSCs derivatives

Historically, the first attempts of retinal neuron replacement using cells derived PSCs concerned the delivery of neural progenitors into the vitreous space or subretinal space, where transplanted cells were expected to acquire mature retinal identity by inductive signals operating in the retinal microenvironment. In 2006, Banin et al. reported the injection of 60 000 -100 000 neural progenitors derived from human ESCs into immune-suppressed Sabra rats (Banin et al., 2006). Integration into the host retina was observed, independently of the site of the injection but only a very low percentage of the engrafted cells (<1.5%) expressed RHODOPSIN, whereas 10% of cells were positive for the proliferative marker Ki67. Nevertheless, no tumor formation was detected by 16 weeks post-operation. Both intravitreal and subretinal transplanted neural progenitors also differentiated into glial and neuronal lineage, indicating a broad neural developmental potential as well as an insufficient competence for photoreceptor generation (Banin et al., 2006).

A similar kind of cell population (human ESC-derived neural progenitors) has been transplanted in not immune-suppressed wild-type mice, in order to investigate the long-term survival together with the differentiation into the host retina (Hambright et al., 2012). Transplanted cells, expressed specific markers of retinal progenitors (RX, SIX6, VSX2 and NEUROD1), but no markers of the photoreceptor lineage such as CRX and NRL. Findings indicated that the survival of xenogenic human grafts was better when the host RPE/choroid was not damaged, confirming that preservation of the integrity of the blood-retinal barrier is correlated with protection from immune-inflammatory response and survival of the transplanted cells. Regarding cell maturation, at 3 months following transplantation, 67.5% of cells within the graft co-expressed RECOVERIN together with the human nuclear protein epitope (HNu), exclusively in the case of subretinal injection but not after intravitreal injection. No immunohistochemical assay for further photoreceptor maturation was reported.

Finally, Wang and colleagues (Lu et al., 2013; Tsai et al., 2015) provided the proof-of-concept that neural progenitors derived from both human ESCs and iPSCs are effective in preserving vision in RCS rats (classically used as a rat model for AMD), thereby exerting a neuroprotective role similarly to the effect observed after grafts of human fetal-derived neural progenitors (Cuenca et al., 2013; Gamm et al., 2007; Luo et al., 2014). Both human ESC- and iPSC-derived neural progenitors remained as phenotypically uncommitted progenitors following transplantation, since they continue to express Nestin but failed to express markers of specific

retinal neurons or RPE cells. A small portion of the cell population was found to be Ki67+ but no tumor formation was observed in any of the studies. Visual function assays (optokinetic response, electroretinogram (ERG) and luminance threshold recording) showed that vision loss was significantly slowed down in grafted eyes even if not completely stopped (Tsai et al., 2015). These findings are in agreement with histological results indicating that transplanted neural progenitors preserved photoreceptors, since the ONL in cell treated eyes was thicker than in the control at all of the time points tested. The authors suggested that photoreceptors and consequently vision preservation was mediated by the capacity of injected neural progenitors to phagocytose photoreceptor outer segments. In support of this hypothesis, they found that human iPSC-derived neural progenitors expressed genes relevant for phagocytosis, and that they could phagocytose and degrade outer segments *in vitro* and *in vivo*, as engulfed membranous discs were detected within the cytoplasm of grafted neural progenitor cells. It seems that human iPSC-derived neural progenitors can compensate for dysfunctional phagocytosis in RCS rats, thus preserving visual function. Nevertheless, an additional paracrine effect of human neural progenitors by the secretion of neurotrophic factors may also play an important role in retarding retinal degeneration in this rodent model (Luo et al., 2014).

The first transplants of human PSCs directed to a retinal fate were reported by the group of Thomas Reh (Lamba et al., 2009). Human ESCs were differentiated for 3 weeks accordingly to their “retinal determination” protocol (Lamba et al., 2006) in order to obtain a population composed of 80% retinal cells. Between 50 000 and 80 000 cells were transplanted without any prior selection and followed for up to 6 weeks, thanks to the labeling with GFP-expressing viruses before transplantation. In a first series of experiments aiming at evaluating the ability of integration and differentiation of transplanted cells into a host retina, cells were injected either into the vitreous of newborn wild-type mice or into the subretinal space of adult wild-type mice. In both cases, cells could integrate and showed expression of rod and cone photoreceptor markers, even if intra-vitreous injections resulted in the differentiation into other retinal neurons, as cell migration was not restricted to the ONL but also to the INL and the GCL (Lamba et al., 2009). Integration of human cells expressing photoreceptor markers into the host inner retinal circuitry was further confirmed by immunohistochemical analysis of synaptic markers, synaptophysin and post-synaptic density protein 95 (PSD95). In order to determine whether these integrated photoreceptors were functional, they performed the same transplantation experiments into *Crx*^{-/-} mice (Lamba et al., 2009). In this model of retinal degeneration, photoreceptors failed to develop outer segments and no ERG response could be recorded (Furukawa et al., 1997). After 2 to 3 weeks from subretinal injection of human ESC-derived retinal cells, a partial restoration of light response was detected by ERG analysis compared to uninjected eyes (Lamba et al. 2006). The amplitude of the B-wave response

correlated with the number of GFP⁺ cells, with an average of 3.000 NRL⁺ cells per retina, even if they did not form any detectable outer segments. With this study, Lamba and colleagues (Lamba et al., 2009) demonstrated that human ESCs following differentiation to a retinal fate are able to integrate into a host retina and form functional photoreceptors similarly to photoreceptor precursors isolated from a postnatal mouse retina (MacLaren et al., 2006).

By using the same retinal differentiation protocol with human iPSCs, a year later the same group successfully obtained photoreceptors and transplanted them into the subretinal space of adult wild-type mice (Lamba et al., 2010). Unlike the previous study, they used a lentiviral vector driving the expression of the GFP under the control of the photoreceptor-specific promoter, Inter-photoreceptor retinol binding protein (IRBP) to identify the photoreceptor population for transplantation. After 8 weeks of differentiation, about 10% of cells within the total population expressed GFP, consistently with the two photoreceptor markers, OTX2 and CRX (Lamba et al., 2010). Following FACS and transplantation of 50.000 cells, only approximately 50 cells per eye were located into the ONL, as FACS was found to affect cell survival. Nevertheless, GFP⁺ cells showed some maturation (RHODOPSIN and RECOVERIN expression), even if they maintained a rounded morphology, with no outer segment formation (Lamba et al., 2010).

After these pioneering transplantation studies involving human PSC-derived retinal cells, a larger number of studies have been subsequently conducted by using differentiated mouse PSCs as source of cells for transplantation (**Table 6**).

In 2011, Tucker et al. published a study presenting a stepwise protocol for the generation of photoreceptors from mouse iPSCs for transplantation and they investigated the safety and the capacity for functional integration of these cells. In brief, by exposing a mouse dsRed-iPSC line to a differentiation medium containing Wnt and BMP pathways inhibitors, plus IGF and FGF-2, they obtained 33% of cells expressing Crx and 22% of cells expressing Recoverin by day 33 of differentiation (Tucker et al., 2011a). However, approximately 30% of the cells were still undifferentiated, as showed by the expression of the pluripotency marker SSEA1, and transplantation of this heterogeneous population resulted in teratoma formation. In order to deplete the cell population of SSEA1⁺ cells, two consecutive rounds of MACS were performed prior subretinal injection into *Rhodopsin*^{-/-} mice. DsRed⁺ cells within the host ONL photoreceptors displayed outer segment formation, indicated by expression of Retinal Outer Segment Membrane Protein 1 (ROM1), which on the contrary were completely absent in dystrophic host photoreceptors. Also, co-localization between several synaptic markers and the donor cells was observed. About 6.4% of cells were considered as integrated into the ONL and ERG analysis of transplanted eyes showed an increase in B-wave amplitude (Tucker et al., 2011a), demonstrating for the first time that transplantation of iPSC-derived photoreceptors

Mouse PSC line used (ref. for retinal differentiation protocol)	Transplanted population	Host	Injection route/ Transplantation results	References
dsRed-miPSCs (Tucker et al. 2011)	D33 differentiated cells containing 30% of undifferentiated cells. Magnetic beads depletion of SSEA1-expressing cells prior to transplantation of 250 000 cells	4 to 6 week- old <i>Rho</i> ^{-/-} mice	Subretinal injection. 6.4% of integrated cells within the outer nuclear layer (16 000 cells out of 250 000). ERG response and c-Fos expression detected in grafted eyes.	Tucker et al. 2011a
mESCs (Eiraku et al. 2011)	200 000 FAC-sorted AAV2/9.RhoP.GFP+ rod photoreceptors after 26, 29 or 34D of differentiation.	Adult <i>Gnat1</i> ^{-/-} mice.	Subretinal injection via trans-scleral route. 0.3% of integrated cells.	Gonzalez-Cordero et al. 2013
Crx:GFP-mESCs (Eiraku et al. 2011)	200 000 FAC-sorted GFP+ photoreceptors after 22, 26 or 30D of differentiation	Adult NOD/SCID mice	Subretinal injection. 800 integrated cells (0.4%).	Decembrini et al. 2014
Rosa26.tdTomato/Rx:GFP mESCs Nrl:GFP miPSCs (Eiraku et al. 2011)	PSC-derived retinal sheets at different time points of differentiation (D11-D24)	6-8 week-old <i>Rd1</i> mice	Subretinal injection via trans-vitreous route. Different graft integration patterns, maturation and structural integrity observed. No difference between miPSC and mESC-derived grafts.	Assawachananont et al. 2014
CBA.YFP-mESCs (Eiraku et al. 2011)	200 000 FAC-sorted rod precursors selected at D27 on their coexpression of CD73, CD24, CD133 and CD47 and absence of CD15 expression	6-8 week-old WT or <i>Gnat1</i> ^{-/-} mice	Subretinal injection via trans-scleral route. Higher integration levels of sorted cells (654 cells) compared to unsorted cells (9 cells).	Lakowski et al. 2015
mESCs (Eiraku et al. 2011)	200 000 CD73+ MAC-sorted rod photoreceptors, selected from D26 organoids (pre-transfected with AAV Rho-GFP)	7-12 week-old WT, <i>Prom1</i> ^{-/-} <i>Cpl/Rho</i> ^{-/-} mice	Subretinal injection via trans-vitreous route. Photoreceptors transplanted in WT and <i>Prom1</i> ^{-/-} mice integrated with similar efficiencies; transplanted cells in <i>Cpl/Rho</i> ^{-/-} did not acquire mature morphology. No functional recovery detected by ERG.	Santos-Ferreira et al. 2016a
WT and Crx-GFP mESCs (Eiraku et al. 2011)	200 000 FAC-sorted GFP+ cells from D16 and D23 Crx-GFP organoids or D26-30 AAV2/9.2.1.GFP transfected organoids	WT and 8 week-old <i>Aipl1</i> ^{-/-} mice	Subretinal injection via trans-scleral route. Transplanted cells within host SRS were positive for cone markers.	Kruczek et al. 2017
mESCs (Eiraku et al. 2011)	200 000 FAC-sorted L/MOpSin.GFP+ cones sorted from D26-30 AAV ShH10.L/MOpSin.GFP transfected organoids	WT, dsRed and <i>Nrl</i> ^{-/-} mice	Subretinal injection via trans-scleral route. 99% of GFP+/DsRed+ cells in dsRed recipients; increased number of GFP+ cells in <i>Nrl</i> ^{-/-} host ONL compared to WT	Waldron et al. 2017
Nrl-GFP/ ROSA::Nrl-CtBP2-tdTomato miPSC line (Eiraku et al. 2011)	D13 miPSC-derived retinal sheets	L7-GFP/ <i>rd1</i>	Subretinal injection via trans-vitreous route. Light-avoidance behavior and MEA responses recorded in some transplanted mice.	Mandai et al. 2017a

Table 6 Transplantation studies with retinal cells derived from mouse PSCs.

D, day; ERG, Electroretinogram; m, mouse; MEA, Multi Electrode Array; ONL, Outer Nuclear Layer; SRS, subretinal space; WT, wild-type.

can mediate vision improvement. In another study, Homma and colleagues also investigated the functionality *in vivo* of mouse iPSC-derived photoreceptors after transplantation. To easily identify differentiating photoreceptor precursors, they used an iPSC line generated from transgenic Nrlp.eGFP mouse fibroblasts. FAC-sorted GFP⁺ cells were transplanted into wild type adult mouse retina. Calcium responses measured in grafted iPSC-derived rods 2 weeks after transplantation were comparable to calcium responses measured in native adult mouse rods, suggesting similar functionality (Homma et al., 2013).

With the publication by Sasai and colleagues of a protocol recapitulating major steps of eye and retinal development (Eiraku et al., 2011), retinal differentiation in 2D was abandoned in favor of an organoid-like approach using mouse ESCs. Different groups have investigated the capability of photoreceptor precursors derived from 3D mouse ESC cultures to integrate into adult host retina and to mature into new photoreceptors. Two early studies have focused on the identification of the ontogenetic equivalent *in vitro* of postnatal photoreceptor precursors *in vivo* (Decembrini et al., 2014; Gonzalez-Cordero et al., 2013). In the study by Gonzalez-Cordero et al., they chose to focus on rod precursors by using an adeno-associated viral vector carrying the GFP under the control of a *Rhodopsin* promoter (AVV2/9.Rhop.GFP). They analyzed and compared gene expression profile of Rhop.GFP⁺ cells from mouse P12 rods, from D26 and D34 mouse ESC-derived retinal organoids; D26 Rhop.GFP⁺ cells were selected for transplantation studies in *Gnat1*^{-/-} mice, as D34 Rhop.GFP⁺ cells resembled more closely to P12 rods. Identification of integrated cells was based on acquisition of mature phenotype and co-expression of Gnat1 and GFP, which was found only in 0.3% out of 200 000 injected cells (Gonzalez-Cordero et al., 2013). The number of integrated cells is consistently lower compared to rate of integration obtained by transplanting primary mouse photoreceptor precursors. Possibly, the choice of P12 rods as primary cells of reference, as well as the choice of Rhodopsin promoter, instead of Nrl, to label the cells of interest may have led to the selection of more mature rod photoreceptors derived from mouse ESCs, and not immature photoreceptor precursors. Transplantation into two additional mouse photoreceptor-degenerative models (*Rho*^{-/-} and *Prph2*^{rd2/rd2}) resulted in lower integration rates than in *Gnat1*^{-/-} mice and different photoreceptor maturation outcomes, in agreement with a previous work showing that the disease type has a major impact on the outcome of primary photoreceptor precursor transplantation (Barber et al., 2013).

Similar level of integration efficiency, close to 0.4%, were reported in another study using photoreceptors from mouse ESC-derived retinal organoid (Decembrini et al., 2014). Adult NOD/SCID mice were used as host model to avoid any influence of the immune system and to evaluate any potential tumor formation. Most importantly, the use of a transgenic a mouse ESC line expressing GFP under the control of Crx promoter minimized the risk of false positive

results deriving from transduction of viral particles. This line also enabled to follow developing photoreceptors in optic cup-like structures and to purify GFP-positive differentiating photoreceptors by FACS. Cells at day 25 of culture had the highest integration competence, forming morphologically mature photoreceptors bearing outer segments and spherule synapses, without any tumor formation (Decembrini et al., 2014).

These studies from different groups were interpreted as a solid demonstration of the competence of photoreceptors, derived from 2D and 3D differentiation of mouse ESC and iPSC cultures, to integrate into a host retina and drive a partial restoration of visual function. Regarding human PSC-derived photoreceptors, the preliminary results obtained from one study using 2D culture of ESCs and one study with iPSCs looked promising. However, subsequent transplantation findings have overturned the key findings presented so far and our common understanding of donor photoreceptor integration.

5.2 Change of perspective on donor photoreceptor integration

The evaluation of donor photoreceptor contribution to host retinal repair in animal models has relied on the presence of donor cells labelled with fluorescent reporters, with the assumption that fluorescent-positive cells corresponded to injected cells. This strategy led to the conclusion that donor photoreceptor precursors transplanted into the subretinal space of different blind mice models can physically integrate into the degenerating retina, differentiate into mature photoreceptors, form synaptic connections and possibly lead to recovery of visual function (Barber et al., 2013; MacLaren et al., 2006; Pearson et al., 2012). Very recently, the interpretation of these results has been reconsidered after the publication of several studies (**Table 7** and **Figure 21**) showing that fluorescent-positive photoreceptors are almost exclusively endogenous host photoreceptors resulting from a cytoplasmic material exchange between donor and host cells (Decembrini et al., 2017; Ortin-Martinez et al., 2017; Pearson et al., 2016; Santos-Ferreira et al., 2016b; Singh et al., 2016). The mechanisms of this process are not clearly understood yet; it does not involve nuclear fusion or the uptake of free-floating proteins, even though the direct contact between host and donor cells does not seem to be required for the transfer of protein and/or RNA. Transplanted photoreceptors do not migrate and integrate within the host ONL, instead they most commonly stay in the subretinal space. Material exchange has been demonstrated to be bidirectional, meaning that host photoreceptors can transfer cytoplasmic compounds to the transplanted cells in the subretinal space (Ortin-Martinez et al., 2017; Pearson et al., 2016; Santos-Ferreira et al., 2016b; Singh et al., 2016).

	Pearson et al. 2016	Santos-Ferreira et al. 2016b	Singh et al. 2016	Decembrini et al. 2017	Ortin-Martinez et al. 2017
Donor cell type(s) or background	Rod precursors, E11 progenitors, mouse ESC-derived PRs, Fibroblasts	Rod precursors	Rod precursors	Cone precursors	Rod precursors, Cone precursors, <i>Nrl^{-/-}</i> cods
Recipient mouse models	BL/6j <i>Prph2^{rd2/rd2}</i> <i>Gnat1^{-/-}</i>	BL/6j B2-Cre	BL/6j Crx-Cre	BL/6j	BL/6j <i>Nrl^{-/-}</i> <i>Crx^{-/-}</i>
	Two-color fluorescence	x	x	x	x
	EdU pre-labeling	-	x	-	x
	Y chromosome FISH	x	x	-	-
Method of donor /host resolution	Donor/Host fate mismatch	-	-	-	x
	Cre-recombinase reporter	x	x	-	-
	Ectopic PR protein	x	-	-	x
Notable observations	Bidirectional material exchange between donor and host rods. eGFP uptake does not involve free-proteins and cannot be elicited by fibroblasts donors.	Material transfer from host to donor rods.	Bidirectional material exchange between donor and host rods. Transfer as early as 3 days post-transplantation.	Cone to rod material transfer.	Material transfer to rods, cones and cods Bidirectional and second order transfer to INL cells.

Table 7 Summary of studies describing material exchange.

Different techniques used to identify material exchange are detailed for each study. Adapted from Nickerson et al., 2018.

E, embryonic day; INL, Inner Nuclear Layer; PR, photoreceptor.

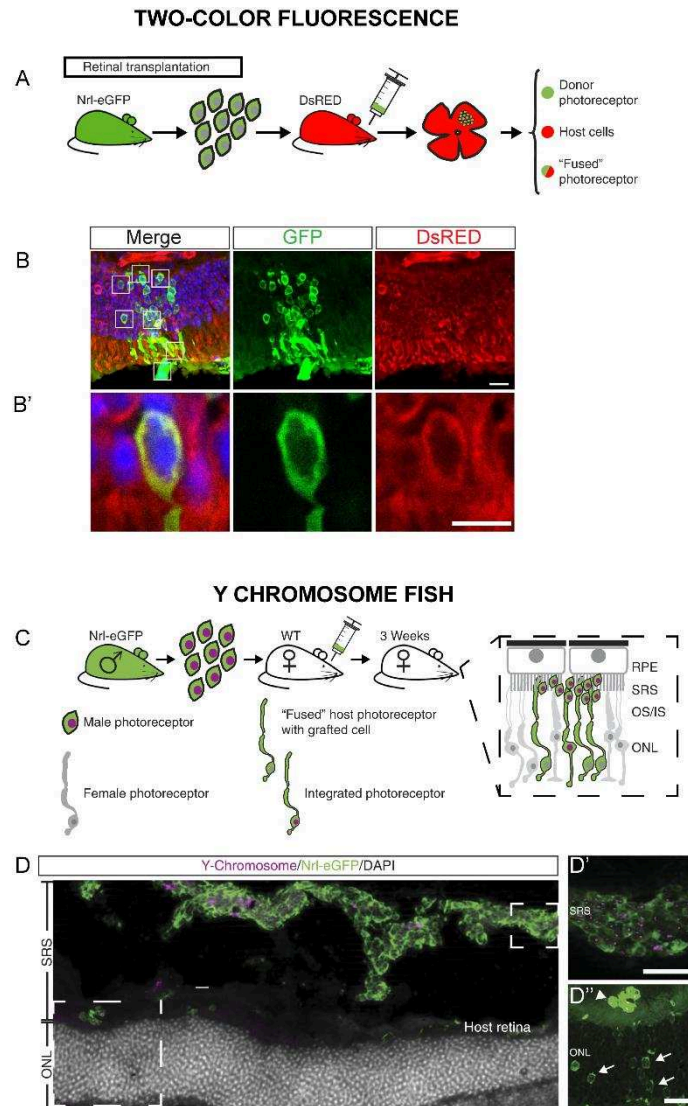


Figure 21 Investigation of donor/host material exchange by two-color fluorescence and Y chromosome FISH.

A-B') Transplantation of Nrl-eGFP donor photoreceptor precursors in DsRED recipient retinas. Co-localization of GFP and DsRED (indicated by squares in B, with a selected magnification in B') indicates exchange of cytoplasmic material. **C-D')** Sex-mismatched transplantation of photoreceptors from male Nrl-eGFP donor into female recipients allow to distinguish between real integrated cells (GFP+/Ychromosome+ in D' and arrowhead in D'') and material transfer events (GFP+/Y- indicated by arrows in D'') D' and D'' are magnification or areas indicated by dotted lines in D. Panel A, C and D-D'' extracted from Santos-Ferreira et al., 2016b; panel B-B' extracted from Singh et al. 2016.

Scale bars: 20 μm (B, D' and D''), 10 μm (B'). WT, wild type; RPE, Retinal Pigment Epithelium; SRS, Subretinal Space; OS, Outer Segment; IS, Inner Segment, ONL, Outer Nuclear Layer.

It is not clear yet whether material exchange could span synaptic connections and extend to host cells within the INL. The presence of low GFP signal beyond the ONL, in bipolar cells and Müller glia, has been reported. These observations were restricted to mouse *Nrl*^{-/-} recipients following *Nrl*:GFP⁺ donor cell transplantation (Ortin-Martinez et al., 2017) and need to be corroborated by further studies in different models.

In addition to being donor cell-stage dependent, the extent of the phenomenon is also in correlation with the host retina cytoarchitecture; specifically, integrity of the outer limiting membrane could play a controversial role in enhancing (Waldron et al., 2017) or impeding (Ortin-Martinez et al., 2017) the material transfer.

According to Robin Ali's group, not only mouse post-natal photoreceptor precursors, but also mouse ESCs-derived photoreceptors can engage into cytoplasmic material exchange (Kruczek et al., 2017; Pearson et al., 2016; Waldron et al., 2017). In particular, these authors sought to determine whether mouse ESC-derived and primary donor-derived cones could truly integrate in different mouse models of retinal degeneration. Results from previous studies using mouse primary cone precursors or cobs (Decembrini et al., 2017; Santos-Ferreira et al., 2015; Smiley et al., 2016; *cf.* 2.5), which failed to produce cells exhibiting cone morphologies, had contributed to raise questions about the nature of integrated cells. Transplantation of cones in a rod-dominant (wild-type) recipients is particularly suitable to investigate donor-host material exchange, as nuclei in cones bear multiple chromocenters and are bigger than rod nuclei (*cf.* 1.3), providing an additional contrast between donor and host cells.

Results from Waldron et al. confirmed that, regardless of their origin, mouse ESC-derived cones, donor-derived cones and cone-like cells undergo material transfer with rods and account for the majority of GFP⁺ cells found in wildtype recipients and in different models of photoreceptor degeneration. As expected, recipient retinal environment had an impact on transplantation outcome, with the highest number of donor cells counted when *Nrl*^{-/-} and *Prph2*^{rd2/rd2} mouse models were used as host retina. These dystrophic retinas, in which OLM integrity is disrupted, supported an increased number of donor cone photoreceptor integration, compared to wildtype recipients, in addition to material transfer events. They hypothesized that the relative contribution of material transfer and donor cell integration to transplantation outcome depends on the etiology of disease and host retinal environment.

To avoid material transfer events, Kruczek et al. transplanted mouse ESC-derived cones, isolated by viral labelling using a M/L opsin-GFP reporter, into *Aipl1*^{-/-} mice, a model of end-stage Leber congenital amaurosis characterized by rapid and extensive photoreceptor loss (Ramamurthy et al., 2004). They first optimized the protocol previously established in the group (Gonzalez-Cordero et al., 2013) for the generation of cones within 3D retinal structures by including a short RA pulse, which increased the proportion of GFP⁺ cones at D26-30 to

15% (± 7), compare to the 3% contained in adult mouse retina. Grafted GFP⁺ cells were analysed for their survival and maturation capacity 3 weeks after injection: despite lacking morphological features of mature photoreceptors, expression of phototransductive and synaptic markers were detected within transplanted cells, clustered in close proximity with host INL (Kruczek et al., 2017). Although further studies assessing functionality of transplanted cells are required, these results showed for the first time that purified mouse ESC-derived cones can survive in a degenerated retinal environment.

Most of the studies so far have been conducted in mouse-to-mouse conditions. Regarding xenotransplantation of human photoreceptors into rodent host retina, the number of studies specifically addressing material transfer from human cell donor to mouse host are still limited. The presence of specie-specific antigens and the nuclear cytological heterogeneity have already proved to be a valuable tools to distinguish, for example, human photoreceptors from mouse photoreceptors (Nickerson et al., 2018). Nevertheless, immunostaining of cytoplasmic components, useful for morphological interpretation, should always be used in combination with nuclear labelling to identify material exchange events.

The importance of appropriate multiple controls has been raised concerning a recent report by Zhu and colleagues. They investigated the transplantation outcome of human ESC-derived retinal cells into a novel immune-privileged model of photoreceptor degeneration, obtained by crossing the immune-compromised *IL2 γ ^{-/-}* mouse onto the *Crx^{ivrm65}* (Zhu et al., 2017a). Human retinal cell were obtained as previously described by the same group (Lamba et al., 2006, 2009) and virally labelled with GFP using lentivirus and a strong ubiquitous promoter, human elongation 1 α promoter (hEF1 α). Donor GFP⁺ cells were detected in recipient retinas up to 9 months after transplantation and they exhibited mature photoreceptor morphology, undistinguishable from host mouse rod morphology. Potential material exchange events had been investigated by immunostaining against the human cytoplasmic marker STEM 121. However, without further staining of human nuclei either using antibodies against the human nuclear antigen (HNA) or using probes for fluorescent in situ hybridization (FISH) specifically recognizing human chromosomes, the results resented in the paper do not convincingly exclude the possibility that observed GFP⁺ cells correspond to host photoreceptors. In retrospective, the two previous studies with human ESC and iPSC-derived retinal cells (Lamba et al., 2009, 2010) should be reconsidered too; the identical morphology exhibited by label donor cells and host photoreceptors might be explained by the exchange of cell material, as it seems unlikely that human cells would have the capacity to adopt the size and the nuclear features of mouse photoreceptors (MacLaren, 2017).

Similarly to experiments with mouse ESC-derived photoreceptors, subsequent transplantation studies with human PSC-derived retinal cells have been performed preferentially in host with no remaining ONL to reduce possibility of labelling artefacts.

A study from Barnea-Cramer et al. described transplantation of retinal cells, obtained with a differentiation protocol for both hESCs and hiPSCs combining multiple 2D and 3D steps (*cf.* 4.1), into *rd1* mice, a wide-used model of end stage RP. As this protocol is supposed to result into the generation of a homogenous population of photoreceptor progenitors, expressing CRX, NRL and NR2E3, retinal cells were directly transduced with AAV driving the GFP expression by the photoreceptor specific rhodopsin-kinase promoter, without any preliminary selection. Subretinal transplantation into fully degenerated *rd1* mice showed survival of GFP+ cells 3 weeks after transplantation in mice treated with cyclosporine to prevent immune-rejection, with GFP+ cells forming a distinct layer in the subretinal space and co-localizing with HNA marker. The authors also showed a limited recovery of visual response by optometric assay but failed to elicit a significant visual recovery using light avoidance assay. They also showed that undifferentiated retinal progenitors did not survive following transplantation, confirming the importance of the developmental stage for donor cells.

All the studies described so far used unsorted human PSC-derived retinal cells differentiated with 2D culture systems (**Table 8**). In 2017, Gonzalez –Cordero and colleagues reported for the first time the transplantation of human cones isolated from human retinal organoids. The development of a new differentiation system, as we have previously detailed in paragraph 4.1, allowed for the generation of 3D retinal structures sufficiently enriched in cones to support efficient isolation by FACS of virally labelled L/M cones expressing GFP (Gonzalez-Cordero et al., 2017). Transplantation were performed in two mouse model, the *Nrl*^{-/-} mouse, in which the ONL is preserved, and the *Aip1*^{-/-} mouse, lacking ONL and already used for mouse ESC-derived cone transplantation (Kruczek et al., 2017). Donor human cells were identified in three ways: using antibodies against human markers (HNA and human mitochondria), comparing the size of nuclei of GFP+ and host photoreceptors, and by performing FISH for mouse Y chromosome and transplanting sex-mismatched human cells. Evidences from these experiments allowed to confirm the human identity of the majority of GFP+ cells, predominantly located within the subretinal space. In *Nrl*^{-/-} recipients, a small number of human GFP+ cells, positively stained with HNA and displaying significantly larger cell bodies and nuclei than surrounding host photoreceptors, were incorporated in the host ONL cells. A minority of GFP+ cells localized within the ONL was positive for mouse Y chromosome but negative for HNA staining, and bore morphologies and nuclear sizes typical of murine photoreceptors, indicating that human photoreceptors could also engage in material exchange with mouse photoreceptors as described for murine-murine rods and cones.

Human PSC line used (ref. for retinal differentiation protocol)	Transplanted population	Host	Injection route/ Transplantation results	References
hESCs (Lamba et al. 2006)	3-week retinal differentiated cells GFP-labeled by infection with lentivirus. (hEFF1aP-eGFP) or adenovirus (CMVP-eGFP). Transplantation of 50 to 80 000 cells.	Neonatal (P0-P3) and adult <i>Crx</i> ^{-/-} mice (cyclosporine treatment)	Intravitreal and subretinal (via trans-scleral route) injections. 3000 integrated cells. Small ERG response detected in grafted eyes.	Lamba et al. 2009
hiPSCs (Lamba et al. 2006)	4 to 8 week retinal differentiated cells GFP-labeled with lentivirus (IRBPP-GFP). Transplantation of 50 000 FAC-sorted GFP+ cells.	WT mice (cyclosporine treatment)	Subretinal injection via trans-scleral route. Only ~50 cells detected in recipient ONL	Lamba et al. 2010
hESCs (Nasokin et al. 2009)	Transplantation of 50 000 unsorted cells corresponding to 50 day-old retinal progenitors expressing EFTFs, NESTIN and TUJ1.	WT mice (no immunosuppression)	Epiretinal and subretinal (trans-vitreous route) injections. Cells in SRS predominantly RECOVERIN+ cells. Epiretinally grafted cells did not mature. Survival of the xenograft correlated with the integrity of the blood retinal barrier.	Hambright et al. 2012
hESCs and hiPSCs (Barnea-Cramer et al. 2016)	Transplantation of 200 000 cells obtained by dissociation of photoreceptor progenitor spheres transduced with adenovirus (GRK1-GFP)	WT and <i>rd1</i> mice aged 10-12 weeks (cyclosporine treatment)	Subretinal injection via trans-scleral route. On average 6.45% hESC-derived cells and 5.7% hiPSC-derived cells survived. Improvement of optomotor response in treated eyes but no difference in light avoidance response.	Barnea-Cramer et al. 2016
Rx::Venus and Crx::Venus hESC lines (Kuwahara et al. 2015)	hESC-derived retinal sheets at different time points of differentiation (D50-120).	NUDE and NUDE S334ter-3 rats, 2 monkey damage-induced models (cyclosporine treatment)	Subretinal injection via trans-vitreous route. Grafts from D50 organoids developed thicker ONLs than those from D100 organoids. In transplanted monkeys, no positive results obtained by focal ERG.	Shirai et al. 2016
hES cells (Lamba et al. 2006)	Transplantation of 500 000 - 750 000 retinal differentiated cells GFP-labeled by infection with lentivirus. (hEFF1aP-eGFP).	4-6 week-old WT, <i>IL2ry</i> ^{-/-} , <i>Crx</i> ^{trm65} , <i>IL2ry</i> ^{-/-/Crx} ^{trm65} mice	Subretinal injection via trans-vitreous route. 3 months following transplantation, robust presence of GFP+ cells in <i>IL2ry</i> ^{-/-} mice (more than 20 000 GFP+ cells on average). Pupillometry and ERG response in <i>IL2ry</i> ^{-/-/Crx} ^{trm65} mice.	Zhu et al. 2017
hESCs and hiPSCs (Gonzalez-Cordero et al. 2017)	Labeling of L/M cones by infection with ShH10.L/Mopsin.GFP. Transplantation of 100 000 FAC-sorted GFP+ cells.	<i>Nrl</i> ^{-/-} and <i>Aipl1</i> ^{-/-} mice (no immunosuppression).	Subretinal injection. Human cell mostly in SRS of recipient retinas. 30 (±34) GFP+ cells negative for human-specific markers detected in the ONL of <i>Nrl</i> ^{-/-} mice.	Gonzalez-Cordero et al. 2017
Crx::Venus hESC line (Kuwahara et al. 2015)	D64-66 hESC-derived retinal sheets	NOG- <i>Pde6b</i> ^{rd12J/rd1-2J}	Subretinal injection via trans-vitreous route. Long term survival (20-27 weeks) and maturation of transplants. Light responses recorded by MEA from host RGCs in 3 out of 8 grafted retinas.	Iraha et al. 2018
hESCs (Zhong et al. 2014)	HESC-derived retinal sheets at different time points of differentiation (D30-65)	NUDE S334ter-3	Subretinal injection via trans-scleral route. OCT imaging showed long-term transplant growth and survival up to 10 months post-surgery. Visual improvements measured by optokinetic testing and electrophysiologic recording in the superior colliculus.	McLelland et al. 2018

Table 8 Transplantation studies with retinal cells derived from human PSCs.

D, day; ERG, Electroretinogram; h, human; MEA, Multi Electrode Array; OCT, Optical Coherence Tomography; ONL, Outer Nuclear Layer; RGCs, Retinal Ganglion Cells; SRS, subretinal space.

However, differently from what have been showed for L/MOpsin-GFP+ mouse ESC-derived cells (Waldron et al., 2017), material transfer does not seem to be the prevalent phenomenon accounting for the presence of human GFP+ cones in *Nrl*^{-/-} mice. Nevertheless, none of the two mechanisms should be excluded when assessing transplantation outcomes in future experiments with human PSC-derived retinal cells.

When transplanted in *Aip1*^{-/-} model, human PSC-derived cones formed a distinct layer adjacent to host INL, in close proximity to host PKC α bipolar cell terminals. Transplanted cells did not develop outer segments and no functional assessment was performed. Interestingly, in both host models, transplants survived in half of the animal injected in the absence of immunosuppressive treatment for 3 weeks after injection, although after 6 weeks only a small number of cells were detected in only 3 animals (Gonzalez-Cordero et al., 2017).

5.3 Transplantation of PSC-derived retinal sheets

As mentioned above, several retinal differentiation protocols allowed for the generation of photoreceptor precursors in an ONL-like layer (Gonzalez-Cordero et al., 2017; Nakano et al., 2012; Reichman et al., 2014; Zhong et al., 2014), providing the possibility of grafting retinal sheets derived from PSCs (**Figure 22**). This approach had been previously explored using as a source for donor grafts either fetal retinal or fetal photoreceptor sheets (paragraph 2.5).

In a proof-of-concept study, the group of Masayo Takahashi reported the first transplantation using mouse ESC- and iPSC-derived 3D retinal sheets into the *rd1* mouse model (Assawachananont et al., 2014). As retinal sheet transplantation has been suggested to be more effective in advanced stage of retinal degeneration when the ONL is completely gone (Seiler and Aramant, 2012), this retinal degenerative model was suitable to recapitulate the clinical scenario of end-stage retinal degeneration, with complete loss of rods occurring by 3 weeks of age (Lolley et al., 1994). Retinal sheets were prepared at different stages from optic cup-like structures generated from both Rx-GFP knockin ESC line and and *Nrl*-GFP knockin iPSC line. Both reporter cell lines could be identically differentiated towards retinal and photoreceptor lineage and no difference in transplantation outcome was observed between retinal tissues derived from the two cell sources. Grafts of retinal derivatives between D11 and 17 of differentiation were found to have the best competence to form structured ONL containing photoreceptors with different degrees of inner and outer segment formation. “Older grafts” (between 18 and 24 days of differentiation) showed the tendency to become disorganized and integration occurred with individual cells, similarly to cell suspension transplantation. In grafts presenting an incomplete INL, photoreceptors could make a direct contact with host bipolar cells.

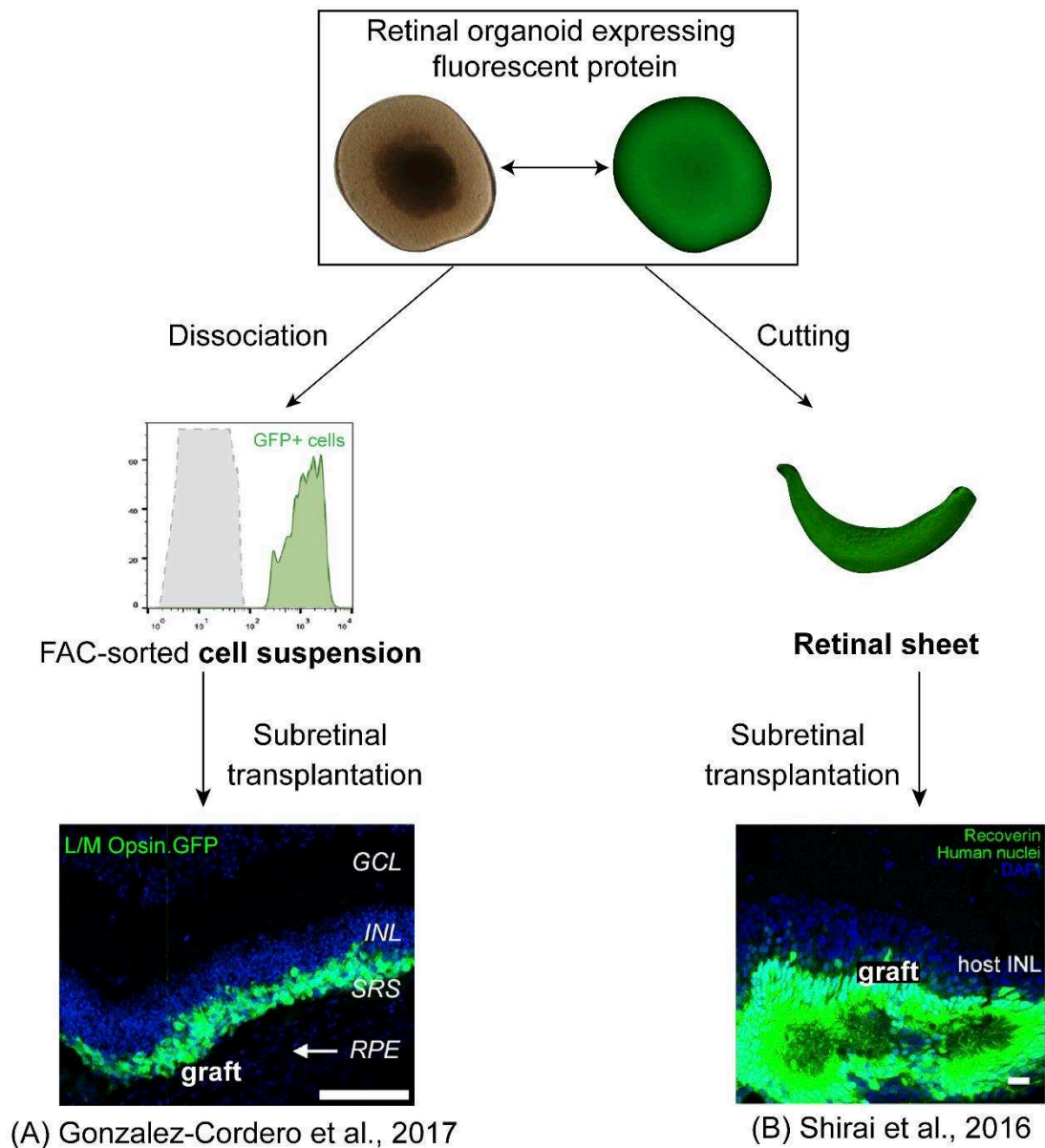


Figure 22 Transplantation of human PSC-derivatives as cell suspension versus retinal sheet. Illustration of the two strategies adopted so far in transplantation studies using human PSC-derived retinal organoids as source of retinal cells. Note that cell injected as cell suspension form a layer in proximity to host INL, whereas transplanted retinal sheets form rosettes.

Scale Bars: 100 μm (A), 20 μm (B). FACS, Fluorescence-Activated Cell Sorting; ONL, Outer Nuclear Layer; INL, Inner Nuclear Layer, GCL, Ganglion Cell Layer; RPE, Retinal Pigment Epithelium; SRS, Subretinal Space.

However, in most of the cases, this type of connections occurred when grafted retinal sheet formed rosettes within the host INL, meaning that on the other side the host RPE was not in contact with the donor photoreceptors (Assawachananont et al., 2014).

Three years later, the same group showed in the same mouse model that their transplantation strategy led to improvement of visual function (Mandai et al., 2017a). They could directly visualize host-graft synaptic contact by using retinal sheet generated from a mouse reporter iPSC line that express CtBP2-tdTomato at photoreceptor synaptic terminals after differentiation (Nrl-GFP/ROSA::Nrl-CtBP2-tdTomato), and transplanting human cells in L7-GFP/*rd1* mice, obtained by crossing *rd1* mice with L7-GFP mice that express GFP in rod bipolar cells. Whole-retina and RGC light-responsive function was analyzed in human iPSC-derived retinal transplants by *ex vivo* MEA recordings. Grafts were responsive to light, although measured amplitudes were smaller than those of wild-type retina and displayed more variable patterns. Light-responsive behavior was analyzed through an adaptation of a shuttle-avoidance system in mice pre-selected to have substantial amount of subretinal grafts. Around half of the tested animals showed responses to light. However, optokinetic test failed to show an improvement in transplanted animals over control.

Human ESC and iPSC-derived retinal sheets have also been demonstrated to have the ability to survive and mature following transplantation in a degenerated retinal environment (Iraha et al., 2018; Shirai et al., 2016). To this end, different animal models have been used. In a first study, human ESC-derived retinal tissues were first transplanted either into NUDE rats or in retinal degenerated S334^{ter} NUDE rats (SD-Foxn1 Tg(S334^{ter})3LavRrrc), to allow long-term maturation (D240-270) of human retinal tissues derived from differentiation of two human ESC reporter lines (RX::Venus and CRX::Venus) (Shirai et al., 2016).

In the majority of rosette-like structures within grafts, development of inner segment/outer segment structures were observed. Often human INL cells were maintained in the graft, preventing direct contact of human photoreceptors with host bipolar cells, which was still observed in a certain number of rosettes. Transplantation was then performed into two new monkey models of retinal degeneration, developed and characterized by the group. In these models, large perimacular areas of the ONL were selectively targeted for damage either by subretinal injection of cobalt chloride or 577-nm optically pumped semiconductor laser photocoagulation. However, in injury-induced models it was difficult to obtain the same pattern of degeneration in every animal, as it is with transgenic or knockout models. Only one eye of the laser-induced model and three eyes of the cobalt-induced model were transplanted with human ESC-derived retinal tissues at around D60 of differentiation.

Given their immature developmental stage, retinal tissues at the moment of transplantation are enriched in proliferating progenitors, potentially dangerous in a clinical context. No tumor

formation was observed, and at the time of graft histological analysis, around 140 days after transplantation, a few proliferative cells were still present. Similarly to experiments in rats, cells within the grafts gave rise to different cell types, including rod and cones but also PKC α + bipolar cells. Although immunohistochemical analysis suggested the formation of host-graft synaptic connections, functional integration could not be detected by focal ERG, maybe in reason of the small size of the graft.

Light responses could be recorded in the following study by the group, where both human iPSC and ESC-derived retinal tissues were transplanted in a new mouse immunodeficient model of retinal degeneration (Iraha et al., 2018). Given the need to monitor xenograft maturation for extended time, they established a new mouse model by crossing *rd1* mouse with immune-compromised *IL2Rg^{null}* (NOG) mouse (*cf.* 2.3). This animal recipient model, where ONL completely degenerates, was preferred over the model established by Zhu et al., as in *Crx^{ivrm65}* mice remaining host photoreceptors could undergo material transfer with donor cells. As in previous study (Shirai et al., 2016), transgenic CRX::Venus human ESC-derived retinal sheets around D60 were used for transplantation; immunohistological and functional analysis were performed around four month later. Light responses were recorded by MEA from 3 out of 8 transplanted retinas, whereas attempts to detect full-field ERG responses were not successful. Interestingly, mouse retinas with human ESC-derived grafts showed a lower responsiveness compared to mouse iPSC-derived transplants, highlighting how the use of allografts versus xenografts can have an impact that should be considered in the evaluation of the transplantation outcome.

Very recently, another study showed the potential for human ESC-derived retinal sheets to restore visual function by using optokinetic test and electrophysiological recording in the superior colliculus (McLelland et al., 2018). Differentiation protocol was adapted from Zhong et al. (2014) and retinal sheets were prepared from retinal organoids between D30 and 65 of differentiation. Immunodeficient rho S334ter-3 rats were used as recipient models. Optical coherence tomography imaging monitored long-term transplant growth and survival up to 10 months post-surgery. Rats tested 2 to 3 months after transplantation performed better in optokinetic test than before transplantation, meaning that transplants improved visual acuity. The difference between transplanted and control eyes increased with time due to the slower development of the human transplant and the increased degeneration of the rat host. 4 to 10 months after transplantation, when no active host photoreceptors are supposed to remain, 9 of 13 rats showed responses to flashes of light in the superior colliculus, with no responses detected in the controls.

These studies showed that, similarly to human primary fetal sheet, human ESC-derived retinal tissues have the capacity to grow, differentiate and mature in a retinal environment mimicking human retinal dystrophies, with promising potential for vision restoration.

5.4 Isolation and transplantation of photoreceptors derived from PSCs

The whole of the studies presented so far showed an increasing attention towards the necessity of selecting the photoreceptor precursors before transplantation. With the exception of the study by Tucker and colleagues (Tucker et al., 2011a), which as described above adopted a negative selection approach, the majority of the works are based on a positive selection of the population of interest (Decembrini et al., 2014; Gonzalez-Cordero et al., 2013; Lamba et al., 2010). These studies have focused on the characterization of the developmental stage of ESC and iPSC-derived photoreceptors corresponding to P4 photoreceptor precursors (MacLaren et al., 2006; Pearson et al., 2012). At this purpose, reporter cell lines have been used, enabling for the identification of photoreceptor cells via the expression of a fluorescent protein under the control of a photoreceptor-specific promoter or knockin in a photoreceptor-specific locus. However, as genetically or virally labeled cells are not suitable for clinical applications, several studies have been focusing on the identification of cell surface markers characterizing photoreceptor precursors. In this context, the plasma membrane protein, Cluster of Differentiation 73 (CD73) also known as ecto-5'-nucleotidase, has been reported to be specifically expressed in the developing photoreceptors in mice retina (Koso et al., 2009), and was concomitantly indicated as an effective surface antigen for the selection of transplantation competent photoreceptor precursor from early postnatal mouse retina (Eberle et al., 2011; Lakowski et al., 2011). Following transplantation of the selected population into wild-type mice, these two studies reported an increased rate of integration than following transplantation of the unsorted population. Selection based on CD73 was equally effective with FACS and MACS approach, leading to a significant enrichment of photoreceptor precursor population with both methods. Lakowski et al. (2011) performed photoreceptor precursor isolation also by using CD73 in combination with another cell surface marker, CD24. Contrary to CD73, CD24 is expressed in embryonic retina and it is down regulated shortly after birth in mouse. Therefore, a combined selection for double-positive CD73/CD24 cells should allow for the exclusive purification of postnatal photoreceptor precursors, by excluding at the same time CD24+ but CD73- immature precursors and mature photoreceptor cells which maintain CD73 expression but lack CD24 expression. Nevertheless, the CD73+ and the double positive CD73/CD24 populations integrated with the same efficiency (Lakowski et al., 2011). As CD73 expression is maintained in mature photoreceptors, an additional combination of four CD markers, CD73, CD24, CD133 and CD47, has been proposed in order to select exclusively

the cell corresponding to post-mitotic precursors in mouse retinal organoids (Lakowski et al., 2015). CD73 and CD133 were found to be highly expressed in Nrl+ rod precursors, conferring specificity for photoreceptor in the context of mouse ESC-derived retinal differentiation; CD47 and CD24 conferred specificity for the appropriate ontogenetic stage (young post-mitotic). At D27, identified as the developmental stage to obtain transplantation-competent cells, the four positive CD markers were expressed in 25% of cells in mouse ESC-derived retinal organoids derived from mouse ESCs. They also identified a marker for the negative selection of potentially harmful mitotically active cells, CD15, therefore proposing for a combination of positive and negative approach as purification strategy. Following transplantation into the subretinal space of either wild-type or *Gnat1*^{-/-} mice of 200.000 cells isolated by FACS some cells were detected into the recipient retina bearing typical rod morphology, probably resulting from donor-host material exchange.

Shortly after, Santos-Ferreira and colleagues demonstrated that the targeting of a single surface antigen, CD73, was sufficient to efficiently enrich a homogenous population of rod precursors from mouse ESC-derived organoids (Santos-Ferreira et al., 2016a). At D26, CD73+ cells corresponded to 60% total cell population from dissociate organoids, consistently with the percentage of CD73+ cells measured in P4 mouse retina (Eberle et al., 2011). After selection by MACS, the proportion of CD73+ cells was enriched to 85%. When CD73+ cells were transplanted into a novel mouse model of severe photoreceptor degeneration (*Cpfl1/Rho*^{-/-}), cells survived in the subretinal space and expressed rod-specific markers, even if the expression of synaptic markers were reduced. ERG recording failed to show functional improvements in transplanted eyes.

In a human context, our group reported for the first time that CD73 was specifically expressed in CRX+/RECOVERIN+ photoreceptor precursors derived from human iPSCs (Reichman et al., 2014), as confirmed recently in fetal and adult human retina *in vivo* (Lakowski et al., 2015, 2018). The panel of surface antigen, CD73(+), CD24(+), CD133(+), CD47(+) and CD15(-), was not suitable for selection of human photoreceptor precursors, as only CD73 and CD133 were identified in a screening for cell surface biomarkers expressed in human adult and fetal retina (Lakowski et al., 2018). The approach consequently proposed by these authors, in order to isolate photoreceptor precursors from human PSC-derived organoids, is to perform a preliminary double negative selection against CD29 and SSEA-1, before proceeding with a positive selection with CD73. However, both the efficiency and the yield of cells following FACS seem still too low to satisfy a potential demand in a cell therapy approach, as triple selected population isolated from human PSC-derived retinal organoids were not enough to be used in transplantation experiments.

Further microarray analysis on P4 mouse rods has led to the identification of three new candidate surface markers, whose expression is exclusively restricted to young rod photoreceptors, *Cacna2d4*, *Kcnv2*, and *Cnga1* (Postel et al., 2013). Their utility for photoreceptor separation has not been validated yet.

With the advancements in RNA sequencing, even to the single cell level, different studies have started looking deeper and comparing transcriptome dynamics of developing human photoreceptors during human development *in vivo* and *in vitro*, within 3D retinal structures derived from PSCs. Kaewkhaw and colleagues generated a human ESC reporter line carrying in the *AAVS1* locus the GFP under the control of *CRX* promoter, gene specifically expressed in post-mitotic photoreceptors (Kaewkhaw et al., 2015). They could not only follow the emergence of photoreceptors in ESC-derived retinal organoids, but, for the first time, they could correlate immunohistochemistry data with photoreceptor transcriptomic profile obtained by RNA-seq of GFP+ cells. Unfortunately, since the analysis was focused on early developmental stages of photoreceptors (37, 47, 67 and 90 days of differentiation), before the onset of OPSIN and RHODOPSIN expression, it does not provide a full characterization of gene expression profiles during rod and cone maturation. Different surface proteins were proposed as candidate cell surface markers for human photoreceptors. KCNV2 was identified as a candidate human photoreceptor marker, as previously suggested for mouse photoreceptors (Postel et al., 2013), as well as SLC6A17, SLC40A1 AND KCNH2. None of these candidate marker has been validated so far. No direct comparison with global gene expression profile of human photoreceptors during embryonic and fetal development was performed in this study, because of the paucity of available data relative to human fetal retina at that time. In 2017, two studies involving the analysis of transcriptome during human retinal development have been published. The work by Hoshino et al. is the most complete, as it presented an extensive histological and transcriptomic analysis of human fetal retina from D52 to D136, and it will be a precious resource to stage human PSC-derived retinal organoids (Hoshino et al., 2017). It also provides a comparison between the transcriptomic profiles of human and mouse retina during development, with mouse embryonic retina (E11-E16) correlating with human D52-D80 and postnatal P0-P4 retina similar to D94-136 human fetal retina. Some gene exhibited a marked difference in their gene expression levels between the two species, such as *DCC* and *NRTK1* (encoding respectively netrin and nerve growth factor receptors), confirming the necessity to investigate further the differences between human and mouse retinal development.

The other study focalized on cone transcriptome during human development, with the intent of comparing fetal and stem-derived cones (Welby et al., 2017). Cones in both retinal explants and organoids were labeled for sorting by using adenovirus carrying GFP under control of the

locus control region and the enhancer of L/M opsin gene (*OPN1LW*, *OPN1MW* and *OPN1MW2*). By analyzing single-cell transcriptome of human fetal L/M opsin cones at different stages of development, they could identify genes differentially expressed during cone maturation, highlighting the concept that, for each specific time point in development, individual cones exist in the retina at different stages of their developmental trajectory. *In vivo* and *in vitro* GFP+ cones shared a similar gene expression signature. These data were used to try to identify cell surface markers upregulated in GFP+ fetal cones to separate cones from both human retinal explants and human retinal organoids. CD73, which had been previously used to isolate cones from a *Nrf1*^{-/-} mouse retina (Santos-Ferreira et al., 2015), was not overexpressed in their dataset and no single surface markers was exclusively expressed in GFP+ population. A combination of different markers, CD26, CD147 and CD133, was proposed to isolate in human L/M opsin cone cells, but the enrichment achieved (30% ±16) requires further optimization (Welby et al., 2017). To this purpose, the use of a more specific construction to identify cones should lead to a refined analysis, as the promoter used in this study (PR2.1) was shown to lead to nonspecific labelling after intraocular injection in the INL and GCL, in addition to cone labelling (Khabou et al., 2018).

Extreme caution should be taken in verifying the pattern of expression resulting from the introduction of fluorescent proteins, either by viral infection or transgenic approaches. The generation of reporter lines is painstaking, with no guarantees of a satisfactory outcome, and in most of the cases multiple reporters would be necessary for a more specific analysis.

In order to avoid the need for a pre-identification of the cell population of interest, single-cell RNA analysis has been proposed as a tool to dissect neural retinal populations within retinal organoids (Phillips et al., 2017). However, analytical methods based on unbiased algorithms were unrevealing, because of the high number of cell expressing mixed signatures. A new method was proposed which classified different cell populations accordingly to the level of expression for some key genes, established as markers of different retinal populations. In this way, it will be possible to identify new genes associated with putative retinal cell types.

To summarize, the need for a marker or a panel of markers to efficiently enrich human photoreceptors is still unmet. A large amount of novel data generated with new sequencing technologies has already expanded our knowledge about molecular markers of retinal developmental stages and their regulatory networks. More information is likely to be uncovered with the development of new analytical methods. With retinal organoids recapitulating more and more faithfully human retinal differentiation, it will be possible to easily validate new candidate markers. The following step required for future therapeutic testing will be the development of a selection process compatible with GMP-grade environment.

Aims

Rescuing the degenerated retina in retinal diseases, such as inherited retinopathies or age-related macular degeneration is a major challenge for which specific cell replacement is one of the most promising approaches. Human iPSCs have the ability to be expanded indefinitely in culture and could be used as an unlimited source of retinal cells. Several data have shown that following various manipulations; human iPSCs can give rise to retinal cells, particularly photoreceptors (*cf.* 4.1). Previous work from our group had led to the development of a protocol (Reichman et al., 2014) that eliminates complicated preliminary steps usually required to differentiate human PSCs into specific retinal lineages, with the simultaneous generation of RPE cells and retinal organoids containing photoreceptors (precursors and matures), needed for regenerative medicine. In the same study, the group could show for the first time that the surface antigen CD73, previously used to isolate both mouse post-natal and mouse ESC-derived photoreceptor precursors (Eberle et al., 2011; Lakowski et al., 2011, 2015; Santos-Ferreira et al., 2016a), was expressed in human iPSC-derived retinal organoids.

For retinal cell therapy, is crucial to adapt iPSC generation and differentiation protocols to GMP conditions. Equally important, an effective strategy for the isolation of a homogenous photoreceptor population, avoiding the use of fluorescent reporters, should be developed.

The major objectives of my PhD project are part of steps necessary for the translation of iPSC technology to the clinic for the treatment of photoreceptor degenerative diseases. The project has been focused on three principal and consecutive aims:

- i) to generate and bank transplantable photoreceptor precursors from human iPSCs in GMP-compatible conditions (Part 1);
- ii) to separate and characterize photoreceptor precursors from human retinal organoids by targeting of a cell surface antigen (Part 1 and 2);
- iii) to conduct pre-clinical studies to evaluate the safety and the functionality of photoreceptor precursors for therapeutic applications (Part 2 and 3).

Results

1. Generation of photoreceptor precursors from human iPSCs in near GMP conditions: identification of a photoreceptor marker and development of a cryopreservation strategy (Paper 1)

Based on our previous differentiation protocol (Reichman et al., 2014), we have developed a new retinal differentiation method of human iPSCs cultured on Vitronectin, as synthetic substrate to replace fibroblast feeder layer in absence of xenogeneic products. We demonstrated that in this environment near to clinical conditions with the use of minimal and GMP-compatible raw materials, human iPSCs were still able to generate self-forming retinal organoids, containing all the different neuro-retinal cell types, and RPE. This xeno-free approach is compatible with the cryopreservation of human iPSC-derived retinal organoids while preserving the photoreceptor population.

I have particularly contributed to characterize the pattern of expression of the cell surface protein CD73 in retinal organoids during the differentiation. I developed a protocol for the dissociation of retinal organoids based on the use of papain allowing to replat and culture retinal dissociated cells into 2D cultures on Poly-D-Lysine and Laminin substrates. I have also showed that papain-dissociated cells still can be cryopreserved and importantly that these cells still expressed CD73.

In conclusion, with this work we could generate retinal organoids using clinical-compatible differentiation media; our new culture conditions support the differentiation and prolonged maturation of photoreceptors. We demonstrated that the surface antigen CD73 is specifically expressed in cells committed into the human photoreceptor lineage, both rods and cones. Enzymatic digestion of retinal organoids with papain efficaciously preserved CD73 expression on dissociated cells, which is important for future development of separation strategy of photoreceptors based on the targeting of CD73. We developed two strategies to cryopreserve retinal cells, as whole organoids or following dissociation, showing that in both cases photoreceptors are preserved and still express CD73. Taken together, these results are an important starting point for the generation and banking of photoreceptors from human iPSCs for clinical applications.

Generation of Storable Retinal Organoids and Retinal Pigmented Epithelium from Adherent Human iPSCs in Xeno-Free and Feeder-Free Conditions

SACHA REICHMAN,^a AMÉLIE SLEMBROUCK,^a GIULIANA GAGLIARDI,^a ANTOINE CHAFFIOL,^a
ANGÉLIQUE TERRAY,^a CÉLINE NANTEAU,^a ANAIS POTEY,^a MORGANE BELLE,^a
ORIANE RABESANDRATANA,^a JENS DUEBEL,^a GAEL ORIEUX,^a EMELINE F. NANDROT,^a
JOSÉ-ALAIN SAHEL,^{a,b} OLIVIER GOUREAU^a

Key Words. Retinal photoreceptors • Retinal pigmented epithelium • Cellular therapy • Induced pluripotent stem cells

^aInstitut de la Vision, Sorbonne Universités, INSERM, CNRS UMR 7210, UPMC Univ Paris 06, Paris, France; ^bCentre Hospitalier National d'Ophtalmologie des Quinze-Vingts, INSERM-DHOS CIC 1423, Paris, France

Correspondence: Olivier Goureau, Ph.D., Institut de la Vision, 17, Rue Moreau, Paris 75012, France. Telephone: (33) 1.53.46.25.33; Fax: (33) 1. 44. 53.46.26.00; e-mail: olivier.goureau@inserm.fr

Received August 9, 2016; accepted for publication January 7, 2017; first published online in STEM CELLS EXPRESS February 8, 2017.

© AlphaMed Press
1066-5099/2017/\$30.00/0

[http://dx.doi.org/
10.1002/stem.2586](http://dx.doi.org/10.1002/stem.2586)

ABSTRACT

Human induced pluripotent stem cells (hiPSCs) are potentially useful in regenerative therapies for retinal disease. For medical applications, therapeutic retinal cells, such as retinal pigmented epithelial (RPE) cells or photoreceptor precursors, must be generated under completely defined conditions. To this purpose, we have developed a two-step xeno-free/feeder-free (XF/FF) culture system to efficiently differentiate hiPSCs into retinal cells. This simple method, relies only on adherent hiPSCs cultured in chemically defined media, bypassing embryoid body formation. In less than 1 month, adherent hiPSCs are able to generate self-forming neuroretinal-like structures containing retinal progenitor cells (RPCs). Floating cultures of isolated structures enabled the differentiation of RPCs into all types of retinal cells in a sequential overlapping order, with the generation of transplantation-compatible CD73⁺ photoreceptor precursors in less than 100 days. Our XF/FF culture conditions allow the maintenance of both mature cones and rods in retinal organoids until 280 days with specific photoreceptor ultrastructures. Moreover, both hiPSC-derived retinal organoids and dissociated retinal cells can be easily cryopreserved while retaining their phenotypic characteristics and the preservation of CD73⁺ photoreceptor precursors. Concomitantly to neural retina, this process allows the generation of RPE cells that can be effortlessly amplified, passaged, and frozen while retaining a proper RPE phenotype. These results demonstrate that simple and efficient retinal differentiation of adherent hiPSCs can be accomplished in XF/FF conditions. This new method is amenable to the development of an in vitro GMP-compliant retinal cell manufacturing protocol allowing large-scale production and banking of hiPSC-derived retinal cells and tissues. STEM CELLS 2017;35:1176–1188

SIGNIFICANCE STATEMENT

Human induced pluripotent stem cells (hiPSCs) can generate an unlimited source of retinal cells for cellular therapies. Protocols using defined conditions free of nonhuman derivatives are preferred for clinical translation. Here, we developed a two-step xeno-free/feeder-free culture system relying on simple culture medium change of adherent hiPSCs, which lead to the efficient generation of both retinal pigmented epithelial cells and self-forming retinal organoids, containing cell populations of major interest for future cell therapy (retinal ganglion cells and photoreceptors). Moreover, retinal organoids can be cryo-banked while retaining their retinal phenotype after thawing. This method provides a new GMP-transferable procedure to generate large-scale of retinal cells which could be then be fast-tracked to the clinic.

INTRODUCTION

The impaired or complete loss of function of photoreceptor cells or supporting retinal pigmented epithelium (RPE) is the main cause of irreversible blindness in retinal diseases, such as inherited

retinopathies and age-related macular degeneration (AMD). The death of retinal ganglion cells (RGCs) in glaucoma also results in irreversible loss of vision. Cell replacement strategies using cell derivatives of pluripotent stem cells are very promising approaches to rescue the degenerated

retina. Stepwise differentiation protocols were designed to mimic retinal differentiation and to successfully generate RPE cells, RGCs, and photoreceptors from human embryonic stem cells (hESCs) and induced pluripotent stem cells (hiPSCs) [1–14]. Recent innovative process demonstrated that hESCs or hiPSCs could efficiently form 3D retinal structures, starting from embryoid bodies [15–18] or simply from confluent hiPSC cultures [19, 20]. The majority of these approaches often rely on animal-derived components in the medium and animal-derived substrate or feeder layer. Therefore, the establishment of a defined and completely xeno-free (XF) culture system following current Good Manufacturing Practice (GMP) guidelines for the generation of transplantable retinal cell types derived from hESCs or hiPSCs is needed for future clinical applications. The use of a feeder-free (FF) system with chemically defined media is now well described for the culture hESCs and hiPSCs [21], as well as for the generation of RPE cells [6, 22–24] including from hESCs in clinical conditions [25]. However, XF/FF culture conditions are poorly documented for differentiation towards retinal neurons [26, 27].

In the current study, we have developed a new retinal differentiation method of hiPSCs in absence of xenogeneic products, based on our simple method allowing both the self-formation of neural retina-like structures and the generation of RPE cells from confluent hiPSCs [19, 28]. This XF approach is compatible with the cryopreservation of hiPSC-derived RPE cells and neural retinal cells. We show for the first time the capability of both hiPSC-derived retinal organoids and dissociated retinal cells to be stored while retaining their phenotypic characteristics, needed for their utilization in cell transplantation.

MATERIALS AND METHODS

Human iPSC Cultures

Established hiPSC-2 clone [19], previously cultured on mitomycin inactivated mouse embryonic fibroblasts, was adapted to feeder-free conditions. iPS colonies from hiPSC-2 clone cells were incubated from 7 to 10 minutes in 2 ml of enzyme-free Gentle cell dissociation reagent (STEMCELL Technologies, Grenoble, France, www.stemcell.com) at room temperature. After aspiration of the dissociation solution, detached cell aggregates were resuspended in 2 ml of prewarmed chemical defined Essential 8 medium (Thermo Fisher Scientific, Courtabouef, France, www.thermofisher.com) by pipetting up and down the center of the iPS colonies without detaching the feeder cells. Human iPSCs were transferred on truncated recombinant human vitronectin (rhVTN-N)-coated dishes with Essential 8 medium. Cells were routinely cultured at 37°C in a standard 5% CO₂/95% air incubator with a daily medium change. iPS cells were passaged with the enzyme-free Gentle cell dissociation reagent (2 ml for 7 minutes at room temperature) every week. Detached cell aggregates were collected in Essential 8 medium and carefully pipetted up and down to obtain uniform suspension of cell aggregates that are replated at ratio of 1/10 to 1/60 depending on the confluence. Feeder free-adapted hiPSCs were subjected to retinal differentiation after 3–5 passages. Adapted at passage 16 (p16), the hiPSC-2 clone was used between p20 and p40 for characterization and differentiation.

Retinal Differentiation and hiPSC-Derived Retinal Cell Cultures

Retinal cell differentiation was based on our previously established protocol [28] with some modifications. Human iPSCs were

expanded to 70–80% confluence in 6-cm diameter dishes coated with rhVTN-N (Thermo Fisher Scientific) in Essential 8 medium. At this time, defined as day 0 (D0), hiPSCs were cultured in chemical defined Essential 6 medium (Thermo Fisher Scientific). After 2 days, the medium was switched to E6N2 medium composed of Essential 6 medium, 1% CTS (Cell Therapy Systems) N2 supplement (Thermo Fisher Scientific), 10 units per ml Penicillin and 10 µg/ml Streptomycin (Thermo Fisher Scientific). The medium was changed every 2–3 days. On D28, identified self-formed retinal organoids were isolated, using a needle, with the surrounding cells and cultured in 6-well-plates (8–12 organoids per well) as floating structures in the ProB27 medium supplemented with 10 ng/ml of animal-free recombinant human FGF2 (Peprotech, Neuilly sur Seine, France, www.peprotech.com) and half of the medium was changed every 2–3 days. ProB27 medium is composed of chemical defined DMEM:Nutrient Mixture F-12 (DMEM/F12, 1:1, L-Glutamine), 1% MEM nonessential amino acids, 2% CTS B27 supplement (Thermo Fisher Scientific), 10 units per ml Penicillin and 10 µg/ml Streptomycin. At D35, FGF2 was removed and half of the ProB27 medium was changed every 2–3 days for the next several weeks.

For hiPSC-derived RPE (hiRPE) cell cultures, identified pigmented patches were cut around D42 and transferred, noted as passage 0 (P0), onto plates coated with CTS CELLStart (Thermo Fisher Scientific). hiRPE cells were expanded in the ProN2 medium composed of DMEM/F12, 1% MEM nonessential amino acids, 1% CTS N2 supplement, 10 units per ml Penicillin, and 10 µg/ml Streptomycin; and the medium was changed every 2–3 days. At confluence, hiRPE cells were dissociated using trypsin and replated at 5×10^4 cells per cm² onto T-25 cm² CTS CellStart-coated dishes for amplification before banking.

Cryopreservation of hiPSC-Derived Retinal Cells

Three to five retinal organoids at D84 were suspended in 250 µl of cold Cryostem freezing medium (Clinisciences, Nanterre, France, www.clinisciences.com) and frozen in a 1.5 ml cryogenic tube (Nunc, Dutscher, Issy les Moulineaux, France, www.dutscher.com) placed in isopropanol-based Mr Frosty freezing container (Thermo Fisher Scientific) at –80°C for a minimum of 4 hours. Frozen tubes were kept in a –150°C freezer for long-term storage. HiRPE cells were frozen at passage 1 in Cryostem freezing medium (1.5×10^6 cells per 250 µl) using the same method with the freezing container and were placed at –150°C for long-term storage. Frozen retinal structures or hiRPEp1 cells were thawed quickly at 37°C in a water bath and resuspended in prewarmed dedicated media for downstream investigations.

Retinal Organoid Immunostaining-Clearing and Imaging

Retinal organoids were first incubated at RT on a rotating shaker in a solution (PBSGT) of PBS 1X containing 0.2% gelatin, 0.5% Triton X-100 and 0.01% thimerosal (Sigma-Aldrich, Saint-Quentin Fallavier, France, www.sigma-aldrich.com) for 3 hours. Samples were next transferred to PBSGT containing the selected primary antibodies (Supporting Information Table S1) and placed at 37°C for 3 days, with rotation at 100 rpm. This was followed by six washes for 30 minutes in PBSGT at RT. Next, samples were incubated with appropriate secondary antibodies conjugated with either Cy3 or Alexa Fluor 594 (Interchim, Montluçon, France, www.interchim.com) diluted at 1:600 in PBSGT overnight. After six 30-minute washes in PBSGT at RT, samples were stored at 4°C

in PBS until the 3D imaging of solvent-cleared organ (3DISCO) clearing procedure [29]. Samples were first dehydrated in a graded series (50%, 80%, and 100%) of tetrahydroflurane (Sigma-Aldrich) diluted in H₂O, during 1 hour for each step. This was followed by a delipidation in dichloromethane (Sigma-Aldrich) for at least 20 minutes, and finally, samples were cleared overnight in dibenzylether (Sigma-Aldrich). 3D imaging was performed either with an ultramicroscope (LaVision BioTec) using the InspectorPro software (LaVision BioTec, Bielefeld, Germany, www.lavisionbiotec.com) or an upright confocal microscope (Olympus FV1000, Rungis, France, www.olympus-lifescience.com) with a numerical 10X objective for high-resolution imaging, as previously described [29]. Images, 3D volume and movies were generated using Imaris x64 software (version 7.6.1, Bitplane) using the “snapshot” and “animation” tools. Movie legends were generated using iMovie 10.0.2.

RESULTS

Generation of Self-Forming Retinal Organoids in Xeno-Free/Feeder-Free Conditions from Confluent hiPSCs

Human iPSC colonies from the integration-free iPS cell line 2 (hiPSC-2), previously generated by episomal approach [19], were adapted to XF/FF culture system using the truncated recombinant human vitronectin (rhVTN-N) as synthetic substrate and chemical defined Essential 8 medium [21]. Under these new conditions, qRT-PCR revealed that the expression of pluripotency genes in hiPSC-2 is still comparable to that seen in hESCs (Supporting Information Fig. S1A). hiPSC-2 expanded in XF/FF conditions express the pluripotency markers OCT4 and SSEA4 or SOX2 and TRA1-60 (Supporting Information Fig. S1B–1G) and exhibited a normal karyotype (Supporting Information Fig. S1H).

At around 70% of confluence, hiPSC colonies cultured in Essential 8 medium were placed in Essential 6 medium (Essential 8 medium without FGF2 and TGFβ) during 2 days to turn off the self-renewal machinery and encourage the spontaneous differentiation. Since we previously reported that N2 supplement alone could be sufficient to direct hiPSCs cultured on feeder layers toward retinal fate [19], we tested different chemically defined media containing 1% of CTS N2 supplement (Fig. 1A). In this XF/FF environment, the use of ProN2 medium validated with hiPSCs on feeder layers [19] led regretfully to cell death (data not shown). Nevertheless, we developed a new retinal differentiation medium (E6N2 medium), corresponding to Essential 6 medium containing 1% of CTS N2 supplement, allowing the self-formation of neuroepithelial-like structures from adherent hiPSCs in 28 days (Fig. 1A). In this XF/FF conditions, differentiating iPSCs started within 14 days (D14) to endogenously express the key BMP and WNT antagonists, DKK1 and NOGGIN, respectively, essential for neural differentiation (Fig. 1B). About 4 weeks after the initiation of differentiation, self-forming neuroepithelial-like structures appeared in the culture dishes (Fig. 1C and Supporting Information Fig. S2A). RT-qPCR analysis of these isolated structures at D28 revealed an eye-field specification with the robust expression of specific markers, such as *SIX3*, *MITF*, *VSX2*, *PAX6*, *RAX*, and *LHX2*, while losing the expression of the pluripotency marker *POU5F1* (*OCT4*) (Fig. 1E). Immunostaining at D28 showed that these structures comprise a

population of mitotic retinal progenitor cells (RPCs) coexpressing *VSX2* and *Ki67* (Fig. 4A). The expression of transcription factors involved in the photoreceptor lineage, such as *CRX*, *NRL*, and *NEUROD1*, was also detected as early as D28 (Fig. 1E).

Following isolation along with surrounding cells at D28, retinal organoids were cultured as floating structures (Fig. 1D and Supporting Information Fig. S2B) in medium containing CTS B27 supplement (ProB27 medium) with human FGF2 during 1 week (Fig. 1A) to favor differentiation of the neural retina [30]. Spherical organoids increased in size and the distal part of the neuroepithelium became pigmented around D42 (Supporting Information Fig. S2B–2D). To confirm the reproducibility of the differentiation process, two other hiPSC lines were subjected to the XF/FF differentiation process. Our results demonstrated that similar retinal organoids can be obtained indifferently from hiPSCs derived from foreskin fibroblasts reprogrammed by an episomal approach (Supporting Information Fig. S2E, 2F) or derived from adult dermal fibroblasts reprogrammed in XF/FF conditions with the Sendai virus (Supporting Information Fig. S2G, 2H). The evaluation of the number of structures that developed per cm² for these three hiPSC lines at D28 revealed some expected intercell line variability in term of efficiency (Supporting Information Fig. S2I).

Transcription factors involved in retinal specification and differentiation were still expressed in retinal organoids during floating cultures in ProB27 medium, with a noticeable increase of *RAX*, *SIX3*, and *VSX2* expression after D35, while expression of the nonretinal forebrain marker *FOXG1* decreased (Fig. 1F). At D35, cells forming retinal organoids coexpressed *RAX* and *PAX6* (Fig. 1H, 1I) confirming their eye-field identity [31]. At this time, *VSX2*⁺ cells were predominantly located in the outer part of the developing neuroepithelium (Fig. 1J–1L), which also expressed also *PAX6* (Fig. 1J, 1K). *MITF*⁺ cells were found mainly in the distal part of the organoids (Fig. 1L, 1M), corresponding to RPE cells. At D35, the *PAX6*⁺/*VSX2*[−] cell population is concentrated at the inner part of neuroepithelium (Fig. 1J, 1K), corresponding to the first postmitotic differentiating retinal neurons, which did not express the *Ki67* proliferation marker (Fig. 1N, 1O). Some cells in the same location were found to be immunoreactive for a specific marker of RGCs, *BRN3A* (Fig. 4B). Nevertheless, at D35, the outer part of retinal organoids still contained proliferative RPCs identified by the coexpression of *VSX2* and *Ki67* (Fig. 1O). Interestingly, RT-qPCR analysis showed that the emergence of photoreceptor precursors can be detected after D42 by up-regulation of *NRL*, *CRX*, and *NEUROD1* expression (Fig. 1G), concomitant to the decrease of *VSX2* and *RAX* expression (Fig. 1F).

Differentiation of RPCs from hiPSC-Derived Retinal Organoids

RT-qPCR analysis on organoid RNA extracts showed that RPCs can be committed in to the photoreceptor lineage, with an increase of *CRX* (Fig. 1G), *RECOVERIN* (*RCVRN*) and *CONE ARRESTIN* (*CAR*) expression (Fig. 2A) throughout the floating culture. The expression of genes specific for mature photoreceptors, such as *RHO-DOPSIN* (*RHO*), *BLUE* or *RED/GREEN* (*R/G*) *OPsin* (*OPS*), emerges only after 100 days (Fig. 2B). Immature photoreceptors immunoreactive for *CRX*, *OTX2*, and *RCVRN* can be identified at D49 (Fig. 2C, 2D), and a stronger expression of these markers was observed at D84 (Fig. 2E). Rods and cones can be clearly identified either by *RHO* or *R/G* *OPS*, *BLUE OPS* and *CAR* immunostaining in

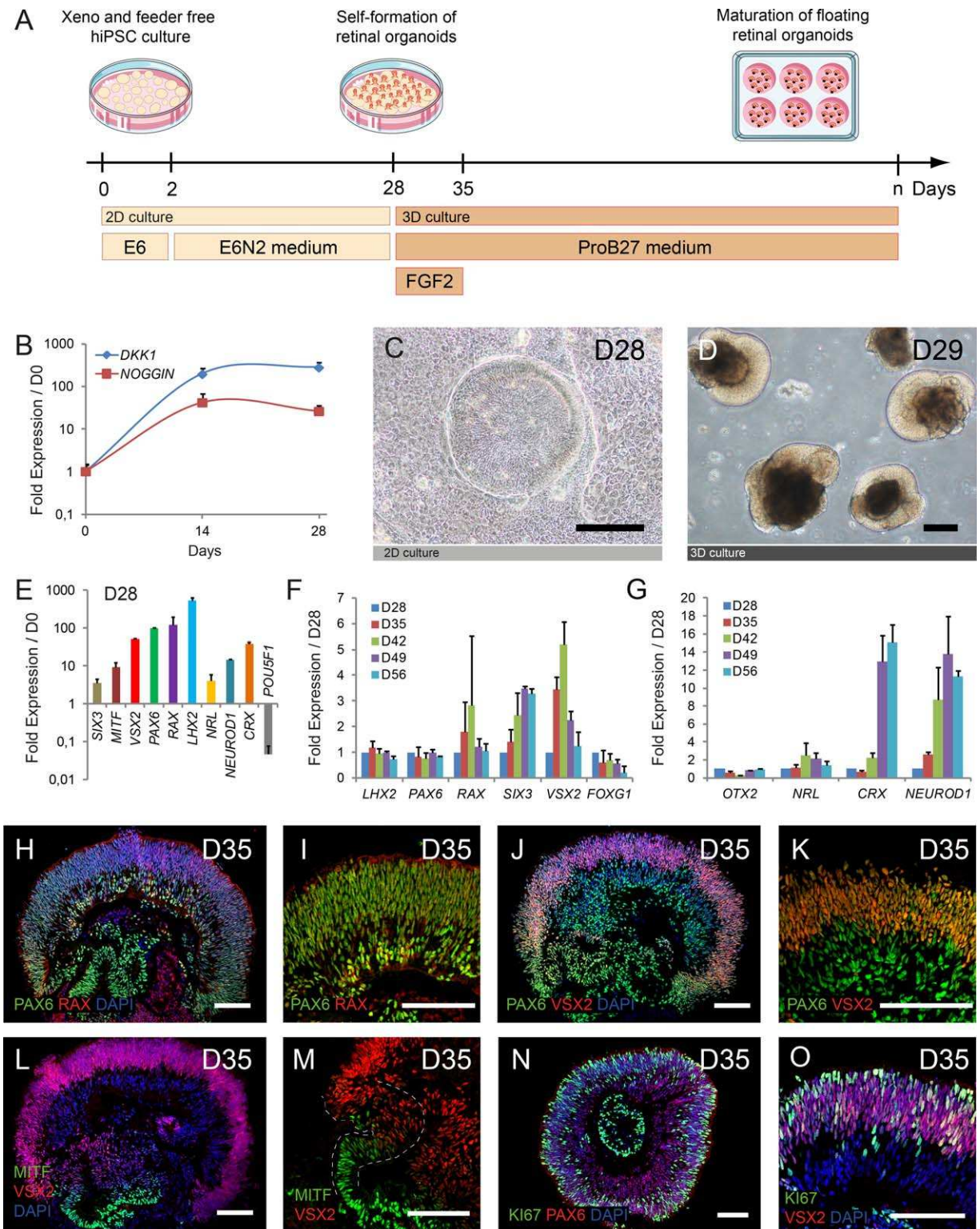


Figure 1. Generation of retinal organoids from adherent hiPSCs in Xeno Free and Feeder Free conditions. **(A)**: Schematic diagram illustrating the protocol for retinal organoid production from hiPSCs. **(B)**: RT-qPCR analysis of *DKK1* and *NOGGIN* during differentiation at D0, D14, and D28. Data are normalized to hiPSC-2 at D0. **(C)**: Self-forming neuroretinal-like structures derived from adherent hiPSCs at D28. Scale bar = 100 μ m. **(D)**: Morphology of representative floating retinal organoids isolated at D29. Scale bar = 100 μ m. **(E)**: RT-qPCR analysis of eye-field transcription factors, *NRL*, *CRX*, *NEUROD1*, and pluripotency marker *POU5F1* in retinal organoids at D28. Data are normalized to hiPSC-2 at D0. **(F, G)**: RT-qPCR time course analysis of eye-field and retinal specific transcription factors and forebrain marker *FOXG1* in retinal organoids between D28 and D56. Data are normalized to retinal organoids at D28. **(H–O)**: Immunostaining of retinal organoid sections at D35 for PAX6, RAX, VSX2, MITF, and Ki67. Picture in panel N correspond to a transverse section of retinal organoids. Scale bars = 100 μ m. Abbreviation: hiPSC, human induced pluripotent stem cell.

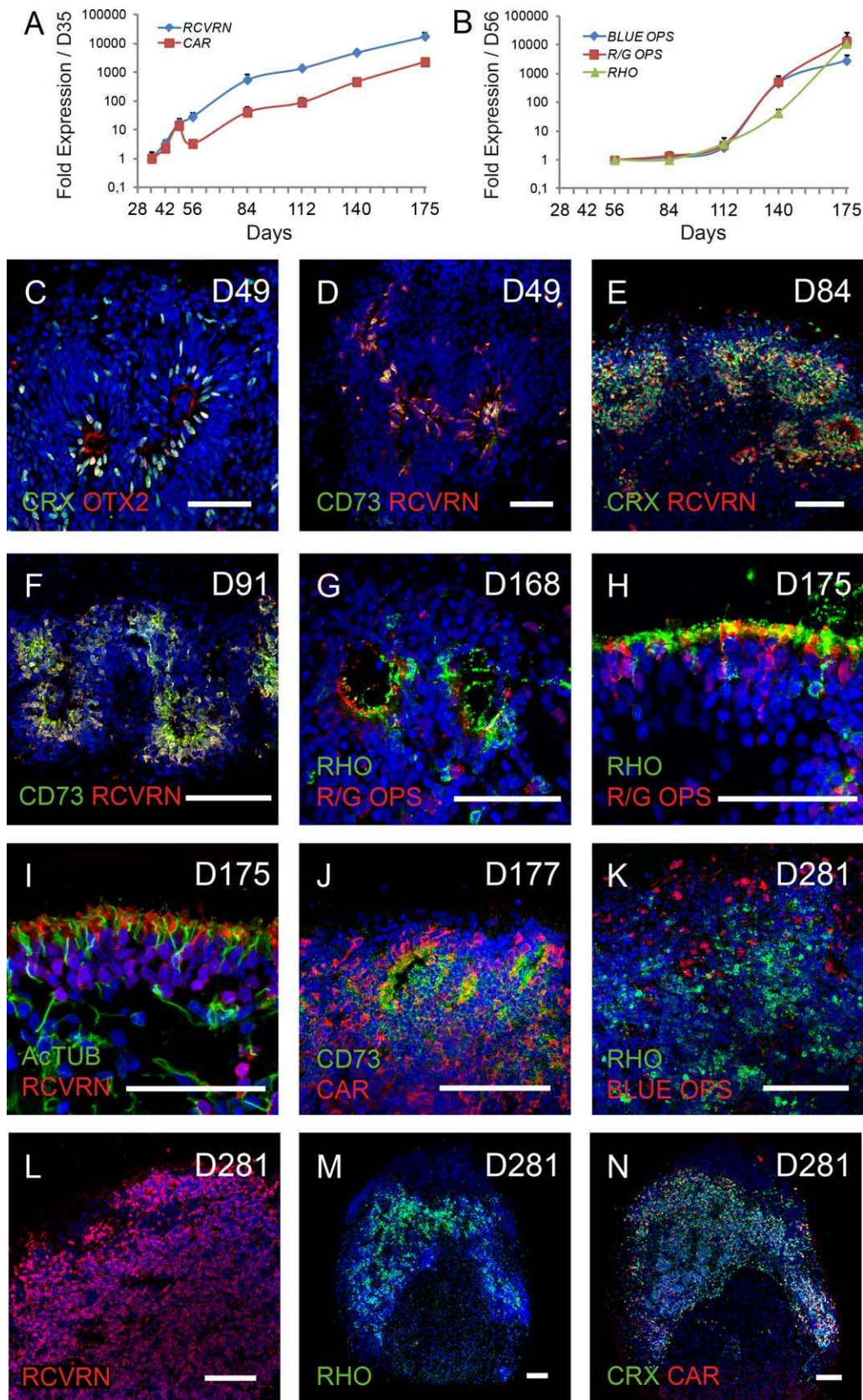


Figure 2. Photoreceptor differentiation in retinal organoids during floating cultures. (A, B): RT-qPCR analysis of photoreceptor markers during differentiation between D35 and D175. Data are normalized to retinal organoids at D35 (A) or D56 (B). (C–N): Immunostaining of retinal organoid sections for CRX (C, E, N), OTX2 (C), CD73 (D, F, J), RECOVERIN (D–F, I, L), RHODOPSIN (G, H, K, M), R/G OPSIN (H), BLUE OPSIN (K), Acetylated TUBULIN (I), and CONE ARRESTIN (J, N) at the indicated time of differentiation. Nuclei were counterstained with DAPI (blue). Scale bars = 50 μm (C, D, G–I) or 100 μm (E, F, J–N).

culture kept for a longer period until D281 (around 9 months) (Fig. 2G–2N). Interestingly, after 40–50 days, differentiating photoreceptors were often found inside rosettes (Fig. 2C–2G), even though an external cell layer resembling the outer nuclear layer can be observed in some iPSC-derived retinal organoids (Fig. 2H, 2I). The cell surface marker CD73 is expressed specifically in differentiating RCVRN⁺ photoreceptors at different times of differentiation (Fig. 2D, 2F and Supporting Information Fig. S3B). The expression of CD73 by photoreceptors was confirmed after D140 by the coexpression with RCVRN, CAR, BLUE OPS, and R/G OPS (Fig. 2J and Supporting Information Fig. S3). Conversely, CD73 was not expressed by PAX6⁺ cells (corresponding to RGCs and horizontal/amacrine cells) located around the rosettes (Supporting Information Fig. S3A). An efficient photoreceptor differentiation was also observed in retinal organoids derived from the two other hiPSC lines showing cells expressing RCVRN, CAR, CRX, RHO, BLUE OPS, and R/G OPS between D77 and D175 (Supporting Information Fig. S4). In 175-days old retinal organoids, the connecting cilium marker acetylated TUBULIN revealed the existence of very thin structures juxtaposed to RCVRN⁺ cells (Fig. 2I), suggesting the formation of cilia and photoreceptor outer segments (POS).

To analyze the spatial distribution of rosettes containing rods and cones, we performed whole-mount immunostaining with photoreceptor specific markers and 3DISCO clearing procedure on D195 retinal organoids. This technology offers the possibility of imaging entire transparent samples without the need of sectioning, when combined with immunohistochemistry [29]. Spatial arrangement of photoreceptors characterized by the expression of RCVRN/RHO and CAR/RHO was observed on 3D-reconstructed images (Fig. 3A, 3B). The precise 3D pattern of rosettes containing RHO⁺ rods or CAR⁺ cones was visualized in the external part of the retinal organoids (Fig. 3C and Supporting Information Movies S1 and S2). High-resolution confocal imaging of RHO staining on cleared D195 organoids revealed an intense fusiform staining reminiscent of emerging POS in the center of rosettes (Fig. 3D). Similar staining was observed with CAR antibody identifying cones in different retinal organoids (Supporting Information Fig. S4J). TUNEL assay performed on 195-days old organoids demonstrated that photoreceptors identified by RCVRN, RHO, or BLUE OPS staining in the rosettes do not seem to undergo apoptosis (Supporting Information Fig. S5). Transmission electronic microscopy analysis confirmed the presence of photoreceptor ultrastructures, such as basal body and connecting cilium with a photoreceptor-specific microtubule arrangement at D112 (Fig. 3E–3K). Some photoreceptors also presented membranous materials, corresponding to developing POS, which were clearly identified at D196 (Fig. 3L).

To test whether the hiPSC-derived photoreceptors are capable of achieving functional maturation, we tested their ability to exhibit an inward dark current (IDC). The IDC corresponding to an influx of Na⁺ and Ca²⁺ through the activation of cyclic nucleotide-gated (CNG) channels is the result of the increase of the cGMP concentration in photoreceptors. To mimic this “dark state,” we used a membrane-permeant cGMP analogue (8-Br-cGMP) to open cationic CNG channels leading to the IDC, as previously described [18]. Ca²⁺ influx was monitored with live two-photon imaging of the intracellular fluorescent Ca²⁺ indicator Fura-2 in dissociated cells from retinal organoids at D175. Forty-eight hours after seeding, some Fura-2-loaded retinal cells showed a calcium influx

when exposed to 8-Br-cGMP, as observed by decreased intracellular fluorescence (Fig. 3M, 3N). Average of maximum fluorescence variation during recording of 11 responsive photoreceptors is $-22.52\% \pm 10.63\%$ (151 cells analyzed, $N = 4$) (Fig. 3O). No decrease of the intracellular fluorescence has been observed in retinal cells exposed to AMES puffs instead of the cGMP analogue (150 cells analyzed, $N = 4$). These functional observations support our morphological data that the XF/FF culture conditions reported here allow a certain level of photoreceptor maturation.

The RPCs within retinal organoids are able to give rise to other retinal cell types. By RT-qPCR and immunostaining using BRN3 markers, we confirmed the early emergence of the RGCs after 35 days of differentiation (Fig. 4C, 4K). Interestingly, BRN3A⁺ RGCs localized around the rosettes containing OTX2⁺ photoreceptors can still be observed in 84-days old organoids when ProB27 medium was used (Fig. 4F). Similar immunofluorescence analysis confirmed the differentiation of RGCs in retinal organoids derived from the two other hiPSC lines (Supporting Information Fig. S4A–4C, S4E), confirming the reproducibility of the differentiation process. Differentiating amacrine and horizontal cells were detected by RT-qPCR with the induction of *GAD2* and *LIM* expression, respectively, (Fig. 4L) and by immunohistochemistry with the presence of AP2⁺/PAX6⁺ and LIM1⁺/PAX6⁺ cells, respectively, (Fig. 4D, 4E). RT-qPCR demonstrated that bipolar cells identified by PKC α expression appear later (Fig. 4M) and immunostaining at D281 confirmed the presence of fully differentiated bipolar cells coexpressing VSX2 and PKC α (Fig. 4I, 4J). The emergence of Müller glial cells was also observed at later time points, as shown by RT-qPCR with the induction of specific markers *GLAST1* and *RLBP1* (Fig. 4M) and by the identification of cells coexpressing the GLUTAMINE SYNTHETASE (*GS*) and *SOX9* (Fig. 4G). At D140, the presence of very rare Ki67⁺ cells (less than five positive cells per section) indicates that retinal organoids reached a “mature state,” confirmed by the absence of mitotic RPCs (Fig. 4H).

Cryopreservation of Photoreceptor Precursors from Retinal Organoids

Considering the potential use of photoreceptor precursors for future cell transplantation [32, 33] and the length of the differentiation, we sought to develop different cryopreservation approaches that would enable the cells to be stored along the differentiation process. The first strategy was to cryopreserve whole retinal organoids at stages of development where CD73 is well expressed (close to D100, as shown by immunofluorescence). Retinal organoids cultured in suspension until D84 were submitted to cryopreservation using cold Cryostem freezing medium and the presence of photoreceptors was examined in organoids 16 days after thawing, at D100, in floating cultures. Frozen retinal organoids showed the presence of intact rosettes containing CRX⁺ and RCVRN⁺ photoreceptor precursors (Fig. 5E, 5F) similar to nonfrozen organoids at the same stage (Fig. 5A, 5B). Interestingly, the CD73⁺ cells, considered as the transplantable cell population [34–36], were still clearly identified. Indeed, as in nonfrozen organoids (Fig. 5C, 5D), CD73 is specifically expressed in RCVRN⁺ cells (Fig. 5G, 5H) confirming their specific expression in photoreceptors. Quantification of CRX⁺ cells at D100 (Fig. 5Q) did not reveal any significant difference between the number of cells in controls (nonfrozen) and frozen retinal organoids ($p = .1344$; $n = 81,450$, and 119,339 counted cells).

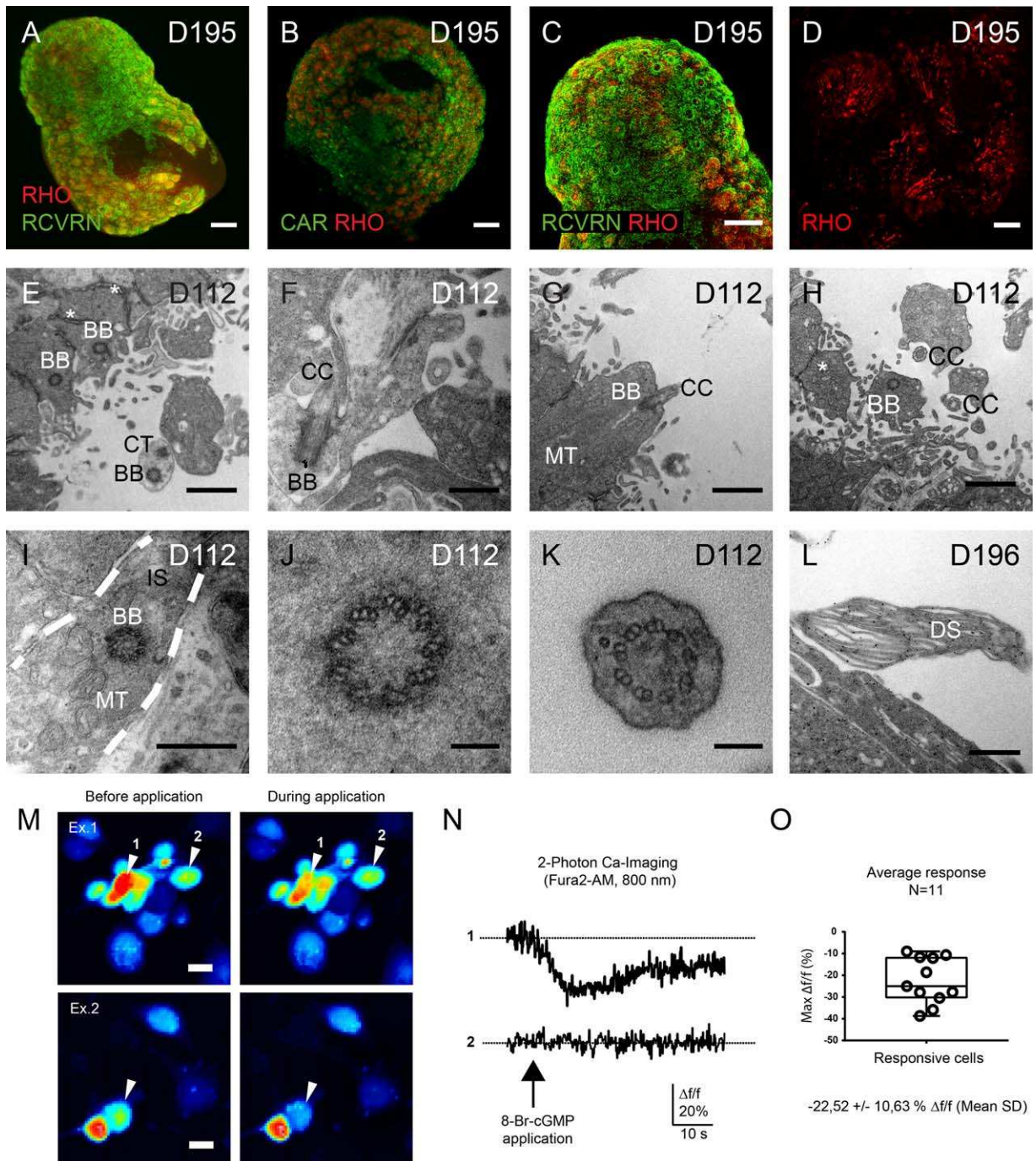


Figure 3. Maturation and electrophysiological analysis of hiPSC-derived photoreceptors. **(A–D):** Immunolabeling for RHODOPSIN (A–D), RECOVERIN (A, C) or CONE ARRESTIN (B), and 3DISCO clearing of D195 retinal organoids. Scale bars = 200 μ m (A–C) and 25 μ m (D). **(E–L):** Transmission electronic microscopy analysis of retinal organoids at D112 and D196 with the presence of external limiting membrane (*), BB, CC, CT, MT, IS, and DS. Photoreceptor-specific microtubule arrangements revealed the presence of the clearly identifiable $9 \times 3 + 0$ basal body complex BB and $9 \times 2 + 0$ CC. Scale bars = 1 μ m (E, G, H); 500 nm (F, I, L); 100 nm (J, K). **(M):** Calcium imaging on dissociated retinal cells at D175. Examples (Ex.1 and Ex.2) of 2-Photon Fura2-AM fluorescence images obtained before (left) and during (right) application of 8-Br-cGMP. White arrows on Ex.1 denoted 1 and 2 represent a responsive and a nonresponsive cell, respectively. On Ex.2, the arrow represents another responsive cell. Fluorescent images are represented in false colors and are averages of 20 seconds of activity before or during stimulation. A cGMP-based calcium influx is reflected by a decrease in Fura2-AM fluorescence, and such a response is observed in both examples in one cell, without affecting neighbor cells. Scale bars = 5 μ m. **(N):** Fluorescence raw traces and effect of cGMP analogue on the cells 1 and 2 displayed on Ex.1, expressed as percentage change from baseline fluorescence ($\Delta f/f$ %). **(O):** Boxplot representing the average decrease in fluorescence amplitude of 11 responsive cells from three independent samples. Abbreviations: BB, basal body; CC, connecting cilia; CT, centrioles; MT, mitochondria; IS, inner segments; DS, disc stacks.

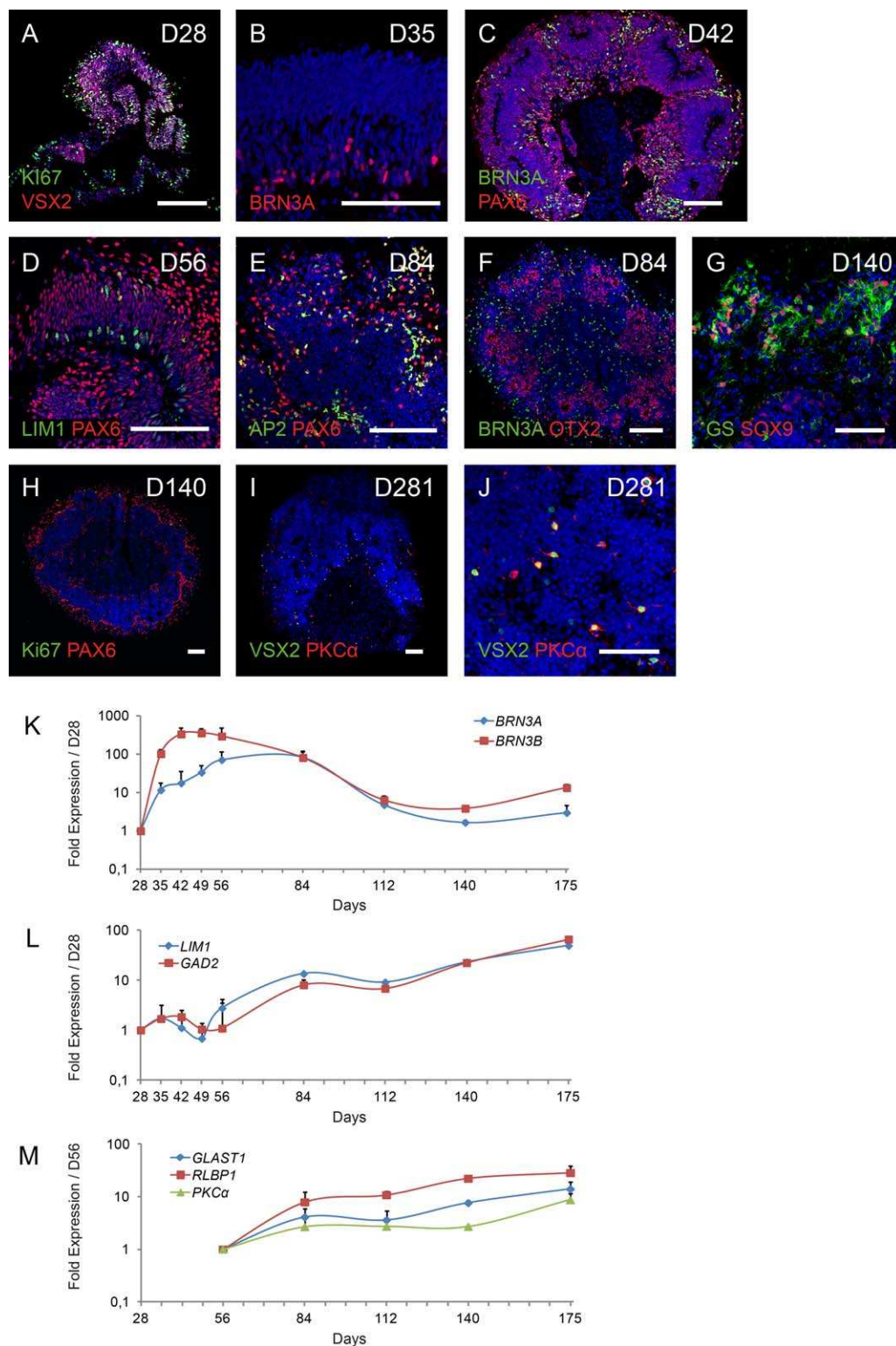


Figure 4. Sequential generation of retinal ganglion cells, horizontal cells, amacrine cells, Müller glial cells, and bipolar cells from floating retinal organoids. **(A)**: Immunofluorescence staining of cryosectioned retinal organoids at D28 for Ki67 and VSX2. **(B–F)**: Immunohistochemical analysis of retinal organoids between D35 and D84 using markers for RGCs (BRN3A, PAX6), horizontal cells (LIM1, PAX6), amacrine cells (AP2, PAX6), and photoreceptors (OTX2). Scale bars = 100 μ m. **(G–J)**: Immunohistochemical analysis of retinal organoids after D140 using markers for proliferating cells (Ki67) and for late retinal cell types, Müller glial cells (GS, SOX9) and bipolar cells (VSX2, PKC α). Nuclei were counterstained with DAPI (blue). Scale bars = 100 μ m (H, I) and 50 μ m (G, J). **(K–M)**: RT-qPCR analysis of selected neural retinal cell types in retinal organoids at different times: RGCs (BRN3A, BRN3B); horizontal cells (LIM1), amacrine cells (GAD2), Müller glial cells (GLAST1, RLBP1), and bipolar cells (PKC α). Data are normalized to retinal organoids at D28 (K, L) or D56 (M).

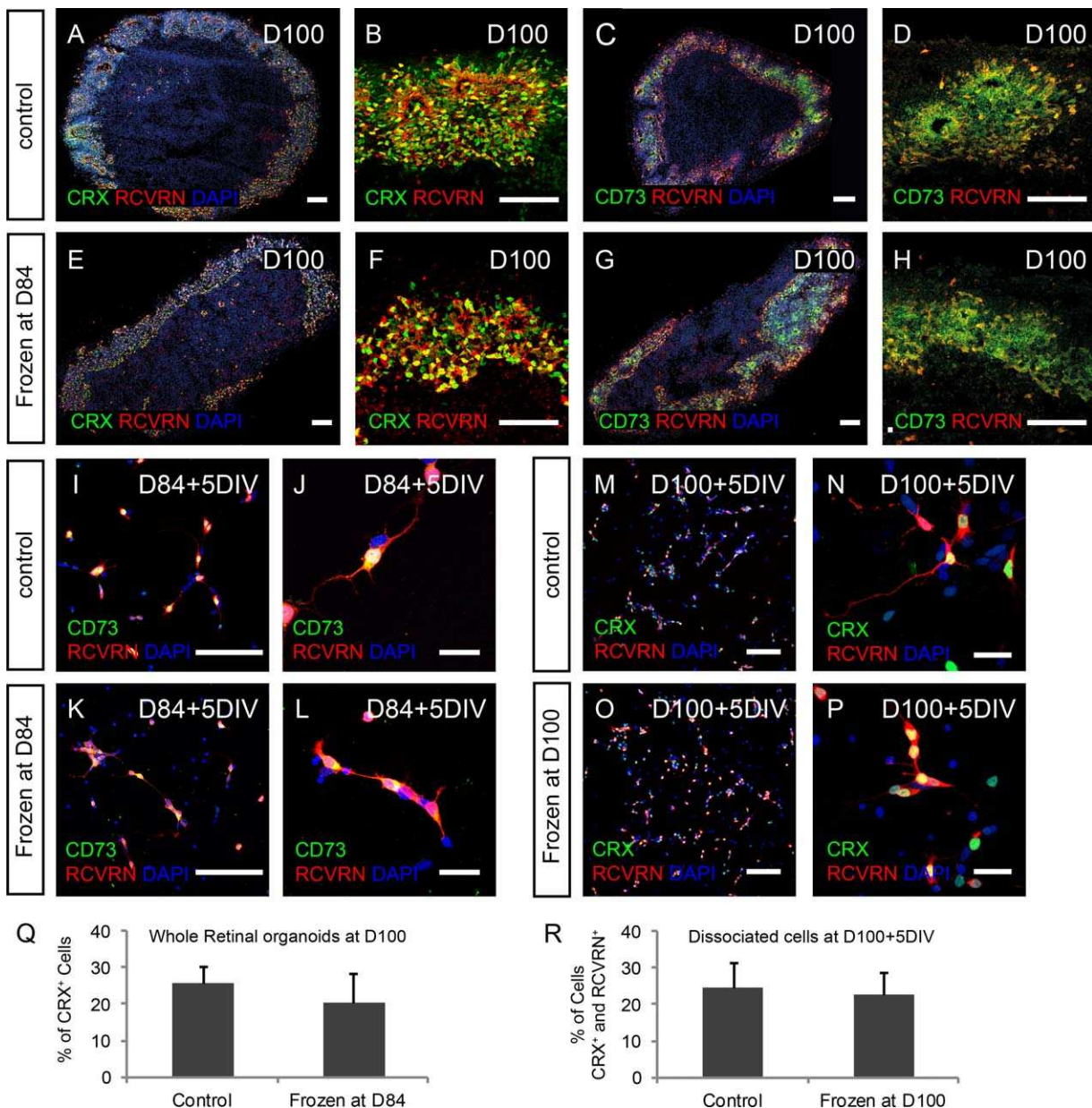


Figure 5. Efficient cryopreservation of photoreceptor precursors in whole retinal organoids or as dissociated cells. **(A–D)**: Immunostaining for CRX (A, B), CD73 (C, D), and RECOVERIN (A–D) on retinal organoids at D100. Scale bars = 100 μ m. **(E–H)**: Immunostaining for CRX (E, F), CD73 (G, H), and RECOVERIN (E–H) on retinal organoids cryopreserved at D84 and cultured for additional 16 days after thawing. Scale bars = 100 μ m. **(I–P)**: Retinal organoids were dissociated at D84 (I–L) or D100 (M–P) and retinal cells were either cultured for 5 days in vitro (DIV) (I, J, M, N) or cryopreserved and cultured for 5 DIV after thawing (K, L, O, P) before immunostaining for CD73 (I–L), CRX (M–P), and RECOVERIN (I–P). Scale bars = 100 μ m (I, K, M, O) and 25 μ m (J, L, N, P). **(Q)**: Quantitative analysis at D100 of CRX-positive cells in unfrozen retinal organoids (control, $N = 7$ organoid sections corresponding to 81,450 cells) or in retinal organoids cryopreserved at D84 ($N = 11$ organoid sections corresponding to 119,339 cells). **(R)**: Quantitative analysis after 5 DIV of double CRX/RECOVERIN-positive cells in fresh (control, $n = 31,303$ cells) or cryopreserved dissociated cell population from D100 retinal organoids ($n = 13,958$ cells).

In a second approach, we examined whether dissociated retinal cells from organoids could be cryopreserved. In this case, retinal organoids cultured until D84 or D100 were dissociated using papain and retinal cells were cryopreserved using the cold Cryostem freezing medium. After thawing, cells were plated on Poly-D-Lysin/Laminin treated coverslips to be cultured for five additional days in vitro (DIV). Immunostaining revealed that frozen RCVRN⁺ photoreceptors have kept their strong CD73 expression as in nonfrozen dissociated cells (Fig. 5I–5L). Similar observations were made on a double CRX⁺ and RCVRN⁺ cell

population (Fig. 5M–5P). Accordingly, quantification showed no significant difference in the number of double CRX⁺ and RCVRN⁺ cells between frozen cells and control cells (Fig. 5R) ($p = .5839$; $n = 31,303$, and 23,958 counted cells).

Generation, Amplification, and Banking of hiPSC-Derived RPE Cells

Human iPS-derived RPE (hiRPE) cells were generated simultaneously to the retinal organoids from confluent hiPSCs cultured in Essential 6 medium with the successive addition after 2 days

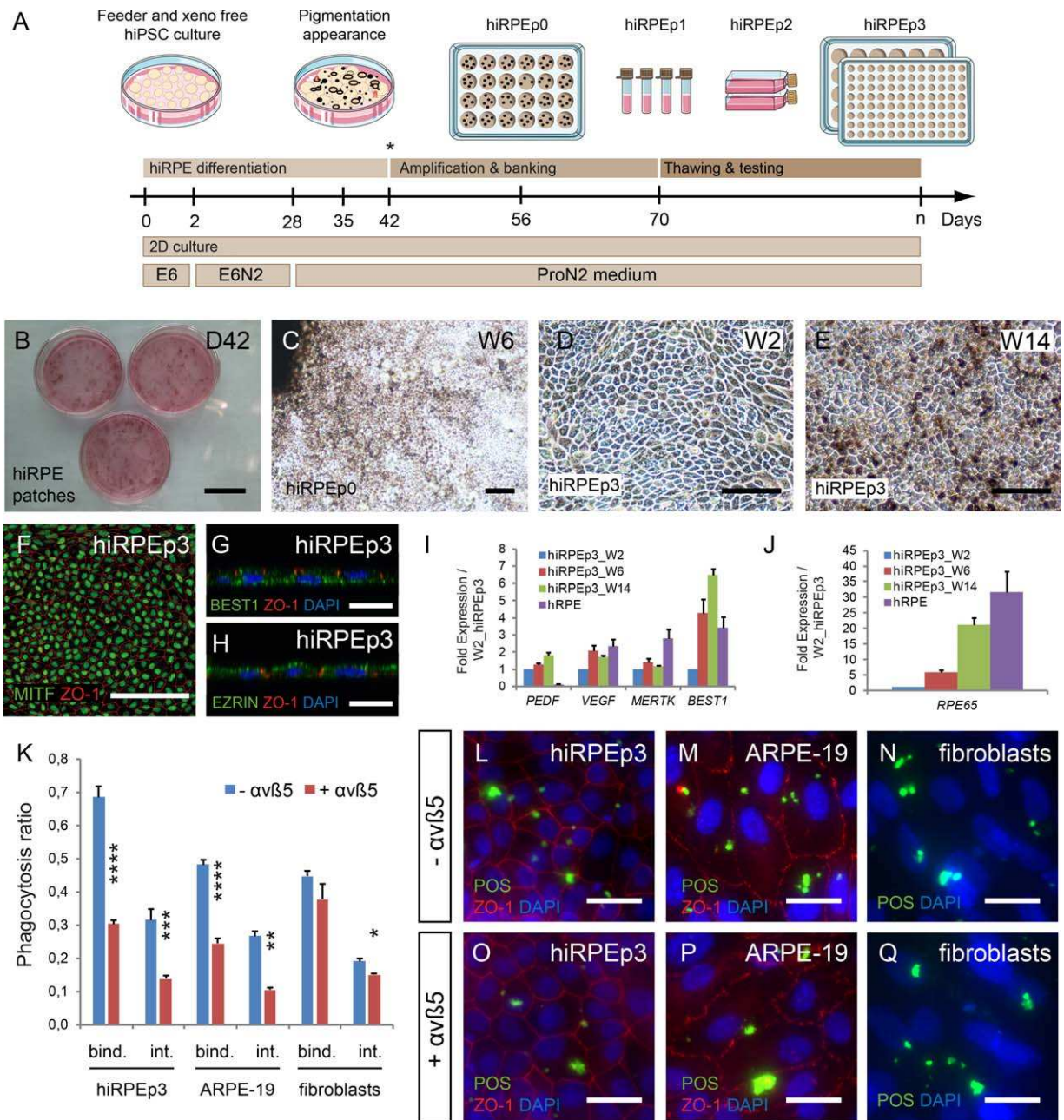


Figure 6. Generation and characterization of hiRPE cells in Xeno-Free and Feeder-Free conditions. **(A):** Schematic diagram illustrating different steps for the generation, amplification, and storage of RPE cells from adherent culture of iPSCs hiPSCs. (*) Pigmented patch picking time. **(B):** Phase-contrast images of pigmented patches of hiRPE cells from hiPSC-2 at D42. Scale bar = 3 cm. **(C–E):** Phase-contrast images of hiRPE cells at passage 0 (hiRPEp0) and at passage 3 (hiRPEp3), respectively, at 6 weeks (W6) after picking and at W2 or W14 after passaging. Scale bars = 100 μm. **(F):** MITF and ZO-1 immunostaining of hiRPEp3 cells, 2 weeks in culture after thawing. Scale bar = 100 μm. **(G, H):** Z-stack confocal images showing typical polarized expression of BEST1 and ERZIN in hiRPEp3 cells. Scale bars = 10 μm. **(I, J):** RT-qPCR analysis of mature RPE-associated markers in hiRPEp3 cells cultured 2 (W2), 6 (W6), or 14 weeks (W14) after thawing. Data are normalized to hiRPEp3 cells at W2. **(K):** Evaluation of RPE cell phagocytic activity: ratios of FITC/DAPI fluorescence were evaluated in hiRPEp3 cells, ARPE-19 cell line and fibroblasts after 3 hours of incubation with FITC-labeled POS to determine binding and uptake of POS in absence (blue bars) or in presence (red bars) of function-blocking antibody anti αvβ5 integrin. Values represent the mean ± SD (*, *p* < .05; **, *p* < .01; ***, *p* < .005; ****, *p* < .001) from three separate experiments. **(L–Q):** Qualitative representation of internalization of FITC-labeled POS (green) by hiRPEp3, ARPE-19 and fibroblasts (nuclei counterstained in blue) in absence or in presence of the anti αvβ5 integrin blocking antibody. Scale bars = 25 μm.

of the CTS N2 supplement until D28 (Fig. 6A). After removal of self-forming retinal organoids, cell cultures were switched to ProN2 medium. Around D42, pigmented patches of cells were picked up and hiRPE cells were amplified from these patches (Fig. 6B, 6C). After 2 weeks, hiRPE cells at passage 1 (hiRPEp1)

were cryopreserved for cell banking and thawed hiRPE cells at passage 3 (hiRPEp3) were used for complete characterization (Fig. 6D, 6E). Generated epithelial cells were immunoreactive for the key RPE-specific transcription factor MITF and the tight junction marker ZO-1 (Fig. 6F). Counting the number of MITF⁺

cells confirmed the purity of the cell culture with $99.83\% \pm 0.31\%$ of positive cells ($n = 208,259$ cells). Immunostaining for BESTROPHIN (BEST1) and EZRIN showed a correct polarization of hiRPE cells in culture with the expression of these proteins at the basolateral membrane and the apical side of the cells, respectively, (Fig. 6G, 6H). RT-qPCR analysis also demonstrates that cells retained the expression of mature RPE-associated markers such as *PEDF*, *VEGF*, *MERTK*, and *BEST1* after freezing and at least for three additional passages (Fig. 6I). Long-term cultures of hiRPEp3 cells depicted a closer RPE phenotype to human primary cultures, particularly for *RPE65*, which is strongly expressed in adult human RPE cells (Fig. 6J). We investigated whether hiRPE cells after banking still exhibited typical native RPE functions. Using ELISA we showed vascular endothelial growth factor (VEGF) and pigment epithelium derived factor (PEDF) secretion by hiRPEp3 cells with respective values of 12.4 ± 0.5 ng/ml and 80.5 ± 8.8 ng/ml ($n = 3$). We also demonstrated the ability of hiRPEp3 cells to carry out specific phagocytosis of FITC-labeled POS similarly to the human immortalized RPE cell line ARPE-19 (Fig. 6K-6Q). Conversely to fibroblasts, POS phagocytosis by both hiRPE and ARPE-19 cells was blocked by an antibody against integrin $\alpha\beta5$, demonstrating the specificity of POS phagocytosis linked to this receptor by RPE cells, as previously demonstrated [37, 38].

DISCUSSION

In the current study, we propose a new protocol to generate retinal organoids and RPE cells from adherent hiPSCs using a defined XF/FF culture system amenable to future clinical grade production. To keep simple a protocol avoiding EB formation and the use of substrates such as Matrigel as previously described in xenogeneic condition [19, 28], retinal differentiation in the XF/FF culture conditions has required the assessment of critical points. We have determined the right time-point to start the differentiation of adherent hiPSCs, developed new chemical defined differentiation medium and established the optimal timing to collect emerging retinal organoids. The replacement of feeders by human vitronectin, which supported pluripotency of hESCs and hiPSCs in a XF defined medium [21], enables the generation of self-forming neuroretinal structures and RPE cells, when expanded iPSC colonies were placed in successive chemically-defined proneural media with animal-free CTS supplements (ThermoFisher Scientific). The endogenous production by hiPSCs of DKK1 and NOGGIN, two inducers of neural and retinal specification, could explain the self-formation of these structures, as previously reported [19]. The presence of recombinant human Insulin in the CTS N2 supplement, could play a similar role to that of IGF-1, generally added to promote the retinal lineage [9, 12]. Isolated structures cultured as floating retinal organoids in ProB27 medium allowed the differentiation of multipotent RPCs in all the retinal cell types in a sequential overlapping order, similar to the one we previously reported in xenogeneic conditions [19]. RGCs were detected as early as D35 followed by horizontal and amacrine cells, whereas mature photoreceptors, expressing OPSIN or RHODOPSIN, and bipolar or Müller glial cells were clearly identified after a D100. Interestingly, our culture conditions allowed the maintenance of both mature S and L/M cones and rods in retinal

organoids until D281 (>9 months). The presence of a specific photoreceptor ultrastructures confirms that our XF/FF conditions permit the maturation of photoreceptors with similar structures to those observed in the developing human retina [39]. Further evidence of the advanced level of maturation is the sensitivity of a proportion of hiPSC-derived photoreceptors to cGMP stimulation in a similar manner to native photoreceptors. Moreover, we demonstrated that adaptation of the tissue clearing procedure 3DISCO [29] to retinal organoids, allowed the analysis of fluorescently labeled retinal cells in transparent organoids while preserving original shape and structure. This approach provides a global view of retinal cell type development, spatial arrangement and connections within the organoids. When combined with high-resolution microscopy, this technique could be used for a rapid and efficient analysis of normal and pathological features in intact retinal organoids generated from patient-specific iPSCs.

For future cell therapy strategies based on purified photoreceptor precursors, our XF/FF protocol allows, in less than 100 days, the generation of CD73⁺ photoreceptor precursors, described as a transplantation-compatible cell population in mouse [34–36]. We have demonstrated that CD73 is a marker of photoreceptor precursors and continues to be expressed in differentiated photoreceptors, particularly cones expressing R/G or BLUE OPSIN, in contrast to mice where rare BLUE OPSIN cones do not express CD73 [40]. Since the transplantation in ONL-degenerated host retinas should also be considered, the intact neuroretinal tissue of the retinal organoids derived from hiPSCs in XF/FF conditions could be of clinical utility, as recently proposed for hESC-derived retinal tissues [41]. In this context of retinal sheet transplantation, the ontogenic stages of differentiated tissues from hESCs or hiPSCs should be clearly defined for successful transplantation. Nevertheless, a therapeutic translation of these cells would require a constant production in terms of cell quantity and consistency that it is not likely to be achieved with a fresh cell therapy product (CTP). Therefore, developing an adequate cryopreservation of the CTP is a crucial aspect to ensure a continual delivery of the cell population of interest. Cryopreservation of the whole retinal organoids demonstrated that in frozen-thawed structures the CD73⁺ photoreceptor precursor population is preserved. This should make it possible to prepare large-scale stocks of retinal organoids at specific stages to deliver pure transplantation-competent CD73⁺ cells when needed. Furthermore, our freezing method enables the cryopreservation of dissociated retinal cells including photoreceptor precursors without loss of membrane expression of CD73. This observation highlights the alternative possibility of using thawed dissociated retinal cells and potentially a thawed and homogenous population of CD73⁺ cells for cell transplantation. However, it will be important to determine what kind of cryopreservation process and purification method induces less cell stress and would be the most effective for subretinal grafting.

In addition to photoreceptor precursors, the production of hiPSC-derived RGCs in our XF/FF conditions could have important implications for the treatment of retinal dystrophies affecting the RGCs such as glaucoma. The fast emergence of RGCs in organoids and the use of CTSTM B27-containing medium that keeps them alive longer compared to N2-containing medium [19], should facilitate the development of cell-based

therapy approaches using hiPSC-derived RGCs. Our cryopreservation technique would be useful to freeze retinal organoids at relatively early stages (before day 50) to make frozen stocks of RGC precursors that could be delivered when needed.

Concomitantly to the neural retina, our protocol allows the generation of RPE cells from hiPSCs that can be easily amplified, passaged and frozen while retaining a proper RPE phenotype and RPE specific functions such as POS phagocytosis and trophic factor secretion. Gene expression assays indicated that hiRPE cell maturation could be achieved by extending the length of culture time. Large-scale production of hiRPE cells can be reached with our XF/FF conditions, since one 6-cm² dish can produce up to 500 millions of hiRPE cells after three passages. Based on previous reports, using either hESC-derived RPE cells in suspension [25] or sheets of hiPSC-derived RPE cells [42], we believe that the XF/FF differentiation protocol reported here could deliver sufficient quantities of cells to perform several thousands of injections. A large-scale production of these cells could be required with the future development of global haplotype hiPSC banking, where a limited number of cell lines with common HLA haplotypes will be derived in order to match a significant portion of the patient population [43, 44].

CONCLUSION

The present study shows that simple and efficient retinal differentiation of adherent hiPSCs can be accomplished in XF/FF environment near to clinical conditions with the use of minimal and GMP-compatible raw materials. This new method is amenable to the development of an in vitro GMP-compliant retinal cell manufacturing protocol allowing for large-scale production and banking of hiPSC-derived retinal cells and tissues. Human iPSCs used in this study have been generated by a nonintegrative approach, thus addressing one major limitation for future clinical applications of hiPSCs generated from integrative delivery systems. Considering these advances, future cell therapy requiring transplantation of RGCs, photoreceptors or RPE cells to treat retinal degeneration could be achieved.

ACKNOWLEDGMENTS

We are grateful to G. Toutirais (Electronic microscopy facility, UPMC-Paris 6) for performing TEM analysis, Dr. C. Craft (Mary D. Allen Laboratory for Vision Research, USC ROSKI Eye

Institute) for cone arrestin antibody and Dr. M. Garita-Hernandez for critical reading. We thank S. Fouquet and D. Godefroy from the imaging facility and M. Lechuga from the automated high content analysis platform, both supported by “Département de Paris and by Région Ile de France” and Dr. N. Oudrhiri and Prof. A. Bennaceur, (Service d’hématologie cytogénétique GHU Paris-Sud APHP, INGESTEM ANR Programme Investissements d’Avenir) for the conventional cytogenetic analysis. This work was supported by grants from the Agence Nationale de la Recherche (ANR) [GPIPS: ANR-2010-RFCS005], the Accelerating Technology Transfer SATT Lutec (CelliPSight), the “Fondation pour la Recherche Médicale” (Bio-engineering program - DBS20140930777) and the Retina France association to O.G. This work was also performed in the frame of the LABEX LIFESENSES [ANR-10-LABX-65] supported by the ANR within the Programme Investissements d’Avenir [ANR-11-IDEX-0004-02]. A.T. was supported by a grant from the Fondation de France (Berthe Fouassier) and O.R. from the Fédération des Aveugles et des Handicapés Visuels de France.

AUTHOR CONTRIBUTIONS

S.R.: Conception and design, collection and/or assembly of data, data analysis and interpretation, manuscript writing, final approval of manuscript; A.S.: Conception and design, collection and/or assembly of data, data analysis and interpretation, final approval of manuscript; G.G.: Collection and/or assembly of data, data analysis and interpretation, manuscript writing, final approval of manuscript; A.C.: Collection and/or assembly of data, data analysis and interpretation, final approval of manuscript; A.T.: Collection and/or assembly of data; C.N.: Collection and/or assembly of data; A.P.: Provision of study material; M.B.: Provision of study material; O.R.: Provision of study material; J.D.: Provision of study material; G.O.: Provision of study material; E.N.: Collection and/or assembly of data, data analysis and interpretation, final approval of manuscript; J.-A.S.: Administrative and financial support, final approval of manuscript; O.G.: Financial support, conception and design, collection and/or assembly of data, data analysis and interpretation, manuscript writing, final approval of manuscript

DISCLOSURE OF POTENTIAL CONFLICTS OF INTEREST

The authors indicate no potential conflicts of interest.

REFERENCES

- Osakada F, Ikeda H, Mandai M et al. Toward the generation of rod and cone photoreceptors from mouse, monkey and human embryonic stem cells. *Nat Biotechnol* 2008; 26:215–224.
- Idelson M, Alper R, Obolensky A et al. Directed differentiation of human embryonic stem cells into functional retinal pigment epithelium cells. *Cell Stem Cell* 2009;5:396–408.
- Krohne TU, Westenskow PD, Kurihara T et al. Generation of retinal pigment epithelial cells from small molecules and OCT4 reprogrammed human induced pluripotent stem cells. *STEM CELLS TRANSL MED* 2012;1:96–109.

- Kokkinaki M, Sahibzada N, Golestaneh N. Human induced pluripotent stem-derived retinal pigment epithelium (RPE) cells exhibit ion transport, membrane potential, polarized vascular endothelial growth factor secretion, and gene expression pattern similar to native RPE. *STEM CELLS* 2011;29:825–835.
- Zahabi A, Shahbazi E, Ahmadi H et al. A new efficient protocol for directed differentiation of retinal pigmented epithelial cells from normal and retinal disease induced pluripotent stem cells. *Stem Cells Dev* 2012;21:2262–2272.
- Buchholz DE, Pennington BO, Croze RH et al. Rapid and efficient directed

differentiation of human pluripotent stem cells into retinal pigmented epithelium. *STEM CELLS TRANSL MED* 2013;2:384–393.

- Maruotti J, Wahlin K, Gorrell D et al. A simple and scalable process for the differentiation of retinal pigment epithelium from human pluripotent stem cells. *STEM CELLS TRANSL MED* 2013;2:341–354.
- Meyer JS, Shearer RL, Capowski EE et al. Modeling early retinal development with human embryonic and induced pluripotent stem cells. *Proc Natl Acad Sci USA* 2009;106:16698–16703.
- Zhu Y, Carido M, Meinhardt A et al. Three-dimensional neuroepithelial culture

from human embryonic stem cells and its use for quantitative conversion to retinal pigment epithelium. *PLoS One* 2013;8:e54552.

10 Zhou S, Flamier A, Abdouh M et al. Differentiation of human embryonic stem cells into cone photoreceptors through simultaneous inhibition of BMP, TGF β and Wnt signaling. *Development* 2015;142:3294–3306.

11 Yanai A, Laver CRJ, Joe AW et al. Differentiation of human embryonic stem cells using size-controlled embryoid bodies and negative cell selection in the production of photoreceptor precursor cells. *Tissue Eng Part C Methods* 2013;19:755–764.

12 Lamba DA, Karl MO, Ware CB et al. Efficient generation of retinal progenitor cells from human embryonic stem cells. *Proc Natl Acad Sci USA* 2006;103:12769–12774.

13 Tucker BA, Mullins RF, Streb LM et al. Patient-specific iPSC-derived photoreceptor precursor cells as a means to investigate retinitis pigmentosa. *Elife* 2013;2:e00824.

14 Mellough CB, Sernagor E, Moreno-Gimeno I et al. Efficient stage-specific differentiation of human pluripotent stem cells toward retinal photoreceptor cells. *STEM CELLS* 2012;30:673–686.

15 Meyer JS, Howden SE, Wallace KA et al. Optic vesicle-like structures derived from human pluripotent stem cells facilitate a customized approach to retinal disease treatment. *STEM CELLS* 2011;29:1206–1218.

16 Nakano T, Ando S, Takata N et al. Self-formation of optic cups and storable stratified neural retina from human ESCs. *Cell Stem Cell* 2012;10:771–785.

17 Zhong X, Gutierrez C, Xue T et al. Generation of three-dimensional retinal tissue with functional photoreceptors from human iPSCs. *Nat Commun* 2014;5:4047.

18 Mellough CB, Collin J, Khazim M et al. IGF-1 signalling plays an important role in the formation of three dimensional laminated neural retina and other ocular structures from human embryonic stem cells. *STEM CELLS* 2015;33:2416–2430.

19 Reichman S, Terray A, Slembrouck A et al. From confluent human iPSC cells to self-forming neural retina and retinal pigmented epithelium. *Proc Natl Acad Sci USA* 2014;111:8518–8523.

20 Singh RK, Mallela RK, Cornuet PK et al. Characterization of three-dimensional retinal tissue derived from human embryonic stem

cells in adherent monolayer cultures. *Stem Cells Dev* 2015;24:2778–2795.

21 Chen G, Gulbranson DR, Hou Z et al. Chemically defined conditions for human iPSC derivation and culture. *Nat Methods* 2011;8:424–429.

22 Vaajasaari H, Ilmarinen T, Juuti-Uusitalo K et al. Toward the defined and xeno-free differentiation of functional human pluripotent stem cell-derived retinal pigment epithelial cells. *Mol Vis* 2011;17:558–575.

23 Pennington BO, Clegg DO, Melkoulmian ZK et al. Defined culture of human embryonic stem cells and xeno-free derivation of retinal pigmented epithelial cells on a novel, synthetic substrate. *STEM CELLS TRANSL MED* 2015;4:165–177.

24 Plaza RA, Petrus-Reurer S, Antonsson L et al. Xeno-free and defined human embryonic stem cell-derived retinal pigment epithelial cells functionally integrate in a large-eyed preclinical model. *Stem Cell Rep* 2015;6:1–9.

25 Schwartz SD, Tan G, Hosseini H et al. Subretinal transplantation of embryonic stem cell-derived retinal pigment epithelium for the treatment of macular degeneration: An assessment at 4 years. *Invest Ophthalmol Vis Sci* 2016;57:ORSFc1–ORSFc9.

26 Tucker BA, Anfinson KR, Mullins RF et al. Use of a synthetic xeno-free culture substrate for induced pluripotent stem cell induction and retinal differentiation. *STEM CELLS TRANSL MED* 2013;2:16–24.

27 Sridhar A, Steward MM, Meyer JS. Non-xenogeneic growth and retinal differentiation of human induced pluripotent stem cells. *STEM CELLS TRANSL MED* 2013;2:255–264.

28 Reichman S, Goureau O. Production of retinal cells from confluent human iPSC cells. *Methods Mol Biol* 2016;1357:339–351.

29 Belle M, Godefroy D, Dominici C et al. A simple method for 3D analysis of immunolabeled axonal tracts in a transparent nervous system. *Cell Rep* 2014;9:1191–1201.

30 Fuhrmann S. Eye morphogenesis and patterning of the optic vesicle. *Curr Top Dev Biol* 2010;93:61–84.

31 Mathers PH, Jamrich M. Regulation of eye formation by the Rx and pax6 homeobox genes. *Cell Mol Life Sci* 2000;57:186–194.

32 MacLaren RE, Pearson RA, MacNeil A et al. Retinal repair by transplantation of photoreceptor precursors. *Nature* 2006;444:203–207.

33 Barber AC, Hippert C, Duran Y et al. Repair of the degenerate retina by photoreceptor transplantation. *Proc Natl Acad Sci USA* 2013;110:354–359.

34 Lakowski J, Han Y-T, Pearson RA et al. Effective transplantation of photoreceptor precursor cells selected via cell surface antigen expression. *STEM CELLS* 2011;29:1391–1404.

35 Eberle D, Schubert S, Postel K et al. Increased integration of transplanted CD73-positive photoreceptor precursors into adult mouse retina. *Invest Ophthalmol Vis Sci* 2011;52:6462–6471.

36 Ferreira TS, Postel K, Stutzki H et al. Daylight vision repair by cell transplantation. *STEM CELLS* 2015;1:1–15.

37 Finnemann SC, Bonilha VL, Marmorstein AD et al. Phagocytosis of rod outer segments by retinal pigment epithelial cells requires $\alpha(v)\beta 5$ integrin for binding but not for internalization. *Proc Natl Acad Sci USA* 1997;94:12932–12937.

38 Nandrot EF, Anand M, Almeida D et al. Essential role for MFG-E8 as ligand for $\alpha v \beta 5$ integrin in diurnal retinal phagocytosis. *Proc Natl Acad Sci USA* 2007;104:12005–12010.

39 Hollenberg MJ, Spira AW. Human retinal development: Ultrastructure of the outer retina. *Am J Anat* 1973;137:357–385.

40 Koso H, Minami C, Tabata Y et al. CD73, a novel cell surface antigen that characterizes retinal photoreceptor precursor cells. *Invest Ophthalmol Vis Sci* 2009;50:5411–5418.

41 Shirai H, Mandai M, Matsushita K et al. Transplantation of human embryonic stem cell-derived retinal tissue in two primate models of retinal degeneration. *Proc Natl Acad Sci USA* 2016;113:201512590.

42 Kamao H, Mandai M, Okamoto S et al. Characterization of human induced pluripotent stem cell-derived retinal pigment epithelium cell sheets aiming for clinical application. *Stem Cell Rep* 2014;2:205–218.

43 Taylor CJ, Peacock S, Chaudhry AN et al. Synthesis generating an iPSC bank for HLA-matched tissue transplantation based on known donor and recipient HLA types. *Cell Stem Cell* 2012;11:147–152.

44 Wilmut I, Leslie S, Martin NG et al. Development of a global network of induced pluripotent stem cell haplobanks. *Regen Med* 2015;10:235–238.



See www.StemCells.com for supporting information available online.

Supplemental Information

Supplemental Materials and Methods

Cryosection

For cryosectioning, retinal organoids were fixed for 15 min in 4% paraformaldehyde at 4°C and washed in PBS. Structures were incubated at 4°C in PBS / 30% Sucrose (Sigma-Aldrich) solution during at least 2 hrs. Structures were embedded in a solution of PBS, 7.5% gelatin (Sigma-Aldrich), 10% sucrose and frozen in isopentane at -50°C. 10 µm-thick cryosections were collected in two perpendicular planes.

Cell dissociation

Floating retinal organoids were collected at D84 or D100. Distal pigmented RPE was discarded from the structures under a stereomicroscope and retinal structures were washed 3 times in Ringer solution (NaCl 155 mM; KCl 5 mM; CaCl₂ 2 mM; MgCl₂ 1 mM; NaH₂PO₄ 2 mM; HEPES 10 mM and Glucose 10 mM). RPE-free retinal organoids were dissociated with two units of pre-activated papain at 28.7 u/mg (Worthington) in Ringer solution during 25 min at 37°C. When cells were homogeneously resuspended with up and down pipetting, then papain was deactivated by adding 1 ml of ProB27 medium. Cells were centrifuged and resuspended in pre-warmed ProB27 medium. Retinal cells were plated in 24 well-plates previously coated with Poly-D-Lysin at 2 µg/cm² and Laminin at 1 µg/cm² (Sigma-Aldrich). Dissociated cells were incubated at 37°C in a standard 5% CO₂ / 95% air incubator and medium was changed every 2 days for the next 5 days, before immunostaining.

Calcium dye loading and two-photon calcium imaging.

Fura 2-AM (Thermo Fisher Scientific) was dissolved in dimethyl sulfoxide mixed with 20% Pluronic F-127 (Thermo Fisher Scientific) and then diluted to reach a final concentration of 10

μM . Dissociated retinal cells seeded on Poly-D-Lysin/Laminin-coated coverslips were dark adapted prior to every recording, and loaded with Fura2-AM (10 μM) for 45 min at 37°C in a standard incubator. Cells were then placed in the recording chamber of a 2-photon microscope and perfused (2 ml/min) with oxygenated (95% O₂/5% CO₂) AMES Ringer's solution (Sigma-Aldrich) for at least 1 hr, in the dark. Cells were later exposed to either 1 mM of 8-Br-cGMP (Sigma-Aldrich), diluted in AMES or AMES for control recordings. Glass pipettes (borosilicate glass capillaries) with a resistance of 4-5 M Ω , filled with the solutions and connected to a Picospritzer II pressure system (General Valve Corporation, pressure 5 psi) were used for applying 10 seconds puffs on small groups of recorded cells. Temperature was kept at 37°C for the duration of the experiment.

Imaging of cells stained by the Fura 2-AM dye was performed using a custom-made two-photon microscope equipped with a 25x water immersion objective (XLPlanN-25x-W-MP/NA1.05, Olympus) and a pulsed femto-second laser (InSightTM DeepSeeTM, Newport Corporation, Irvine, CA). Images were acquired using the excitation laser at a wavelength of 800 nm. Square regions (minimum 50x50 μm) of neighbor cells positioned in the puffing area were imaged and analyzed. For each experiment we started by recording 20 seconds of baseline spontaneous activity before puffing. The interval between two consecutive puff stimulations was at least two minutes. An increase in calcium concentration in a cell was detected as a decrease in Fura-2 fluorescence intensity, which was calculated using the formula $\% \Delta F/F_0$, in which $\Delta F = F - F_0$, and where F_0 was average baseline cell intensity during the 20 sec prestimulus period.

Immunostaining and imaging on retinal sections and dissociated retinal cells

Sections, retinal dissociated cells or hiRPE cells were fixed with 4% PAF in PBS for 5 min before immunostaining. After washes with PBS, nonspecific binding sites were blocked for 1 hr at room temperature with a PBS solution containing 0.2% gelatin and 0.25% Triton X-100 (blocking buffer) and then overnight at 4°C with the primary antibody (Table S1) [19, 45] diluted in blocking buffer. Slides were washed three times in PBS with 0.1% Tween and then incubated

for 1 hour at room temperature with appropriate secondary antibodies conjugated with either AlexaFluor 488, 594 or 647 (Interchim) diluted at 1:600 in blocking buffer with 4',6-diamidino-2-phenylindole (DAPI) diluted at 1:1000 to counterstain nuclei. TUNEL assays were performed using the in situ cell death detection kit, TMR red (Roche, Sigma-Aldrich) according to the manufacturer's recommendations. Fluorescent staining signals were captured with a DM6000 microscope (Leica Microsystems) equipped with a CCD CoolSNAP-HQ camera (Roper Scientific) or using an Olympus FV1000 confocal microscope equipped with 405, 488, 543 and 633 nm lasers. Confocal images were acquired using a 1.55 or 0.46 μm step size and corresponded to the projection of 20 to 40 optical sections.

Karyotype analysis

Samples for conventional cytogenetic analysis were prepared as previously described [46] with slight modifications. For obtention of mitotic preparations, cells were cultured 2 hours in E8 medium supplemented with 100 ng/ml Colcemid (ThermoFisher Scientific) before osmotic shock in 0.075 M KCl (ThermoFisher Scientific) and fixation with methanol/acetic acid solution (3:1). For each cell line, a minimum of 10 metaphases were analyzed.

RNA extraction and Taqman Assay

Total RNAs were extracted using Nucleospin RNA II kit (Macherey-Nagel) according to the manufacturer's protocol, and RNA yields and quality were checked with a NanoDrop spectrophotometer (Thermo Fischer Scientific). cDNA were synthesized from 250 ng of mRNA using the QuantiTect reverse transcription kit (Qiagen) following manufacturer's recommendations. Synthesized cDNA were then diluted at 1/20 in DN^{ase}-free water before performing quantitative PCR. qPCR analysis was performed on a Applied Biosystems real-time PCR machine (7500 Fast System) with custom TaqMan® Array 96-Well Fast plates and TaqMan® Gene expression Master Mix (Thermo Fischer Scientific) following manufacturer's instructions. All primers and MGB probes labeled with FAM for amplification (Table S2) were purchased from Thermo Fischer Scientific. Results were normalized against 18S and

quantification of gene expression was based on the DeltaCt Method in three minimum independent biological experiments.

Transmission electron microscopy (TEM)

Retinal organoids were fixed with 2% glutaraldehyde and 1% PAF in 0.1 M PBS (pH 7.4), for 1 hr at room temperature and washed in PBS. Samples were postfixed in 1% osmium-bidistilled water for 1 hr at room temperature. After washes in bidistilled water, the samples were dehydrated in increasing concentrations of ethanol. Samples were then infiltrated in 1:1 ethanol: epon resin for 1 hr and finally 100% epon resin for 48 hrs at 60°C for polymerization. 70 nm-thick sections were cut with an ultracut UCT microtome (Leica Microsystems) and picked up on copper rhodium-coated grids. Grids were stained for 2 min in Uranylless (DELTA Microscopies) and for 5 min in 0,2% lead citrate and further analyzed on an electron microscope (EM 912 OMEGA, ZEISS) at 80 kV. Images were captured with digital camera (Side-Mounted TEM CCD, Veleta 2kx2k).

VEGF and PEDF ELISA

HiRPEp3 (hiPSC-2) were plated at 50 000 cells/cm² and cultured in ProN2 medium. The cultured medium from confluent hiRPE p3 cells was collected 48hrs after the medium change and stored at -80°C until the assay was performed. VEGFA and PEDF secretion levels were measured by respectively the Human VEGF Quantikine ELISA kit and the Human SerpinF1/PEDF DuoSet ELISA (R&D Systems), according to the manufacturer's instructions.

Phagocytosis assay.

Banked hiRPE cells at passage1 were thawed, cultured and confluent hiRPE cells were plated onto 96-well CellStart®-coated plates at 5x10⁴ cells/cm² and cultured in ProN2 medium for at least 4 weeks before the phagocytosis assay. HiRPEp3 cells were challenged for 3 hrs with 1×10⁶ FITC-labeled photoreceptor outer segments (POS) before detection of surface-bound and internalized FITC-POS particles according to established procedures [37]. Each well was

rinsed three times with PBS containing 1 mM MgCl₂ and 0.2 mM CaCl₂ (PBS-CM). For exclusive detection of internalized particles, fluorescence of surface-bound FITC-POS was selectively quenched by incubation in 0.2% trypan blue in PBS-CM for 10 min before cell fixation. Cells were fixed by incubation in ice cold methanol for 5 min followed by rehydration and incubation for 10 min at room temperature with DAPI for nuclei counterstaining. Fluorescent signals were quantified with the Infinite M1000 Pro (Tecan) and cells were imaged with a DM6000 microscope equipped with a CCD CoolSNAP-HQ camera.. To assess the specificity of the POS phagocytosis machinery used, cells were pre-incubated 30 min in the presence of 50 µg/ml of the anti-integrin $\alpha v\beta 5$ (function blocking antibody, P1F6 Millipore) and subsequently during POS phagocytosis as described above. The human ARPE-19 cell line was used as a positive control for phagocytic activity, and fibroblasts were used as a negative control for the phagocytic machinery used for POS uptake.

Statistical analysis

Statistical analysis was performed using Prism 6 (GraphPad software) with unpaired parametric Student's *t* test with Welch's correction for unequal variances when required (one-to-one comparisons). Values of $P < 0.05$ were considered statistically significant.

Supplemental References

45. Li A, Zhu X, Brown B, et al. Gene expression networks underlying retinoic acid-induced differentiation of human retinoblastoma cells. *Invest. Ophthalmol. Vis. Sci.* 2003;44(3):996–1007.
46. Tosca L, Feraud O, Magniez A, et al. Genomic instability of human embryonic stem cell lines using different passaging culture methods. *Mol. Cytogenet.* 2015;8:30.

Table S1. List of antibodies used for immunohistochemistry analysis.

Antigen	Species	Dilution	Source
Acetylated TUBULIN	Mouse monoclonal	1:1000	Sigma
AP2	Mouse monoclonal	1:100	DSHB
BESTROPHIN	Mouse monoclonal	1:1000	Novus
BLUE OPSIN	Rabbit polyclonal	1:500	Millipore
BRN3A	Mouse monoclonal	1:250	Millipore
CD73	Mouse monoclonal	1:100	BioLegend
CONE ARRESTIN	Rabbit polyclonal	1:2000	Millipore
	Rabbit polyclonal	1:10 000	gift from Dr C. Craft
CRX	Mouse monoclonal	1:5000	Abnova
EZRIN	Mouse monoclonal	1:250	Sigma
GLUTAMIN SYNTHASE	Mouse monoclonal	1:500	Millipore
KI67	Mouse monoclonal	1:200	BD Pharmagen
LIM1 (LHX1)	Mouse monoclonal	1:20	DSHB
LHX2	Goat polyclonal	1:100	Santa Cruz
MITF	Mouse monoclonal	1:200	DAKO
OCT4	Rabbit monoclonal	1:100	Cell Signaling
R/G OPSIN	Rabbit polyclonal	1:500	Millipore
OTX2	Rabbit polyclonal	1:5000	Millipore
PAX6	Rabbit polyclonal	1:1000	Millipore
PKC α	Rabbit polyclonal	1:5000	Santa Cruz
RAX/RX	Rabbit polyclonal	1:10 000	Abcam
RHODOPSIN	Mouse monoclonal	1:250	Millipore
RECOVERIN	Rabbit polyclonal	1:2000	Millipore
SSEA4	Mouse monoclonal	1:200	Cell Signaling
SOX2	Rabbit monoclonal	1:400	Cell Signaling
SOX9	Rabbit polyclonal	1:1000	Millipore
TRA1-60	Mouse monoclonal	1:100	Cell Signaling
VSX2 (CHX10)	Goat polyclonal	1:2000	Santa Cruz
ZO1	Rabbit polyclonal	1:250	ThermoFischer Sci

Table S2. List of TaqMan® Gene Expression ID Assays used for qRT-PCR:

Gene Symbols	Assays IDs
18S	18S-Hs99999901_s1
BEST1	BEST1-Hs00188249_m1
BLUE OPSIN	OPN1SW-Hs00181790_m1
BRN3A	POU4F1-Hs00366711_m1
BRN3B	POU4F2-Hs00231820_m1
CONE ARRESTIN	ARR3-Hs00182888_m1
CRX	CRX-Hs00230899_m1
DKK1	DKK1-Hs00183740_m1
DNMT3B	DNMT3B-Hs00171876_m1
GAD2	GAD2-Hs00609534_m1
GDF3	GDF3-Hs00220998_m1
GLAST1	SLC1A3-Hs00188193_m1
LHX2	LHX2-Hs00180351_m1
LIM1	LHX1-Hs00232144_m1
LIN28A	LIN28A-Hs00702808_s1
MERTK	MERTK-Hs01031973_m1
MITF	MITF-Hs01117294_m1
NANOG	NANOG-Hs02387400_g1
NEUROD1	NEUROD1-Hs00159598_m1
NODAL	NODAL-Hs00415443_m1
NOGGIN	NOG-Hs00271352_s1
NRL	NRL-Hs00172997_m1
OCT4 (POU5F1)	POU5F1-Hs00999632_g1
PAX6	PAX6-Hs00240871_m1
PDEF	SERPINF1-Hs01106934_m1
PKCα	PRKCA-Hs00925195_m1
R/G OPSIN	OPN1MW-Hs00241039_m1
RAX	RAX-Hs00429459_m1
RECOVERIN	RCVRN-Hs00610056_m1
RHODOPSIN	RHO-Hs00892431_m1
RLBP1	RLBP1-Hs00165632_m1
RPE65	RPE65-Hs01071462_m1
SIX3	SIX3-Hs00193667_m1
TERT	TERT-Hs00972656_m1
VEGF	VEGFA-Hs00900055_m1
VSX2	VSX2-Hs00766959_s1

Supplemental figures

Goureau, Supplemental figure 1, top

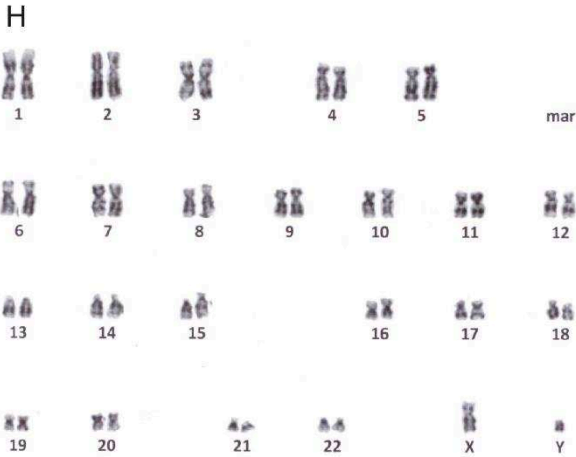
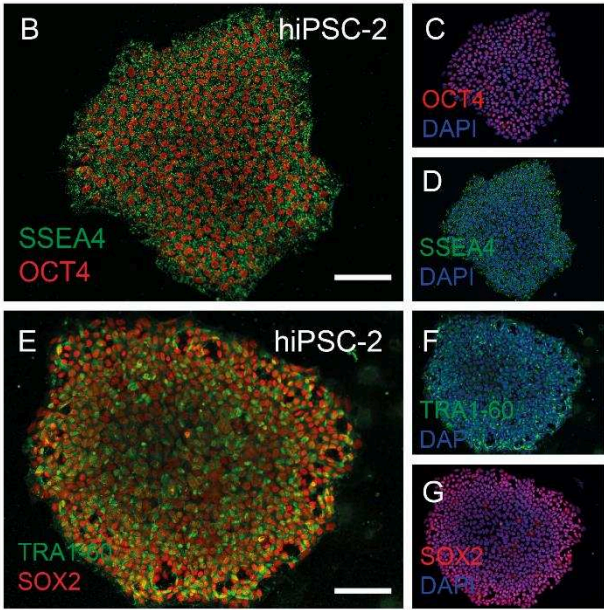
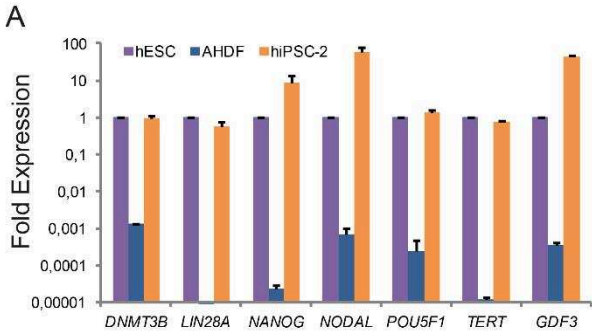


Figure S1: Characterization of integration-free hiPSCs (hiPSC-2) adapted to Xeno Free and Feeder Free conditions.

(A) RT-qPCR analysis of pluripotency and self-renewal markers in hESCs, hiPSC-2 and adult human dermal fibroblasts (AHDF). Data are normalized to hESCs. (B-G) Immunohistochemistry of pluripotency markers (SSEA4, OCT4, TRA1-60, and SOX2) in hiPSC-2. Scale bars = 100 μ m (H) Karyotype analysis of hiPSC-2.

Goureau, Supplemental figure 2, top

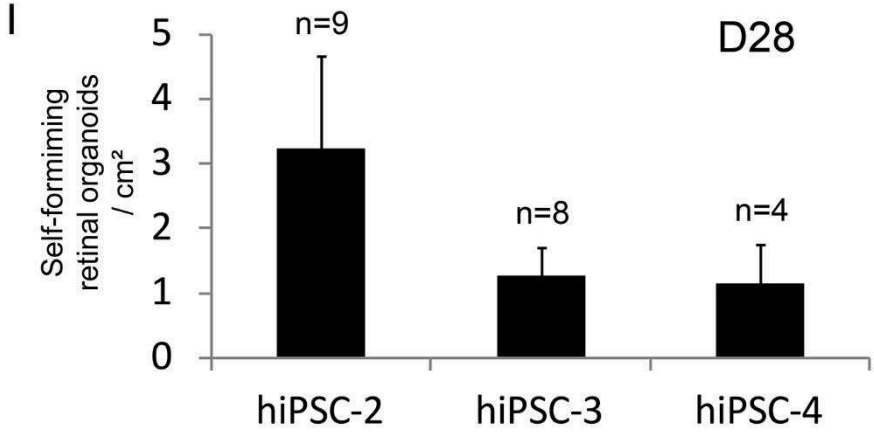
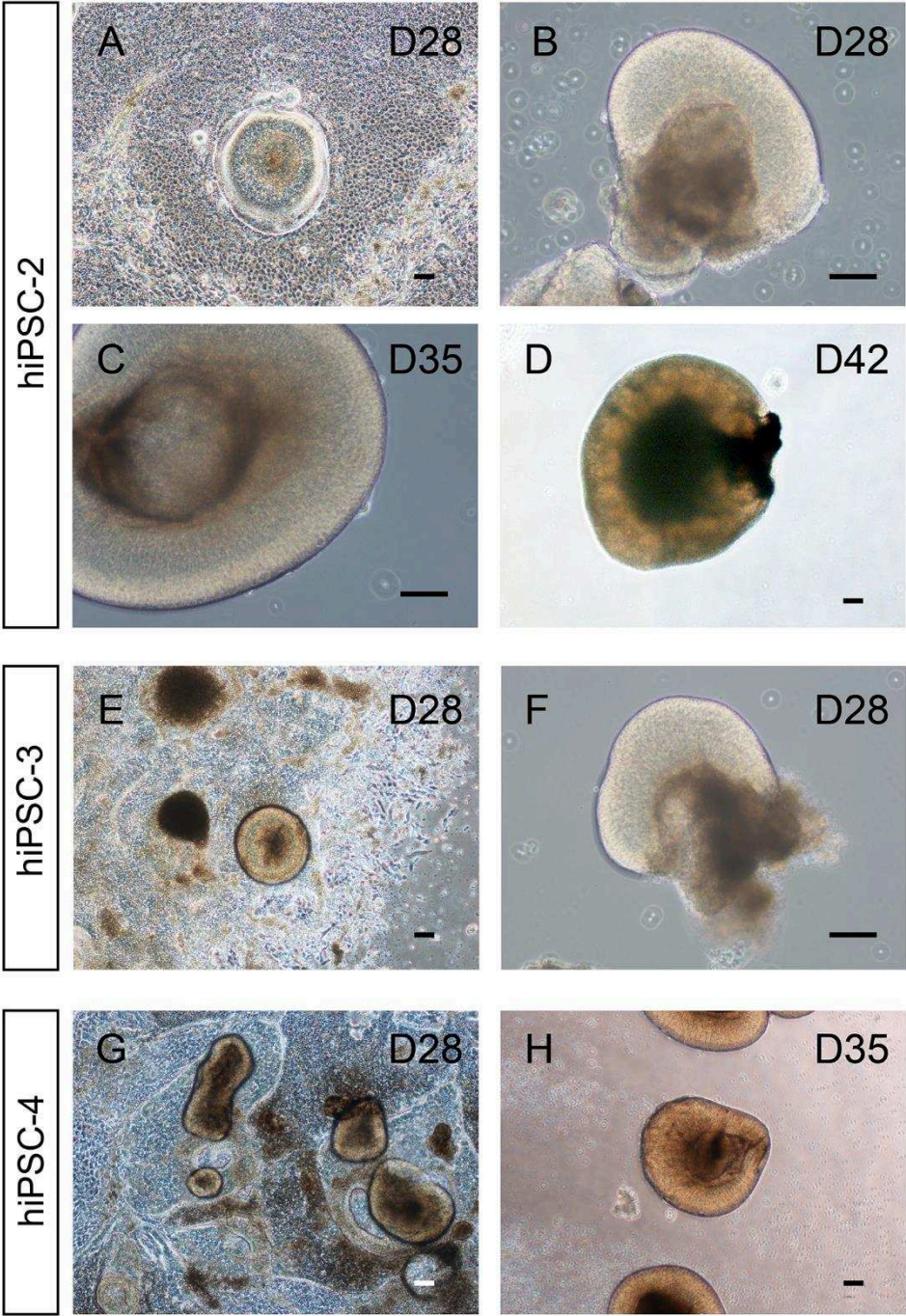


Figure S2: Reproducibility of the retinal organoid formation with different hiPSC lines.

Morphology of the self-forming neuroretina-like structures at D28 (A, E, G) and derived retinal organoids at D28 (B, F), D35 (C, H) and D42 (D), generated from three different integration-free hiPSCs: hiPSC-2 derived from adult dermal fibroblasts reprogrammed by an episomal approach (A-D); hiPSC-3 derived from neonatal foreskin fibroblasts reprogrammed by an episomal approach (E, F) and hiPSC-4 derived from adult dermal fibroblasts reprogrammed by the Sendai virus method (G, H). Scale bars = 100 μm . Efficiency of retinal organoid formation was determined by calculating the number of structures per cm^2 at D28 for the three different hiPSC lines (I). The number of independent differentiation experiments is noted for each hiPSC lines.

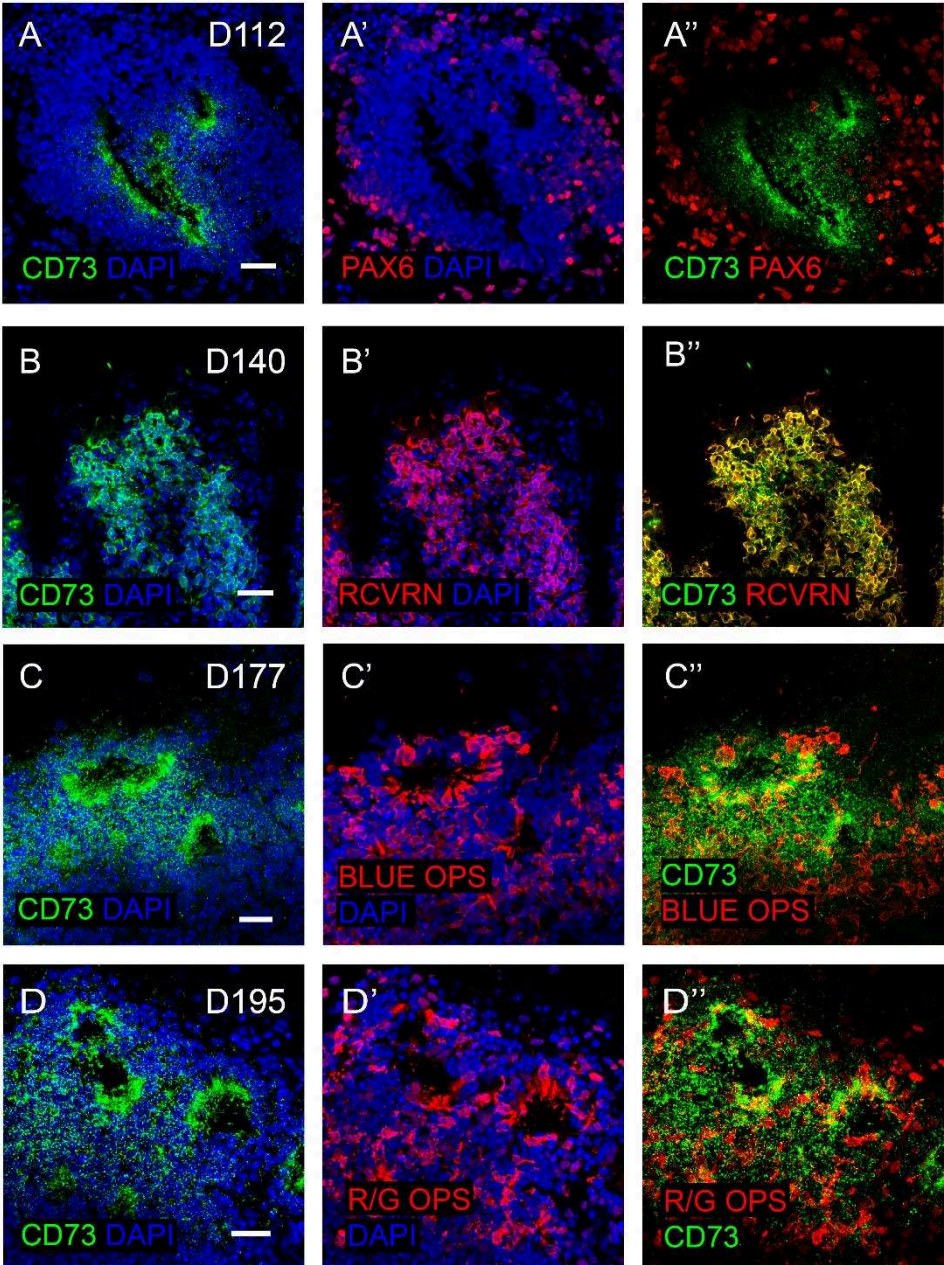


Figure S3: Expression of surface antigen CD73 in hiPSC-derived photoreceptors.

Immunofluorescence staining of cryosectioned retinal organoids at different times of differentiation for CD73 (A-D) and either PAX6 (A') or different photoreceptor markers, RECOVERIN (B'), BLUE OPSIN (C') and R/G OPSIN (D'). A" to D" correspond to merge image of panels A-A' to D-D' without DAPI staining, demonstrating the co-localization of CD73 exclusively with different photoreceptor markers. Scale bars = 25 μ m.

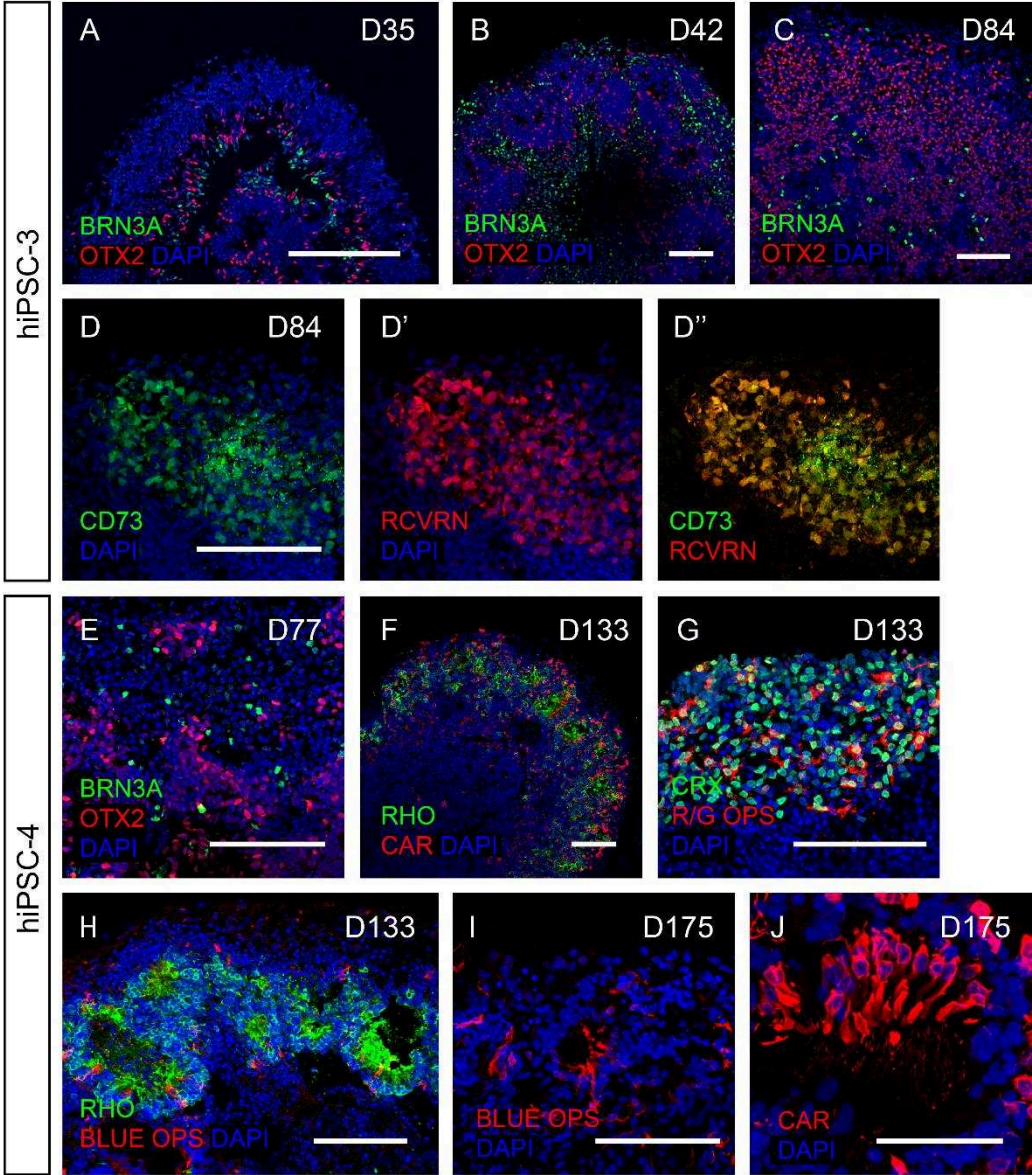


Figure S4: Efficient generation of RGCs and photoreceptors in retinal organoids derived from different hiPSC lines.

Immunofluorescence staining of cryosectioned retinal organoids derived from hiPSC-3 and hiPSC-4 at different times of differentiation using markers for RGCs (BRN3A) and photoreceptors (OTX2, RECOVERIN, CONE ARRESTIN, R/G OPSIN, RHODOPSIN, BLUE OPSIN). Scale bars = 100 μm (A-I), 50 μm (J).

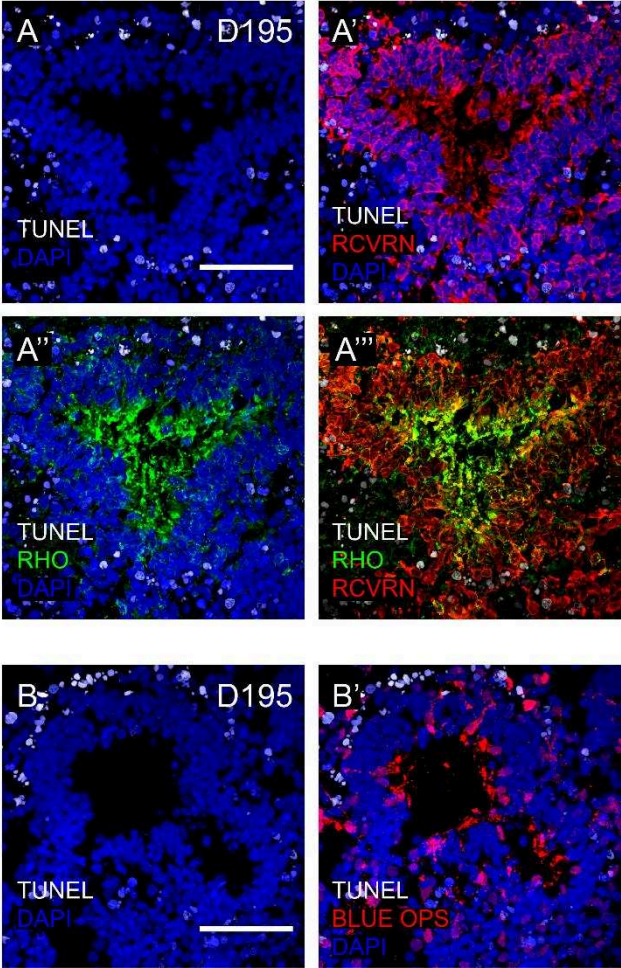


Figure S5: Absence of apoptosis in the rosettes containing hiPSC-derived photoreceptors. Immunohistological staining of D195-old retinal organoid sections for apoptotic cells (TUNEL) and photoreceptor markers, RECOVERIN (A', A'''), RHODOPSIN (A'', A''') and BLUE OPSIN (B'). Merged images showed no TUNEL-positive photoreceptors in the rosettes. Scale bars = 50 μ m.

Supplemental movie legends

Movie S1: 3D Movie of a D195 retinal organoid labelled with anti-Recoverin (green) and anti-Rhodopsin (red).

Movie S2: 3D Movie of a D195 retinal organoid labelled with anti-Cone Arrestin (green) and anti-Rhodopsin (red).

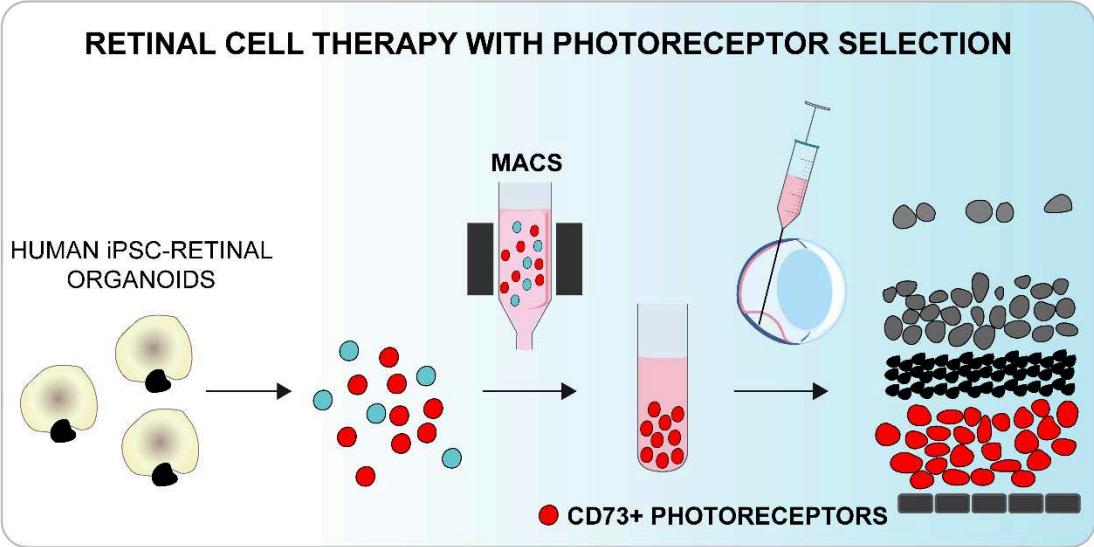
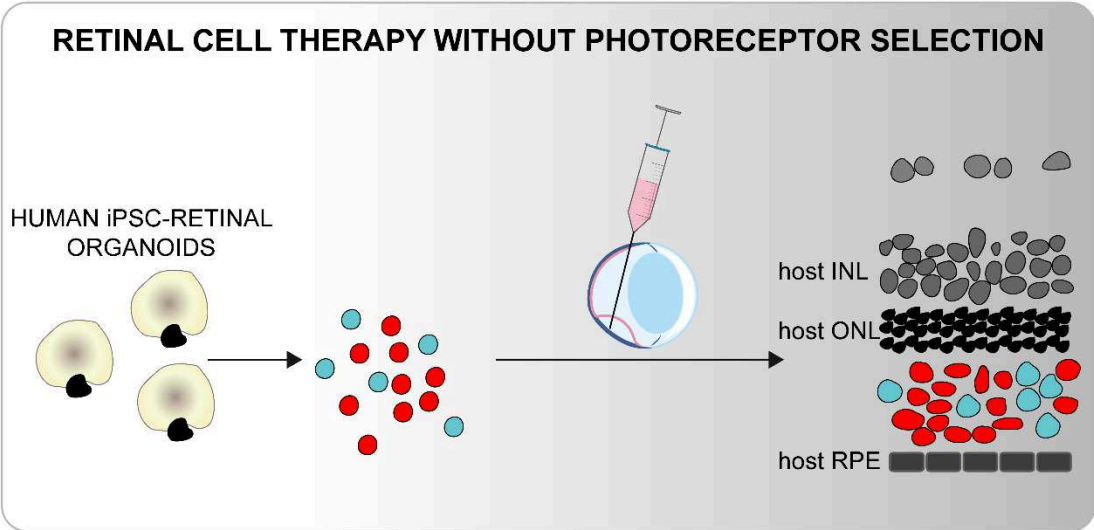
2. Separation and characterization of photoreceptor precursors from human retinal organoids by targeting of a cell surface antigen (Paper 2)

Having validated the expression of CD73 in retinal organoids generated with our xeno-free and feeder-free differentiation protocol (Reichman et al., 2017), we have proceeded with a deeper characterization of CD73-positive cells, in order to evaluate their utility for future treatments based on photoreceptor cell replacement.

In the article presented here, we could report the efficient separation of human iPSC-derived photoreceptors via CD73-based MACS, with both *in vitro* and *in vivo* characterization of CD73-positive cells isolated from retinal organoids. In addition, we used the CRISPR-Cas9 technology to generate a reporter iPSC line for the identification of cells committed into the photoreceptor lineage via the expression of the fluorescent protein mCherry. We used this approach to further confirm the photoreceptor identity of CD73-positive cells.

Absence of hyperproliferation following transplantation in immune-compromised hosts, the NUDE rats, demonstrated the safety of CD73 cells. Transplantation in the P23H rat model of RP confirmed that the selected population was homogenously composed by photoreceptors, which survived up to 2.5 months in the subretinal space after transplantation and expressed both rod and cone markers.

GRAPHICAL ABSTRACT



Article

Characterization and Transplantation of CD73-Positive Photoreceptors Isolated from Human iPSC-Derived Retinal Organoids

Giuliana Gagliardi,¹ Karim Ben M'Barek,² Antoine Chaffiol,¹ Amélie Slembrouck-Brec,¹ Jean-Baptiste Conart,¹ Céline Nanteau,¹ Oriane Rabesandratana,¹ José-Alain Sahel,^{1,3,4} Jens Duebel,¹ Gael Orieux,¹ Sacha Reichman,¹ and Olivier Goureau^{1,*}

¹Institut de la Vision, Sorbonne Université, INSERM, CNRS, 17, Rue Moreau, Paris 75012, France

²INSERM U861, UEVE, CECS, AFM, Institute for Stem Cell Therapy and Exploration of Monogenic Diseases, Corbeil-Essonnes 91100, France

³CHNO des Quinze-Vingts, DHU Sight Restore, INSERM-DHOS CIC, Paris 1423, France

⁴Department of Ophthalmology, University of Pittsburgh School of Medicine, Pittsburgh, PA 15213, USA

*Correspondence: olivier.goureau@inserm.fr

<https://doi.org/10.1016/j.stemcr.2018.07.005>

SUMMARY

Photoreceptor degenerative diseases are a major cause of blindness for which cell replacement is one of the most encouraging strategies. For stem cell-based therapy using human induced pluripotent stem cells (hiPSCs), it is crucial to obtain a homogenous photoreceptor cell population. We confirmed that the cell surface antigen CD73 is exclusively expressed in hiPSC-derived photoreceptors by generating a fluorescent cone rod homeobox (Crx) reporter hiPSC line using CRISPR/Cas9 genome editing. We demonstrated that CD73 targeting by magnetic-activated cell sorting (MACS) is an effective strategy to separate a safe population of transplantable photoreceptors. CD73+ photoreceptor precursors can be isolated in large numbers and transplanted into rat eyes, showing capacity to survive and mature in close proximity to host inner retina of a model of photoreceptor degeneration. These data demonstrate that CD73+ photoreceptor precursors hold great promise for a future safe clinical translation.

INTRODUCTION

Retinal diseases caused by the cell death of photoreceptors (PRs) and/or supporting retinal pigment epithelium (RPE), such as age-related macular degeneration and retinitis pigmentosa, are the increasingly significant cause of incurable sight loss. Cell replacement represents a potential vision restoration strategy for advanced stage of disease with severe cell loss (Dalkara et al., 2016; Zhao et al., 2017). While RPE replacement alone may be used for specific disease indications, transplantation of PRs—as a retinal sheet or as a suspension of dissociated cells—is required after extensive PR degeneration (Jayakody et al., 2015; Santos-Ferreira et al., 2017; Zhao et al., 2017). Prior studies in animal models revealed that transplantation of post-mitotic PR precursors, isolated from mouse neonatal retinae, might be feasible (Pearson et al., 2012; Santos-Ferreira et al., 2015; Singh et al., 2013). Donor PRs derived from mouse pluripotent stem cells (PSCs) have been transplanted into the subretinal space (SRS) of different blind mice models, showing integration into the degenerating retina, differentiation into mature PRs, and formation of synaptic connections, possibly leading to partial recovery of visual function (Decembrini et al., 2014; Gonzalez-Cordero et al., 2013; Mandai et al., 2017; Santos-Ferreira et al., 2016a; Tucker et al., 2011). However, recent work has indicated that functional recovery may be achieved by transferring of cytoplasmic material from transplanted mouse PRs to remaining host PRs, rather than through real integration into the recipient outer nuclear layer

(ONL) (Decembrini et al., 2017; Ortin-Martinez et al., 2017; Pearson et al., 2016; Santos-Ferreira et al., 2016b; Singh et al., 2016). It is unclear whether human PRs may also be able to transfer cytoplasmic material to host cells (Zhu et al., 2017).

The most promising source for the unlimited generation of human PRs for cell therapy is represented by human PSCs. Different protocols have been reported allowing for the differentiation of both rod and cone PRs starting from a serum-free floating culture of embryoid body-like aggregates (SFEB) (Lamba et al., 2006; Meyer et al., 2009; Osakada et al., 2008). Considerable progress has been made over the last few years with 3D retinal organoid formation from an optimized SFEB system (Mellough et al., 2015; Nakanokawa et al., 2012; Tucker et al., 2013; Zhong et al., 2014) or from adherent human PSCs (Gonzalez-Cordero et al., 2017; Reichman et al., 2014). Some of these protocols have been recently adapted to Good Manufacturing Practice (GMP) guidelines required for the generation of transplantable cells for future clinical applications (Reichman et al., 2017; Sridhar et al., 2013; Wiley et al., 2016). Despite continuous improvements, efficiency in generating a homogeneous cell population of post-mitotic PR precursors, corresponding to the appropriate donor cell population for cell therapy, remains to be addressed. Ensuring safety is of particular importance; transplantable cells must be devoid of mitotically active cells or residual undifferentiated PSCs that could be teratogenic (Tucker et al., 2011). As genetic engineering or viral labeling of the cells are not suitable for clinical applications, several studies have

been focusing on the identification of cell surface markers characterizing precursor and mature PRs derived from human induced pluripotent stem cells (hiPSCs) and in human retina (Kaewkhaw et al., 2015; Lakowski et al., 2018; Welby et al., 2017). However, low levels of both purity and cell yields resulting from the separation approaches used so far require further optimization, representing a challenge for future applications.

Using our GMP-compliant retinal differentiation protocol (Reichman et al., 2017), we have demonstrated that PRs express the cell surface antigen CD73, previously described for the enrichment of mouse PSC-derived PRs (Lakowski et al., 2015; Santos-Ferreira et al., 2016a). In this study, we reported a complete characterization of CD73+ cells during maturation of hiPSC-derived retinal organoids and we demonstrated that the simple CD73-based magnetic-associated cell sorting (MACS) results in selection of PRs. Transplantation of isolated CD73+ PRs in a rat model of retinal degeneration supported the usefulness of our separation strategy, which could be implemented for the development of stem cell-based therapy to treat retinal diseases due to PR cell death.

RESULTS

Expression of CD73 in hiPSC-Derived Retinal Organoids

We first sought to determine the expression of the *NT5E* gene coding for the surface antigen CD73 during the maturation of hiPSC-derived retinal organoids, in floating culture conditions, based on our retinal differentiation protocol (Reichman et al., 2017). qRT-PCR analysis showed that *NT5E* (CD73) starts to be expressed at day 50 (D50); this expression sharply increases until 150 days of differentiation and is maintained in organoids at later stages of maturation. As expected, expression levels of PR-specific genes *CRX* and *RECOVERIN* (*RCVRN*) were also increased, with an earlier peak of induction around D100 (Figure 1A). CD73 was present in post-mitotic cells (Ki67⁻) committed in the PR lineage (Figure S1). PR precursors in retinal organoids could further differentiate in all PR subtypes, rods, and red/green and blue cones, as shown by the increased expression of rhodopsin (*RHO*), red/green opsin (*OPN1LW/MW*), and blue opsin (*OPN1SW*), respectively (Figure 1B). Evaluation of CD73 expression by flow cytometry indicated that the percentage of CD73+ cells steadily increased from 7% ± 12% at D85 to 55% ± 2% at D200 of differentiation (Figure 1C, n = 10 organoids from N ≥ 3 differentiations, **p < 0.01, Kruskal-Wallis test). Therefore, targeting the CD73+ cell population at different time of differentiation should result in isolating populations of either precursor or mature PRs (Figure 1D).

To evaluate if timing of CD73 expression was dependent on the hiPSC line used for the generation of the retinal organoids, we carried out additional characterization studies with another hiPSC line derived from adult Müller glial cells. Furthermore, to easily identify the entire PR population within the retinal organoids, we used this iPSC line to generate, using the CRISPR-Cas9 system, a fluorescent *CRX* hiPSC reporter line, in which a nuclear form of the fluorescent protein mCherry under the control of the mouse *Crx* promoter (Furukawa et al., 2002) was inserted into the AAVS1 site (Figure S2A). We selected a puromycin-resistant clone (*CRX-c2*), carrying a copy of the insert in both AAVS1 locus (Figure S2B) for further retinal differentiation. qRT-PCR analysis of *NT5E* and PR-specific gene expression in retinal organoids from AAVS1:*CrxP_H2BmCherry* hiPSC line (Figures S2C and S2D) led to similar results obtained on organoids from hiPSC line 2 (Figures 1A and 1B). In whole retinal organoids, endogenous mCherry signal was visible by D49 and it allowed tracing the differentiating mCherry+ PRs (Figure S2E). Immunostaining of sections from D100 organoids confirmed the expected nuclear localization of mCherry, due to the presence of the Histone-2B (H2B) sequence (Figure S2F). By combining whole-mount immunostaining for *CRX* and a clearing procedure 3DISCO (Belle et al., 2014) on D75 organoids, we showed that mCherry expression was restricted to *CRX*+ cells in the entire organoid (Figures 1E and S2F; Video S1), demonstrating the specificity of the mouse *Crx* promoter in the human context. The presence of both CONE ARRESTIN (hCAR)+/mCherry+ cells and RHODOPSIN+/mCherry+ cells identified by immunostaining (Figure S2G) confirmed that mCherry+ cells were both cone and rods. Importantly, CD73 expression was restricted to mCherry+ cells both in retinal organoid sections (Figure 1F) and in dissociated cells from organoids, where all the *RECOVERIN*+ cells presented a mCherry+ nucleus (Figure 1G).

Enrichment of PRs by MACS Based on Expression of CD73 in Dissociated Retinal Organoid Cells

Since we aimed at separating the PR population from organoids by targeting CD73, we developed a protocol based on the magnetic labeling of CD73+ cells, previously used to obtain PR enrichment from post-natal mice (Eberle et al., 2011). Efficiency of the MACS process was evaluated by flow cytometry using a PE-conjugated CD73 primary antibody on dissociated retinal organoids older than D100 of differentiation, because MACS at earlier stages did not lead to a satisfactory enrichment of CD73+ cells (data not shown). We showed that the MACS-positive fraction contained 87% ± 7% of CD73+ cells (n = 20 organoids, N = 3 differentiations; Figure 2A), a rate of enrichment consistent with previously published results from

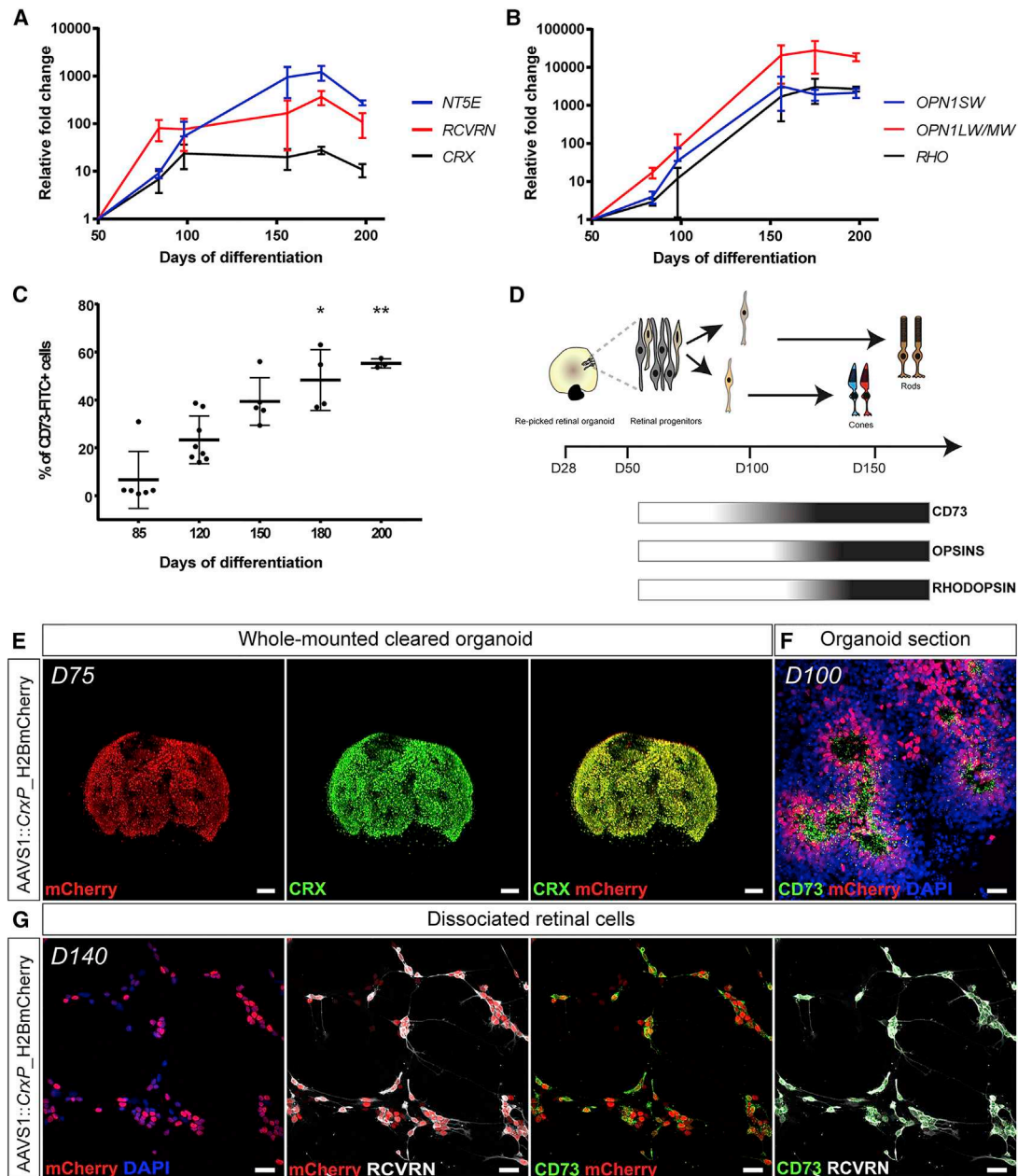


Figure 1. Analysis of CD73 Expression in hiPSC-Derived Retinal Organoids

(A and B) qRT-PCR analysis of *NT5E* (coding for CD73) and PR markers during differentiation between D50 and D200 (mean \pm SD; n = 5 organoids from N = 3 differentiations per time point). Gene expression at each time point is indicated relative to organoids at D50.

(C) Percentage of CD73⁺ cells in organoids between D85 and D200 of differentiation analyzed by flow cytometry using CD73-FITC antibody (mean \pm SD; n = 10 organoids from N \geq 3 differentiations D85 versus D180 *p < 0.05, D85 versus D200 **p < 0.01, multiple comparisons Kruskal-Wallis test).

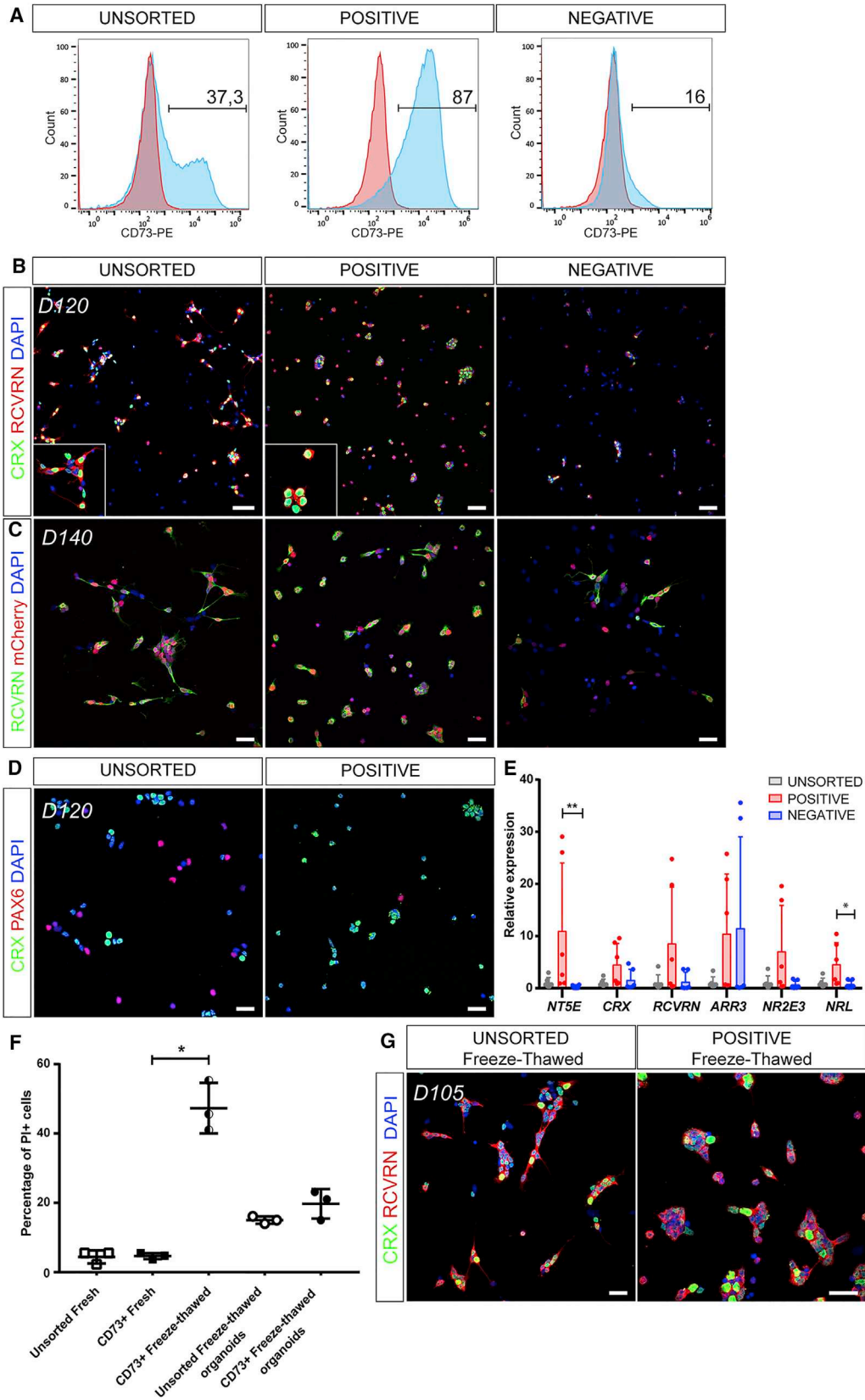
(D) Schematic summarizing temporal expression of CD73 and mature PR markers in organoids.

(E) Endogenous mCherry staining (red) and CRX immunolabeling (green) on solvent-cleared D75 organoid generated from the AAVS1:*CrxP_H2BmCherry* hiPSC line.

(F) Immunostaining showing the expression of CD73 in mCherry⁺ PRs in section of D100 AAVS1:*CrxP_H2BmCherry* retinal organoid.

(G) Dissociated mCherry⁺ cells (red) from D140 AAVS1:*CrxP_H2BmCherry* retinal organoids co-expressing RECOVERIN (gray) and CD73 (green). Nuclei were counterstained with DAPI (blue) in the first left panel.

Scale bars, 100 μ m (E), 25 μ m (F and G).



(legend on next page)



post-natal mouse retinae or retinal cells from mPSCs (Eberle et al., 2011; Santos-Ferreira et al., 2016a). CD73+ fractions from D120 organoids revealed relative enrichment in CRX+/RECOVERIN+ cells ($66\% \pm 15\%$) compared with the unsorted fractions ($32\% \pm 7\%$) (Figure 2B), with the percentage of CRX+ cells being increased from $53\% \pm 10\%$ in unsorted fractions to $79\% \pm 11\%$ in CD73+ fractions ($n = 10$ images, $N = 3$ differentiations, **** $p < 0.0001$, two-way ANOVA with Tukey's multiple comparisons test). MACS for CD73 was performed on D140 organoids generated from the AAVS1:*CrxP*_H2BmCherry hiPSC line to validate the efficacy and the reproducibility of our separation strategy. As expected, almost all CD73+ cells in the MACS-positive fraction displayed mCherry+ nuclei ($98\% \pm 0.7\%$, $n = 12$ images, $N = 3$ differentiations), as well as RECOVERIN-positive immunostaining (Figure 2C). A qualitative depletion of mCherry+ cells was observed in the CD73- fraction, as opposed to the clear enrichment observed in the CD73+ fraction. Immunostaining for PAX6, corresponding to horizontal, amacrine, and retinal ganglion cells in retinal organoids (Reichman et al., 2017), demonstrated that PAX6+ cells constituted an abundant population in unsorted fractions from D120 organoids, while the MAC-sorted CD73+ cell population contained very few PAX6+ cells (Figure 2D). qRT-PCR analysis confirmed that *NT5E* expression level was significantly higher in CD73+ cells than in CD73- cells at D120 (Figure 2E). Other markers of PR specification were expressed at increased levels in CD73+ cells (Figure 2E). The relatively modest increase of CRX+ cells could be due to the ontogenetic stage of organoids, where the differentiating CRX+/CD73- cells present in D120 organoids were still present in the negative fractions. Ratios of gene expression levels between CD73+ and CD73- fractions confirm increased expression in CD73+ cells for the PR genes analyzed (Figure S3A). All together, these data support the use of CD73 as a marker of both differentiating cone and rod PRs and

validate the MACS of CD73+ cells around D120 of differentiation as an efficient strategy to obtain a homogeneous and viable population of hiPSC-derived PR precursors.

With the perspective of developing a cell therapy product, we have tested the possibility to cryopreserve the isolated population of CD73+ cells directly after MACS. The evaluation of cell viability in freeze-thawed CD73+ cells by flow cytometry using propidium iodide (PI) revealed that $47\% \pm 7\%$ of the cells are apoptotic (PI+) after thawing (compared with $4.6\% \pm 0.9\%$ in fresh CD73+ cells, $n = 15$ organoids, $N = 3$ differentiations, * $p < 0.05$, Kruskal-Wallis test) (Figure 2F). Having already developed a simple cryopreservation procedure of whole retinal organoids with no impact on CD73 expression (Reichman et al., 2017), we tested whether freeze-thawed organoids could still represent a source for MACS of viable CD73+ PR precursors. Retinal organoids, frozen at D90 of differentiation, were thawed and put back into floating cultures for an additional 2 weeks before performing MACS. In these conditions, MACS of CD73 cells still resulted in efficient enrichment of PR precursors, as shown by co-immunostaining with CRX and RECOVERIN (Figure 2G). The assessment of cell viability demonstrated that freeze-thawing resulted in a small, but not significant, increase in the number of apoptotic cells from $4.4\% \pm 1.9\%$ to $15\% \pm 1\%$ of PI+ cells in unsorted fractions from fresh and freeze-thawed organoids respectively ($n = 15$ organoids, $N = 3$ differentiations). MACS alone did not significantly affect cell viability in any condition: $4.4\% \pm 1.9\%$ compared with $4.6\% \pm 0.9\%$ and $15\% \pm 1\%$ to $19.7\% \pm 4.2\%$ of PI+ cells for fresh and freeze-thawed organoids respectively ($n = 15$ organoids, $N = 3$ differentiations) (Figure 2F).

Maturation of CD73+ PRs

To analyze more deeply the cell identity of CD73+ cells, MACS for CD73 was performed on 200-day-old retinal

Figure 2. Selection of hiPSC-Derived PRs by Targeting of CD73

- (A) Representative CD73-PE flow cytometry analysis plot (specific staining in blue, isotype control staining in red) on unsorted, and MAC-sorted CD73+ and CD73- fractions from D120 organoids showing the percentage of CD73+ cells.
- (B) Immunofluorescence analysis of PR markers CRX and RECOVERIN in dissociated cells from D120 organoids (unsorted fraction) and in CD73+ and CD73- fractions after MACS.
- (C) Immunolabeling of RECOVERIN+ cells in unsorted, and sorted CD73+ and CD73- fractions from D140 AAVS1:*CrxP*_H2BmCherry retinal organoids.
- (D) Exclusive expression of CRX and PAX6 in dissociated cells from D120 organoids (unsorted) and after MACS targeting CD73 (positive).
- (E) qRT-PCR expression analysis of PR-specific genes in cells from unsorted (gray), and CD73+ (red) and CD73- (blue) fractions after MACS at D120 (mean \pm SD; $n = 25$ organoids from $N = 6$ differentiations, * $p < 0.05$, ** $p < 0.01$, multiple comparisons Kruskal-Wallis test). Gene expression is indicated relative to organoids at D120.
- (F) Quantitative analysis by flow cytometry of apoptotic (PI+) cells on unsorted and CD73+ fractions in dissociated cells from: unfrozen retinal organoids (unsorted and CD73+ fresh), freeze-thawed CD73+ cells, freeze-thawed retinal organoids (unsorted and CD73+ freeze-thawed organoids) (* $p < 0.05$, multiple comparisons Kruskal-Wallis test).
- (G) Co-expression of CRX and RECOVERIN in unsorted or sorted CD73+ cells from dissociated freeze-thawed organoids.
- Scale bars, 50 μ m (B), 25 μ m (C, D, and G).

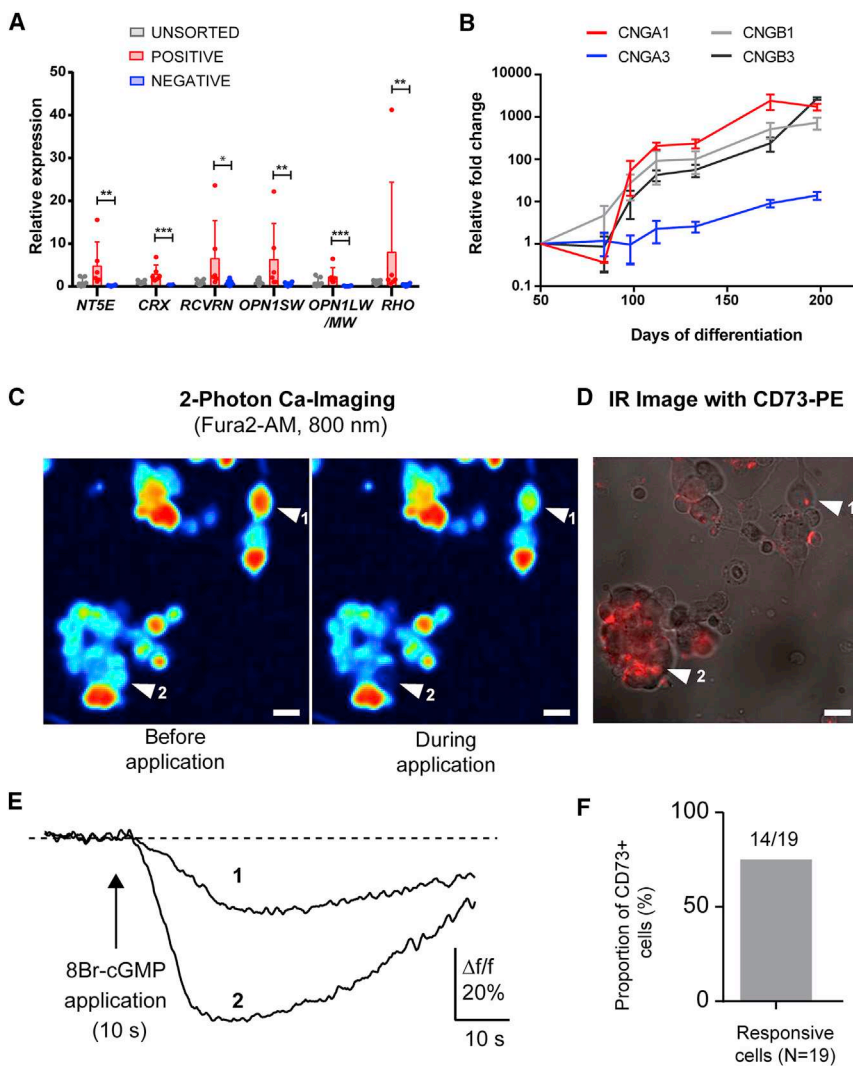


Figure 3. Characterization of CD73+ Cells from Mature Retinal Organoids

(A) qRT-PCR expression analysis of PR-specific genes in cells from unsorted (gray), and CD73+ (red) and CD73- (blue) fractions after MACS at D200 (mean \pm SD; n = 25 organoids from N = 6 differentiations, *p < 0.05, **p < 0.01, ***p < 0.001, multiple comparisons Kruskal-Wallis test). Gene expression is indicated relative to organoids at D200.

(B) qRT-PCR time course analysis of CNG channel subunits in organoids between D50 and D200 (mean \pm SD; n = 5 organoids from N = 3 differentiation per time point). Gene expression at each time point is indicated relative to organoids at D50.

(C) Representative examples of 2-Photon Fura2-AM fluorescence images (calcium imaging) obtained before (left) and during (right) application of 8-Br-cGMP on dissociated retinal cells at D190. White arrows 1 and 2 represent two responsive cells.

(D) Infra-red (IR) image showing CD73-PE staining on dissociated retinal cells at D190. White arrows indicate responsive cells denoted 1 and 2 from image (C).

(E) Fluorescence traces after application of cGMP analog on cells 1 and 2 displayed in (C and D), expressed as percentage change from baseline fluorescence ($\Delta f/f\%$).

(F) Percentage of CD73+ cells among the 8-Br-cGMP-responsive cell population (n = 19 from N = 5). Scale bars, 10 μ m (C and D).

organoids containing mature rods and cones (Reichman et al., 2014, 2017). qRT-PCR analysis clearly showed a significant overexpression of both mature cone- (*OPN1SW* and *OPN1LW/M*) and rod-specific (*RHO*) genes in CD73+ cells compared with CD73- cells (Figures 3A and S3B), in agreement with previous immunostaining data revealing the co-expression of CD73 with CONE ARRESTIN, BLUE OPSIN, and RED/GREEN OPSIN in retinal organoids (Reichman et al., 2017). The increased expression of *NTSE*, as well as *CRX* and *RCVRN*, in the CD73- positive fraction, confirmed the efficacy of the MACS process in retinal organoids from mature stages (Figures 3A and S3B). qRT-PCR analysis of the different subunits of cyclic nucleotide-gated ion (CNG) channels, expressed in functional PRs, showed that the expression of both rod-specific CNG channel subunits (CNGA1 and CNGB1) and of cone-specific CNG channel subunits (CNGA3 and CNGB3)

started between D50 and D100 and increased after D150 (Figure 3B). To assess whether the functionality of CD73+ cells was consistent with PR electrophysiological behavior, we studied CNG channel activity in dark-like conditions in adherent cultures of dissociated retinal organoids. By combining live two-photon calcium imaging with infra-red imaging, we monitored in CD73+ cells, labeled with a PE-conjugated CD73 antibody, the variations in intracellular Ca^{2+} levels in response to the addition of a cGMP analog (8-Br-cGMP), as described previously (Mellough et al., 2015; Reichman et al., 2017). As dissociated cells from D120 organoids did not show any functional response (data not shown), experiments were performed in D190 dissociated cells when the expression of all subunits is optimal. Fura-2-loaded cells showed an increase in intracellular Ca^{2+} when exposed to 8-Br-cGMP, as demonstrated by decreased intracellular fluorescence



($-22.42\% \pm 2.67\%$, $n = 34$, $N = 8$) (Figures 3C–3E). More importantly, the majority of the responsive cells were CD73[−] PE⁺ cells (Figure 3F). Consistently with their gene expression profile, CD73⁺ cells displayed a PR-specific response to the cGMP analog, supporting the use of CD73 as a marker of the PR cell population.

Safety Assessment of hiPSC-Derived Retinal Cells

Since the use of PSC-derived cells is associated with the risk of the presence of potentially tumorigenic undifferentiated cells (Tucker et al., 2011), we evaluated by immunofluorescence the presence of residual undifferentiated PSCs and mitotic cells in retinal organoids. No expression of pluripotency markers OCT4, NANOG, or SSEA-4 were detected in dissociated retinal cells from D120 organoids, excluding the presence of undifferentiated PSCs. In contrast to undifferentiated hiPSC colonies (Figure 4A), very few cells were positive for the mitotic marker Ki67 at D120, corresponding to remaining retinal progenitor cells (Figure 4B). These data demonstrated the rarity of proliferative cells already before the selection of the PR by MACS. The safety of both unsorted and sorted CD73⁺ cells was assessed by transplanting 300,000 unsorted cells or MAC-sorted CD73⁺ cells from D120 organoids in the SRS of adult immunodeficient NUDE rats. As expected, no hyper-proliferation was observed after 8 weeks in animals engrafted with differentiated retinal cells (Figure 4C). Half of the NUDE rats transplanted with undifferentiated hiPSCs developed tumors in the eye (Figure 4D). Immunostaining with antibodies specifically directed against a cytoplasmic (STEM 121) or a human nuclear antigen (HNA) demonstrated the presence of human cells in the SRS 8 weeks after transplantation with both unsorted and sorted CD73⁺ cells (Figures 4E and 4F). The absence of Ki67⁺ cells in the SRS confirmed that both transplanted unsorted and CD73⁺ cells do not contain mitotically active cells (Figure 4F), confirming that retinal cells derived from D120 organoids are suitable for safe transplantation studies.

Transplantation of Unsorted and CD73⁺ Cells into the Dystrophic P23H Rat Retina

Next, we sought to study the transplantation competence of CD73⁺ cells in a host environment recapitulating degenerative conditions. The P23H transgenic rat, which carries a P23H mutated *Rhodopsin* transgene, is a well-characterized model of rod-cone dystrophies, displaying progressive PR degeneration starting from 1 month after birth (Orhan et al., 2015). We transplanted unsorted retinal cells or sorted CD73⁺ cells from D120 organoids into 6-week-old hemizygous P23H rats, corresponding to an intermediate stage of PR degeneration (Orhan et al., 2015). One week after transplantation, unsorted cells survived in the SRS, identified by the expression of human-specific markers,

STEM121, HNA, and human cytochrome *c* oxidase (MTCO2) (Figure 5A). hiPSC-derived retinal cells do not seem to migrate into the host ONL. Instead, S121⁺ cells were densely packed in the SRS, forming a new distinct layer of cells between host PRs and RPE even 4 weeks after transplantation (Figures 5B and 5C). Interestingly, the primary antibody against RECOVERIN, directed against an epitope of the human protein, led to a stronger signal against human cells than against host rat PRs and bipolar cells (Figure 5C). Although the RECOVERIN staining in the rat retina was still clearly detectable and highly specific (Figure 5D), this difference in the signal intensity can be used as an additional strategy to distinguish the xenotransplant. Another parameter allowing for a straightforward identification of transplanted cells was the striking difference in the size and heterochromatin distribution of the nuclei in rat and human PRs. Consistent with previous observations (Gonzalez-Cordero et al., 2017), human nuclei were bigger in size (Figure 5E) with multiple chromocenters (Solovei et al., 2009); conversely rat PRs had smaller nuclei and highly condensed heterochromatin at their center (Figure 5E). While a large part of human transplanted cells stained with anti-RECOVERIN antibody, double S121⁺/PAX6⁺ cells were also detected (Figure 5F), confirming the heterogeneous identity of unsorted cells.

In contrast to unsorted cells, xeno-grafts with CD73⁺ cells gave rise to a homogeneous population of cells, co-expressing S121 and RECOVERIN (Figure 6A) and completely devoid of PAX6⁺ cells 4 weeks after transplantation (Figure 6B). Further characterization of grafted CD73⁺ cells showed a high enrichment in cones, stained by human-specific CONE ARRESTIN (hCAR) antibody, while only few RHODOPSIN⁺ cells were detected (Figure 6C). hCAR⁺ cells corresponded predominantly to red/green cones (Figure 6D) and few human HNA⁺ cones expressed BLUE OPSIN (Figure 6E). When the host PRs are mostly degenerated in some animals, human PRs could be directly in contact with the host inner nuclear layer (INL), and the expression of the pre-synaptic protein RIBEYE could be observed as immunoreactive spots, distributed at the extremities of hCAR⁺ cells (Figure 6F). Immunostaining with PKC α antibody allowed the visualization of tight apposition between human S121⁺ cells and PKC α ⁺ bipolar cells 4 weeks after transplantation (Figures 6G and 6G').

In a few animals ($n = 2/7$) we observed, at 10 weeks post-transplantation, clusters of human PRs co-expressing S121 and RECOVERIN intercalated in the host retina (Figure 7A), indicating the ability of CD73⁺ cells to survive for a relatively long time in the presence of immunosuppressive treatment. The limited efficacy of the immunosuppressive regimen and possible blood-retina barrier damage subsequent to surgery could explain the limited number of animals in which human cells can be detected 10 weeks

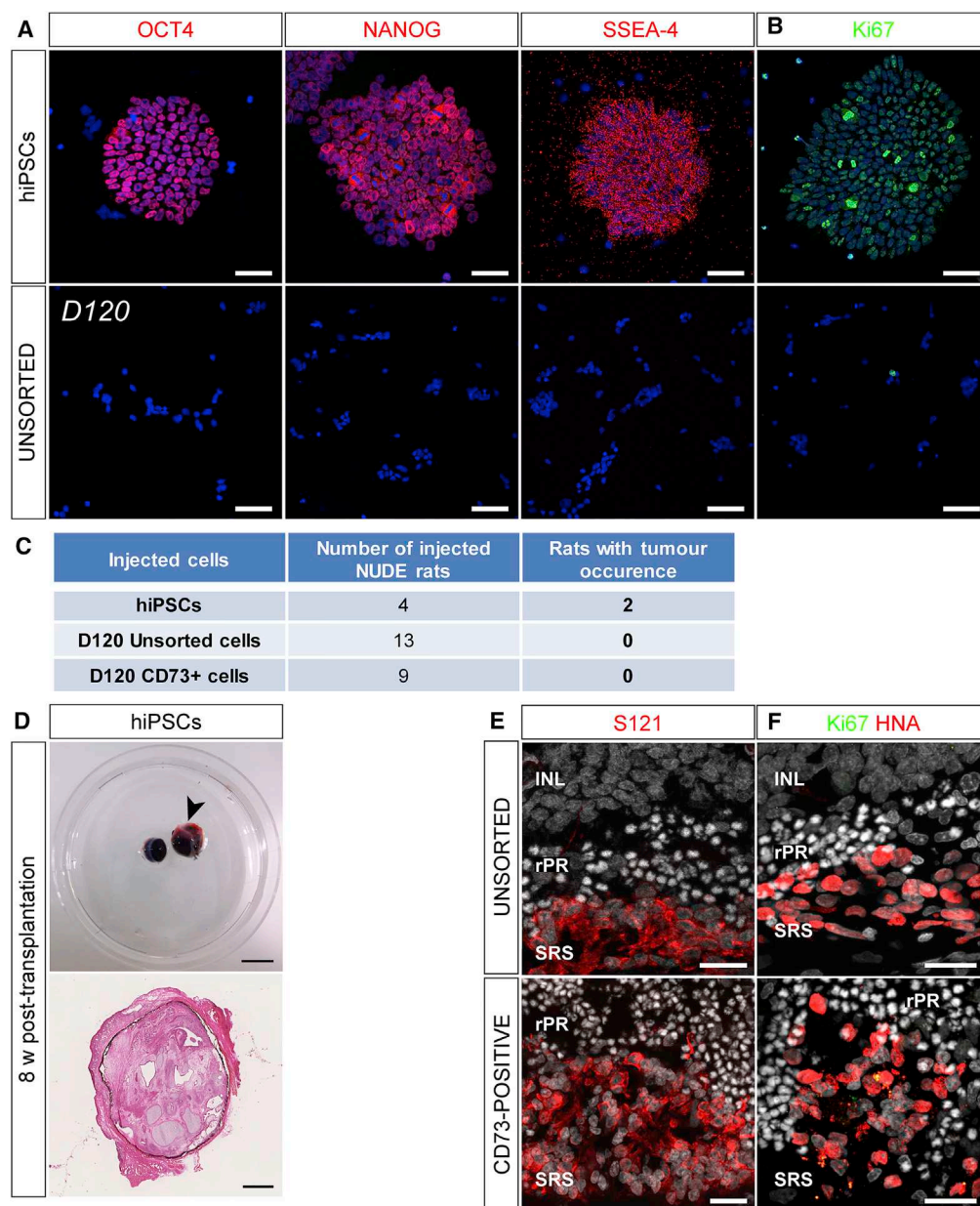


Figure 4. Safety Assessment of hiPSC-Derived Retinal Cells

(A) Immunostaining showing the expression of pluripotency markers OCT4, NANOG, and SSEA-4 in iPSC colonies (hiPSCs) but not in dissociated cells (unsorted) from D120 retinal organoids.

(B) Immunolabeling for Ki67 protein, associated with cell proliferation, in a representative iPSC colony and dissociated cells from D120 retinal organoids. Note loss of Ki67 expression in retinal cells.

(C) Table recapitulating the tumorigenicity test after subretinal transplantation into NUDE rats of dissociated hiPSCs and D120 unsorted or MAC-sorted CD73+ cells. Observations were made 8 weeks after the transplantation.

(D) Example of eyeballs of NUDE rats 8 weeks after subretinal transplantation of hiPSCs (black arrow) compared with non-transplanted eye. Bottom panel illustrates H&E staining of cross-section of the same hiPSC-transplanted eye.

(E) Representative confocal images showing the presence of human S121+ cells in the SRS of NUDE rat 8 weeks after transplantation of D120 unsorted cells or MAC-sorted CD73+ cells. Nuclei were counterstained with DAPI (gray).

(F) Absence of double Ki67+/HNA+ cells in unsorted and sorted CD73+ grafted cells 8 weeks after transplantation. Nuclei were counterstained with DAPI (gray). Scale bars, 1 cm (D) (top panel), 1 mm (D) (bottom panel), 50 μ m (A and B), 20 μ m (E and F). SRS, subretinal space; rPR, rat photoreceptors.

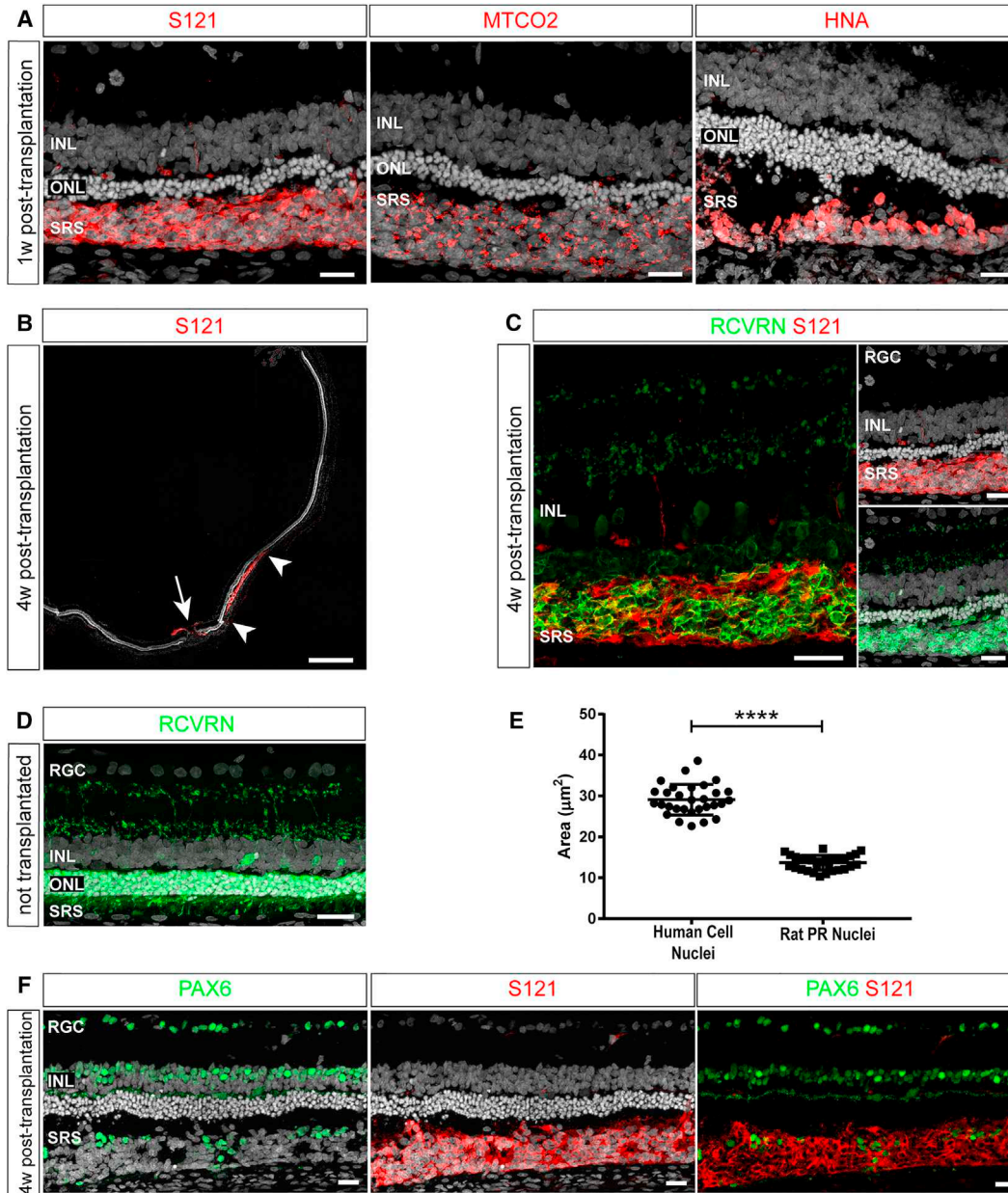


Figure 5. Transplantation of hiPSC-Derived Retinal Cells into a Rat Model of Retinal Degeneration

(A) Identification of donor human cells 1 week after transplantation by using three different human-specific antibodies (red): STEM 121 (left), MTCO2 (center), and HNA (right).

(B) Confocal mosaic image of D120 unsorted cell-transplanted eye showing the distribution of human S121+ cells in the SRS 4 weeks after transplantation. Arrowheads delimitate the spread of the grafted cells; the site of injection is indicated with an arrow.

(C) Most transplanted human retinal cells (S121+ cells) coexpress RECOVERIN. Note that RECOVERIN staining is lower in rat cells than in human cells.

(D) Example of RECOVERIN immunostaining in a non-grafted retina from P23H rat at 10 weeks of age. RECOVERIN antibody specifically labels rat PRs and part of the bipolar cells within the INL.

(E) Size of nuclei area of transplanted human cells and endogenous rat PRs 4 weeks after transplantation (mean \pm SD, n = 30 nuclei measured, N = 3 grafted retinas; ****p < 0.0001, Mann-Whitney test).

(F) Some transplanted human S121+ retinal cells express the transcription factor PAX6.

Nuclei were counterstained with DAPI (gray). Scale bars, 20 μm (A, C, D, and F), 500 μm (B). SRS, subretinal space; ONL, outer nuclear layer, INL, inner nuclear layer; RGC, retinal ganglion cell layer.

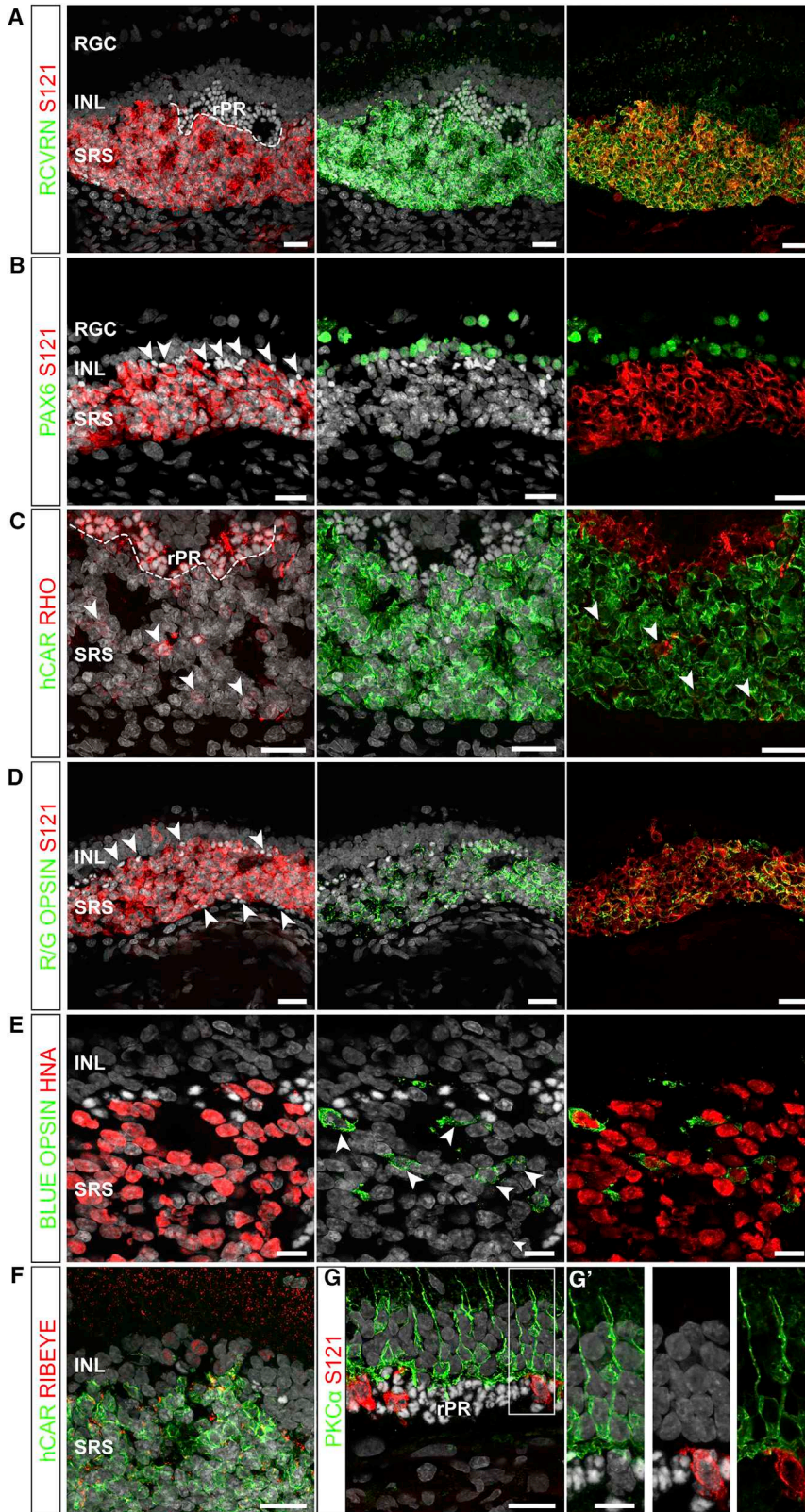


Figure 6. Transplantation of hiPSC-Derived CD73+ Photoreceptors into the P23H Rat Model of Retinal Degeneration

(A) Human S121+ cells co-expressing PR marker RECOVERIN located in close proximity to the rat INL. The residual rat PRs are delimited by the white dotted line.

(B) Absence of double S121/PAX6-positive cells. Transplanted CD73+ cells labeled by S121 are in close proximity with host PAX6+ cells within the INL. Arrowheads indicate residual rat PR nuclei.

(C) Labeling of human cone PRs by human-specific CONE ARRESTIN antibody (hCAR) and rod PRs by RHODOSPIN antibody. Arrowheads indicate human RHODOSPIN+ cells. Residual rat Rhodopsin+ PRs are delimited by the white dotted line.

(D) Human S121+ cells co-expressing cone PR marker R/G OPSIN. Residual S121-rat PRs (arrowheads) can be recognized by their nuclei features (smaller size and brightness).

(E) Some human HNA+ cells express blue cone marker BLUE OPSIN (arrowheads).

(F) Staining for synaptic protein RIBEYE and human CONE ARRESTIN (hCAR) showing localized punctate RIBEYE expression in human cone PRs directly in contact with the INL.

(G) Rat PKC α + bipolar cells are in close proximity to human S121+ cells inserted within the host ONL. The area delimited by the line indicates the location of high-magnification images presented in (G').

All observations were made 4 weeks after transplantation. Nuclei were counterstained with DAPI (gray). Scale bars, 20 μ m (A–D), 10 μ m (E–G'). SRS, subretinal space; rPR, rat photoreceptors; INL, inner nuclear layer; RGC, retinal ganglion cell layer.

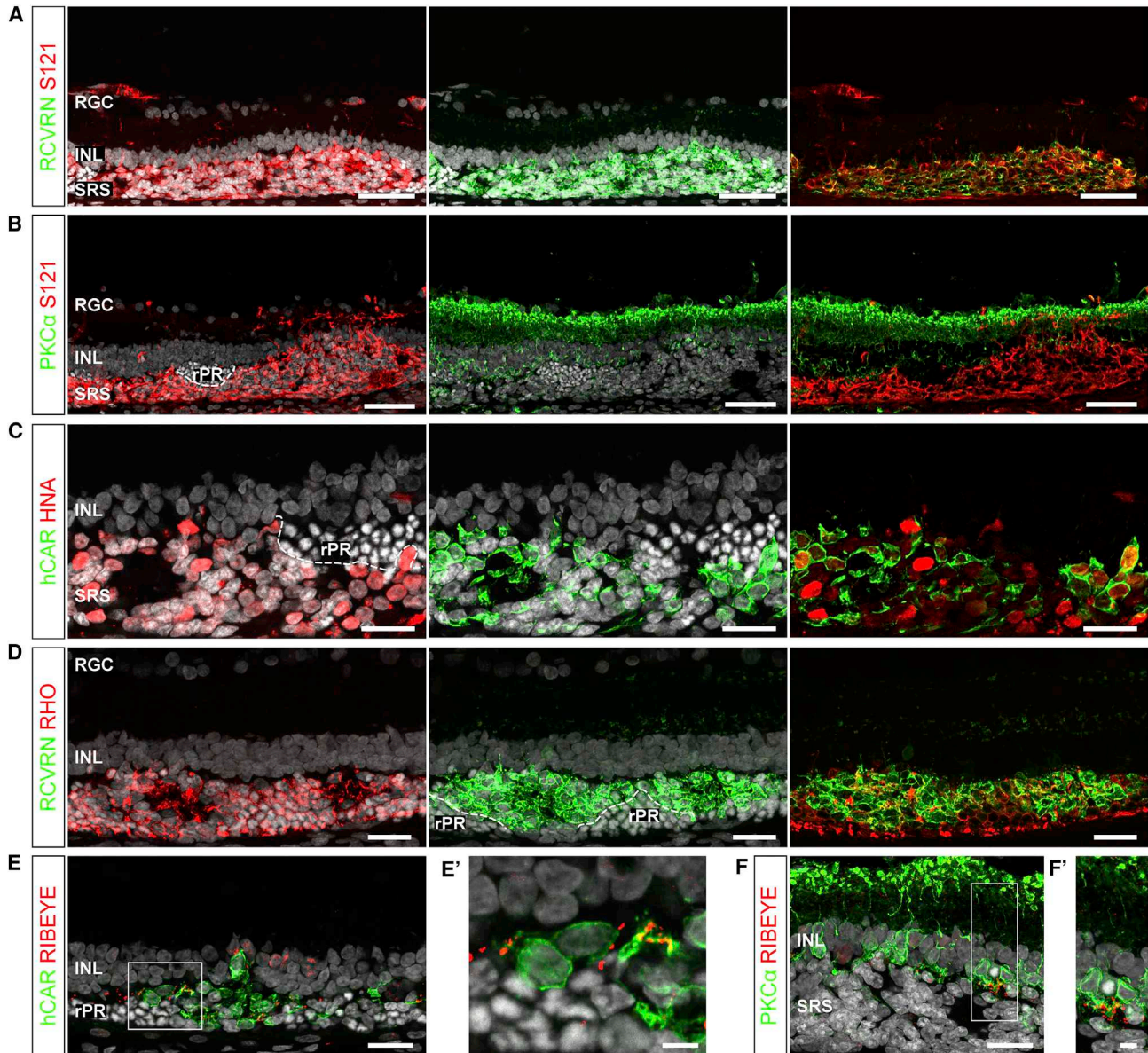


Figure 7. Long-Term Survival of Transplanted CD73+ Cells

(A) CD73+ human PRs, co-expressing S121 and RECOVERIN, are intercalated within the rat retina.

(B) Example of the distribution of human S121+ cells in close proximity to rat PKC α + bipolar cells.

(C) Transplanted PRs co-expressing human CONE ARRESTIN (hCAR) and human marker HNA. The residual rat PRs are delimited by the white dotted line.

(D) Staining for human and rat rod PRs with RHODOPSIN and RECOVERIN antibodies.

(E) RIBEYE protein expression in the rat outer plexiform layer close to human cone PRs (hCAR+ cells). The area delimited by the line indicates the location of the high-magnification image presented in (E').

(F) RIBEYE protein expression in close proximity to the synaptic terminals of rat PKC α + bipolar cells. The area delimited by the line indicates the location of the high-magnification image presented in (F').

All observations were made 10 weeks after transplantation. Nuclei were counterstained with DAPI (gray). Scale bars, 50 μ m (A and B), 20 μ m (C–E and F), 5 μ m (E' and F'). SRS, subretinal space; rPR, rat photoreceptors; INL, inner nuclear layer; RGC, retinal ganglion cell layer.



after transplantation. Human S121+ PRs were located in close proximity to the rat PKC α + bipolar cells (Figure 7B). As in xeno-grafts analyzed 4 weeks after transplantation (Figure 6), again a large part of transplanted human HNA+ cells corresponded to cones (hCAR+ cells), even though few rods co-expressing bright RECOVERIN and RHODOPSIN can be observed (Figures 7C and 7D). Interestingly, some of the transplanted hCAR+ cones closest to the host INL expressed the pre-synaptic marker RIBEYE (Figures 7E and 7E'). Consistently, some of the rat PKC α + bipolar cells closest to the human cells, distinguishable by their nuclear morphology, expressed RIBEYE at their synaptic terminals extending into the outer plexiform layer (Figures 7F and F').

DISCUSSION

In this study, we have developed a strategy based on the MACS of CD73+ cells to efficiently isolate PRs from hiPSC-derived retinal organoids and we demonstrated that CD73+ PR precursors could be safely transplanted into a host retina. One of the major challenges ahead for the development of a stem cell-based therapy to replace PRs is to obtain a consistent cell therapy product by complying with GMP guidelines, with no variations in terms of purity, yields, and quality of the manufactured cells. Using our retinal differentiation protocol combined with CD73- cell sorting, we obtained a large number of cells corresponding to a homogeneous population of PR precursors, as shown by *in vitro* and *in vivo* characterization. Our differentiation protocol is based on a feeder-free iPSC culture system and uses exclusively chemically defined xeno-free compounds. GMP-compliant MACS enrichment is already used in clinical trials (Menasché et al., 2015), with no negative impact or long-term side effects due to the microbeads at the surface of MAC-sorted cells (Handgretinger et al., 1998). Thus, our entire protocol to manufacture a cell therapy product should be easily GMP transferable. Moreover, MACS could be performed using cryopreserved organoids, ensuring the possibility to store the organoids at the appropriate stage of differentiation for downstream applications.

Despite a reasonable variability, an adequate number of viable CD73+ cells for transplantation can be still isolated by MACS. Starting from 20 million dissociated retinal cells at D120 of differentiation, MACS yielded 5 ± 1.8 million CD73+ cells, corresponding to the $25\% \pm 9\%$ of the total cell population, demonstrating that large-scale production of a homogeneous PR precursor cell population can be reached. We proposed that 120-day-old retinal organoids represent the most suitable source of transplantable PRs, since at this stage the CD73+ cell population is

mostly composed of immature PRs expressing CRX and RECOVERIN, but not OPSIN and RHODOPSIN. The precise definition of the ontogenetic stage of donor cells is very important for transplantation success, as previously demonstrated in mice, where only early post-natal PR precursors are able to efficiently integrate into the retina (Pearson et al., 2012; Waldron et al., 2017). The temporal profile of the expression of PR genes in our retinal organoids is very similar to the profile recently reported in human fetal retina (Hoshino et al., 2017; Welby et al., 2017). Also, expression of genes in D115-D136 human fetal retina was correlated to mouse P2-P4 retina in a comparative analysis of human and mouse transcriptome during retinal development (Hoshino et al., 2017), corroborating our choice of the differentiation stage of hiPSC-derived retinal organoids to isolate transplantable PR precursors. Recent transcriptome analysis of developing human PRs derived from PSCs should be also helpful for the isolation of PSC-derived PRs at the right stage of development, compatible for future transplantation studies (Kaewkhaw et al., 2015; Phillips et al., 2017; Welby et al., 2017).

One major advantage of the separation strategy presented here relies on the targeting of one single-cell surface antigen, CD73. Positive selection of retinal cells expressing CD73 has been mainly focused on rods, using Nrl:GFP mice or AAVs carrying a rhodopsin-driven GFP to specifically label rods (Eberle et al., 2011; Lakowski et al., 2011, 2015; Santos-Ferreira et al., 2016a). Nevertheless, CD73 has also been used for the enrichment of cone-like cells from a Nrl-/- mouse retina (Santos-Ferreira et al., 2015). Very recently, a comparative analysis of the transcriptome of human fetal and iPSC-derived cones, identified with the use of an AAV2/9-pR2.1:GFP reporter, and screening for cell surface-specific markers for cones in GFP+ cells, has been reported. Interestingly, NT5E (CD73) expression was not upregulated in GFP+ cones isolated by fluorescence-activated cell sorting (FACS) (Welby et al., 2017). This may be explained by the fact that CD73 is expressed by both rods and cones. Hence, in the absence of rods, no overexpression of CD73 is expected. Indeed, in our study, we found that hiPSC-derived retinal MAC-sorted CD73+ cells overexpress both rod- and cone-specific genes compared with CD73- cells.

Remarkably, the enrichment in PR precursors obtained after CD73-based MACS from D120 retinal organoids is in agreement with recent data reported on human retinal tissues (Lakowski et al., 2018). Indeed, FACS for CD73 from fetal retinae after 14 weeks of gestation allowed an enrichment for PRs, despite a large variability between different fetal samples ($50\% \pm 24\%$). The ontogenetic stage of retinal organoids is critical for CD73-based PR selection, since previous RNA sequencing analysis in CRX-GFP+ cells isolated from hESC-derived retinal organoids younger than



90 days failed to identify CD73 as a marker of early PR precursors (Kaewkhaw et al., 2015).

Transplantation studies demonstrated that CD73-sorted PR precursors survive and mature into normal and degenerating rat retinæ during several weeks. Surprisingly, a large part of transplanted CD73+ cells could be identified as cones in the SRS of P23H rats, suggesting that exogenous factors present within the host retina may favor either differentiation or survival of cones. Another explanation may reside in the temporal window of CD73 sorting, which may correspond to the peak of cone generation. Previous transplantation studies in mouse degenerative models had reported the presence of hiPSC-derived PRs within host mouse ONL, identified by GFP expression obtained via viral labeling (Gonzalez-Cordero et al., 2017; Lamba et al., 2009; Zhu et al., 2017). Gonzalez-Cordero and colleagues were able to confirm the human origin of most of the virally labeled human PSC-derived PRs by immunostaining with human-specific nuclear antigen. Importantly, they also reported the presence of small numbers of GFP+/HNA- within host ONL, whose morphology closely resembled that of mouse PRs, thereby demonstrating for the first time that human PSC-derived PRs can also engage in cytoplasmic material transfer following transplantation (Gonzalez-Cordero et al., 2017). The absence of a morphological difference between human GFP+ cells and mouse PRs may lead to a reconsideration of the human identity of GFP+ cells in previous studies (Lamba et al., 2009; Zhu et al., 2017). Donor-host cytoplasmic exchange has never been reported in transplantation studies in the rat retina. In our study, transplanted human PRs can be clearly distinguished from rat PRs thanks to both specific immunolabeling and cytological features. Remarkably, no HNA+ or S121+ cell displaying nuclear morphology peculiar to rat PRs was detected in host eyes, suggesting that transfer of cytoplasmic material between donor CD73+ PRs and host rat PRs does not seem to occur in the animal model presented here. Nevertheless, further studies would be necessary to undoubtedly exclude this process in the rat retina.

Despite the ability of CD73+ PRs to specifically respond to cGMP *in vitro*, no significant functional improvement was detected by electroretinography in P23H rats transplanted with unsorted or CD73+ cells compared with untreated eyes. Since human PRs were incorporated in a small area of the retina, more suitable strategies should be applied to determine the functionality of transplanted CD73+ cells. Also, in light of recent findings highlighting the structural divergence between rodent and human in proteins essential to PR synaptogenesis (Laver and Matsuura, 2017), more closely related species such as non-human primates would be more appropriate to evaluate the efficacy of human PR grafts.

In summary, we have reported the generation and the separation of an hiPSC-derived PR precursor cell population amenable to GMP manufacturing and compatible for future cell replacement therapy. The simplicity and the robustness of our separation strategy represent a reliable source to obtain PRs, not only in the context of cell replacement, but also for a broad spectrum of applications, such as disease modeling or drug screening.

EXPERIMENTAL PROCEDURES

See [Supplemental Experimental Procedures](#) for detailed protocols and [Supplemental Information](#) for antibodies (Table S1) and qPCR probes (Table S2).

MACS

Retinal organoids at various time points of differentiation were dissociated with papain (Worthington) according to the protocol described in Reichman et al. (2017). To remove residual aggregates, cell suspensions were filtered through a 30- μ m strainer (Miltenyi Biotec). Dissociated cells were resuspended in MACS buffer and incubated first with CD73 antibody (BioLegend) for 10 min at 4°C at a dilution of 1:10 and then, after washing, with 20 μ L of anti-mouse IgG1 MicroBeads (Miltenyi Biotec) per 10^7 cells for 15 min at 4°C. Cells resuspended in 500 μ L of MACS buffer were applied onto a pre-equilibrated mass spectrometry column fixed to a MACS separator (Miltenyi Biotec). The flow-through containing negative or unlabeled cells was collected by three washes with 500 μ L MACS buffer. The positive fraction was eluted with 1 mL of MACS buffer following removal of the column from the magnet.

Cell Transplantation

All protocols were approved by the local ethical committee (Charles Darwin ethical committee for animal experimentation C2EA-05) in strict accordance with French and European regulation for animal use in research (authorization number 05033). Cell suspension (4 μ L) containing 300,000 cells in MACS buffer was injected with a trans-vitreous approach into the SRS of adult NUDE rats or 6-week-old hemizygous P23H rats. From 2 days before transplantation to the end of the follow-up, P23H rats were maintained under immunosuppression through cyclosporine treatment (210 mg/L) in the drinking water.

SUPPLEMENTAL INFORMATION

Supplemental Information includes Supplemental Experimental Procedures, four figures, two tables, and one video and can be found with this article online at <https://doi.org/10.1016/j.stemcr.2018.07.005>.

AUTHOR CONTRIBUTIONS

G.G. contributed to the conception, design, execution, and analysis/interpretation of all experiments and writing of the manuscript. K.B.M. contributed to surgery, histological processing, analysis of results, and revision of manuscript. A.C. performed calcium live imaging and analysis of results. A.S.-B. contributed to iPSC



culture and histological processing. J.-B.C. contributed to surgery. C.N. and O.R. contributed to iPSC culture. J.-A.S. contributed to administrative and financial support. J.D. contributed to analysis of calcium imaging. G.O. contributed to cell culture, clearing experiments, and revision of manuscript. S.R. contributed to interpretation of experiments and revision of manuscript. O.G. contributed to the conception, design, and interpretation of experiments, manuscript writing, and financial support.

ACKNOWLEDGMENTS

We are grateful to J. Dégardin, M. Simonutti, and the staff of the Animal and Phenotyping facilities for help. We thank S. Fouquet from the Imaging facility, L. Riancho from the FACS facility, and A. Potey from the High Content Screening facility. We thank Dr. F. Sennlaub, X. Guillonnet, and Garita-Hernandez (Institut de la Vision, Paris) for helpful comments and Dr. C. Craft (Mary D. Allen Laboratory for Vision Research, USC ROSKI Eye Institute) for Cone arrestin antibody. This work was supported by grants from ANR (GPIPS: ANR-2010-RFCS005) (ANR-16-CE17-0008-02-SIGHTREPAIR), the Technology Transfer company SATT Lutech, LABEX REVIVE (ANR-10-LABX-73), and Retina France Association. This work was also performed in the frame of the LABEX LIFESENSES (ANR-10-LABX-65) within the Program Investissements d'Avenir (ANR-11-IDEX-0004-02). G.G. was a recipient of a PhD fellowship from the French Ministry of Higher Education and Research, K.B.M. was a recipient of a fellowship from the LABEX REVIVE (ANR-10-LABX-73), and O.R. was a recipient of a PhD fellowship from Fédération des Aveugles de France.

Received: March 7, 2018
Revised: July 9, 2018
Accepted: July 10, 2018
Published: August 9, 2018

REFERENCES

Belle, M., Godefroy, D., Dominici, C., Heitz-Marchaland, C., Zelina, P., Hellal, F., Bradke, F., and Chedotal, A. (2014). A simple method for 3D analysis of immunolabeled axonal tracts in a transparent nervous system. *Cell Rep.* *9*, 1191–1201.

Dalkara, D., Goureau, O., Marazova, K., and Sahel, J.-A. (2016). Let there be light: gene and cell therapy for blindness. *Hum. Gene Ther.* *27*, 134–147.

Decembrini, S., Koch, U., Radtke, F., Moulin, A., and Arsenijevic, Y. (2014). Derivation of traceable and transplantable photoreceptors from mouse embryonic stem cells. *Stem Cell Reports* *2*, 853–865.

Decembrini, S., Martin, C., Sennlaub, F., Chemtob, S., Biel, M., Samardzija, M., Moulin, A., Behar-Cohen, F., and Arsenijevic, Y. (2017). Cone genesis tracing by the Chrn4-EGFP mouse line: evidences of cellular material fusion after cone precursor transplantation. *Mol. Ther.* *25*, 634–653.

Eberle, D., Schubert, S., Postel, K., Corbeil, D., and Ader, M. (2011). Increased integration of transplanted CD73-positive photoreceptor precursors into adult mouse retina. *Invest. Ophthalmol. Vis. Sci.* *52*, 6462.

Furukawa, A., Koike, C., Lippincott, P., Cepko, C.L., and Furukawa, T. (2002). The mouse *Crx* 5'-upstream transgene sequence directs cell-specific and developmentally regulated expression in retinal photoreceptor cells. *J. Neurosci.* *22*, 1640–1647.

Gonzalez-Cordero, A., West, E.L., Pearson, R.A., Duran, Y., Carvalho, L.S., Chu, C.J., Naeem, A., Blackford, S.J.I., Georgiadis, A., Lakowski, J., et al. (2013). Photoreceptor precursors derived from three-dimensional embryonic stem cell cultures integrate and mature within adult degenerate retina. *Nat. Biotechnol.* *31*, 741–747.

Gonzalez-Cordero, A., Kruczek, K., Naeem, A., Fernando, M., Kloc, M., Ribeiro, J., Goh, D., Duran, Y., Blackford, S.J.I., Abelleira-Hervas, L., et al. (2017). Recapitulation of human retinal development from human pluripotent stem cells generates transplantable populations of cone photoreceptors. *Stem Cell Reports* *9*, 820–837.

Handgretinger, R., Lang, P., Schumm, M., Taylor, G., Neu, S., Koscielnak, E., Niethammer, D., and Klingebiel, T. (1998). Isolation and transplantation of autologous peripheral CD34+ progenitor cells highly purified by magnetic-activated cell sorting. *Bone Marrow Transplant.* *21*, 987–993.

Hoshino, A., Ratnapriya, R., Brooks, M.J., Chaitankar, V., Wilken, M.S., Zhang, C., Starostik, M.R., Gieser, L., La Torre, A., Nishio, M., et al. (2017). Molecular anatomy of the developing human retina. *Dev. Cell* *43*, 763–779.e4.

Jayakody, S.A., Gonzalez-Cordero, A., Ali, R.R., and Pearson, R.A. (2015). Cellular strategies for retinal repair by photoreceptor replacement. *Prog. Retin. Eye Res.* *46*, 31–66.

Kaewkhaw, R., Kaya, K.D., Brooks, M., Homma, K., Zou, J., Chaitankar, V., Rao, M., and Swaroop, A. (2015). Transcriptome dynamics of developing photoreceptors in three-dimensional retina cultures recapitulates temporal sequence of human cone and rod differentiation revealing cell surface markers and gene networks. *Stem Cells* *33*, 3504–3518.

Lakowski, J., Han, Y.T., Pearson, R.A., Gonzalez-Cordero, A., West, E.L., Gualdoni, S., Barber, A.C., Hubank, M., Ali, R.R., and Sowden, J.C. (2011). Effective transplantation of photoreceptor precursor cells selected via cell surface antigen expression. *Stem Cells* *29*, 1391–1404.

Lakowski, J., Gonzalez-Cordero, A., West, E.L., Han, Y.T., Welby, E., Naeem, A., Blackford, S.J.I., Bainbridge, J.W.B., Pearson, R.A., Ali, R.R., et al. (2015). Transplantation of photoreceptor precursors isolated via a cell surface biomarker panel from embryonic stem cell-derived self-forming retina. *Stem Cells* *33*, 2469–2482.

Lakowski, J., Welby, E., Budinger, D., Di Marco, F., Di Foggia, V., Bainbridge, J.W.B., Wallace, K., Gamm, D.M., Ali, R.R., and Sowden, J.C. (2018). Isolation of human photoreceptor precursors via a cell surface marker panel from stem cell-derived retinal organoids and fetal retinae. *Stem Cells* *36*, 709–722.

Lamba, D.A., Karl, M.O., Ware, C.B., and Reh, T.A. (2006). Efficient generation of retinal progenitor cells from human embryonic stem cells. *Proc. Natl. Acad. Sci. USA* *103*, 12769–12774.

Lamba, D.A., Gust, J., and Reh, T.A. (2009). Transplantation of human embryonic stem cell-derived photoreceptors restores some visual function in *Crx*-deficient mice. *Cell Stem Cell* *4*, 73–79.



- Laver, C.R.J., and Matsubara, J.A. (2017). Structural divergence of essential triad ribbon synapse proteins among placental mammals – implications for preclinical trials in photoreceptor transplantation therapy. *Exp. Eye Res.* *159*, 156–167.
- Mandai, M., Fujii, M., Hashiguchi, T., and Sunagawa, G.A. (2017). iPSC-derived retina transplants improve vision in rd1 end-stage retinal-degeneration mice. *Stem Cell Reports* *8*, 69–83.
- Mellough, C.B., Collin, J., Khazim, M., White, K., Sernagor, E., Steel, D.H.W., and Lako, M. (2015). IGF-1 signaling plays an important role in the formation of three-dimensional laminated neural retina and other ocular structures from human embryonic stem cells. *Stem Cells* *33*, 2416–2430.
- Menasché, P., Vanneaux, V., Hagege, A., Bel, A., Cholley, B., Cacciapuoti, I., Parouchev, A., Benhamouda, N., Tachdjian, G., Tosca, L., et al. (2015). Human embryonic stem cell-derived cardiac progenitors for severe heart failure treatment: first clinical case report. *Eur. Heart J.* *36*, 2011–2017.
- Meyer, J.S., Shearer, R.L., Capowski, E.E., Wright, L.S., Wallace, K.A., McMillan, E.L., Zhang, S.-C., and Gamm, D.M. (2009). Modeling early retinal development with human embryonic and induced pluripotent stem cells. *Proc. Natl. Acad. Sci. USA* *106*, 16698–16703.
- Nakano, T., Ando, S., Takata, N., Kawada, M., Muguruma, K., Sekiguchi, K., Saito, K., Yonemura, S., Eiraku, M., and Sasai, Y. (2012). Self-formation of optic cups and storable stratified neural retina from human ESCs. *Cell Stem Cell* *10*, 771–785.
- Orhan, E., Dalkara, D., Neullé, M., Lechavue, C., Michiels, C., Picaud, S., Léveillard, T., Sahel, J.A., Naash, M.I., LaVail, M.M., et al. (2015). Genotypic and phenotypic characterization of P23H line 1 rat model. *PLoS One* *10*, e0127319.
- Ortin-Martinez, A., Tsai, E.L.S., Nickerson, P.E., Bergeret, M., Lu, Y., Smiley, S., Comanita, L., and Wallace, V.A. (2017). A reinterpretation of cell transplantation: GFP transfer from donor to host photoreceptors. *Stem Cells* *35*, 932–939.
- Osakada, F., Ikeda, H., Mandai, M., Wataya, T., Watanabe, K., Yoshimura, N., Akaike, A., Sasai, Y., and Takahashi, M. (2008). Toward the generation of rod and cone photoreceptors from mouse, monkey and human embryonic stem cells. *Nat. Biotechnol.* *26*, 215–224.
- Pearson, R.A., Barber, A.C., Rizzi, M., Hippert, C., Xue, T., West, E.L., Duran, Y., Smith, A.J., Chuang, J.Z., Azam, S.A., et al. (2012). Restoration of vision after transplantation of photoreceptors. *Nature* *485*, 99–103.
- Pearson, R.A., Gonzalez-Cordero, A., West, E.L., Ribeiro, J.R., Aghaizu, N., Goh, D., Sampson, R.D., Georgiadis, A., Waldron, P.V., Duran, Y., et al. (2016). Donor and host photoreceptors engage in material transfer following transplantation of postmitotic photoreceptor precursors. *Nat. Commun.* *7*, 13029.
- Phillips, J., Jiang, P., Howden, S., Barney, P., Min, J., York, N., Chu, L., Capowski, E., Cash, A., Jain, S., et al. (2017). A novel approach to single cell RNA-sequence analysis facilitates in silico gene reporting of human pluripotent stem cell-derived retinal cell types. *Stem Cells* *36*, 1–16.
- Reichman, S., Terray, A., Slembrouck, A., Nanteau, C., Orioux, G., Habeler, W., Nandrot, E.F., Sahel, J.-A., Monville, C., and Goureau, O. (2014). From confluent human iPSC cells to self-forming neural retina and retinal pigmented epithelium. *Proc. Natl. Acad. Sci. USA* *111*, 8518–8523.
- Reichman, S., Slembrouck, A., Gagliardi, G., Chaffiol, A., Terray, A., Nanteau, C., Potey, A., Belle, M., Rabesandratana, O., Duebel, J., et al. (2017). Generation of storable retinal organoids and retinal pigmented epithelium from adherent human iPSC cells in xeno-free and feeder-free conditions. *Stem Cells* *35*, 1176–1188.
- Santos-Ferreira, T., Postel, K., Stutzki, H., Kurth, T., Zeck, G., and Ader, M. (2015). Daylight vision repair by cell transplantation. *Stem Cells* *33*, 79–90.
- Santos-Ferreira, T., Völkner, M., Borsch, O., Haas, J., Cimalla, P., Vassudevan, P., Carmeliet, P., Corbeil, D., Michalakis, S., Koch, E., et al. (2016a). Stem cell-derived photoreceptor transplants differentially integrate into mouse models of cone-rod dystrophy. *Invest. Ophthalmol. Vis. Sci.* *57*, 3509–3520.
- Santos-Ferreira, T., Llonch, S., Borsch, O., Postel, K., Haas, J., and Ader, M. (2016b). Retinal transplantation of photoreceptors results in donor–host cytoplasmic exchange. *Nat. Commun.* *7*, 13028.
- Santos-Ferreira, T.F., Borsch, O., and Ader, M. (2017). Rebuilding the missing part—a review on photoreceptor transplantation. *Front. Syst. Neurosci.* *10*, 1–14.
- Singh, M.S., Charbel Issa, P., Butler, R., Martin, C., Lipinski, D.M., Sekaran, S., Barnard, A.R., and MacLaren, R.E. (2013). Reversal of end-stage retinal degeneration and restoration of visual function by photoreceptor transplantation. *Proc. Natl. Acad. Sci. USA* *110*, 1101–1106.
- Singh, M.S., Balmer, J., Barnard, A.R., Aslam, S.A., Moralli, D., Green, C.M., Barnea-Cramer, A., Duncan, I., and MacLaren, R.E. (2016). Transplanted photoreceptor precursors transfer proteins to host photoreceptors by a mechanism of cytoplasmic fusion. *Nat. Commun.* *7*, 13537.
- Solovei, I., Kreysing, M., Lanctôt, C., Kösem, S., Peichl, L., Cremer, T., Guck, J., and Joffe, B. (2009). Nuclear architecture of rod photoreceptor cells adapts to vision in mammalian evolution. *Cell* *137*, 356–368.
- Sridhar, A., Steward, M.M., and Meyer, J.S. (2013). Nonxenogeneic growth and retinal differentiation of human induced pluripotent stem cells. *Stem Cells Transl. Med.* *2*, 255–264.
- Tucker, B.A., Park, I.H., Qi, S.D., Klassen, H.J., Jiang, C., Yao, J., Rendenti, S., Daley, G.Q., and Young, M.J. (2011). Transplantation of adult mouse iPSC cell-derived photoreceptor precursors restores retinal structure and function in degenerative mice. *PLoS One* *6*, e18992.
- Tucker, B.A., Mullins, R.F., Streb, L.M., Anfnson, K., Eyestone, M.E., Kaalberg, E., Riker, M.J., Drack, A.V., Braun, T.A., and Stone, E.M. (2013). Patient-specific iPSC-derived photoreceptor precursor cells as a means to investigate retinitis pigmentosa. *Elife* *2013*, 1–18.
- Waldron, P.V., Di Marco, F., Kruczek, K., Ribeiro, J., Graca, A.B., Hippert, C., Aghaizu, N.D., Kalargyrou, A.A., Barber, A.C., Grimaldi, G., et al. (2017). Transplanted donor- or stem cell-derived cone photoreceptors can both integrate and undergo material



transfer in an environment-dependent manner. *Stem Cell Reports* *10*, 1–16.

Welby, E., Lakowski, J., Di Foggia, V., Budinger, D., Gonzalez-Cordero, A., Lun, A.T.L., Epstein, M., Patel, A., Cuevas, E., Kruczek, K., et al. (2017). Isolation and comparative transcriptome analysis of human fetal and iPSC-derived cone photoreceptor cells. *Stem Cell Reports* *9*, 1898–1915.

Wiley, L.A., Burnight, E.R., DeLuca, A.P., Anfinson, K.R., Cranston, C.M., Kaalberg, E.E., Penticoff, J.A., Affatigato, L.M., Mullins, R.F., Stone, E.M., et al. (2016). cGMP production of patient-specific iPSCs and photoreceptor precursor cells to treat retinal degenerative blindness. *Sci. Rep.* *6*, 30742.

Zhao, C., Wang, Q., and Temple, S. (2017). Stem cell therapies for retinal diseases: recapitulating development to replace degenerated cells. *Development* *144*, 1368–1381.

Zhong, X., Gutierrez, C., Xue, T., Hampton, C., Vergara, M.N., Cao, L.-H., Peters, A., Park, T.S., Zambidis, E.T., Meyer, J.S., et al. (2014). Generation of three-dimensional retinal tissue with functional photoreceptors from human iPSCs. *Nat. Commun.* *5*, 1–14.

Zhu, J., Cifuentes, H., Reynolds, J., and Lamba, D.A. (2017). Immunosuppression via loss of IL2 γ enhances long-term functional integration of hESC-derived photoreceptors in the mouse retina. *Cell Stem Cell* *20*, 374–384.e5.

Supplemental Information

**Characterization and Transplantation of CD73-Positive Photoreceptors
Isolated from Human iPSC-Derived Retinal Organoids**

Giuliana Gagliardi, Karim Ben M'Barek, Antoine Chaffiol, Amélie Slembrouck-Brec, Jean-Baptiste Conart, Céline Nanteau, Oriane Rabesandratana, José-Alain Sahel, Jens Duebel, Gael Orioux, Sacha Reichman, and Olivier Goureau

Supplemental Information

Supplemental Figures

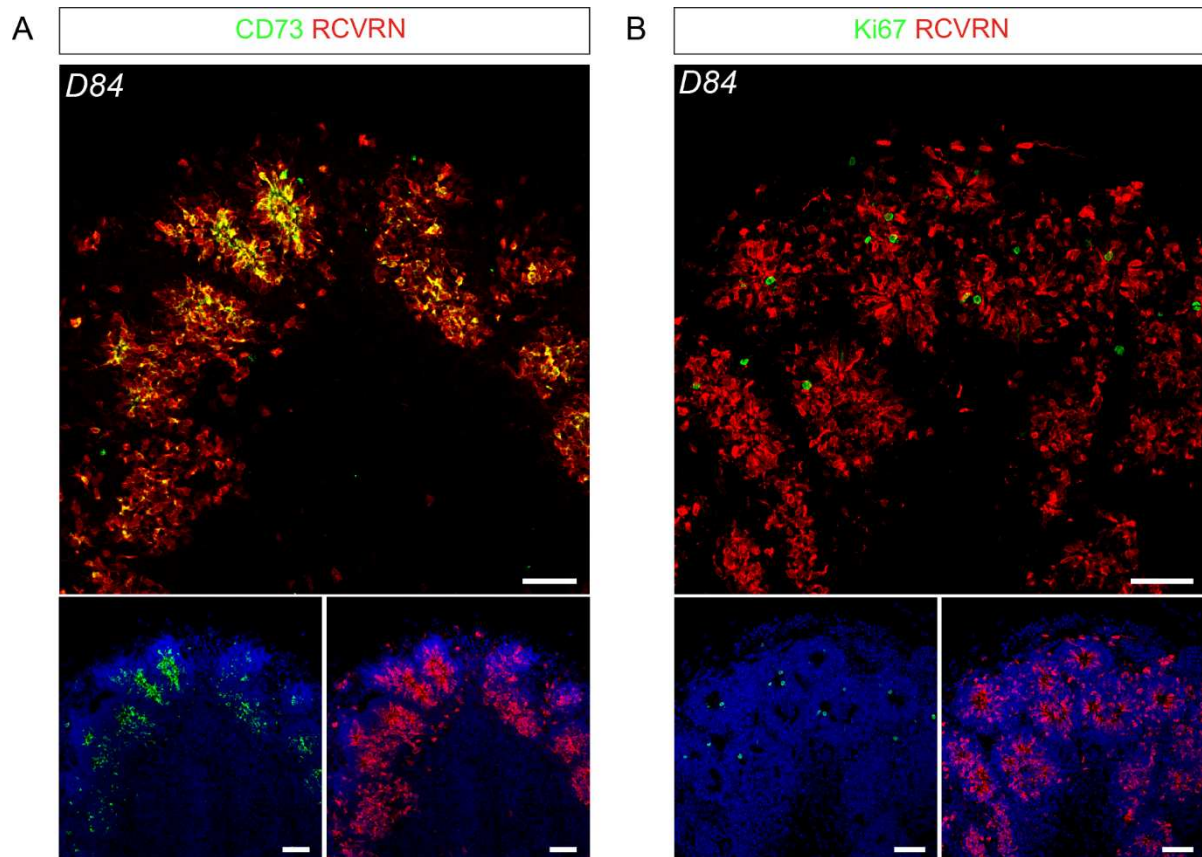


Figure S1. Expression of CD73 in post-mitotic photoreceptor precursors in hiPSC-derived retinal organoids. Related to Figure 1.

(A) Co-expression of CD73 (green) and RECOVERIN (red) by immunohistochemistry in a section from D84-old organoid. Note that CD73 is exclusively expressed in RCVRN⁺ cells.

(B) Immunostaining with mitotic marker Ki67 (green) and RECOVERIN (red) in a section from D84-old organoid. Note that all of the RCVRN⁺ cells do not express Ki67, confirming that RCVRN⁺ cells correspond to post-mitotic PR precursors.

Nuclei were counterstained with DAPI (blue). Scale bars: 50 μ m.

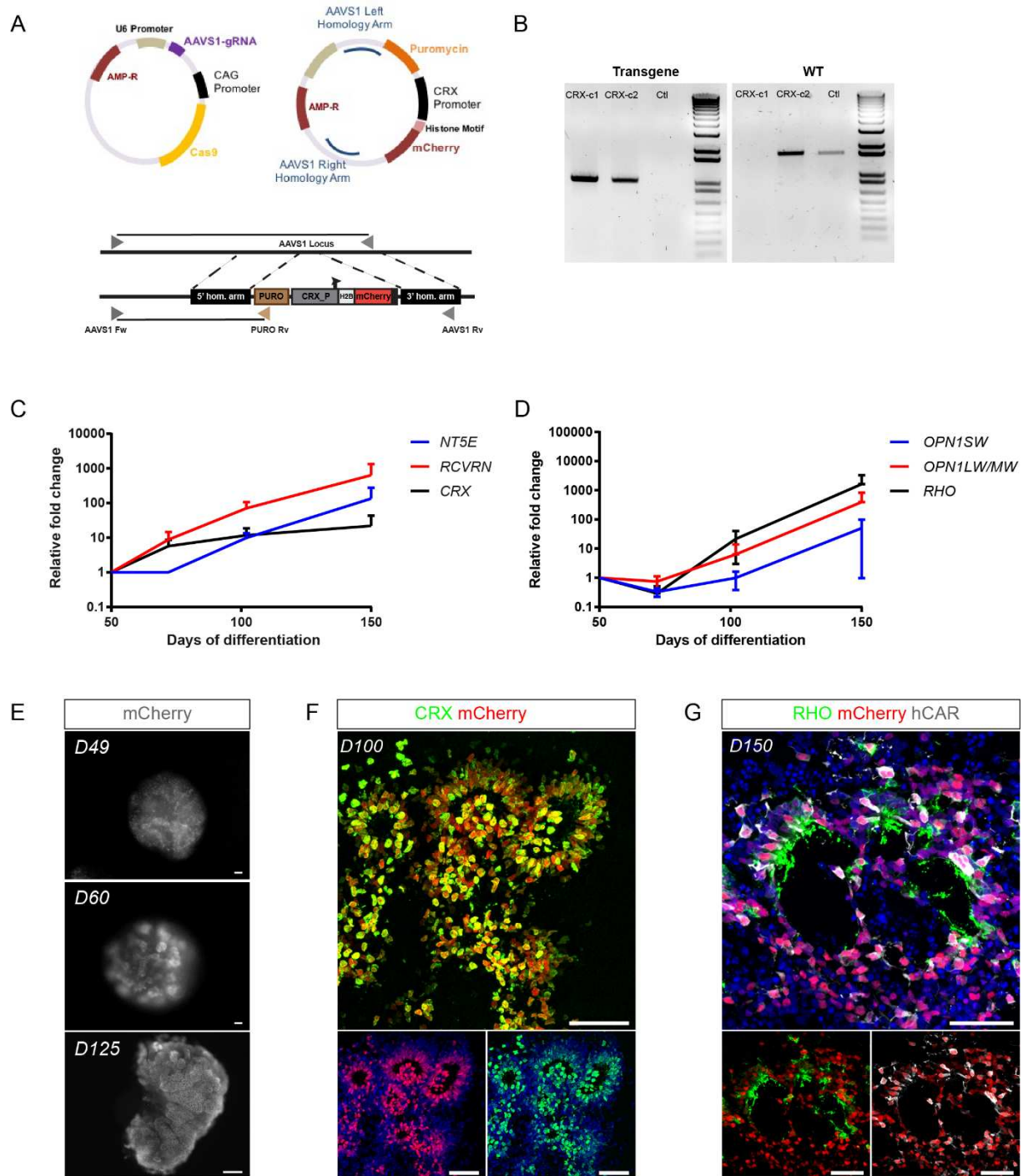


Figure S2. Generation and characterization of AAVS1::CrxP_H2BmCherry hiPSC line. Related to Figures 1 and 2.

(A) Schematic representation of CRISPR/Cas9 and donor plasmids used for the generation of the AAVS1::CrxP_H2BmCherry hiPSC line. Triangles on the bottom schema indicate the homology region of the primers (AAVS1 Fw, PURO Rv, AAVS1 Rv) used to validate the insertion of the fluorescent cassette.

(B) Results of the PCR evaluating the integration of CrxP_H2BmCherry construct into AAVS1 site. Gel on the left shows the presence of the transgene in clone CRX-c1 and CRX-c2, corresponding to the amplification product with AAVS1 Fw and PURO Rv primers, as indicated in A. The transgene was not amplified in DNA from WT hiPSCs (control, Ctl). Picture of the gel on the right shows the result of the PCR with AAVS1 Fw and AAVS1 Rv primers amplifying exclusively the WT form of the AAVS1 locus (Ctl), allowing for distinction between heterozygous (CRX-c2) or homozygous integration (CRX-c1).

(C-D) RT-qPCR analysis of *NT5E* (coding for CD73) and PR markers during differentiation from AAVS1::*CrxP*_H2BmCherry hiPSC line between D50 and D150 (mean \pm SD; n=5 organoids from N=3 differentiations per time point). Gene expression at each time point is indicated relative to organoids at D50.

(E) Endogenous expression of mCherry detected in AAVS1::*CrxP*_H2BmCherry retinal organoids at different time of differentiation.

(F) Immunostaining with CRX antibody confirming the specific co-localization between CRX+ cells and mCherry+ nuclei in section of D100 AAVS1::*CrxP*_H2BmCherry retinal organoid.

(G) Immunostaining showing the expression of RHODOPSIN (RHO) and human specific CONE ARRESTIN (hCAR) in mCherry+ cells in section of D100 AAVS1::*CrxP*_H2BmCherry retinal organoid, confirming that mCherry+ cells correspond to both rods and cones.

Scale bars: 100 μ m (E), 50 μ m (F,G).

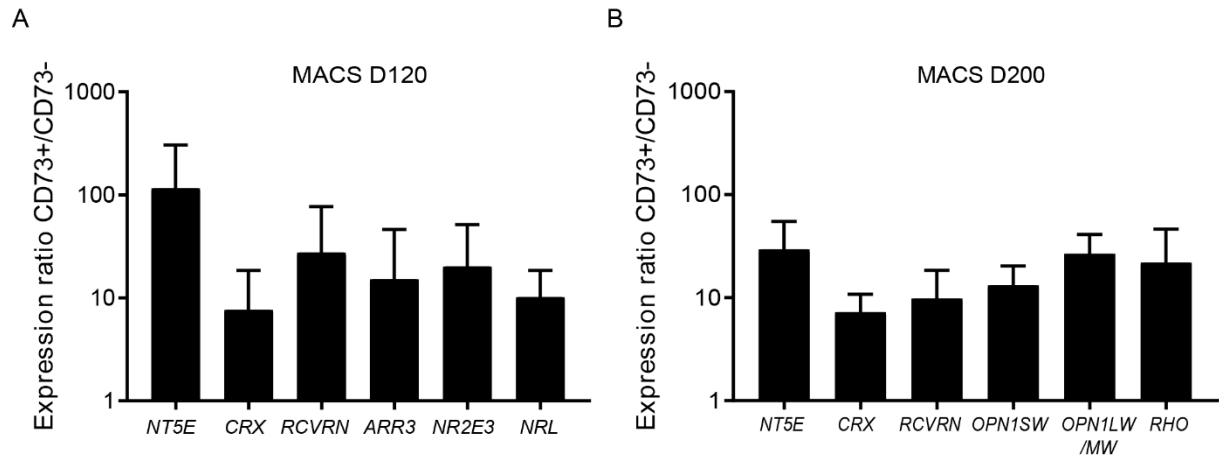


Figure S3. Increased expression of PR genes in CD73-positive fractions. Related to Figures 2 and 3.

(A) RT-qPCR expression ratio of PR-specific genes between cells from CD73-positive and negative fractions after MACS at D120 (mean \pm SD; n=25 organoids from N=6 differentiations).

(B) RT-qPCR expression ratio of PR-specific genes between cells from CD73-positive and negative fractions after MACS at D200 (mean \pm SD; n=25 organoids from N=6 differentiations).

For all of the analysis, the relative expression to unsorted cells was calculated first (values shown in Figures 2E and 3A). The ratio values were obtained by dividing the expression values from CD73-positive fractions by corresponding values from CD73-negative fractions.

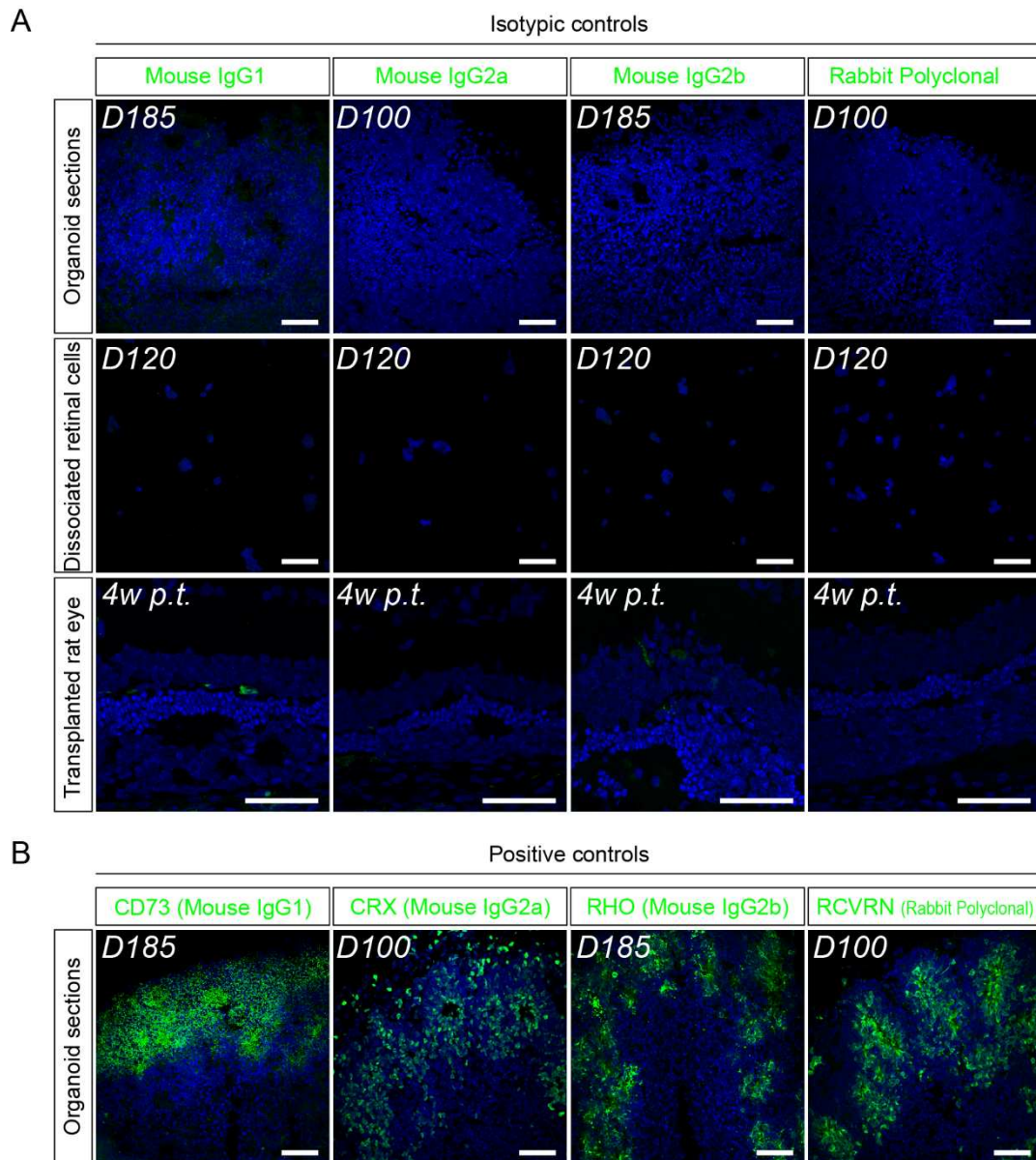


Figure S4. Negative isotypic controls confirm specificity of primary antibody immunostainings. Related to Figures 1, 2, 5, 6 and 7.

(A) Immunostaining on retinal organoid sections, dissociated retinal cells and rat retinal sections with isotypic control antibodies. The absence of signal or its non-specific localization (in rat retina sections) confirm the specificity of the primary antibodies used in this study. Each isotypic antibody was used at the highest concentration within the concentration range used for corresponding primary antibodies.

(B) Immunostainings on retinal organoid sections with different primary antibodies, performed as positive controls.

Scale bars: 50 μm (A,B).

Supplemental movie legends

Movie S1: Movie of a D75 AAVS1::*CrxP*_H2BmCherry retinal organoid labelled with anti-CRX (green)
(related to Figures 1 and S2)

Supplemental Tables

Table S1. List of antibodies used for immunohistochemistry analysis
(related to Figures 1-7, S1, S2 and S4)

Antigen	Species	Dilution	Source
Primary antibodies			
CD73	Mouse IgG1	1:100	BioLegend (AD2/344002)
CD73-FITC	Mouse IgG1	1:1000	BioLegend (AD2/344015)
CD73-PE	Mouse IgG1	1:10	Miltenyi (AD2/130-097-943)
CONE ARRESTIN (human specific)	Rabbit Polyclonal	1:10 000	Gift from Dr C. Craft
CRX	Mouse IgG2a	1:5000	Abnova (H00001406-M02)
HNA (human specific)	Mouse IgG1	1:500	Millipore (MAB1281)
KI67	Mouse IgG1	1:200	BD Pharmagen (550609)
	Rabbit Polyclonal	1 :500	Abcam (ab15580)
MTCO2 (human specific)	Mouse Polyclonal	1:500	Abcam (ab3298)
NANOG	Rabbit Polyclonal	1:2000	Cell Signaling (D73G4)
OCT4	Rabbit Polyclonal	1:100	Cell Signaling (C30A3)
BLUE OPSIN	Rabbit Polyclonal	1 :500	Millipore (AB5407)
RED/GREEN OPSIN	Rabbit Polyclonal	1:500	Millipore (AB5405)
PAX6	Rabbit Polyclonal	1:1000	Millipore (AB2237)
PKC α	Rabbit Polyclonal	1:1000	Sigma-Aldrich (P34334)
RHODOPSIN	Mouse IgG2b	1:500	Millipore (MABN15)
RIBEYE (CtBP2)	Mouse IgG1	1:500	BD Bioscience (612044)
RECOVERIN	Rabbit Polyclonal	1:5000	Millipore (AB5535)
SSEA4	Mouse IgG	1:200	Cell Signaling (MC813)
STEM 121(human specific)	Mouse IgG1	1:500	Takara Bio (Y40410)
Primary Control Isotype			
Isotype Control	Mouse IgG1		Cell Signaling (G3A1)
Isotype Control	Mouse IgG2a		Cell Signaling (E5Y6Q)
Isotype Control	Mouse IgG2b		Cell Signaling (E7Q5L)
Isotype Control	Rabbit Polyclonal		Cell Signaling
Secondary antibodies			
Alexa Fluor-488 anti mouse	Donkey	1:600	Jackson ImmunoResearch (715-545-150)
Alexa Fluor-488 anti rabbit	Donkey	1:600	Jackson ImmunoResearch (711-545-152)
Alexa Fluor-594 anti mouse	Donkey	1:600	Jackson ImmunoResearch (715-585-150)
Alexa Fluor 594 anti rabbit	Donkey	1:600	Jackson ImmunoResearch (715-585-152)

Table S2. List of TaqMan® Gene Expression ID Assays used for qRT-PCR
(related to Figures 1, 2, 3, S2 and S3)

Gene Symbols	Assays IDs
<i>18S</i>	<i>18S-Hs99999901_s1</i>
<i>OPN1SW</i>	<i>OPN1SW-Hs00181790_ml</i>
<i>NT5E (CD73)</i>	<i>NT5E-Hs00159686_ml;</i>
<i>CNGA1</i>	<i>CNGA1-Hs00175586_ml</i>
<i>CNGA3</i>	<i>CNGA3-Hs00175667_ml</i>
<i>CNGB1</i>	<i>CNGB1-Hs00974374_ml</i>
<i>CNGB3</i>	<i>CNGB3-Hs01555863_ml</i>
<i>CONE ARRESTIN</i>	<i>ARR3-Hs00182888_ml</i>
<i>CRX</i>	<i>CRX-Hs00230899_ml</i>
<i>NRL</i>	<i>NRL-Hs00172997_ml</i>
<i>NR2E3</i>	<i>NR2E3-Hs00183915_ml</i>
<i>OPN1LW/MW</i>	<i>OPN1LW/MW-Hs00241039_ml</i>
<i>RECOVERIN</i>	<i>RCVRN-Hs00610056_ml</i>
<i>RHODOPSIN</i>	<i>RHO-Hs00892431_ml</i>

Supplemental Experimental Procedures

Human iPSC maintenance and retinal differentiation

Human iPSCs derived from dermal fibroblasts (hiPSC-2 clone, Reichman et al., 2014) and *AAVS1::CrxP H2BmCherry hiPSC line* derived from human retinal Müller glial cells were cultured on truncated recombinant human vitronectin-coated dishes with Essential 8™ medium (ThermoFisher Scientific) as previously described (Reichman et al., 2017). For retinal differentiation adherent iPSCs were expanded to 70-80 %, then FGF-free medium was added to the cultures for 2 days followed by a neural induction period allowing the appearance of retinal structures. Identified retinal organoids were manually isolated and cultured as floating structures for the next several weeks to follow retinal differentiation as previously described (Reichman et al., 2017).

Magnetic-Activated Cell Sorting

Retinal organoids at various time points of differentiation were dissociated with papain (Worthington) accordingly to the protocol described in Reichman et al., 2017. To remove residual aggregates, cell suspensions were filtered through a 30 µm strainer (Miltenyi Biotec) pre-hydrated with 1 ml of ProB27 medium (Reichman et al. 2017). After counting, cells were centrifuged and resuspended in MACS buffer, composed of 2 mM EDTA (Sigma-Aldrich) and 1% FBS in PBS (ThermoFisher Scientific). For the labelling with the primary antibody, cells were incubated with CD73 antibody (BioLegend) for 10 minutes at 4°C at a dilution of 1:10. Cells were washed by adding 1-2 ml of MACS buffer per 10⁷ cells and centrifuged 5 minutes at 300 g. Cell pellet was resuspended in 80 µl of buffer and 20 µl of anti-mouse IgG1 MicroBeads (Miltenyi Biotec) were added per 10⁷ cells. After 15 minute-incubation at 4°C, cells were washed once in MACS buffer, resuspended in 500 µl of MACS buffer and applied onto a pre-equilibrated MS column fixed to a MACS separator (Miltenyi Biotec). The flow-through containing negative or unlabeled cells was collected by three washes with 500 µl MACS buffer. Column was removed from the magnet and the positive fraction was eluted with 1 ml of MACS buffer in a new collection tube. Cells from both CD73-negative and positive fractions were quantified before being used for successive experiments.

Flow cytometry analysis

Following dissociation of retinal organoids by papain digestion, 2x10⁵ cells were resuspended in 100 µl of MACS buffer and incubated 10 minutes at 4°C with CD73-FITC antibody (BioLegend) diluted 1:1000. Cells were washed once and resuspended in 300 µl MACS buffer for analysis. Background fluorescence and non-specific binding were measured using unstained cells and isotypic control.

To evaluate cell viability, dissociated cells were resuspended in MACS buffer at the concentration of 1x10⁶ cells/ml. Propidium Iodide (ThermoFisher Scientific) was added to the cells at a final concentration of 1 µg/ml, incubated for 30 minutes at 4°C in the dark. Samples were analyzed without additional washings. Analysis was performed at FC500 flow cytometer (Beckman Coulter). Flow cytometry files were analyzed using FlowJo software (Treestar).

Cryopreservation of hiPSC-derived retinal organoids and MAC-sorted CD73+ cells

Five retinal organoids at D100 were suspended in 250 µl of cold Cryostem freezing medium (Clinisciences) and frozen as described (Reichman et al., 2017). Between 1 and 2 million of MAC-sorted CD73+ cells were suspended in 250 µl of cold Cryostem freezing medium (Clinisciences) and frozen using the same method. Frozen retinal structures and CD73+ cells were thawed quickly at 37°C in a water bath and resuspended in prewarmed dedicated media for downstream investigations.

Adherent culture of dissociated retinal cells

Unsorted or MAC-sorted retinal cells were plated in 24 well-plates previously coated with Poly-D-Lysin at 2 µg/cm² and Laminin at 1 µg/cm² (Sigma-Aldrich). Dissociated cells were incubated at 37°C in a standard 5% CO₂ / 95% air incubator and medium was changed after 24 hours. After 48 hours cells were fixed with 4% PFA in PBS for 10 minutes at 4°C and kept in PBS until immunostaining.

Generation of AAVS1::CrxP H2BmCherry hiPSC line

To construct donor plasmid for the expression of H2BmCherry under the control of Crx promoter from the AAVS1 locus, AAV-CAGGS-EGFP1 plasmid (Addgene #22212) (Hockemeyer et al., 2009) was modified. H2BmCherry extracted from NucBow plasmid (Loulrier et al., 2014) and synthetic 2.5kB mouse CRX promoter (Furukawa et al., 2002) were subcloned by a XbaI/MluI digestion between AAVS1 homology arms of 800 bp each (HA-L and HA-R). We used pX330-U6-Chimeric_BB-CBh-hSpCas9 (addgene#42230) (Cong et al., 2013) to construct the CRISPR/Cas9 vector by annealing and ligating in BbsI sites an oligonucleotide pairs (5'-CACCGGGGCCACTAGGGACAGGAT-3' / 3'-CCCCGGTGATCCCTGTCTACAAA-5') encoding a 20-nt AAVS1 guide sequence according to the protocol of Ran et al. (Ran et al., 2013). Plasmids are prepared using a Plasmid MidiPrep kit (Macherey-Nagel) and verified by restriction digest and gel electrophoresis for identity and

integrity, and quantity determined by NanoDrop (ThermoFisher Scientific) before storage at 1–2 mg/ml in sterile Tris buffer (pH 8.0). To generate stable cell lines, hiPSC line derived from retinal Müller glial cells (Slembrock-Brec et al., manuscript in preparation) were grown for 24 hours in 6-well plates before overnight transfection at 37°C with CRISPR/Cas9 and donor plasmids using FuGene HD (Promega). Two days after transfection, selection of recombinant cells was started in presence of 0.25 µg/ml Puromycin (ThermoFisher Scientific) for the first 48 hours; the concentration of Puromycin was then increased to 0.5 µg/ml until picking of single colonies. Genomic DNA from Puromycin-resistant clones was extracted with Nucleospin Tissue Kit (Macherey-Nagel) according to the manufacturer instruction. Correct reporter integration was evaluated by PCR using a forward primer upstream to the left arm of recombination of AAVS1 and a reverse primer either within the reporter cassette or in the AAVS1 right homologous arm (Figure S1A). The PCR was composed of 32 cycles including 3 successive steps at 95°C, 60°C and 72°C for respectively 30 seconds, 30 seconds and 2 minutes. The genotype was finally visualized after migration of the DNA in a 1.2 % agarose gel. After validation by sequencing, one homozygous reporter integration cell line (CRX-c1) was selected for generation of retinal organoids. Importantly, hiPSCs remained pluripotent after CRISPR/Cas9 gene editing, keeping a hESC-like morphology with no genomic alteration, evaluated by SNP genotyping.

Retinal organoid immunostaining-clearing and imaging

Retinal organoids were first incubated at RT on a rotating shaker in a solution (PBSGT) of PBS 1X containing 0.2% gelatin, 0.5% Triton X-100 and 0.01% thimerosal (Sigma-Aldrich) for 3 hours. Samples were next transferred to PBSGT containing primary antibody against CRX (Table S1) and placed at 37°C for 3 days, with rotation at 100 rpm. This was followed by six washes for 30 minutes in PBSGT at RT. Next, samples were incubated with appropriate secondary antibodies conjugated with Cy3 (Interchim) diluted at 1:600 in PBSGT overnight. After six 30-minute washes in PBSGT at RT, samples were stored at 4°C in PBS until the 3D imaging of solvent-cleared organ (3DISCO) clearing procedure (Belle et al., 2014). 3D imaging was performed with an ultramicroscope (LaVision BioTec) using the InspectorPro software (LaVision BioTec), as previously described (Belle et al., 2014). Images, 3D volume and movies were generated using Imaris x64 software (version 7.6.1, Bitplane) using the “snapshot” and “animation” tools.

Calcium dye loading and two-photon calcium imaging

Retinal cells dissociated from 200-day old retinal organoids were incubated for 10 minutes at 4°C with CD73-PE antibody diluted at 1:1000 in MACS buffer. Cells were then washed in MACS buffer and resuspended in culture medium and plated on Poly-D-Lysin/Laminin-coated coverslips. The intracellular calcium indicator Fura 2-AM (ThermoFisher Scientific) was dissolved in DMSO mixed with 20% Pluronic F-127 (ThermoFisher Scientific) before being diluted to the final concentration of 10 µM. In a standard incubator, dark-adapted retinal cells were loaded with Fura2-AM (10 µM) for 45 minutes at 37°C, and later placed in the recording chamber of a 2-photon microscope. Cells were perfused (2 ml/min) with oxygenated (95% O₂/5% CO₂) AMES Ringer’s solution (Sigma-Aldrich) for at least 1 hour in the dark, and later exposed to 1 mM of 8-Br-cGMP (Sigma-Aldrich) puffs, diluted in AMES. Glass pipettes (borosilicate glass capillaries) with a resistance of 5 MΩ, filled with the solutions and connected to a Picospritzer II pressure system (General Valve Corporation, pressure 5 psi) were used for applying 10 seconds puffs on small groups of recorded cells. Temperature was kept at 37°C for the duration of the experiment. A custom-made two-photon microscope equipped with a 25x water immersion objective (XLPlanN-25x-W-MP/NA1.05, Olympus) and a pulsed femto-second laser (InSight™ DeepSee™, Newport Corporation, Irvine, CA) were used to image cells stained by the Fura 2-AM dye. We acquired and analyzed image sequences of neighbor cells positioned in the puffing area (square regions of at least 50x50 µm), using the excitation laser at a wavelength of 800 nm. The interval between two consecutive puff stimulations was at least two minutes and 20 seconds of baseline spontaneous activity were recorded before every puff experiment. An increase in calcium concentration in a cell was detected as a decrease in Fura-2 fluorescence intensity, which was calculated using the formula % ΔF/F₀, in which ΔF=F-F₀, and where F₀ was average baseline cell intensity during the 20-second prestimulus period.

Animals

Adult nude rats (CrI:NIH-Foxn1^{nu}) were purchased from Charles River Laboratories. Transgenic homozygous P23H-1 rats obtained from the laboratory of S. Picaud (Vision Institute, Paris) were crossed with WT albino Sprague-Dawley rats purchased from Charles River Laboratories to produce hemizygous P23H-1 rats. Animals were kept on a 12-hour light/12-hour dark cycle in plastic cages and allowed to eat and drink ad libitum in the animal facility of the Vision Institute (agreement number A751202). All experiments were carried out in strict accordance with the Association for Research in Vision and Ophthalmology statement for animal research in ophthalmology. Moreover, protocols were approved by the local ethical committee (Charles Darwin ethical committee for animal experimentation C2EA-05) in strict accordance with French and European regulation for animal use in research (authorization number 05033).

Cell transplantation

From 2 days before transplantation to the end of the follow-up, 6-week-old hemizygous P23H rats were maintained under immunosuppression through cyclosporine treatment (210 mg/liter) in the drinking water (M'Barek et al., 2017). Rats were first anesthetized by 5% isoflurane inhalation for 5 minutes and they were maintained in deep anesthesia with 2% isoflurane inhalation. A few drops of a local anesthetic (oxybuprocaine; Thea) and tropicamide (Mydriaticum 0.5%; Thea) were added onto the cornea of the eye to be transplanted. Surgery was performed under an operating microscope (Leica F18). Cells were resuspended in MACS buffer at 75000 cells per μl . A microsyringe pump injector (UMP3 UltraMicroPump and Micro4 controller, World Precision Instruments) connected to a 80-gauge glass microcapillary (Eppendorf) containing 4 μl of cell suspension was inserted into the eye approximately 2 mm posterior to the limbus. Then the microcapillary was slowly advanced into the vitreous space, placed nasally in the subretinal space where cell suspension was slowly injected, so that soft retina was focally detached from comparatively hard retinal pigmented epithelium. 6-week-old Nude rats were subjected to the same surgical procedures for subretinal transplantation. Animals with signs of major intraocular hemorrhage during the surgery or with disrupted retina/absence of graft based on optical coherence tomography evaluation were excluded (about 20% of animals).

Cryosection

For cryosectioning, retinal organoids and rat eye cups were fixed respectively for 10 minutes and 6 hours in 4% paraformaldehyde at 4°C and washed in PBS. Structures were incubated at 4°C in PBS / 30% Sucrose (Sigma-Aldrich) solution during at least 2 hours. Structures were embedded in a solution of PBS, 7.5% gelatin (Sigma-Aldrich), 10% sucrose and frozen in isopentane at -50°C. 10 μm -thick cryosections were collected for analysis.

Immunostaining, imaging and cell counting

Sections and dissociated retinal cells on coverslips were subjected to immunostaining as previously described (Orioux et al., 2014; Reichman et al., 2014). Primary antibodies, their isotopic controls as well as secondary antibodies are listed in Table S1. Fluorescent staining signals were captured with an Olympus FV1000 confocal microscope and images were acquired using a 1.55, 0.54 or 0.46 μm step size and corresponded to the projection of 20 to 40 optical sections. To assess the specificity of primary antibody, these were replaced with isotype controls at the highest concentration. For all antibodies no non-specific binding was observed (Figure S4). For cell counting, images were acquired using a ThermoFisher Scientific ArrayScan VTI and analyzed using the target activation protocol by HCS Studio Software 6.6.0.

RNA extraction and Taqman Assay

Total RNAs were extracted using Nucleospin RNA II kit (Macherey-Nagel) and cDNA synthesized from 250 ng of RNA using the QuantiTect reverse transcription kit (Qiagen) following manufacturer's recommendations. qPCR analysis was performed on diluted cDNA (1/20) in 20 μl final volume in microplate using a Applied Biosystems real-time PCR machine (7500 Fast System) with TaqMan® Gene expression Master Mix (ThermoFisher Scientific) as previously described (Reichman et al., 2014). All primers and MGB probes labeled with FAM for amplification (Table S2) were purchased from ThermoFisher Scientific. 18S was used as internal control to normalize expression of analyzed genes. Quantification of relative gene expression was based on the DeltaCt Method in three minimum independent biological experiments.

Statistical analysis

n corresponds to number of organoids or images from each independent differentiation, or number of animals; N indicates the number of independent experiments performed (e.g. the number of independent retinal differentiations). Statistical analysis is based on at least three independent experiments. Statistical analysis was performed using Prism 7 (GraphPad software) with appropriate statistical test including Mann-Whitney test, one-way, two-way ANOVA or Kruskal-Wallis test followed when necessary by multiple comparison test (post-hoc analysis) such as the Tukey's test. Values of $P < 0.05$ were considered statistically significant.

Supplemental References

- Cong, L., Ran, F.A., Cox, D., Lin, S., Barretto, R., Hsu, P.D., Wu, X., Jiang, W., and Marraffini, L.A. (2013). Multiplex Genome Engineering Using CRISPR/VCas Systems. *Science* (80-). *339*, 819–823.
- Hockemeyer, D., Soldner, F., Beard, C., Gao, Q., Mitalipova, M., Dekelver, R.C., Katibah, G.E., Amora, R., Boydston, E.A., Zeitler, B., et al. (2009). Efficient targeting of expressed and silent genes in human ESCs and iPSCs using zinc-finger nucleases. *Nat. Biotechnol.* *27*, 851–857.
- Loulier, K., Barry, R., Mahou, P., Franc, Y. Le, Supatto, W., Matho, K.S., Ieng, S., Fouquet, S., Dupin, E., Benosman, R., et al. (2014). Multiplex Cell and Lineage Tracking with Combinatorial Labels. *Neuron* *81*, 505–520.
- M'Barek, K. Ben, Habeler, W., Plancheron, A., Jarraya, M., Regent, F., Terray, A., Yang, Y., Chatrousse, L., Domingues, S., Masson, Y., et al. (2017). Human ESC-derived retinal epithelial cell sheets potentiate rescue of photoreceptor cell loss in rats with retinal degeneration. *Sci. Transl. Med.* *9*.
- Orieux, G., Picault, L., Slembrouck, A., Roger, J.E., Guillonneau, X., Sahel, J.-A., Saule, S., McPherson, J.P., and Goureau, O. (2014). Involvement of Bcl-2-Associated Transcription Factor 1 in the Differentiation of Early-Born Retinal Cells. *J. Neurosci.* *34*, 1530–1541.
- Ran, F.A., Hsu, P.D., Wright, J., Agarwala, V., Scott, D.A., and Zhang, F. (2013). Genome engineering using the CRISPR-Cas9 system. *Nat. Protoc.* *8*, 2281–2308.

3. Additional results

3.1 Characterization of human transplants by fluorescence in situ hybridization

Material exchange between donor and host photoreceptors account for the majority of apparent integrated cells in transplantation studies with murine photoreceptors. Since this mechanism has been very limitedly described for both donor human cells and rat host cells, we have extensively characterized donor cells in recipient retinas (Paper 2). We measured morphological features and we used several human specific antibodies directed against antigens localized in different cellular compartments (nucleus, cytoplasm and mitochondria). Importantly, we performed a co-staining using antibodies against human specific nuclear marker (HNA) and against human form of CONE ARRESTIN (cone cytoplasmic marker), and we validated the co-localization of these markers. Another technique that has been used in several studies to distinguish donor cells from host cells and investigate cytoplasmic material transfer is fluorescence in situ hybridization (FISH) (see **Table 7**). FISH probes have the advantage of targeting specific chromosome features, offering the possibility to identify cell nuclei and to detect nuclear fusion events.

Since one of the human iPSC line used for the generation of retinal cells was established from a male donor (Reichman et al., 2014), we have performed FISH using a probe specific for the human Y chromosome (XCP Y Orange, Metasystems) as previously described (Santos-Ferreira et al., 2016b). We combined FISH with immunostaining for the cytoplasmic human marker STEM121 (S121) to verify the specificity of the probe signal and to detect any event of material exchange. FISH signal was detected exclusively in cells displaying nuclear morphology typical of human cells (**Figure 23A and B**), as previously described (Paper 2). All the S121+ cells were also positively labelled by the probe against the human Y chromosome. As expected, host rat photoreceptors (rPR), and more generally host rat retinal cells, were not stained with the human Y chromosome FISH probe or with S121 antibody. Analysis was performed on retinal sections at both 1 month (**Figure 23A**) and 2.5 months (**Figure 23B**) after transplantation, with equivalent results.

We did not detect any event of material transfer, corresponding to S121+/Y- cells, or nuclear fusion, as we did not observe any Y+ cell displaying rat nuclear morphology. These additional findings validated our results obtained by immunostaining and morphological characterization (Paper 2).

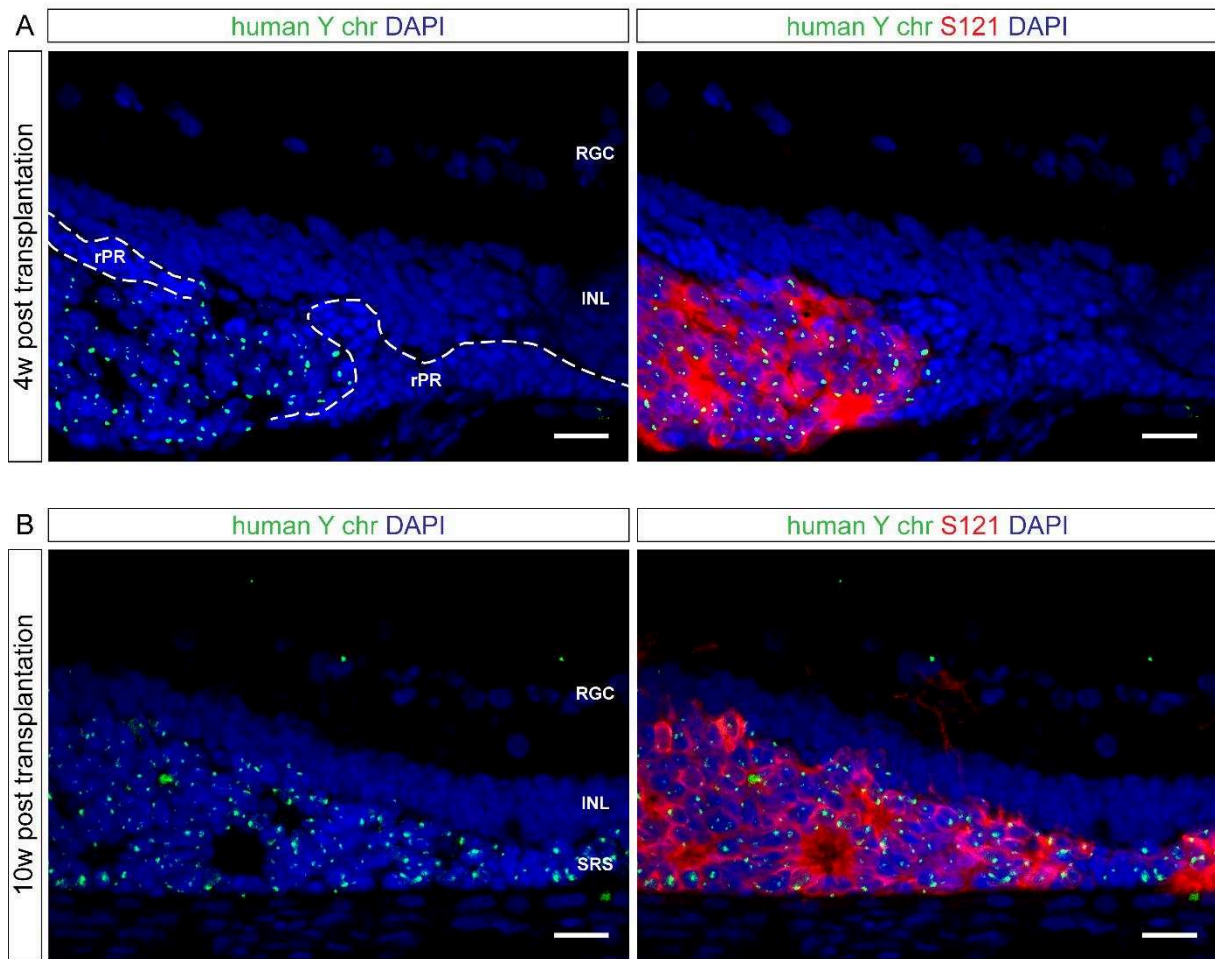


Figure 23: Identification of transplanted human cells by FISH and immunolabeling.

FISH for human Y chromosome (green) with immunostaining for human cytoplasmic antigen S121 (red) in P23H rat recipients at 4 weeks (A) and 10 weeks (B) after transplantation.

Scale bars 20 μ m. rPR, rat photoreceptors

3.2 Evaluation of the visual function in P23H rats by full field ERG recording

Although we could demonstrate some functionality *in vitro* of CD73+ mature photoreceptors (Paper 2), we could not detect a significant rescue of the visual function in transplanted P23H rats. Here, we present in more details the data we could collect in two different transplantation studies.

Three days after injection, eye fundus were examined by *in vivo* by fundus photography (bright field) following dilation with Tropicamide (1%) and using a Phoenix Micron III Retinal Imaging Microscope (Phoenix) according to the manufacturer's instructions.

Before ERG recording, all animals were kept in the dark overnight for adaptation. Rats were anesthetized during the entire procedure. Gold electrodes were placed on each cornea, which were humidified with an ophthalmic gel (Lacrinorm 0.2%, Bausch & Lomb). Ground and reference electrodes were placed on the back and cheeks. Full field ERGs were recorded simultaneously in both eyes using Visiosystem (SIEM Bio-Medicale) after light stimulation (Ganzfeld stimulator, SIEM Bio-Medicale). Seven levels of stimulus intensity ranging from 0.000003 cd·s/m² to 10 cd·s/m² were used for ERG recording. Each individual response is the mean of five measures.

Spectral domain optical coherence tomography (SD-OCT) was performed immediately after ERG to obtain a morphological analysis of the retina, with an OCT imaging device (Bioptigen 40 nm HHP) coupled to InVivoVue software (Bioptigen). Rectangular scans were used to acquire b-scans near the optic nerve. En face SD-OCT images were reconstructed from b-scans using ImageJ software (reslice and maximal projection tools).

We first measured the light responses before transplantation from hemizygous P23H rats aged of 5 weeks (**Figure 24A**). Levels of measured b-wave amplitudes were quite variable between different samples, especially for responses to higher light stimuli, between 0.3 and 10 cd·s/m². Interocular differences were also quite marked, with a significant difference in b-wave amplitudes registered in left and right eyes at high light stimulus (n=20, *p<0.05, **p<0.01, 2 way ANOVA followed by Sidak's multiple comparison post hoc test), reflecting as expected, a certain variability in the degeneration rate of photoreceptors between different individuals, as well as within the same individual.

In the first series of experiments animals at 6 weeks of age were transplanted in their left eye by injection in the subretinal space via trans-vitreous route (**Figure 24B**). One group of rats had received a sham injection, with MACS buffer, while a second group was grafted with CD73+ cells. Three days after transplantation the left eye fundus was examined to verify the presence of retinal detachment at the site of injection (**Figure 24C**).

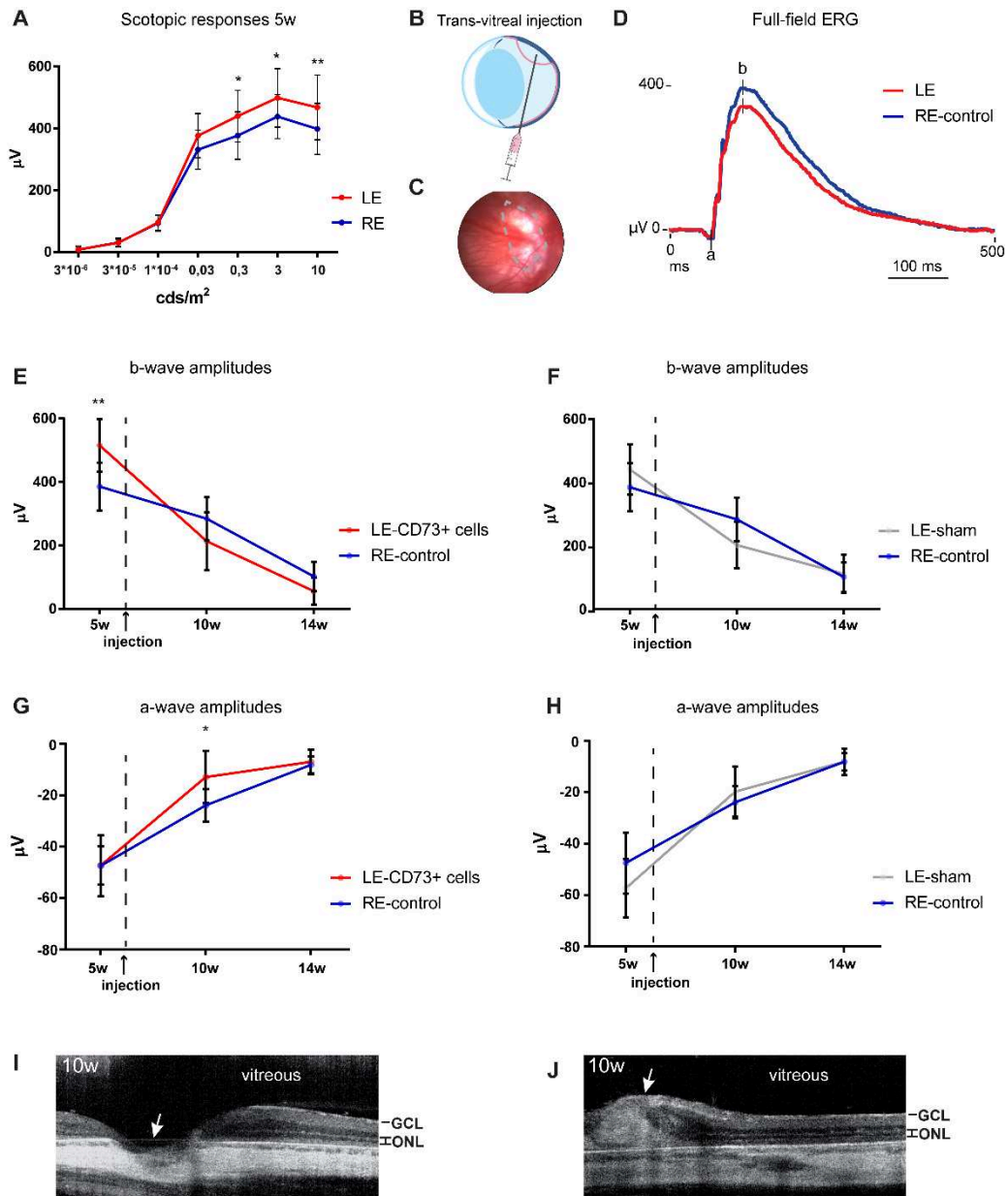


Figure 24 ERG recordings and SD-OCT images from P23H rats after trans-vitreous injection.

A) B-wave amplitudes measured in left eye (LE) and right eye (RE) of hemizygous P23H rats aged of 5 weeks, before transplantation. **B)** Illustration of the subretinal injection strategy. **C)** Eye-fundus image of a P23H rat 3 days after subretinal injection. Dotted lines delimitate site of retinal detachment resulting from injection. **D)** Representative waveforms registered with a 0.3 cds/m² stimulus from left and right eyes at 10 weeks. a-wave (a) and b-wave (b) peaks are indicated. **E)** b-wave amplitudes recorded with a 0.3 cds/m² stimulus from injected eyes with CD73+ cells (LE) and uninjected eyes (RE) before (5 weeks) and after transplantation (10 and 14 weeks). The time of injection is indicated by the dotted line. **F)** b-wave amplitudes recorded from uninjected eyes (RE) and eyes injected with MACS buffer used for cell resuspension (sham) at different time points. **G)** a-wave amplitudes recorded with a 0.3 cds/m² stimulus from sham-injected eyes (LE) and uninjected eyes (RE) as a function of age. Note that a-values are negative, so that increasing values actually indicate a reduction of visual function. **H)** a-wave amplitudes recorded with a 0.3 cds/m² stimulus from injected eyes with CD73+ cells (LE) and uninjected eyes (RE) as a function of age. **I)** Image obtained by SD-OCT illustrating retinal damage at the site of injection (indicated by the arrow). **J)** SD-OCT image of a P23H rat retina 4 weeks after transplantation with CD73+ cells. Arrow indicate the retinal bulge possibly containing donor cells. All data are represented as mean±SD. *p<0.05, **p<0.01, 2 way ANOVA followed by Sidak's multiple comparison post hoc test.

W, weeks; LE, left eye; RE, right eye; GCL, Ganglion Cell Layer; ONL, Outer Nuclear Layer.

4 weeks and 8 weeks following transplantation, we performed ERG recordings on the injected animals, which were aged of 10 and 14 weeks respectively.

Based on the b-wave amplitudes measured for each different light intensity in uninjected animals, we decided to focus the analysis of ERG responses, both a and b waves, on amplitudes recorded with a stimulus of 0.3 cds/m². At this light intensity, a negative peak for the a-wave, deriving from photoreceptor hyperpolarization, as well as a positive peak for the b-wave, corresponding to the entire retina response, could be easily identified without any risk of visual response saturation (**Figure 24D**).

Light responses recorded from injected eyes were not improved in any of the two conditions (**Figures E-H**). Indeed, compared to values registered before transplantation (5w), visual responses keep decreasing similarly in uninjected and injected eyes over the two months following transplantation. In all samples, b-wave and a-wave amplitudes recorded from transplanted eyes were smaller, even if not always significantly, than responses measured in non-transplanted eyes, indicating that the surgical procedure could have negatively affected vision function in transplanted animals. Analyses of grafted retinas by SD-OCT confirmed retinal damages that could be observed in some samples, reflecting the entry site of the needle corresponding to the injection site (**Figure 24I**). In some retinas, a bulge was visible in the SRS that could correspond to the transplanted cells (**Figure 24J**). Nevertheless, immunofluorescence analysis on retinal sections of P23H rats injected with CD73+ cells, reported in paper 2 (Figures 6 and 7), showed that transplanted cells could survive in the subretinal space of injected eyes.

Since trans-vitreous injections for cell delivery into the subretinal space are more prone to retinal damage because retina is pierced twice, we decided to test a different injection strategy to target the subretinal space, by introducing the needle through the choroid and the RPE to better preserve the integrity of the retina (**Figure 25A**). Therefore, with trans-scleral injections the neural retina should not be pierced. *In vivo* eye fundus examination excluded retinal abnormalities and confirmed the presence of retinal detachment at the site of injection (**Figure 25B**).

P23H rats were transplanted with CD73+ cells at 6 weeks of age, and subsequently analyzed at 10 and 14 weeks of age, corresponding to 4 weeks and 8 weeks after transplantation respectively. No significant differences in b-wave and a-wave amplitudes were observed in transplanted eyes compared to uninjected eyes in 10- or 14-week-old rats (**Figure 25C and D**). Interestingly, both b-wave and a-wave amplitudes showed a reduction, even if not significant, at 14 weeks compared to 10 weeks in uninjected eye. Differently, this decrease between 10 and 14 weeks was not observed in eyes transplanted with CD73+ cells: b-wave amplitudes remained stable, whereas a-wave amplitudes were slightly, not significantly, improved at 2 months compared to 1 month after injection. Imaging of the retina by SD-OCT,

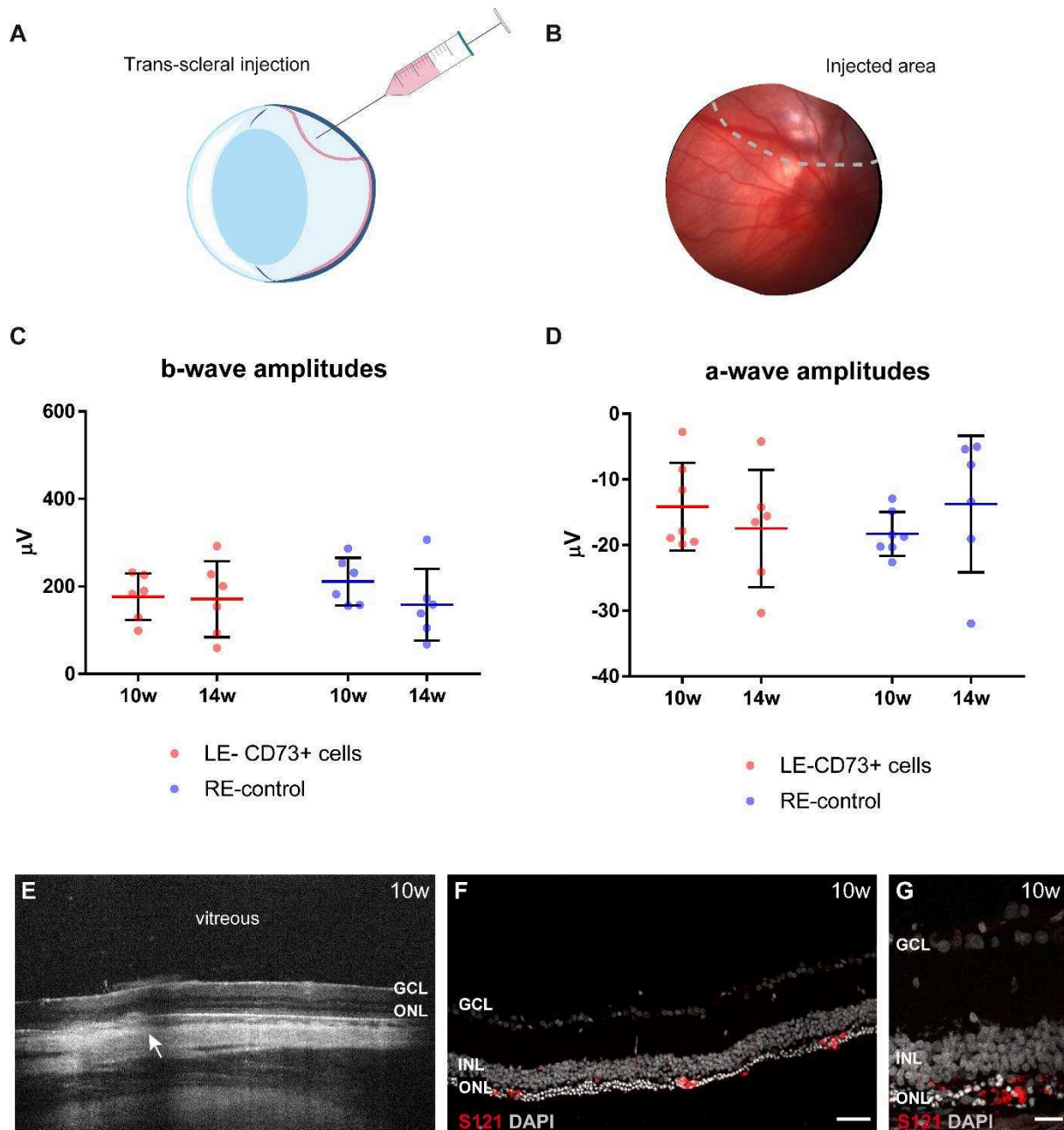


Figure 25: ERG recordings and SD-OCT images from P23H rats after trans-scleral injection.

A) Schematic illustrating the trans-scleral route to deliver cells in subretinal space. **B)** Eye-fundus image of a P23H rat 3 days after subretinal injection. Dotted lines delimitate site of retinal detachment resulting from injection. **C)** b-wave amplitudes recorded with 0.3cds/m² stimuli from injected (LE) and uninjected eyes (RE) of hemizygous P23H rats 4 weeks and 8 weeks after transplantation with CD73+ cells. **D)** a-wave amplitudes recorded with 0.3cds/m² stimuli from injected (LE) and uninjected eyes (RE) of hemizygous P23H rats 4 weeks and 8 weeks after transplantation with CD73+ cells. Note that a-values are negative, so that more negative values actually indicate an improvement of visual function. **E)** SD-OCT image of a P23H rat retina 4 weeks after transplantation with CD73+ cells. Arrow indicates the presumptive injection site. **F)** and **G)** Immunostaining on section of injected retina against human specific marker S121 (red). Nuclei were counterstained with DAPI (gray).

Scatter dot plots with mean \pm SD, n=6. Scale bars: 50 μ m (F), 20 μ m (G). W, weeks; LE, Left Eye; RE, Right eye; GCL, Ganglion Cell Layer; INL, Inner Nuclear Layer; ONL, Outer Nuclear Layer.

showed that the whole retina did not present any abnormalities and the injection site was undetectable in most of the samples (**Figure 25E**). However, when we analyzed retinal sections by immunostaining, very few human cells can be detected in recipient subretinal space (**Figure 25F and G**). Donor cells were detected in very few retinas injected by trans-scleral approach and in a lower quantity compared to retinas injected by the trans-vitreous method. For this reason, we could not establish a direct correlation between the rescue of the functionality and the presence of the grafted cells. For example, the increased reduction of ERG responses in uninjected eye compared to treated eyes could be due to interocular variability in the rate of photoreceptor degeneration (**Figure 24A**).

These results show the necessity to develop a surgical procedure allowing for a reduced detrimental impact on the host retina while ensuring an effective delivery and survival of grafted cells in the subretinal space.

Discussion and Perspectives

1. *In vitro* photoreceptor differentiation, maturation and isolation

We reported the generation of retinal organoids from three different human iPSC lines by a new feeder-free and xeno-free differentiation protocol. We also reported a complete characterization of the pattern of expression of the cell surface antigen CD73 in retinal organoids generated from two different human iPSC lines. This demonstrated the robustness of our differentiation protocol. Expected variability in CD73 expression levels within retinal organoids were reported by RT-qPCR and flow cytometry; nevertheless, we could perform CD73-based MACS using retinal organoids generated with both human iPSC lines, obtaining equivalent homogenous photoreceptor populations. Reproducibility and minimization of not only inter-cell line variability, but also batch-to batch variability, are crucial points for the manufacturing of a cell therapy product. Our differentiation protocol is based on the endogenous secretion of morphogens that lead to the spontaneous generation of retinal organoids. Differential abilities of iPSC lines to secrete inhibitors of both TGF β /BMP and Wnt pathways could affect the efficacy of retinal lineage differentiation. Extensive cell line characterization, as proposed by Bock et al. (Bock et al., 2011), will be useful to identify the most suitable pluripotent cell lines. The lack of exogenous molecules and reduction of complicated steps is the distinctive trait of our protocol and it represents more of a strength point than a liability, considering the potential for scalability and automatization.

The human iPSC lines used in the study presented here were initially established on feeders by episomal reprogramming and were adapted to feeder-free conditions in a second time. Although they have not been generated and cultured under full GMP-conditions, also because our laboratory is not a GMP-compliant facility, we used clinical-grade media and supplements (Thermo Scientific CTS grade) for the entire protocol of iPSC maintenance and retinal differentiation. Concerning photoreceptor separation, adaptation to full GMP conditions for manufacturing of cell therapy product, CD73+ cells, should benefit from the fact that MACS-derived products has already entered the clinic. For example, MAC-sorted SSEA-1+ cardiac progenitors derived from human ESCs entered phase I clinical trial (Menasché et al., 2015). We preferred MACS because it is faster and preserved better cell viability than FACS (Eberle et al., 2011), with satisfactory levels of purity (higher than 85%). We adapted previously published protocols for the enrichment of rods from mouse post-natal retinas and mouse ESC-derived organoids (Eberle et al., 2011; Santos-Ferreira et al., 2016a). CD73-based MACS from 120-day-old human retinal organoids produced sufficient amounts of transplantation-competent photoreceptors. For example, in the hypothesis of treating patients with 1 million

cells per eye, the appropriate number of CD73+ cells could be obtained from as little as five to ten 120-day-old retinal organoids.

Efforts for a clinical translation must include the development of a cryopreservation strategy. Banking of cell therapy products ensures the possibility to generate and characterize at once a large batch of cells, which can be subsequently divided and stored as multiple doses ready for administration, reducing costs of production. Neurons are particularly sensitive to freezing, but, for example, cryopreservation procedures already exist for human ESC-derived dopaminergic neurons that will soon enter clinical trials for Parkinson Disease in different countries (Barker et al., 2017).

We developed different strategies for the banking of retinal cells derived from human iPSCs. The most promising in terms of preservation of cell viability is the cryopreservation of whole retinal organoids. Freeze-thawed organoids could be put back into culture to allow further retinal maturation or to serve as a source of cells for CD73-based MACS. Freezing of MAC-sorted CD73+ cells led to 50% of apoptotic cells after thawing, probably due to an increased cell fragility after sorting. Levels of cell recovery should be further improved to attain at least 60-80% of living cells, as reported for thawed dopaminergic neuron precursors (Niclis et al., 2017; Nolbrant et al., 2017). Different cryopreservation media, possibly devoid of DMSO, should be tested to determine whether is possible to store purified populations of immature photoreceptors. Other parameters that could have an impact on freeze-thawing efficacy include number of frozen cells, cell density, and speed of both freezing and thawing.

In mouse retina, the expression of CD73 has been described to follow Crx induction, but to precede Nrl expression. Similarly, in human retinal organoids we showed that CD73 is exclusively detected in photoreceptors expressing CRX and RECOVERIN. Thus, CD73 is not a marker of early photoreceptor lineage commitment, unlike CRX, and it cannot be used as a marker of photoreceptor at the most immature stages (before D100), in agreement with previous study from Kaewkhaw et al. Indeed, they did not identified CD73 as a marker of CRX+ cells in human retinal organoids younger than D90 using a CRX fluorescent reporter iPSC line (Kaewkhaw et al., 2015). Nevertheless, CD73 cannot be considered uniquely as a marker of mature photoreceptors, as its expression anticipates RHODOPSIN, RED/GREEN OPSIN and BLUE OPSIN expression. Our conclusion is that CD73 starts to be expressed in cells already committed to the photoreceptor lineage (*i.e.* photoreceptor precursors); CD73 then continues to be expressed during photoreceptor maturation and its expression is maintained in both mature rods and cones. Therefore, by performing CD73-based MACS on organoids between D100 and D130 of differentiation it is possible to separate photoreceptor precursors,

expressing CRX and RECOVERIN, while conducting CD73-based MACS on organoids at advanced stages of maturation (>D150) allows the isolation of mature rods and cones.

Our results concerning the pattern of expression of CD73 and its utility to separate photoreceptors are not in complete agreement with those from a very recent study using human fetal retina and PSC-derived retinal organoids (Lakowski et al., 2018). Lakowski et al. showed that FAC-sorting of CD73+ cells resulted in a significant enrichment of photoreceptors from sample of fetal retina older than 14 weeks of gestation, consistently with our conclusions. This enrichment was further increased when combined with a double negative selection for SSEA-1 and CD29. However, they reported that targeting of CD73 alone failed to enrich for CRX+/RECOVERIN+ cells in human PSC-derived retinal organoids, obtained accordingly to a modified version of the protocol by David Gamm's group (Meyer et al., 2009). Surprisingly, optic vesicle-like structures were not lifted by cutting as in the original protocol, but were maintained in adherent cultures following neural induction. Arguably, they concluded that CD73 was not specifically expressed in photoreceptors, even if separation of photoreceptors by triple selection with SSEA-1-/CD29-/CD73+ increased the proportion of photoreceptors compared to separation by double negative selection based on SSEA-1 and CD29. It is important to consider that this study was exclusively based on flow cytometry analysis and immunostaining of the FAC-sorted cell populations; no immunostaining or gene expression analysis for CD73, CD29 and SSEA-1 was performed on retinal organoids or fetal retinal tissues before FACS. Given the efficacy of CD73 sorting with fetal retinal samples, it seems likely that their culture system failed to induce an adequate expression of CD73 in retinal organoids. Although the isolation of photoreceptors by negative selection is interesting because it would avoid the injection of immunolabeled cells, the need for multiple markers is disadvantageous because it increases the time required for cell sorting while reducing cell viability as well as cell yields.

Another problematic concerned whether the expression of CD73 in the human retina is localized specifically in rods or both in rods and cones. The study by Lakowski et al. reported that the majority of SSEA-1-/CD29-/CD73+ cells from human fetal retina were positive for RHODOPSIN immunostaining (Lakowski et al., 2018). Another publication by Welby et al. failed to identify CD73 within the genes overexpressed in human fetal cone population, isolated by viral labeling with AAV2/9 driving GFP under the control of the OPSINpR2.1 promoter (Welby et al., 2017).

Since our protocol allowed the generation of organoids containing both rods and cones roughly in the same proportion, we undoubtedly showed by immunostaining that CD73 co-localized with cone markers CONE ARRESTIN, RED/GREEN OPSIN AND BLUE OPSIN. By analyzing

the expression of principal photoreceptor markers in CD73+ cell population we demonstrated that both rods and cones are enriched in CD73+ fraction after MACS. Characterization of CD73+ cell *in vivo*, following transplantation into the P23H rat, indicated that actually the majority of human transplanted cells expressed CONE ARRESTIN.

It would be interesting to identify distinct surface markers for rods and cones, in order to select exclusively one population of photoreceptors. A combination of four different CD markers has been proposed for cone selection on the basis on human cone transcriptomic analysis (*cf.* 5.4, Welby et al., 2017). However, the levels of enrichment for cone photoreceptors and the quantity of isolated cells are still unsatisfactory and their validity has not been confirmed *in vivo*. It would be also useful trying to guide the differentiation alternatively toward cone or rod cell lineage. For example, COCO has been shown to increase the proportion of S-cones (Zhou et al., 2015). Tuning of retinoic acid (RA) supplementation could be used to increase or decrease the final proportion of cones in retinal organoids. Continuous culture of mouse ESC-derived organoids in the presence of RA resulted into an inhibition of cone fate specification; on the contrary, supplementing cultures with a short pulse of RA in correspondence of the peak for cone generation increased the expression of S Opsin (Kruczek et al., 2017). Suppression of RA, with cross-regulation between RA and FGF8 signaling, has also been shown to be important for the patterning of the fovea area in chicken (da Silva and Cepko, 2017). Timed inhibition of RA may be required for the induction of fovea-like structures, highly enriched in cones, in retinal organoids.

We used B27 supplement that contains vitamin A, a precursor of RA, for the entire duration of floating cultures. We have not investigated whether vitamin A is actually processed to RA and in what proportion. Although we have not performed a precise quantification of the cone population within our retinal organoids, results from CONE ARRESTIN immunostaining suggest that the proportion of cone is higher than 5%, corresponding to the total cone population in the human retina. Thus, our organoids could have a cone/rod ratio more similar to that within the cone-enriched macula in human retina. It seems likely that isolation of cone-enriched cell population will be based on both the use of appropriate guiding molecules and time-specific selection, as the peak of cone generation precedes that of rods (Carter-Dawson and Lavail, 1979; Young, 1985).

We are currently testing new culture conditions to implement long-term photoreceptor survival and maturation. This will be of particular utility for disease modelling applications. In this perspective, the use of CD73 as a marker of photoreceptors could offer the possibility to focus pathophysiological investigations on the isolated population of photoreceptors. We attempted to increase maturation of photoreceptor precursors after sorting in 2D cultures, but we failed to obtain the expression of mature markers. Cell survival in this condition was limited to a

maximum of three weeks, probably because the coating we tested (Poly-D-Lysine and Laminin) was not optimized for long-term culture of photoreceptors. 3D culture conditions offered a more suitable environment for terminal maturation of photoreceptors. We could not detect any light-responsive cell within retinal organoids or following dissociation, probably because outer segments are not adequately structured in our conditions. The absence of RPE cells, required for the chromophore recycling, could also explain this absence of light-response (Strauss, 2005).

Taurine, a byproduct of the sulphurous amino acids cysteine and methionine has been used in a large number of retinal differentiation protocol (listed in **Table 4**) to enhance photoreceptor maturation. In our culture system, we found that addition of Taurine during floating culture of retinal organoids did not have any effect on maturation of photoreceptors.

At the same time, we attempted to shorten the differentiation time to achieve photoreceptors expressing CD73. Similarly to our previous protocol (Reichman et al., 2014), we treated retinal organoids with DAPT concomitantly with induction of CRX and RECOVERIN expression (D42-49 or D49-56). Inhibition of the Notch pathway was effective in increasing the proportion of RECOVERIN⁺ cells by inducing RPCs to exit the cell cycle. However, maturation of photoreceptors was not accelerated, so that sustained expression of CD73 was not reached before D100, similarly to control culture conditions. It is unlikely that delaying addition of DAPT during induction of CD73 (around D80) would be effective, because the majority of the cells are already post-mitotic at that time.

Reporter PSC lines could be highly useful for the optimization of culture conditions for photoreceptor generation and maturation. More in general, they provide a tool for the analysis of specific cell types and lineages in cultures. In this context, we generated a Crx reporter cell line to follow the differentiation of iPSCs towards the photoreceptor lineage and the use of this reporter cell line allowed us to confirm the photoreceptor identity of CD73⁺ cells. Transgenic expression driven by CRX promoter has already been adopted to investigate the hPSC-derived photoreceptor population, by using different strategies, and the validity of this approach has been largely demonstrated (Collin et al., 2016; Homma et al., 2017; Kaewkhaw et al., 2015; Nakano et al., 2012; Phillips et al., 2017). We first used Zinc Finger Nucleases to perform a knock-in the CRX locus, in order to put the expression of the fluorescent protein under control of the endogenous CRX promoter, as previously shown (Collin et al., 2016; Nakano et al., 2012). This strategy required, after the selection of the recombinant clone by Neomycin selection, the excision of the antibiotic-resistance cassette, by transient transfection with a Cre-encoding plasmid, that otherwise would have interfered with the expression of the fluorescent protein. Because the insertion of the reporter construction resulted in the disruption of one CRX allele, only clones carrying one copy of the insert could have been used for the generation of retinal organoids. While we could achieve targeted insertion in the CRX locus with relatively

high efficiency, the isolation of clones having correctly excised the Neomycin-resistance cassette following Cre recombination proved to be particularly difficult. Therefore, we opted for an alternative strategy based on the use of CRISPR-Cas9 technology to insert a nuclear-targeted form of the fluorescent protein mCherry under control of mouse Crx promoter into the AAVS1 locus, similarly to the Crx reporter line generated by Kaewkhaw et al. Although the expression of the fluorescent protein was not driven by the endogenous promoter, we could confirm that the reporter construct recapitulated endogenous CRX expression in human iPSC-derived organoids. Given the relative ease of achieving transgene insertion into the AAVS1 locus, we are currently developing new reporter human iPSC lines, with specific minimal promoters of Opsin and Rhodopsin that will provide new tools for the characterization and manipulation of specific photoreceptor cell population in retinal organoids.

2. *In vivo* cell integration, maturation and functionality

We performed transplantation of unsorted retinal cells and CD73+ photoreceptors in two animal models, NUDE and P23H rats. Although most of transplantation studies have been performed in mouse models (**Table 2**), we have preferred rat over mouse models because the bigger size of their eyes should have facilitated surgical procedures. In addition, retinal degeneration has been extensively characterized in different lines of P23H transgenic rats (LaVail et al., 2018; Orhan et al., 2015) and previously used at our institute in a transplantation study with rat postnatal photoreceptors (Yang et al., 2010).

Achieving high rate of photoreceptor survival and integration, while always ensuring safety, are the two most relevant aspects to be considered in transplantation studies. Cells were detected 8 weeks after transplantation without any sign of hyper-proliferation in all NUDE rats transplanted with human iPSC-derived retinal cells. Further safety studies should be conducted on a longer period (at least 6 months) and evaluate the bio-distribution of injected cells in different organs.

Transplanted cells survived 10 weeks after injection only in two P23H rats under immunosuppressive treatment. We believe that immune-mediated cell rejection is one of the principal causes of poor transplantation outcome and that transplanted cells can only be detected after a long time in correctly immunosuppressed animals. Oral administration of cyclosporine, by addition in the drinking water, is an immunosuppressive regimen classically used but very difficult to control and with limited efficacy (Kamao et al., 2014; Ben M'Barek et al., 2017).

In the works published so far modulation of the host immune system is not a consistent factor, varying from use of immune-compromised host, use of immunosuppressive drugs and no

immunosuppression at all (**Table 8**). Zhu and colleagues demonstrated the necessity to use immunosuppressed recipient to achieve long-term cell survival (Zhu et al., 2017a), and the use of immune-compromised photoreceptor degenerative models in the case of xenografts is becoming more common (Iraha et al., 2018; McLelland et al., 2018; Shirai et al., 2016). This strategy seems more reliable when long-term immunosuppression is needed compared to immunosuppressive drugs. Importantly, it avoids the severe side effects caused by long-term immunosuppressive treatment.

In our experience, it was very difficult to maintain rats under cyclosporine regimen over 2 months after transplantation. In a number of studies transplanted animals are analyzed 3 weeks after surgery, which is a short time especially for human xenotransplants, considering the length of human photoreceptor maturation both *in vivo* (human fetuses) and within retinal organoids. In two recent works (Iraha et al., 2018; McLelland et al., 2018), the use of immunodeficient retinal degeneration rodent models at end-stage of photoreceptor degeneration allowed post-surgical following of human retinal sheet for up to 10 months. They reported the presence of structures resembling to putative outer segments localized in the inner face of neural rosettes within donor ONL.

In our study, we detected human cells expressing RHODOPSIN, RED/GREEN OPSIN and BLUE OPSIN at both 4 and 10 weeks after transplantation. However, these cells did not display the morphological features of mature photoreceptors, including the presence of outer segments contacting the host RPE, consistently with previous results concerning injection of human PSC-derived retinal cells under suspension (Barnea-Cramer et al., 2016; Gonzalez-Cordero et al., 2017).

In addition to adaptive immune system, innate immune system has been shown to play a role following photoreceptor transplantation. Specifically, in mouse the mesencephalic astrocyte-derived neurotrophic factor (MANF) expression in innate immune cells promote retinal repair after injury and when MANF was supplemented to donor mouse photoreceptors, the number of grafted cells in the recipient retina increased (Neves et al., 2016). Nevertheless, it is still unclear how to regulate this mechanism. With transplantation surgery potentially damaging the blood-retina barrier, the subretinal microenvironment would no longer be immunoprivileged because immune cells may enter the retina and favoured grafted cell rejection. In this respect, we think that transplantation via trans-scleral approach may incur an increased risk of cell rejection resulting from possible damage to the choroid vessels. As a consequence, grafted cell survival may be reduced. Cells could also be lost by reflux at the moment of needle withdrawal. All these factors together may explain the reduced number of transplanted cells in the subretinal space of eye injected via a trans-scleral route.

At the same time, we found that the method of injection can affect visual function as showed by ERG recordings. The reduced responses observed in most of the animals having received a trans-vitreous injection, including the sham group, indicate that the surgical act can negatively impact on the functionality of the retina. Subretinal injections are very delicate surgery, which present several possible complications, including haemorrhage, partial to complete retinal detachment and retinal gliosis, as shown by OCT analysis. In rodents, the surgical procedure is even more complicated because of the reduced size of the eye, the large volume occupied by the lens and the impossibility to clearly visualize the impacted area during the injection (**Figure 1** and **Table 1**). In primates, where the trans-vitreous approach is the sole injection route possible, the injection of cell suspensions should be safer as the surgical procedure is camera-assisted and the vitreous cavity has a larger volume.

Recently, LaVail et al. reported in the P23H a thinning of ONL in proximity to the injection site, independently of the solution injected, containing PBS only or different neurotrophic factors (LaVail et al., 2018). This injury-response may negatively affect the outcome of cell transplantation in this model of photoreceptor degeneration. It would be important to elucidate the mechanisms of this process, in order to determine whether or not the P23H rat is an appropriate model to perform subretinal injections.

The lack of a significant visual improvement measured by ERG recording is consistent with previous reports (Iraha et al., 2018; Shirai et al., 2016), reflecting a generalized difficulty in obtaining a measurable rescue of the visual function by this technique. This is principally due to the fact that ERG measures the response from the entire retina, while only a small area of the retina is targeted by cell replacement, so that an eventual functional improvement in the treated region would be too small to positively affect the global response in a degenerated retina. To obviate this problem, focal ERG (fERG) has been developed to determine response specifically from a delimited area, allowing for a direct comparison between treated and untreated regions within the same eye. This strategy would also eliminate the error deriving from variability between left to right eye. Indeed, we found that in some case this difference can be significant and could lead to misleading results. So far, this technique has been mostly implemented on non-human primates, whereas recording fERGs from mice and rats is still challenging because of the difficulty in focusing the stimuli on focal areas in small eyes and in eliminating the effects of stray light (Fujii et al., 2016).

MEA can be used to record spontaneous and light-evoked responses from RGCs *ex vivo*, providing a possible evaluation of the synaptic connection and the transmission of the visual stimulus from transplanted cells to the other cells of the retina. A number of studies have also

shown that MEA can also be used to record responses from isolated mouse retinas (Homma et al., 2009; Stett et al., 2003), called micro ERGs, and that micro ERGs recorded by MEA display a and b waves similarly to full-field ERG recordings (Fujii et al., 2016). Given its higher spatial resolution and higher sensitivity compared to full-field ERG, MEA recordings should detect the response elicited even by a single photoreceptor. Interestingly, this approach has been recently used to measure light responses from grafted regions of dystrophic *rd1* mouse retina, while full-field ERGs were not detected in those grafted retinas (Iraha et al., 2018). The major limitation of this technique is the difficulty to distinguish between responses originated by residual host retinal cells and transplanted donor cells. For this reason, MEA could not be used to evaluate functionality of our grafted human cells, since even at 10 weeks after transplantation, corresponding to 4-month-old rats, hemizygous P23H rats still bore a residual ONL. Because degeneration in homozygous P23H rats is faster than in hemizygotes (LaVail et al., 2018), we believed that transplantation into homozygous P23H rats at end-degenerative stage, where no residual light responses could be produced by host cells would have been more informative. Despite the absence of full-field ERG responses and the complete degeneration of ONL, analysed by OCT, light-evoked responses were detected by MEA from residual cones in retinas from homozygous P23H rat aged of 9 and 11 months, similarly to previous results obtained with retinas from heterozygous P23H rats at the same age (Kolomiets et al., 2010). These observations suggest that transplantation and functional assessment of grafted cells by MEA in the P23H rat model could not be performed in animals younger than 12-18 months.

Visually guided behavioural tests have also been used to evaluate visual rescue following transplantation (**Table 8**). Unfortunately, optokinetic test cannot be performed on P23H rats because of the reduced visual acuity in albino strains. More in general, considering that vision in rodents is not as much as important as in humans, the pertinence of this test is arguable. In this sense, transplantation studies in non-human primates would be more appropriate, especially in reason of their cone-enriched macula. The high similarity of retinal anatomy between humans and monkeys should allow the evaluation of cell number for injection and the development of an appropriate strategy for cell delivery. Additionally, similarity at a molecular level of the proteins essential to photoreceptor synaptogenesis has been suggested to affect the outcome of photoreceptor transplantation. In particular, the protein pikachurin, a key triad ribbon synapse protein, was predicted to diverge significantly between rodent and human (Laver and Matsubara, 2017). These findings may explain why the extent of visual rescue measured after xenotransplantation of human cells in mice or rats was always reduced compared to functional improvements measured following allografts in rodents (Iraha et al., 2018; Mclelland et al., 2018). Consistently with these observations, transplantation of rat

postnatal photoreceptors in P23H rats led to an improvement in ERG responses (Yang et al., 2010), while transplantation of human iPSC-derived photoreceptors in our study did not. With a molecular architecture of synaptic terminals more similar to humans, monkeys should represent a more convenient model to evaluate functional restoration.

Non-human primates would be also useful as an alternative to classical xenograft experiments by using specific macaque iPSC-derived photoreceptors to evaluate allogeneic transplantation in major histocompatibility (MHC)-matched monkeys. Currently, the major scientific limitation to research with non-human primates is the lack of models of inherited-retinal degeneration, which should be tackled with the latest developments in genome engineering. The results obtained so far have been conducted on a very restricted number of animals and are very preliminary (Chao et al., 2017; Shirai et al., 2016).

We also need to investigate cell material exchange in different transplantation scenarios, such as in allografts and xenografts in non-human primates and lastly in humans. As we have seen, the majority of the studies have focused on murine-murine transplantation (**Table 7**) and only one study has investigated the exchange of cytoplasmic material between donor human cells and mouse recipients (Gonzalez-Cordero et al., 2017). In our study, we could not detect any material exchange event between human donor cells and recipient rat cells. Further studies are required to try understanding the impact and the mechanism of this process.

As recently proposed by Nickerson et al., a minimum of set standards to distinguish *bona fide* cell integration from material exchange events should be adopted in future transplantation studies. Characterization of host-graft tissues should include combination of cytoplasmic (reporter, antibody) and nuclear markers, sex-mismatched probes for FISH and, in case of xenotransplants, specie-specific antibodies and FISH probes (Nickerson et al., 2018).

It is important to further define when host/donor material exchange can happen and to understand mechanisms underlying this process. Having excluded complete cell-cell fusion and the uptake of free molecules, transient cell-cell connections, tunnelling nanotubes or vesicular transport should be investigated (Santos-Ferreira et al., 2017). The elucidation of material exchange process could lead to new therapeutic options. Reconsidering previous studies concerning transplantation of photoreceptors, we are now aware that when transplantation is performed in animal recipient model with residual ONL, functional improvement as well phenotypic rescue may be mediated by exchange of cytoplasmic material between host and donor photoreceptors. While these findings have reopened questions about the optimal developmental stage, maturation and functional integration capabilities of transplanted cells, they may open new pathways for cell therapy applications, in which donor cells can be considered as a vector to deliver a missing protein or other molecules to the endogenous mutated photoreceptors. For example, rod α -transducin was detected in *Gnat1*^{-/-}

recipients following transplantation of wild type photoreceptor precursors (Pearson et al., 2016). For the repair of cardiac tissue, it has been shown that cell-free components, such as exosomes, are the main mediators of regenerative response in target cells, as stem cell-derived exosomes recapitulated the same effects obtained with stem cell therapy (Singla, 2016). A similar approach may be considered for the treatment of certain photoreceptor degenerative diseases, at least for the stages when the ONL is totally or partially intact.

Current photoreceptor replacement strategies with PSC-derivatives, transplanted either as retinal sheet or as photoreceptor cell suspension, showed some limitations. Retinal sheet transplants could lead to some functional restoration; nevertheless, the presence of retinal cell types other than photoreceptors, as well as the assembling into neural rosettes reduces the ability of transplanted retinal cells to integrate within host tissue and restore visual function. The lack of direct contact between photoreceptors and host INL prevents larger formation of synaptic connections, while lack of direct contact between photoreceptors and host RPE may affect long term survival and functionality. On the contrary, transplantation of cell suspension, if appropriately selected as we could demonstrate, can lead to a homogenous population of photoreceptors, although only a fraction of these cells can survive after the injection. Photoreceptor replacement should be performed at advanced stage of degeneration to allow photoreceptors being in direct contact with host INL and RPE. Nevertheless, despite the expression of RHODOPSIN, RED/GREEN OPSIN and BLUE OPSIN, photoreceptor morphological and functional maturation is still unsatisfactory.

The use of bio-scaffolds, such inclusion in hydrogels, have been proposed as a method to enhance cell distribution, survival and integration (Ballios et al., 2015). Alternatively, advancements in 3D printing technologies have made possible the creation of polymers with tightly controlled structure, in addition to chemical and mechanical features. Two-photon polymerization, a high-resolution 3D printing technique, has been used to create structures that facilitated the alignment of retinal progenitor cells, maximizing their density on the surface and facilitating nutrient diffusion throughout the scaffold (Worthington et al., 2017). It has not been shown yet the ability of these cells to differentiate into photoreceptors and to mature with the formation of an outer segment structure. It would be interesting to test the combination of our photoreceptor separation strategy with the use of this, or different type of scaffold, as a strategy for photoreceptor replacement. Bioprinting should allow to precisely control the distribution of cells on scaffolds and to obtain multilayered structures combining RPE and retinal neurons (Shi et al., 2018). This approach could provide a more appropriate treatment for advanced stages of AMD, when both RPE and photoreceptors need to be replaced.

An alternative option, given the difficulty of transplanted photoreceptors to form functional outer segments, may be offered by the combination of stem cell therapy with optogenetics. The

introduction of optogenetic tools in PSC-derived photoreceptor precursors could bypass the need for a functional maturation of transplanted cells, while preserving the localization of photosensitive cells as initial triggers in the transmission chain of visual signal. Differently, conferring light-sensitivity to bipolar cells or RGCs would necessarily alter the retinal circuitry and the final codification of visual message transmitted to the brain. More importantly, the insertion of light-sensors into PSC-derived photoreceptor precursors would make transplanted cells immediately able to respond to light, independently from the formation of outer segments and the presence of RPE. Downstream transmission of visual signals to the other retinal neurons relies on the capacity of transplanted cells to form synaptic connections. Additionally, the major obstacle to clinical translation of this technology is that microbial opsins used so far would not be activated in normal daylight, requiring illumination at specific wavelengths and intensities. Further engineering of new light-sensors together with improved integration of transplanted cells may represent substantial advancements for the efficacy of cell replacement.

As recapitulated in **Figure 26**, the achievement of fully successful photoreceptor replacement will rely on co-implementation of multiple strategies in all the steps leading to cell therapy application, from cell product manufacturing, to surgical delivering and functional restoration. While significant hurdles need to be addressed before achieving any therapeutic ends, most of these open challenges do not concern exclusively the development of outer retinal cell therapies, but they are common to all stem cell-based treatments. Collaborative efforts from not only distinct stem cell domains, but also different scientific disciplines (biologists, engineers and clinicians) should accelerate the progress of regenerative medicine.

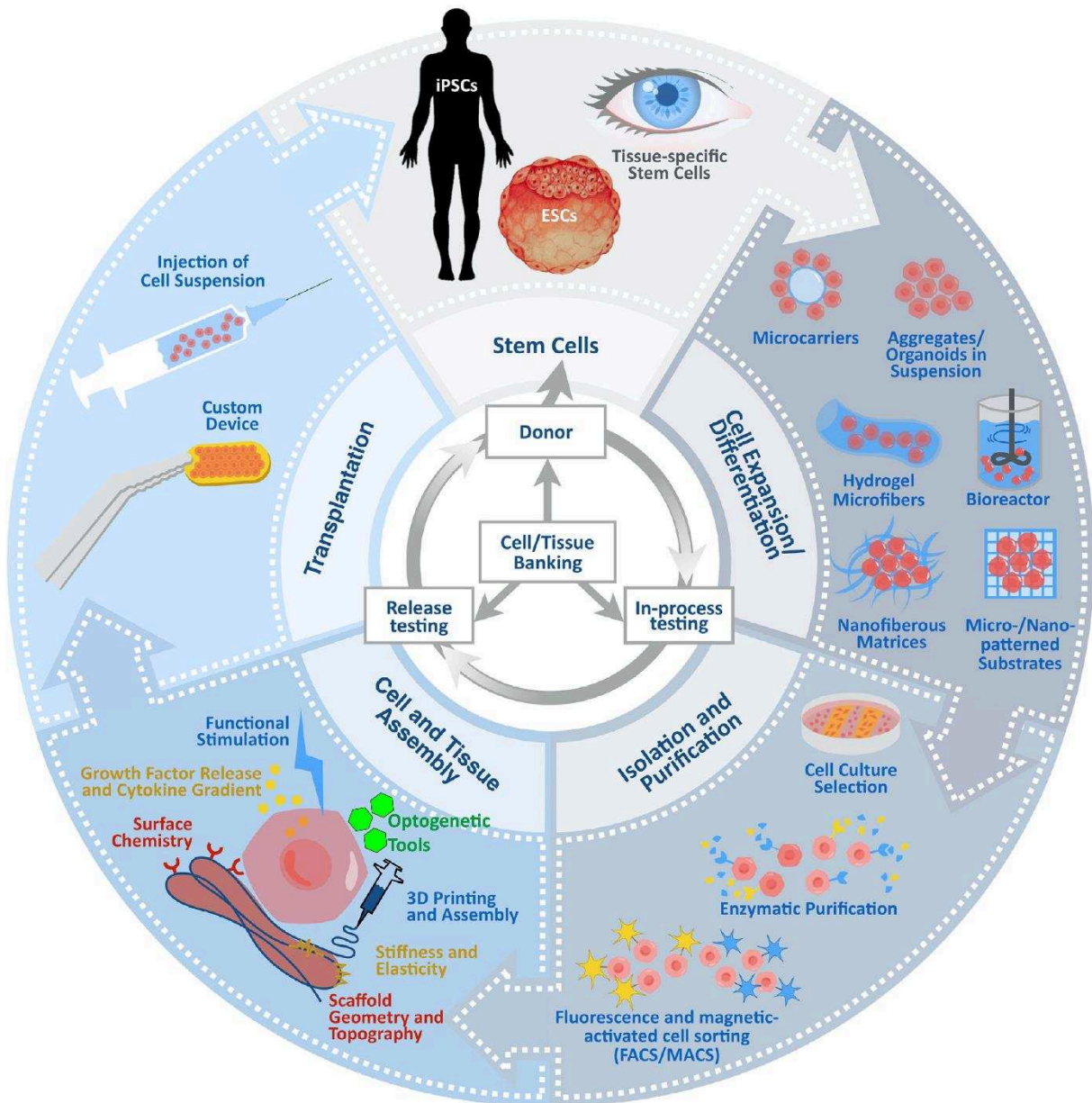


Figure 26 Different strategies for the implementation of production and delivery of cell therapy products for the treatment of outer retinal dystrophies.
Adapted from Stern et al., 2018.

Conclusions

The work presented here aimed at contributing to the development of a cell therapy product for the treatment of photoreceptor degenerative diseases. We have demonstrated the possibility to generate and store retinal organoids from human iPSCs using GMP-grade cell culture media. We have characterized the surface antigen CD73 as a marker of photoreceptors in human retinal organoids. We established a protocol allowing for the separation of a homogenous population of photoreceptors, and we could demonstrate their safety. Finally, CD73-positive cells had the ability to survive and to reach a certain degree of maturation in a dystrophic retinal environment. Improving the survival and the establishment of synaptic connections of transplanted cells is an imperative to achieve a significant rescue of the visual function.

Bibliography

- Acland, G.M., Aguirre, G.D., Ray, J., Zhang, Q., Aleman, T.S., Cideciyan, A. V., Pearce-Kelling, S.E., Anand, V., Zeng, Y., Maguire, A.M., et al. (2001). Gene therapy restores vision in a canine model of childhood blindness. *Nat. Genet.* *28*, 92–95.
- Adler, R., and Canto-Soler, M.V. (2007). Molecular mechanisms of optic vesicle development: complexities, ambiguities and controversies. *Dev. Biol.* *305*, 1–13.
- Aftab, U., Jiang, C., Tucker, B., Kim, J.Y., Klassen, H., Miljan, E., Sinden, J., and Young, M. (2009). Growth kinetics and transplantation of human retinal progenitor cells. *Exp. Eye Res.* *89*, 301–310.
- Ahmad, I., Tang, L., and Pham, H. (2000). Identification of neural progenitors in the adult mammalian eye. *Biochem. Biophys. Res. Commun.* *270*, 517–521.
- Akimoto, M., Cheng, H., Zhu, D., Brzezinski, J.A., Khanna, R., Filippova, E., Oh, E.C.T., Jing, Y., Linares, J.-L., Brooks, M., et al. (2006). Targeting of GFP to newborn rods by Nrl promoter and temporal expression profiling of flow-sorted photoreceptors. *Proc. Natl. Acad. Sci. U. S. A.* *103*, 3890–3895.
- Aldiri, I., Xu, B., Wang, L., Chen, X., Hiler, D., Griffiths, L., Valentine, M., Shirinifard, A., Thiagarajan, S., Sablauer, A., et al. (2017). The Dynamic Epigenetic Landscape of the Retina During Development, Reprogramming, and Tumorigenesis. *Neuron* *94*, 550–568.e10.
- Allikmets, R., Singh, N., Sun, H., Shroyer, N.F., Hutchinson, A., Chidambaram, A., Gerrard, B., Baird, L., Stauffer, D., Peiffer, A., et al. (1997). A photoreceptor cell-specific ATP-binding transporter gene (ABCR) is mutated in recessive Stargardt macular dystrophy. *Nat. Genet.* *15*, 236–246.
- Amirpour, N., Karamali, F., Rabiee, F., Rezaei, L., Esfandiari, E., Razavi, S., Dehghani, A., Razmju, H., Nasr-Esfahani, M.H., and Baharvand, H. (2012). Differentiation of Human Embryonic Stem Cell-Derived Retinal Progenitors into Retinal Cells by Sonic Hedgehog and/or Retinal Pigmented Epithelium and Transplantation into the Subretinal Space of Sodium Iodate-Injected Rabbits. *Stem Cells Dev.* *21*, 42–53.
- Applebury, M.L., Antoch, M.P., Baxter, L.C., Chun, L.L.Y., Falk, J.D., Farhangfar, F., Kage, K., Krzystolik, M.G., Lyass, L.A., and Robbins, J.T. (2000). The Murine Cone Photoreceptor. *Neuron* *27*, 513–523.
- Aramant, R.B., and Seiler, M.J. (2002). Retinal transplantation - Advantages of intact fetal sheets. *Prog. Retin. Eye Res.*
- Aramant, R.B., Seiler, M.J., and Ball, S.L. (1999). Successful cotransplantation of intact sheets of fetal retina with retinal pigment epithelium. *Investig. Ophthalmol. Vis. Sci.*
- Assawachananont, J., Mandai, M., Okamoto, S., Yamada, C., Eiraku, M., Yonemura, S., Sasai, Y., and Takahashi, M. (2014). Transplantation of embryonic and induced pluripotent stem cell-derived 3D retinal sheets into retinal degenerative mice. *Stem Cell Reports* *2*, 662–674.
- Audo, I., Manes, G., Mohand-Saïd, S., Friedrich, A., Lancelot, M.E., Antonio, A., Moskova-Doumanova, V., Poch, O., Zanlonghi, X., Hamel, C.P., et al. (2010). Spectrum of rhodopsin mutations in French autosomal dominant rod-cone dystrophy patients. *Investig. Ophthalmol. Vis. Sci.* *51*, 3687–3700.
- Avilion, A.A., Nicolis, S.K., Pevny, L.H., Perez, L., Vivian, N., and Lovell-Badge, R. (2003). Multipotent cell lineages in early mouse development depend on SOX2 function. *Genes Dev.* *17*, 126–140.
- Baehr, W., and Frederick, J. (2006). Inherited Retinal Diseases: Vertebrate Animal Models. In *Encyclopedia of Life Sciences*, (Chichester, UK: John Wiley & Sons, Ltd), p.
- Bakondi, B., Lv, W., Lu, B., Jones, M.K., Tsai, Y., Kim, K.J., Levy, R., Akhtar, A.A., Breunig, J.J., Svendsen, C.N., et al. (2016). In vivo CRISPR/Cas9 gene editing corrects retinal dystrophy in the S334ter-3 rat model of autosomal dominant retinitis pigmentosa. *Mol. Ther.* *24*, 556–563.
- Ballios, B.G., Cooke, M.J., Donaldson, L., Coles, B.L.K., Morshead, C.M., Van Der Kooy, D., and Shoichet, M.S. (2015). A Hyaluronan-Based Injectable Hydrogel Improves the Survival and Integration of Stem Cell Progeny following Transplantation. *Stem Cell Reports* *4*, 1031–1045.
- Banin, E., Obolensky, A., Idelson, M., Hemo, I., Reinhardt, E., Pikarsky, E., Ben-Hur, T., and

- Reubinoff, B. (2006). Retinal incorporation and differentiation of neural precursors derived from human embryonic stem cells. *Stem Cells* *24*, 246–257.
- Barber, A.C., Hippert, C., Duran, Y., West, E.L., Bainbridge, J.W.B., Warre-Cornish, K., Luhmann, U.F.O., Lakowski, J., Sowden, J.C., Ali, R.R., et al. (2013). Repair of the degenerate retina by photoreceptor transplantation. *Proc. Natl. Acad. Sci.* *110*, 354–359.
- Barker, R.A., Parmar, M., Studer, L., and Takahashi, J. (2017). Human Trials of Stem Cell-Derived Dopamine Neurons for Parkinson's Disease: Dawn of a New Era. *Cell Stem Cell* *21*, 569–573.
- Barnea-Cramer, A.O., Wang, W., Lu, S.-J., Singh, M.S., Luo, C., Huo, H., McClements, M.E., Barnard, A.R., MacLaren, R.E., and Lanza, R. (2016). Function of human pluripotent stem cell-derived photoreceptor progenitors in blind mice. *Sci. Rep.* *6*, 29784.
- Bartsch, U., Oriyakhel, W., Kenna, P.F., Linke, S., Richard, G., Petrowitz, B., Humphries, P., Farrar, G.J., and Ader, M. (2008). Retinal cells integrate into the outer nuclear layer and differentiate into mature photoreceptors after subretinal transplantation into adult mice. *Exp. Eye Res.* *86*, 691–700.
- Bassett, E.A., and Wallace, V.A. (2012). Cell fate determination in the vertebrate retina. *Trends Neurosci.* *35*, 565–573.
- Ben-David, U., Gan, Q.F., Golan-Lev, T., Arora, P., Yanuka, O., Oren, Y.S., Leikin-Frenkel, A., Graf, M., Garippa, R., Boehringer, M., et al. (2013). Selective elimination of human pluripotent stem cells by an oleate synthesis inhibitor discovered in a high-throughput screen. *Cell Stem Cell* *12*, 167–179.
- Bendall, S.C., Stewart, M.H., Menendez, P., George, D., Vijayaragavan, K., Werbowetski-Ogilvie, T., Ramos-Mejia, V., Rouleau, A., Yang, J., Bossé, M., et al. (2007). IGF and FGF cooperatively establish the regulatory stem cell niche of pluripotent human cells in vitro. *Nature* *448*, 1015–1021.
- Berger, W., Kloeckener-Gruissem, B., and Neidhardt, J. (2010). The molecular basis of human retinal and vitreoretinal diseases. *Prog. Retin. Eye Res.* *29*, 335–375.
- Bock, C., Kiskinis, E., Verstappen, G., Gu, H., Boulting, G., Smith, Z.D., Ziller, M., Croft, G.F., Amoroso, M.W., Oakley, D.H., et al. (2011). Reference maps of human es and ips cell variation enable high-throughput characterization of pluripotent cell lines. *Cell* *144*, 439–452.
- Boije, H., MacDonald, R.B., and Harris, W.A. (2014). Reconciling competence and transcriptional hierarchies with stochasticity in retinal lineages. *Curr. Opin. Neurobiol.* *27*, 68–74.
- Boland, M.J., Hazen, J.L., Nazor, K.L., Rodriguez, A.R., Gifford, W., Martin, G., Kupriyanov, S., and Baldwin, K.K. (2009). Adult mice generated from induced pluripotent stem cells. *Nature* *461*, 91–94.
- Boucherie, C., Mukherjee, S., Henckaerts, E., Thrasher, A.J., and Sowden, J.C. (2013). Brief report: Self-organizing neuroepithelium from human pluripotent stem cells facilitates derivation of photoreceptors. *Stem Cells* *31*, 408–414.
- Bourne, M.C., Campbell, D.A., and Tansley, K. (1938). Hereditary degeneration of the rat retina. *Br. J. Ophthalmol.* *22*, 613–622.
- Bowmaker, J.K., and Hunt, D.M. (2006). Evolution of vertebrate visual pigments. *Curr. Biol.* *16*, R484–R489.
- Bravery, C.A. (2015). Do Human Leukocyte Antigen-Typed Cellular Therapeutics Based on Induced Pluripotent Stem Cells Make Commercial Sense? *Stem Cells Dev.* *24*, 1–10.
- Brzezinski, J.A., and Reh, T.A. (2015). Photoreceptor cell fate specification in vertebrates. *Development* *142*, 3263–3273.
- Brzezinski, J.A., Uoon Park, K., and Reh, T.A. (2013). Blimp1 (Prdm1) prevents re-specification of photoreceptors into retinal bipolar cells by restricting competence. *Dev. Biol.* *384*, 194–204.
- Burnight, E.R., Wiley, L.A., Drack, A. V., Braun, T.A., Anfinson, K.R., Kaalberg, E.E., Halder, J.A., Affatigato, L.M., Mullins, R.F., Stone, E.M., et al. (2014). CEP290 gene transfer rescues Leber congenital amaurosis cellular phenotype. *Gene Ther.* *21*, 662–672.
- Burnight, E.R., Gupta, M., Wiley, L.A., Anfinson, K.R., Tran, A., Triboulet, R., Hoffmann, J.M.,

- Klaahsen, D.L., Andorf, J.L., Jiao, C., et al. (2017). Using CRISPR-Cas9 to Generate Gene-Corrected Autologous iPSCs for the Treatment of Inherited Retinal Degeneration. *Mol. Ther.* *25*, 1999–2013.
- Burnight, E.R., Giacalone, J.C., Cooke, J.A., Thompson, J.R., Bohrer, L.R., Chirco, K.R., Drack, A. V., Fingert, J.H., Worthington, K.S., Wiley, L.A., et al. (2018). CRISPR-Cas9 genome engineering: Treating inherited retinal degeneration. *Prog. Retin. Eye Res.* 1–22.
- Buskamp, V., Krol, J., Nelidova, D., Daum, J., Szikra, T., Tsuda, B., Jüttner, J., Farrow, K., Scherf, B.G., Alvarez, C.P.P., et al. (2014). MiRNAs 182 and 183 Are Necessary to Maintain Adult Cone Photoreceptor Outer Segments and Visual Function. *Neuron* *83*, 586–600.
- Byrne, L.C., Dalkara, D., Luna, G., Fisher, S.K., Clérin, E., Sahel, J.A., Léveillard, T., and Flannery, J.G. (2015). Viral-mediated RdCVF and RdCVFL expression protects cone and rod photoreceptors in retinal degeneration. *J. Clin. Invest.* *125*, 105–116.
- Calvert, P.D., Krasnoperova, N. V., Lyubarsky, A.L., Isayama, T., Nicolo, M., Kosaras, B., Wong, G., Gannon, K.S., Margolskee, R.F., Sidman, R.L., et al. (2000). Phototransduction in transgenic mice after targeted deletion of the rod transducin alpha -subunit. *Proc. Natl. Acad. Sci.* *97*, 13913–13918.
- Carter-Dawson, L.D., and Lavail, M.M. (1979). Rods and cones in the mouse retina. II. Autoradiographic analysis of cell generation using tritiated thymidine. *J. Comp. Neurol.* *188*, 263–272.
- Cepko, C. (2014). Intrinsically different retinal progenitor cells produce specific types of progeny. *Nat. Rev. Neurosci.* *15*, 615–627.
- Chambers, I., Colby, D., Robertson, M., Nichols, J., Lee, S., Tweedie, S., and Smith, A. (2003). Functional expression cloning of Nanog, a pluripotency sustaining factor in embryonic stem cells. *Cell* *113*, 643–655.
- Chang, B., Hawes, N.L., Hurd, R.E., Davisson, M.T., Nusinowitz, S., and Heckenlively, J.R. (2002). Retinal degeneration mutants in the mouse. *Vision Res.* *42*, 517–525.
- Chang, B., Grau, T., Dangel, S., Hurd, R., Jurklics, B., Sener, E.C., Andreasson, S., Dollfus, H., Baumann, B., Bolz, S., et al. (2009). A homologous genetic basis of the murine cpfl1 mutant and human achromatopsia linked to mutations in the PDE6C gene. *Proc. Natl. Acad. Sci. U. S. A.* *106*, 19581–19586.
- Chao, J.R., Lamba, D.A., Klesert, T.R., Torre, A. La, Hoshino, A., Taylor, R.J., Jayabalu, A., Engel, A.L., Khuu, T.H., Wang, R.K., et al. (2017). Transplantation of Human Embryonic Stem Cell-Derived Retinal Cells into the Subretinal Space of a Non-Human Primate. *Transl. Vis. Sci. Technol.* *6*, 4.
- Chen, J., Rattner, A., and Nathans, J. (2005). The rod photoreceptor-specific nuclear receptor Nr2e3 represses transcription of multiple cone-specific genes. *J. Neurosci.* *25*, 118–129.
- Chen, S., Wang, Q.L., Nie, Z., Sun, H., Lennon, G., Copeland, N.G., Gilbert, D.J., Jenkins, N.A., and Zack, D.J. (1997). Crx, a novel Otx-like paired-homeodomain protein, binds to and transactivates photoreceptor cell-specific genes. *Neuron* *19*, 1017–1030.
- Cheng, H., Aleman, T.S., Cideciyan, A. V, Khanna, R., Jacobson, S.G., and Swaroop, A. (2006). In vivo function of the orphan nuclear receptor NR2E3 in establishing photoreceptor identity during mammalian retinal development. *Hum. Mol. Genet.* *15*, 2588–2602.
- Collin, J., Mellough, C.B., Dorgau, B., Przyborski, S., Moreno-Gimeno, I., and Lako, M. (2016). Using Zinc Finger Nuclease Technology to Generate CRX-Reporter Human Embryonic Stem Cells as a Tool to Identify and Study the Emergence of Photoreceptors Precursors during Pluripotent Stem Cell Differentiation. *Stem Cells* *34*, 311–321.
- Cuenca, N., Fernández-Sánchez, L., McGill, T.J., Lu, B., Wang, S., Lund, R., Huhn, S., and Capela, A. (2013). Phagocytosis of photoreceptor outer segments by transplanted human neural stem cells as a neuroprotective mechanism in retinal degeneration. *Invest. Ophthalmol. Vis. Sci.* *54*, 6745–6756.
- Cuenca, N., Fernanndez-Sanchez, L., Sauvé, Y., Segura, F.J., Marti-nez-Navarrete, G., Tamarit, J.M., Fuentes-Broto, L., Sanchez-Cano, A., and Pinilla, I. (2014). Correlation between SD-OCT, immunocytochemistry and functional findings in an animal model of retinal degeneration. *Front. Neuroanat.* *8*.

- D’Cruz, P.M., Yasumura, D., Weir, J., Matthes, M.T., Abderrahim, H., LaVail, M.M., and Vollrath, D. (2000). Mutation of the receptor tyrosine kinase gene *Mertk* in the retinal dystrophic RCS rat. *Hum. Mol. Genet.* *9*, 645–651.
- Daiger, S.P., Sullivan, L.S., and Bowne, S.J. (2013). Genes and mutations causing retinitis pigmentosa. *Clin. Genet.* *84*, 132–141.
- Dalkara, D., Goureau, O., Marazova, K., and Sahel, J.-A. (2016). Let There Be Light: Gene and Cell Therapy for Blindness. *Hum. Gene Ther.* *27*, 134–147.
- Daniele, L.L., Lillo, C., Lyubarsky, A.L., Nikonov, S.S., Philp, N., Mears, A.J., Swaroop, A., Williams, D.S., and Pugh, E.N. (2005). Cone-like morphological, molecular, and electrophysiological features of the photoreceptors of the *Nrl* knockout mouse. *Investig. Ophthalmol. Vis. Sci.* *46*, 2156–2167.
- Decembrini, S., Koch, U., Radtke, F., Moulin, A., and Arsenijevic, Y. (2014). Derivation of traceable and transplantable photoreceptors from mouse embryonic stem cells. *Stem Cell Reports* *2*, 853–865.
- Decembrini, S., Martin, C., Sennlaub, F., Chemtob, S., Biel, M., Samardzija, M., Moulin, A., Behar-Cohen, F., and Arsenijevic, Y. (2017). Cone Genesis Tracing by the *Chrb4*-EGFP Mouse Line: Evidences of Cellular Material Fusion after Cone Precursor Transplantation. *Mol. Ther.* *25*, 634–653.
- Deering, M.F. (2004). A Photon Accurate Model of the Human Eye. ACM SIGGRAPH 2005 Pap. - SIGGRAPH ’05 1–14.
- Deng, W.L., Gao, M.L., Lei, X.L., Lv, J.N., Zhao, H., He, K.W., Xia, X.X., Li, L.Y., Chen, Y.C., Li, Y.P., et al. (2018). Gene Correction Reverses Ciliopathy and Photoreceptor Loss in iPSC-Derived Retinal Organoids from Retinitis Pigmentosa Patients. *Stem Cell Reports* *10*, 1267–1281.
- DiSanto, J.P., Muller, W., Guy-Grand, D., Fischer, A., and Rajewsky, K. (1995). Lymphoid development in mice with a targeted deletion of the interleukin 2 receptor gamma chain. *Proc Natl Acad Sci U S A* *92*, 377–381.
- DiStefano, T., Chen, H.Y., Panebianco, C., Kaya, K.D., Brooks, M.J., Gieser, L., Morgan, N.Y., Pohida, T., and Swaroop, A. (2017). Accelerated and Improved Differentiation of Retinal Organoids from Pluripotent Stem Cells in Rotating-Wall Vessel Bioreactors. *Stem Cell Reports* *10*, 1–14.
- Dryja, T.P., McGee, T.L., Hahn, L.B., Cowley, G.S., Olsson, J.E., Reichel, E., Sandberg, M.A., and Berson, E.L. (1990a). Mutations within the rhodopsin gene in patients with autosomal dominant retinitis pigmentosa. *N Engl J Med* *323*, 1302–1307.
- Dryja, T.P., McGee, T.L., Reichel, E., Hahn, L.B., Cowley, G.S., Yandell, D.W., Sandberg, M.A., and Berson, E.L. (1990b). A point mutation of the rhodopsin gene in one form of retinitis pigmentosa. *Nature* *343*, 364–366.
- Eberle, D., Schubert, S., Postel, K., Corbeil, D., and Ader, M. (2011). Increased Integration of Transplanted CD73-Positive Photoreceptor Precursors into Adult Mouse Retina. *Investig. Ophthalmology Vis. Sci.* *52*, 6462.
- Eberle, D., Kurth, T., Santos-Ferreira, T., Wilson, J., Corbeil, D., and Ader, M. (2012). Outer Segment Formation of Transplanted Photoreceptor Precursor Cells. *PLoS One* *7*.
- Eggan, K., Parmar, M., Takahashi, M., and Yamanaka, S. (2016). 10 Questions: Clinical Outlook for iPSCs. *Cell Stem Cell* *18*, 170–173.
- Eiraku, M., Takata, N., Ishibashi, H., Kawada, M., Sakakura, E., Okuda, S., Sekiguchi, K., Adachi, T., and Sasai, Y. (2011). Self-organizing optic-cup morphogenesis in three-dimensional culture. *Nature* *472*, 51–56.
- Emerson, M.M., Surzenko, N., Goetz, J.J., Trimarchi, J., and Cepko, C.L. (2013). *Otx2* and *Onecut1* promote the fates of cone photoreceptors and horizontal cells and repress rod photoreceptors. *Dev. Cell* *26*, 59–72.
- Evans, M.J., and Kaufman, M.H. (1981). Establishment in culture of pluripotential cells from mouse embryos. *Nature* *292*, 154–156.
- Fan, Y., Wu, J., Ashok, P., Hsiung, M., and Tzanakakis, E.S. (2015). Production of Human Pluripotent

Stem Cell Therapeutics under Defined Xeno-free Conditions: Progress and Challenges. *Stem Cell Rev. Reports* 11, 96–109.

Fuhrmann, S. (2010). Eye morphogenesis and patterning of the optic vesicle. *Curr. Top. Dev. Biol.* 93, 61–84.

Fuhrmann, S., Zou, C., and Levine, E.M. (2014). Retinal pigment epithelium development, plasticity, and tissue homeostasis. *Exp. Eye Res.* 123, 141–150.

Fujieda, H., Bremner, R., Mears, A.J., and Sasaki, H. (2009). Retinoic acid receptor-related orphan receptor alpha regulates a subset of cone genes during mouse retinal development. *J. Neurochem.* 108, 91–101.

Fujii, M., Sunagawa, G.A., Kondo, M., Takahashi, M., and Mandai, M. (2016). Evaluation of micro Electroretinograms Recorded with Multiple Electrode Array to Assess Focal Retinal Function. *Sci. Rep.* 6.

Furukawa, T., Morrow, E.M., and Cepko, C.L. (1997). Crx, a novel otx-like homeobox gene, shows photoreceptor-specific expression and regulates photoreceptor differentiation. *Cell* 91, 531–541.

Furukawa, T., Morrow, E.M., Li, T., Davis, F.C., and Cepko, C.L. (1999). Retinopathy and attenuated circadian entrainment in Crx-deficient mice. *Nat. Genet.* 23, 466–470.

Fusaki, N., Ban, H., Nishiyama, A., Saeki, K., and Hasegawa, M. (2009). Efficient induction of transgene-free human pluripotent stem cells using a vector based on Sendai virus, an RNA virus that does not integrate into the host genome. *Proc. Jpn. Acad., Ser. B* 85.

Gamm, D.M., Wang, S., Lu, B., Girman, S., Holmes, T., Bischoff, N., Shearer, R.L., Sauv e, Y., Capowski, E., Svendsen, C.N., et al. (2007). Protection of visual functions by human neural progenitors in a rat model of retinal disease. *PLoS One* 2, e338.

Gomes, F.L.A.F., Zhang, G., Carbonell, F., Correa, J.A., Harris, W.A., Simons, B.D., and Cayouette, M. (2011). Reconstruction of rat retinal progenitor cell lineages in vitro reveals a surprising degree of stochasticity in cell fate decisions. *Development* 138, 227–235.

Gonzalez-Cordero, A., West, E.L., Pearson, R.A., Duran, Y., Carvalho, L.S., Chu, C.J., Naeem, A., Blackford, S.J.I., Georgiadis, A., Lakowski, J., et al. (2013). Photoreceptor precursors derived from three-dimensional embryonic stem cell cultures integrate and mature within adult degenerate retina. *Nat. Biotechnol.* 31, 741–747.

Gonzalez-Cordero, A., Kruczek, K., Naeem, A., Fernando, M., Kloc, M., Ribeiro, J., Goh, D., Duran, Y., Blackford, S.J.I., Abelleira-Hervas, L., et al. (2017). Recapitulation of Human Retinal Development from Human Pluripotent Stem Cells Generates Transplantable Populations of Cone Photoreceptors. *Stem Cell Reports* 9, 820–837.

Gonzalez Cordero, A., Goh, D., Kruczek, K., Naeem, A., Fernando, M., kleine Holthaus, S.-M., Takaaki, M., Blackford, S.J.I., Kloc, M., Agundez, L., et al. (2018). Assessment of AAV vector tropisms for mouse and human pluripotent stem cell-derived RPE and photoreceptor cells. *Hum. Gene Ther.* hum.2018.027.

Gore, A., Li, Z., Fung, H.-L., Young, J.E., Agarwal, S., Antosiewicz-Bourget, J., Canto, I., Giorgetti, A., Israel, M.A., Kiskinis, E., et al. (2011). Somatic coding mutations in human induced pluripotent stem cells. *Nature* 471, 63–67.

Graw, J. (2010). Eye Development. *Curr. Top. Dev. Biol.* 90, 343–386.

Guerin, C.J., Anderson, D.H., and Fisher, S.K. (1990). Changes in intermediate filament immunolabeling occur in response to retinal detachment and reattachment in primates. *Investig. Ophthalmol. Vis. Sci.* 31, 1474–1482.

Gust, J., and Reh, T.A. (2011). Adult donor rod photoreceptors integrate into the mature mouse retina. *Investig. Ophthalmol. Vis. Sci.* 52, 5266–5272.

Haider, N.B., Cruz, N.M., Allocca, M., and Yuan, J. (2014). Pathobiology of the Outer Retina: Genetic and Nongenetic Causes of Disease (Elsevier Inc.).

- Haji Abdollahi, S., and Hirose, T. (2013). Stargardt-Fundus Flavimaculatus: Recent Advancements and Treatment. *Semin. Ophthalmol.* *28*, 372–376.
- Hambricht, D., Park, K.-Y., Brooks, M., McKay, R., Swaroop, A., and Nasonkin, I.O. (2012). Long-term survival and differentiation of retinal neurons derived from human embryonic stem cell lines in un-immunosuppressed mouse retina. *Mol. Vis.* *18*, 920–936.
- Hamel, C. (2006). Retinitis pigmentosa. *Orphanet J. Rare Dis.* *1*, 1–40.
- Hanna, J., Wernig, M., Markoulaki, S., Sun, C.W., Meissner, A., Cassady, J.P., Beard, C., Brambrink, T., Wu, L.C., Townes, T.M., et al. (2007). Treatment of sickle cell anemia mouse model with iPS cells generated from autologous skin. *Science* (80-.). *318*, 1920–1923.
- Hartong, D.T., Berson, E.L., and Dryja, T.P. (2006). Retinitis pigmentosa. *Lancet* *368*, 1795–1809.
- Hatakeyama, J., and Kageyama, R. (2004). Retinal cell fate determination and bHLH factors. *Semin. Cell Dev. Biol.* *15*, 83–89.
- Haverkamp, S. (2005). The Primordial, Blue-Cone Color System of the Mouse Retina. *J. Neurosci.* *25*, 5438–5445.
- He, J., Zhang, G., Almeida, A.D., Cayouette, M., Simons, B.D., and Harris, W.A. (2012). How variable clones build an invariant retina. *Neuron* *75*, 786–798.
- Hennig, A.K., Peng, G.-H., and Chen, S. (2008). Regulation of photoreceptor gene expression by Crx-associated transcription factor network. *Brain Res.* *1192*, 114–133.
- Hiler, D., Chen, X., Hazen, J., Kupriyanov, S., Carroll, P.A., Qu, C., Xu, B., Johnson, D., Griffiths, L., Frase, S., et al. (2015). Quantification of Retinogenesis in 3D Cultures Reveals Epigenetic Memory and Higher Efficiency in iPSCs Derived from Rod Photoreceptors. *Cell Stem Cell* *17*, 101–115.
- Hirami, Y., Osakada, F., Takahashi, K., Okita, K., Yamanaka, S., Ikeda, H., Yoshimura, N., and Takahashi, M. (2009). Generation of retinal cells from mouse and human induced pluripotent stem cells. *Neurosci. Lett.* *458*, 126–131.
- Ho, A.C., Humayun, M.S., Dorn, J.D., Da Cruz, L., Dagnelie, G., Handa, J., Barale, P.O., Sahel, J.A., Stanga, P.E., Hafezi, F., et al. (2015). Long-Term Results from an Epiretinal Prosthesis to Restore Sight to the Blind. *Ophthalmology* *122*, 1547–1554.
- den Hollander, A.I., Roepman, R., Koenekoop, R.K., and Cremers, F.P.M. (2008). Leber congenital amaurosis: genes, proteins and disease mechanisms. *Prog. Retin. Eye Res.* *27*, 391–419.
- Homma, K., Osakada, F., Hiram, Y., Jin, Z.B., Mandai, M., and Takahashi, M. (2009). Detection of localized retinal malfunction in retinal degeneration model using a multielectrode array system. *J. Neurosci. Res.* *87*, 2175–2182.
- Homma, K., Okamoto, S., Mandai, M., Gotoh, N., Rajasimha, H.K., Chang, Y.S., Chen, S., Li, W., Cogliati, T., Swaroop, A., et al. (2013). Developing rods transplanted into the degenerating retina of Crx-knockout mice exhibit neural activity similar to native photoreceptors. *Stem Cells* *31*, 1149–1159.
- Homma, K., Usui, S., and Kaneda, M. (2017). Knock-in strategy at 3'-end of *Crx* gene by CRISPR/Cas9 system shows the gene expression profiles during human photoreceptor differentiation. *Genes to Cells* *22*, 250–264.
- Hoon, M., Okawa, H., Della Santina, L., and Wong, R.O.L. (2014). Functional architecture of the retina: Development and disease. *Prog. Retin. Eye Res.* *42*, 44–84.
- Hoshino, A., Ratnapriya, R., Brooks, M.J., Chaitankar, V., Wilken, M.S., Zhang, C., Starostik, M.R., Gieser, L., La Torre, A., Nishio, M., et al. (2017). Molecular Anatomy of the Developing Human Retina. *Dev. Cell* *43*, 763–779.e4.
- Hou, P., Li, Y., Zhang, X., Liu, C., Guan, J., Li, H., Zhao, T., Ye, J., Yang, W., Liu, K., et al. (2013). Pluripotent stem cells induced from mouse somatic cells by small-molecule compounds. *Science* *341*, 651–654.
- Howland, H.C., Merola, S., and Basarab, J.R. (2004). The allometry and scaling of the size of

- vertebrate eyes. *Vision Res.* **44**, 2043–2065.
- Hughes, A. (1979). A schematic eye for the rat. *Vision Res.* **19**, 569–588.
- Humphries, M.M., Rancourt, D., Farrar, G.J., Kenna, P., Hazel, M., Bush, R.A., Sieving, P.A., Sheils, D.M., McNally, N., Creighton, P., et al. (1997). Retinopathy induced in mice by targeted disruption of the rhodopsin gene. *Nat. Genet.* **15**, 216–219.
- Hunt, N.C., Hallam, D., Karimi, A., Mellough, C.B., Chen, J., Steel, D.H.W., and Lako, M. (2017). 3D culture of human pluripotent stem cells in RGD-alginate hydrogel improves retinal tissue development. *Acta Biomater.* **49**, 329–343.
- Hussein, S.M., Batada, N.N., Vuoristo, S., Ching, R.W., Autio, R., Narvää, E., Ng, S., Sourour, M., Hämälä, R., Olsson, C., et al. (2011). Copy number variation and selection during reprogramming to pluripotency. *Nature* **471**, 58–62.
- Ikeda, H., Osakada, F., Watanabe, K., Mizuseki, K., Haraguchi, T., Miyoshi, H., Kamiya, D., Honda, Y., Sasai, N., Yoshimura, N., et al. (2005). Generation of Rx+/Pax6+ neural retinal precursors from embryonic stem cells. *Proc. Natl. Acad. Sci. U. S. A.* **102**, 11331–11336.
- Illing, M.E., Rajan, R.S., Bence, N.F., and Kopito, R.R. (2002). A rhodopsin mutant linked to autosomal dominant retinitis pigmentosa is prone to aggregate and interacts with the ubiquitin proteasome system. *J. Biol. Chem.* **277**, 34150–34160.
- Iraha, S., Tu, H.Y., Yamasaki, S., Kagawa, T., Goto, M., Takahashi, R., Watanabe, T., Sugita, S., Yonemura, S., Sunagawa, G.A., et al. (2018). Establishment of Immunodeficient Retinal Degeneration Model Mice and Functional Maturation of Human ESC-Derived Retinal Sheets after Transplantation. *Stem Cell Reports* **10**, 1059–1074.
- Ito, M., Hiramatsu, H., Kobayashi, K., Suzue, K., Kawahata, M., Hioki, K., Ueyama, Y., Koyanagi, Y., Sugamura, K., Tsuji, K., et al. (2002). NOD/SCID/gamma(c)(null) mouse: an excellent recipient mouse model for engraftment of human cells. *Blood* **100**, 3175–3182.
- Jacobs, G.H., Neitz, J., and Deegan, J.F.I. (1991). Retinal receptors in rodents maximally sensitive to ultraviolet light. *Nature* **353**, 737–740.
- Jadhav, A.P., Mason, H.A., and Cepko, C.L. (2006). Notch 1 inhibits photoreceptor production in the developing mammalian retina. *Development* **133**, 913–923.
- Jayakody, S.A., Gonzalez-Cordero, A., Ali, R.R., and Pearson, R.A. (2015). Cellular strategies for retinal repair by photoreceptor replacement. *Prog. Retin. Eye Res.* **46**, 31–66.
- Jia, L., Oh, E.C.T., Ng, L., Srinivas, M., Brooks, M., Swaroop, A., and Forrest, D. (2009). Retinoid-related orphan nuclear receptor RORbeta is an early-acting factor in rod photoreceptor development. *Proc. Natl. Acad. Sci. U. S. A.* **106**, 17534–17539.
- Jin, Z.B., Okamoto, S., Osakada, F., Homma, K., Assawachananont, J., Hirami, Y., Iwata, T., and Takahashi, M. (2011). Modeling retinal degeneration using patient-specific induced pluripotent stem cells. *PLoS One* **6**.
- Jones, B.W., and Marc, R.E. (2005). Retinal remodeling during retinal degeneration. *Exp. Eye Res.* **81**, 123–137.
- de Jong, P.T.V.M. (2006). Age-Related Macular Degeneration. *N. Engl. J. Med.* **355**, 1474–1485.
- Junying, Y., Kejin, H., Kim, S.O., Shulan, T., Stewart, R., Slukvin, I.I., and Thomson, J.A. (2009). Human induced pluripotent stem cells free of vector and transgene sequences. *Science* (80-.). **324**, 797–801.
- Kaewkhaw, R., Kaya, K.D., Brooks, M., Homma, K., Zou, J., Chaitankar, V., Rao, M., and Swaroop, A. (2015). Transcriptome Dynamics of Developing Photoreceptors in Three-Dimensional Retina Cultures Recapitulates Temporal Sequence of Human Cone and Rod Differentiation Revealing Cell Surface Markers and Gene Networks. *Stem Cells* **33**, 3504–3518.
- Kamao, H., Mandai, M., Okamoto, S., Sakai, N., Suga, A., Sugita, S., Kiryu, J., and Takahashi, M. (2014). Characterization of human induced pluripotent stem cell-derived retinal pigment epithelium cell

sheets aiming for clinical application. *Stem Cell Reports* 2, 205–218.

Katoh, K., Omori, Y., Onishi, A., Sato, S., Kondo, M., and Furukawa, T. (2010). Blimp1 suppresses Chx10 expression in differentiating retinal photoreceptor precursors to ensure proper photoreceptor development. *J. Neurosci.* 30, 6515–6526.

Keeler, C. (1966). Retinal degeneration in the mouse is rodless retina. *J. Hered.* 57, 50.

Kelava, I., and Lancaster, M.A. (2016). Dishing out mini-brains: Current progress and future prospects in brain organoid research. *Dev. Biol.* 420, 199–209.

Khabou, H., Garita-Hernandez, M., Chaffiol, A., Reichman, S., Jaillard, C., Brazhnikova, E., Bertin, S., Forster, V., Desrosiers, M., Winckler, C., et al. (2018). Noninvasive gene delivery to foveal cones for vision restoration. *JCI Insight* 3, 96029.

Kim, D., Kim, C.-H., Moon, J.-I., Chung, Y.-G., Chang, M.-Y., Han, B.-S., Ko, S., Yang, E., Cha, K.Y., Robert, L., et al. (2009). Generation of human induced pluripotent stem cells by direct delivery of reprogramming proteins. *Cell Stem Cell* 4, 472–476.

Kim, K., Doi, A., Wen, B., Ng, K., Zhao, R., Cahan, P., Kim, J., Aryee, M.J., Ji, H., Ehrlich, L.I.R., et al. (2010). Epigenetic memory in induced pluripotent stem cells. *Nature* 467, 285–290.

Klassen, H., Schwartz, P.H., Ziaieian, B., Nethercott, H., Young, M.J., Bragadottir, R., Tullis, G.E., Warfvinge, K., and Narfstrom, K. (2007). Neural precursors isolated from the developing cat brain show retinal integration following transplantation to the retina of the dystrophic cat. *Vet. Ophthalmol.* 10, 245–253.

Klassen, H.J., Ng, T.F., Kurimoto, Y., Kirov, I., Shatos, M., Coffey, P., and Young, M.J. (2004). Multipotent retinal progenitors express developmental markers, differentiate into retinal neurons, and preserve light-mediated behavior. *Investig. Ophthalmol. Vis. Sci.* 45, 4167–4173.

Koike, C., Nishida, A., Ueno, S., Saito, H., Sanuki, R., Sato, S., Furukawa, A., Aizawa, S., Matsuo, I., Suzuki, N., et al. (2007). Functional roles of Otx2 transcription factor in postnatal mouse retinal development. *Mol. Cell. Biol.* 27, 8318–8329.

Kolomiets, B., Dubus, E., Simonutti, M., Rosolen, S., Sahel, J.A., and Picaud, S. (2010). Late histological and functional changes in the P23H rat retina after photoreceptor loss. *Neurobiol. Dis.* 38, 47–58.

Koso, H., Minami, C., Tabata, Y., Inoue, M., Sasaki, E., Satoh, S., and Watanabe, S. (2009). CD73, a novel cell surface antigen that characterizes retinal photoreceptor precursor cells. *Investig. Ophthalmol. Vis. Sci.* 50, 5411–5418.

Kraft, T.W., Allen, D., Petters, R.M., Hao, Y., Peng, Y.-W., and Wong, F. (2005). Altered light responses of single rod photoreceptors in transgenic pigs expressing P347L or P347S rhodopsin. *Mol. Vis.* 11, 1246–1256.

Krohne, T.U., Westenskow, P.D., Kurihara, T., Friedlander, D.F., Lehmann, M., Dorsey, A.L., Li, W., Zhu, S., Schultz, A., Wang, J., et al. (2012). Generation of Retinal Pigment Epithelial Cells from Small Molecules and OCT4 Reprogrammed Human Induced Pluripotent Stem Cells. *Stem Cells Transl. Med.* 1, 96–109.

Kruczek, K., Gonzalez-Cordero, A., Goh, D., Naeem, A., Jonikas, M., Blackford, S.J.I., Kloc, M., Duran, Y., Georgiadis, A., Sampson, R.D., et al. (2017). Differentiation and Transplantation of Embryonic Stem Cell-Derived Cone Photoreceptors into a Mouse Model of End-Stage Retinal Degeneration. *Stem Cell Reports* 8, 1659–1674.

Kuwahara, A., Ozone, C., Nakano, T., Saito, K., Eiraku, M., and Sasai, Y. (2015). Generation of a ciliary margin-like stem cell niche from self-organizing human retinal tissue. *Nat. Commun.* 6, 6286.

Lakowski, J., Han, Y.T., Pearson, R.A., Gonzalez-Cordero, A., West, E.L., Gualdoni, S., Barber, A.C., Hubank, M., Ali, R.R., and Sowden, J.C. (2011). Effective transplantation of photoreceptor precursor cells selected via cell surface antigen expression. *Stem Cells* 29, 1391–1404.

Lakowski, J., Gonzalez-Cordero, A., West, E.L., Han, Y.T., Welby, E., Naeem, A., Blackford, S.J.I., Bainbridge, J.W.B., Pearson, R.A., Ali, R.R., et al. (2015). Transplantation of Photoreceptor

Precursors Isolated via a Cell Surface Biomarker Panel from Embryonic Stem Cell-Derived Self-Forming Retina. *Stem Cells* 33, 2469–2482.

Lakowski, J., Welby, E., Budinger, D., Di Marco, F., Di Foggia, V., Bainbridge, J.W.B., Wallace, K., Gamm, D.M., Ali, R.R., and Sowden, J.C. (2018). Isolation of Human Photoreceptor Precursors via a Cell Surface Marker Panel from Stem Cell-derived Retinal Organoids and Fetal Retinae. *Stem Cells*.

Lamba, D.A., Karl, M.O., Ware, C.B., and Reh, T.A. (2006). Efficient generation of retinal progenitor cells from human embryonic stem cells. *Proc. Natl. Acad. Sci. U. S. A.* 103, 12769–12774.

Lamba, D.A., Gust, J., and Reh, T.A. (2009). Transplantation of human embryonic stem cell-derived photoreceptors restores some visual function in Crx-deficient mice. *TL - 4. Cell Stem Cell* 4 *VN-re*, 73–79.

Lamba, D.A., McUsic, A., Hirata, R.K., Wang, P.-R., Russell, D., and Reh, T.A. (2010). Generation, Purification and Transplantation of Photoreceptors Derived from Human Induced Pluripotent Stem Cells. *PLoS One* 5, e8763.

LaVail, M.M., Nishikawa, S., Steinberg, R.H., Naash, M.I., Duncan, J.L., Trautmann, N., Matthes, M.T., Yasumura, D., Lau-Villacorta, C., Chen, J., et al. (2018). Phenotypic characterization of P23H and S334ter rhodopsin transgenic rat models of inherited retinal degeneration. *Exp. Eye Res.* 167, 56–90.

Laver, C.R.J., and Matsubara, J.A. (2017). Structural divergence of essential triad ribbon synapse proteins among placental mammals – Implications for preclinical trials in photoreceptor transplantation therapy. *Exp. Eye Res.* 159, 156–167.

Lee, M.-O., Moon, S.H., Jeong, H.-C., Yi, J.-Y., Lee, T.-H., Shim, S.H., Rhee, Y.-H., Lee, S.-H., Oh, S.-J., Lee, M.-Y., et al. (2013). Inhibition of pluripotent stem cell-derived teratoma formation by small molecules. *Proc. Natl. Acad. Sci. U. S. A.* 110, E3281-90.

Lin, B., McLelland, B.T., Mathur, A., Aramant, R.B., and Seiler, M.J. (2018). Sheets of human retinal progenitor transplants improve vision in rats with severe retinal degeneration. *Exp. Eye Res.* 174, 13–28.

Lister, R., Pelizzola, M., Kida, Y.S., Hawkins, R.D., Nery, J.R., Hon, G., Antosiewicz-Bourget, J., Ogmalley, R., Castanon, R., Klugman, S., et al. (2011). Hotspots of aberrant epigenomic reprogramming in human induced pluripotent stem cells. *Nature* 471, 68–73.

Liu, M.M., and Zack, D.J. (2013). Alternative splicing and retinal degeneration. *Clin. Genet.* 84, 142–149.

Livesey, F.J., and Cepko, C.L. (2001). Vertebrate neural cell-fate determination: lessons from the retina. *Nat. Rev. Neurosci.* 2, 109–118.

Llonch, S., Carido, M., and Ader, M. (2018). Organoid technology for retinal repair. *Dev. Biol.* 433, 132–143.

Lolley, R.N., Rong, H., and Craft, C.M. (1994). Linkage of photoreceptor degeneration by apoptosis with inherited defect in phototransduction. *Invest. Ophthalmol. Vis. Sci.* 35, 358–362.

Lu, B., Morgans, C.W., Girman, S., Luo, J., Zhao, J., Du, H., Lim, S., Ding, S., Svendsen, C., Zhang, K., et al. (2013). Neural Stem Cells Derived by Small Molecules Preserve Vision. *Transl. Vis. Sci. Technol.* 2, 1.

Lund, R.J., Närvä, E., and Lahesmaa, R. (2012). Genetic and epigenetic stability of human pluripotent stem cells. *Nat. Rev. Genet.* 13, 732–744.

Luo, J., Baranov, P., Patel, S., Ouyang, H., Quach, J., Wu, F., Qiu, A., Luo, H., Hicks, C., Zeng, J., et al. (2014). Human retinal progenitor cell transplantation preserves vision. *J. Biol. Chem.* 289, 6362–6371.

Ben M'Barek, K., Habeler, W., Plancheron, A., Jarraya, M., Regent, F., Terray, A., Yang, Y., Chatrousse, L., Domingues, S., Masson, Y., et al. (2017). Human ESC-derived retinal epithelial cell sheets potentiate rescue of photoreceptor cell loss in rats with retinal degeneration. *Sci. Transl. Med.* 9, eaai7471.

- MacLaren, R.E. (2017). Cone fusion confusion in photoreceptor transplantation. *Stem Cell Investig.* *4*, 71–71.
- MacLaren, R.E., Pearson, R.A., MacNeil, A., Douglas, R.H., Salt, T.E., Akimoto, M., Swaroop, A., Sowden, J.C., and Ali, R.R. (2006). Retinal repair by transplantation of photoreceptor precursors. *Nature* *444*, 203–207.
- Mandai, M., Fujii, M., Hashiguchi, T., and Sunagawa, G.A. (2017a). iPSC-Derived Retina Transplants Improve Vision in rd1 End-Stage Retinal-Degeneration Mice. *Stem Cell Reports* *8*, 69–83.
- Mandai, M., Watanabe, A., Kurimoto, Y., Hirami, Y., Morinaga, C., Daimon, T., Fujihara, M., Akimaru, H., Sakai, N., Shibata, Y., et al. (2017b). Autologous Induced Stem-Cell-Derived Retinal Cells for Macular Degeneration. *N. Engl. J. Med.* *376*, 1038–1046.
- Masland, R.H. (2001). The fundamental plan of the retina. *Nat. Neurosci.* *4*, 877–886.
- Masland, R.H. (2012). The Neuronal Organization of the Retina. *Neuron* *76*, 266–280.
- Massof, R.W., and Chang, F.W. (1972). A revision of the rat schematic eye. *Vision Res.* *12*, 793–796.
- Mathur, P., and Yang, J. (2015). Usher syndrome: Hearing loss, retinal degeneration and associated abnormalities. *Biochim. Biophys. Acta* *1852*, 406–420.
- Mclelland, B.T., Lin, B., Mathur, A., Aramant, R.B., Thomas, B.B., Keirstead, H.S., and Seiler, M.J. (2018). Transplanted hESC-Derived Retina Organoid Sheets Differentiate, Integrate, and Improve Visual Function in Retinal Degenerate Rats.
- Mead, B., Berry, M., Logan, A., Scott, R.A.H., Leadbeater, W., and Scheven, B.A. (2015). Stem cell treatment of degenerative eye disease. *Stem Cell Res.* *14*, 243–257.
- Mears, A.J., Kondo, M., Swain, P.K., Takada, Y., Bush, R.A., Saunders, T.L., Sieving, P.A., and Swaroop, A. (2001). Nr1 is required for rod photoreceptor development. *Nat. Genet.* *29*, 447–452.
- Mellough, C.B., Sernagor, E., Moreno-Gimeno, I., Steel, D.H.W., and Lako, M. (2012). Efficient stage-specific differentiation of human pluripotent stem cells toward retinal photoreceptor cells. *Stem Cells* *30*, 673–686.
- Mellough, C.B., Collin, J., Khazim, M., White, K., Sernagor, E., Steel, D.H.W., and Lako, M. (2015). IGF-1 Signaling Plays an Important Role in the Formation of Three-Dimensional Laminated Neural Retina and Other Ocular Structures from Human Embryonic Stem Cells. *Stem Cells* *33*, 2416–2430.
- Menasché, P., Vanneau, V., Hagège, A., Bel, A., Cholley, B., Cacciapuoti, I., Parouchev, A., Benhamouda, N., Tachdjian, G., Tosca, L., et al. (2015). Human embryonic stem cell-derived cardiac progenitors for severe heart failure treatment: first clinical case report: Figure 1. *Eur. Heart J.* *36*, 2011–2017.
- Mendes, H.F., Van Der Spuy, J., Chapple, J.P., and Cheetham, M.E. (2005). Mechanisms of cell death in rhodopsin retinitis pigmentosa: Implications for therapy. *Trends Mol. Med.* *11*, 177–185.
- Meyer, J.S., Shearer, R.L., Capowski, E.E., Wright, L.S., Wallace, K. a, McMillan, E.L., Zhang, S.-C., and Gamm, D.M. (2009). Modeling early retinal development with human embryonic and induced pluripotent stem cells. *Proc. Natl. Acad. Sci. U. S. A.* *106*, 16698–16703.
- Meyer, J.S., Howden, S.E., Wallace, K.A., Verhoeven, A.D., Wright, L.S., Capowski, E.E., Pinilla, I., Martin, J.M., Tian, S., Stewart, R., et al. (2011). Optic vesicle-like structures derived from human pluripotent stem cells facilitate a customized approach to retinal disease treatment. *Stem Cells* *29*, 1206–1218.
- Mitsui, K., Tokuzawa, Y., Itoh, H., Segawa, K., Murakami, M., Takahashi, K., Maruyama, M., Maeda, M., and Yamanaka, S. (2003). The homeoprotein nanog is required for maintenance of pluripotency in mouse epiblast and ES cells. *Cell* *113*, 631–642.
- Mockel, A., Perdomo, Y., Stutzmann, F., Letsch, J., Marion, V., and Dollfus, H. (2011). Retinal dystrophy in Bardet-Biedl syndrome and related syndromic ciliopathies. *Prog. Retin. Eye Res.* *30*, 258–274.

- Mustafi, D., Engel, A.H., and Palczewski, K. (2009). Structure of cone photoreceptors. *Prog. Retin. Eye Res.* *28*, 289–302.
- Naash, M.I., Hollyfield, J.G., al-Ubaidi, M.R., and Baehr, W. (1993). Simulation of human autosomal dominant retinitis pigmentosa in transgenic mice expressing a mutated murine opsin gene. *Proc. Natl. Acad. Sci. U. S. A.* *90*, 5499–5503.
- Nakano, T., Ando, S., Takata, N., Kawada, M., Muguruma, K., Sekiguchi, K., Saito, K., Yonemura, S., Eiraku, M., and Sasai, Y. (2012). Self-formation of optic cups and storable stratified neural retina from human ESCs. *Cell Stem Cell* *10*, 771–785.
- Nakatsuji, N., Nakajima, F., and Tokunaga, K. (2008). HLA-haplotype banking and iPS cells. *Nat. Biotechnol.* *26*, 739–740.
- Neofytou, E., Brien, C.G.O., Couture, L.A., and Wu, J.C. (2015). Hurdles to clinical translation of human induced pluripotent stem cells. *J. Clin. Invest.* *125*, 2551–2557.
- Neves, J., Zhu, J., Sousa-Victor, P., Konjikusic, M., Riley, R., Chew, S., Qi, Y., Jasper, H., and Lamba, D.A. (2016). Immune modulation by MANF promotes tissue repair and regenerative success in the retina. *Science* (80-.). *353*, aaf3646.
- Newman, E., and Reichenbach, A. (1996). The Muller cell: A functional element of the retina. *Trends Neurosci.* *19*, 307–312.
- Ng, L., Hurley, J.B., Dierks, B., Srinivas, M., Saltó, C., Vennström, B., Reh, T. a, and Forrest, D. (2001). A thyroid hormone receptor that is required for the development of green cone photoreceptors. *Nat. Genet.* *27*, 94–98.
- Nichols, J., Zevnik, B., Anastassiadis, K., Niwa, H., Klewe-Nebenius, D., Chambers, I., Schöler, H., and Smith, A. (1998). Formation of pluripotent stem cells in the mammalian embryo depends on the POU transcription factor Oct4. *Cell* *95*, 379–391.
- Nickerson, P.E.B., Ortin-Martinez, A., and Wallace, V.A. (2018). Material Exchange in Photoreceptor Transplantation: Updating Our Understanding of Donor/Host Communication and the Future of Cell Engraftment Science. *Front. Neural Circuits* *12*.
- Nickle, B., and Robinson, P.R. (2007). The opsins of the vertebrate retina: Insights from structural, biochemical, and evolutionary studies. *Cell. Mol. Life Sci.* *64*, 2917–2932.
- Niclis, J.C., Gantner, C.W., Alsanie, W.F., McDougall, S.J., Bye, C.R., Elefanty, A.G., Stanley, E.G., Haynes, J.M., Pouton, C.W., Thompson, L.H., et al. (2017). Efficiently Specified Ventral Midbrain Dopamine Neurons from Human Pluripotent Stem Cells Under Xeno-Free Conditions Restore Motor Deficits in Parkinsonian Rodents. *Stem Cells Transl. Med.* *6*, 937–948.
- van Nie, R., Iványi, D., and Démant, P. (1978). A New H-2-Linked Mutation, rds, Causing Retinal Degeneration in the Mouse. *Tissue Antigens* *12*, 106–108.
- Nishida, A., Furukawa, A., Koike, C., Tano, Y., Aizawa, S., Matsuo, I., and Furukawa, T. (2003). Otx2 homeobox gene controls retinal photoreceptor cell fate and pineal gland development. *Nat. Neurosci.* *6*, 1255–1263.
- Niwa, H., Miyazaki, J.I., and Smith, A.G. (2000). Quantitative expression of Oct-3/4 defines differentiation, dedifferentiation or self-renewal of ES cells. *Nat. Genet.* *24*, 372–376.
- Noggle, S., Fung, H.L., Gore, A., Martinez, H., Satriani, K.C., Prosser, R., Oum, K., Paull, D., Druckenmiller, S., Freeby, M., et al. (2011). Human oocytes reprogram somatic cells to a pluripotent state. *Nature* *478*, 70–75.
- Nolbrant, S., Heuer, A., Parmar, M., and Kirkeby, A. (2017). Generation of high-purity human ventral midbrain dopaminergic progenitors for in vitro maturation and intracerebral transplantation. *Nat. Protoc.* *12*, 1962–1979.
- Oh, E.C.T., Cheng, H., Hao, H., Jia, L., Khan, N.W., and Swaroop, A. (2008). Rod differentiation factor NRL activates the expression of nuclear receptor NR2E3 to suppress the development of cone photoreceptors. *Brain Res.* *1236*, 16–29.

- Ohsawa, R., and Kageyama, R. (2008). Regulation of retinal cell fate specification by multiple transcription factors. *Brain Res.* *1192*, 90–98.
- Okita, K., Ichisaka, T., and Yamanaka, S. (2007). Generation of germline-competent induced pluripotent stem cells. *Nature* *448*, 313–317.
- Okita, K., Matsumura, Y., Sato, Y., Okada, A., Morizane, A., Okamoto, S., Hong, H., Nakagawa, M., Tanabe, K., Tezuka, K.I., et al. (2011). A more efficient method to generate integration-free human iPSC cells. *Nat. Methods* *8*, 409–412.
- Olsson, J.E., Gordon, J.W., Pawlyk, B.S., Roof, D., Hayes, A., Molday, R.S., Mukai, S., Cowley, G.S., Berson, E.L., and Dryja, T.P. (1992). Transgenic mice with a rhodopsin mutation (Pro23His): A mouse model of autosomal dominant retinitis pigmentosa. *Neuron* *9*, 815–830.
- Orhan, E., Dalkara, D., Neullé, M., Lechauve, C., Michiels, C., Picaud, S., Léveillard, T., Sahel, J.A., Naash, M.I., LaVail, M.M., et al. (2015). Genotypic and phenotypic characterization of P23H line 1 rat model. *PLoS One* *10*.
- Ortin-Martinez, A., Tsai, E.L.S., Nickerson, P.E., Bergeret, M., Lu, Y., Smiley, S., Comanita, L., and Wallace, V.A. (2017). A Reinterpretation of Cell Transplantation: GFP Transfer From Donor to Host Photoreceptors. *Stem Cells* *35*, 932–939.
- Osakada, F., Ikeda, H., Mandai, M., Wataya, T., Watanabe, K., Yoshimura, N., Akaike, A., Sasai, Y., and Takahashi, M. (2008). Toward the generation of rod and cone photoreceptors from mouse, monkey and human embryonic stem cells. *Nat. Biotechnol.* *26*, 215–224.
- Osakada, F., Jin, Z.-B., Hirami, Y., Ikeda, H., Danjyo, T., Watanabe, K., Sasai, Y., and Takahashi, M. (2009). In vitro differentiation of retinal cells from human pluripotent stem cells by small-molecule induction. *J. Cell Sci.* *122*, 3169–3179.
- Ovando-Roche, P., West, E.L., Branch, M.J., Sampson, R.D., Fernando, M., Munro, P., Georgiadis, A., Rizzi, M., Kloc, M., Naeem, A., et al. (2018). Use of bioreactors for culturing human retinal organoids improves photoreceptor yields. *Stem Cell Res. Ther.* *9*, 156.
- Ozawa, Y., Nakao, K., Shimazaki, T., Takeda, J., Akira, S., Ishihara, K., Hirano, T., Oguchi, Y., and Okano, H. (2004). Downregulation of STAT3 activation is required for presumptive rod photoreceptor cells to differentiate in the postnatal retina. *Mol. Cell. Neurosci.* *26*, 258–270.
- Panda-Jonas, S., Jonas, J.B., Jakobczyk, M., and Schneider, U. (1994). Retinal Photoreceptor Count, Retinal Surface Area, and Optic Disc Size in Normal Human Eyes. *Ophthalmology* *101*, 519–523.
- Parfitt, D.A., Lane, A., Ramsden, C.M., Carr, A.J.F., Munro, P.M., Jovanovic, K., Schwarz, N., Kanuga, N., Muthiah, M.N., Hull, S., et al. (2016). Identification and Correction of Mechanisms Underlying Inherited Blindness in Human iPSC-Derived Optic Cups. *Cell Stem Cell* *18*, 769–781.
- Pearson, R.A., Barber, A.C., Rizzi, M., Hippert, C., Xue, T., West, E.L., Duran, Y., Smith, A.J., Chuang, J.Z., Azam, S.A., et al. (2012). Restoration of vision after transplantation of photoreceptors. *Nature* *485*, 99–103.
- Pearson, R.A., Gonzalez-Cordero, A., West, E.L., Ribeiro, J.R., Aghaizu, N., Goh, D., Sampson, R.D., Georgiadis, A., Waldron, P. V., Duran, Y., et al. (2016). Donor and host photoreceptors engage in material transfer following transplantation of post-mitotic photoreceptor precursors. *Nat. Commun.* *7*, 13029.
- Peng, G.H., Ahmad, O., Ahmad, F., Liu, J., and Chen, S. (2005). The photoreceptor-specific nuclear receptor Nr2e3 interacts with Crx and exerts opposing effects on the transcription of rod versus cone genes. *Hum. Mol. Genet.* *14*, 747–764.
- Petters, R.M., Alexander, C.A., Wells, K.D., Collins, E.B., Sommer, J.R., Blanton, M.R., Rojas, G., Hao, Y., Flowers, W.L., Banin, E., et al. (1997). Genetically engineered large animal model for studying cone photoreceptor survival and degeneration in retinitis pigmentosa. *Nat. Biotechnol.* *15*, 965–970.
- Phillips, J., Jiang, P., S, H., P, B., Min, J., York, N., Chu, L., Capowski, E., Cash, A., Jain, S., et al. (2017). A Novel Approach to Single Cell RNA-Sequence Analysis Facilitates In Silico Gene Reporting

of Human Pluripotent Stem Cell-Derived Retinal Cell Types. *Stem Cells* 1–16.

Phillips, M.J., Wallace, K.A., Dickerson, S.J., Miller, M.J., Verhoeven, A.D., Martin, J.M., Wright, L.S., Shen, W., Capowski, E.E., Percin, E.F., et al. (2012). Blood-derived human iPS cells generate optic vesicle-like structures with the capacity to form retinal laminae and develop synapses. *Invest. Ophthalmol. Vis. Sci.* 53, 2007–2019.

Phillips, M.J., Perez, E.T., Martin, J.M., Reshel, S.T., Wallace, K.A., Capowski, E.E., Singh, R., Wright, L.S., Clark, E.M., Barney, P.M., et al. (2014). Modeling human retinal development with patient-specific induced pluripotent stem cells reveals multiple roles for visual system homeobox 2. *Stem Cells* 32, 1480–1492.

Pittler, S.J., Keeler, C.E., Sidman, R.L., and Baehr, W. (1993). PCR analysis of DNA from 70-year-old sections of rodless retina demonstrates identity with the mouse rd defect. *Proc. Natl. Acad. Sci.* 90, 9616–9619.

Polo, J.M., Liu, S., Figueroa, M.E., Kulalert, W., Eminli, S., Tan, K.Y., Apostolou, E., Stadtfeld, M., Li, Y., Shioda, T., et al. (2010). Cell type of origin influences the molecular and functional properties of mouse induced pluripotent stem cells. *Nat. Biotechnol.* 28, 848–855.

Postel, K., Bellmann, J., Splith, V., and Ader, M. (2013). Analysis of cell surface markers specific for transplantable rod photoreceptors. *Mol. Vis.* 19, 2058–2067.

Puri, M.C., and Nagy, A. (2012). Concise review: Embryonic stem cells versus induced pluripotent stem cells: The game is on. *Stem Cells* 30, 10–14.

Qi, X., Li, T.-G., Hao, J., Hu, J., Wang, J., Simmons, H., Miura, S., Mishina, Y., and Zhao, G.-Q. (2004). BMP4 supports self-renewal of embryonic stem cells by inhibiting mitogen-activated protein kinase pathways. *Proc. Natl. Acad. Sci. U. S. A.* 101, 6027–6032.

Quadrato, G., Nguyen, T., Macosko, E.Z., Sherwood, J.L., Yang, S.M., Berger, D.R., Maria, N., Scholvin, J., Goldman, M., Kinney, J.P., et al. (2017). Cell diversity and network dynamics in photosensitive human brain organoids. *Nature* 545, 48–53.

Radtke, N.D., Aramant, R.B., Petry, H.M., Green, P.T., Pidwell, D.J., and Seiler, M.J. (2008). Vision improvement in retinal degeneration patients by implantation of retina together with retinal pigment epithelium. *Am. J. Ophthalmol.* 146, 172–182.e1.

Ramamurthy, V., Niemi, G. a, Reh, T. a, and Hurley, J.B. (2004). Leber congenital amaurosis linked to AIPL1: A mouse model reveals destabilization of cGMP phosphodiesterase. *Proc. Natl. Acad. Sci.* 101, 13897–13902.

Reichenbach, A., Siegel, A., Rickmann, M., Wolff, J.R., Noone, D., and Robinson, S.R. (1995). Distribution of Bergmann glial somata and processes: implications for function. *J. Für Hirnforsch.* 36, 509–517.

Reichman, S., Terray, A., Slembrouck, A., Nanteau, C., Orioux, G., Habeler, W., Nandrot, E.F., Sahel, J.-A., Monville, C., and Goureau, O. (2014). From confluent human iPS cells to self-forming neural retina and retinal pigmented epithelium. *Proc. Natl. Acad. Sci. U. S. A.* 111, 8518–8523.

Reichman, S., Slembrouck, A., Gagliardi, G., Chaffiol, A., Terray, A., Nanteau, C., Potey, A., Belle, M., Rabesandratana, O., Duebel, J., et al. (2017). Generation of Storable Retinal Organoids and Retinal Pigmented Epithelium from Adherent Human iPS Cells in Xeno-Free and Feeder-Free Conditions. *Stem Cells* 35, 1176–1188.

Remtulla, S., and Hallett, P.E. (1985). A schematic eye for the mouse, and comparisons with the rat. *Vision Res.* 25, 21–31.

Rhee, K. Do, Goureau, O., Chen, S., and Yang, X.-J. (2004). Cytokine-induced activation of signal transducer and activator of transcription in photoreceptor precursors regulates rod differentiation in the developing mouse retina. *J. Neurosci.* 24, 9779–9788.

Roberts, M.R., Hendrickson, A., McGuire, C.R., and Reh, T.A. (2005). Retinoid X receptor (gamma) is necessary to establish the S-opsin gradient in cone photoreceptors of the developing mouse retina. *Invest. Ophthalmol. Vis. Sci.* 46, 2897–2904.

- Roorda, A., Metha, A.B., Lennie, P., and Williams, D.R. (2001). Packing arrangement of the three cone classes in primate retina. In *Vision Research*, pp. 1291–1306.
- Sakaguchi, D.S., Van Hoffelen, S.J., Theusch, E., Parker, E., Orasky, J., Harper, M.M., Benediktsson, A., and Young, M.J. (2004). Transplantation of neural progenitor cells into the developing retina of the Brazilian opossum: An in vivo system for studying stem/progenitor cell plasticity. *Dev. Neurosci.* *26*, 336–345.
- Sakami, S., Maeda, T., Bereta, G., Okano, K., Golczak, M., Sumaroka, A., Roman, A.J., Cideciyan, A. V., Jacobson, S.G., and Palczewski, K. (2011). Probing mechanisms of photoreceptor degeneration in a new mouse model of the common form of autosomal dominant retinitis pigmentosa due to P23H opsin mutations. *J. Biol. Chem.* *286*, 10551–10567.
- Saliba, R.S., Munro, P.M.G., Luthert, P.J., and Cheetham, M.E. (2002). The cellular fate of mutant rhodopsin: quality control, degradation and aggregate formation. *J. Cell Sci.* *115*, 2907–2918.
- Santos-Ferreira, T., Postel, K., Stutzki, H., Kurth, T., Zeck, G., and Ader, M. (2015). Daylight vision repair by cell transplantation. *Stem Cells* *33*, 79–90.
- Santos-Ferreira, T., Völkner, M., Borsch, O., Haas, J., Cimalla, P., Vasudevan, P., Carmeliet, P., Corbeil, D., Michalakis, S., Koch, E., et al. (2016a). Stem cell-derived photoreceptor transplants differentially integrate into mouse models of cone-rod dystrophy. *Investig. Ophthalmol. Vis. Sci.* *57*, 3509–3520.
- Santos-Ferreira, T., Llonch, S., Borsch, O., Postel, K., Haas, J., and Ader, M. (2016b). Retinal transplantation of photoreceptors results in donor–host cytoplasmic exchange. *Nat. Commun.* *7*, 13028.
- Santos-Ferreira, T.F., Borsch, O., and Ader, M. (2017). Rebuilding the Missing Part—A Review on Photoreceptor Transplantation. *Front. Syst. Neurosci.* *10*, 1–14.
- Satoh, S., Tang, K., Iida, A., Inoue, M., Kodama, T., Tsai, S.Y., Tsai, M.-J., Furuta, Y., and Watanabe, S. (2009). The spatial patterning of mouse cone opsin expression is regulated by bone morphogenetic protein signaling through downstream effector COUP-TF nuclear receptors. *J. Neurosci.* *29*, 12401–12411.
- Scott, P.A., Fernandez de Castro, J.P., Kaplan, H.J., and McCall, M.A. (2014). A Pro23His mutation alters prenatal rod photoreceptor morphology in a transgenic swine model of retinitis pigmentosa. *Investig. Ophthalmol. Vis. Sci.* *55*, 2452–2459.
- Scott, P.A., de Castro, J.P.F., DeMarco, P.J., Ross, J.W., Njoka, J., Walters, E., Prather, R.S., McCall, M.A., and Kaplan, H.J. (2017). Progression of Pro23His Retinopathy in a Miniature Swine Model of Retinitis Pigmentosa. *Transl. Vis. Sci. Technol.* *6*, 4.
- Segre, J.A., Nemhauser, J.L., Taylor, B.A., Nadeau, J.H., and Lander, E.S. (1995). Positional cloning of the nude locus: Genetic, physical, and transcription maps of the region and mutations in the mouse and rat. *Genomics* *28*, 549–559.
- Seiler, M.J., and Aramant, R.B. (1998). Intact sheets of fetal retina transplanted to restore damaged rat retinas. *Investig. Ophthalmol. Vis. Sci.*
- Seiler, M.J., and Aramant, R.B. (2012). Cell replacement and visual restoration by retinal sheet transplants. *Prog. Retin. Eye Res.* *31*, 661–687.
- Seiler, M.J., Aramant, R.B., Thomas, B.B., Peng, Q., Satta, S.R., and Keirstead, H.S. (2010). Visual restoration and transplant connectivity in degenerate rats implanted with retinal progenitor sheets. *Eur. J. Neurosci.* *31*, 508–520.
- Seiler, M.J., Aramant, R.B., Jones, M.K., Ferguson, D.L., Bryda, E.C., and Keirstead, H.S. (2014). A new immunodeficient pigmented retinal degenerate rat strain to study transplantation of human cells without immunosuppression. *Graefes Arch. Clin. Exp. Ophthalmol.* *252*, 1079–1092.
- Seiler, M.J., Lin, R.E., McLelland, B.T., Mathur, A., Lin, B., Sigman, J., De Guzman, A.T., Kitzes, L.M., Aramant, R.B., and Thomas, B.B. (2017). Vision recovery and connectivity by fetal retinal sheet transplantation in an immunodeficient retinal degenerate rat model. *Investig. Ophthalmol. Vis. Sci.* *58*,

614–630.

Shi, P., Tan, Y.S.E., Yeong, W.Y., Li, H.Y., and Laude, A. (2018). A bilayer photoreceptor-retinal tissue model with gradient cell density design: A study of microvalve-based bioprinting. *J. Tissue Eng. Regen. Med.* *12*, 1297–1306.

Shi, Y., Inoue, H., Wu, J.C., and Yamanaka, S. (2017). Induced pluripotent stem cell technology: A decade of progress. *Nat. Rev. Drug Discov.* *16*, 115–130.

Shirai, H., Mandai, M., Matsushita, K., Kuwahara, A., Yonemura, S., Nakano, T., Assawachananont, J., Kimura, T., Saito, K., Terasaki, H., et al. (2016). Transplantation of human embryonic stem cell-derived retinal tissue in two primate models of retinal degeneration. *Proc. Natl. Acad. Sci.* *113*, E81–E90.

Shultz, L.D., Schweitzer, P.A., and Christianson, S.W. (1995). Multiple defects in innate and adaptive immunological function in NOD/LtSz-scid mice. *J. Immunol.* *154*, 180–191.

Sieving, P.A., Caruso, R.C., Tao, W., Coleman, H.R., Thompson, D.J.S., Fullmer, K.R., and Bush, R.A. (2006). Ciliary neurotrophic factor (CNTF) for human retinal degeneration: Phase I trial of CNTF delivered by encapsulated cell intraocular implants. *Proc. Natl. Acad. Sci.* *103*, 3896–3901.

da Silva, S., and Cepko, C.L. (2017). Fgf8 Expression and Degradation of Retinoic Acid Are Required for Patterning a High-Acuity Area in the Retina. *Dev. Cell* *42*, 68–81.e6.

Singh, M.S., Charbel Issa, P., Butler, R., Martin, C., Lipinski, D.M., Sekaran, S., Barnard, A.R., and MacLaren, R.E. (2013). Reversal of end-stage retinal degeneration and restoration of visual function by photoreceptor transplantation. *Proc. Natl. Acad. Sci. U. S. A.* *110*, 1101–1106.

Singh, M.S., Balmer, J., Barnard, A.R., Aslam, S.A., Moralli, D., Green, C.M., Barnea-Cramer, A., Duncan, I., and MacLaren, R.E. (2016). Transplanted photoreceptor precursors transfer proteins to host photoreceptors by a mechanism of cytoplasmic fusion. *Nat. Commun.* *7*, 13537.

Singh, R.K., Mallela, R.K., Cornuet, P.K., Reifler, A.N., Chervenak, A.P., West, M.D., Wong, K.Y., and Nasonkin, I.O. (2015). Characterization of Three-Dimensional Retinal Tissue Derived from Human Embryonic Stem Cells in Adherent Monolayer Cultures. *Stem Cells Dev.* *24*, scd.2015.0144.

Singla, D.K. (2016). Stem cells and exosomes in cardiac repair. *Curr. Opin. Pharmacol.* *27*, 19–23.

Sinha, D., Phillips, J., Joseph Phillips, M., and Gamm, D.M. (2016). Mimicking Retinal Development and Disease With Human Pluripotent Stem Cells. *Investig. Ophthalmology Vis. Sci.* *57*, ORSF11.

Slijkerman, R.W.N., Song, F., Astuti, G.D.N., Huynen, M.A., van Wijk, E., Stieger, K., and Collin, R.W.J. (2015). The pros and cons of vertebrate animal models for functional and therapeutic research on inherited retinal dystrophies. *Prog. Retin. Eye Res.* *48*, 137–159.

Small, K.W., DeLuca, A.P., Whitmore, S.S., Rosenberg, T., Silva-Garcia, R., Udar, N., Puech, B., Garcia, C.A., Rice, T.A., Fishman, G.A., et al. (2016). North Carolina Macular Dystrophy Is Caused by Dysregulation of the Retinal Transcription Factor PRDM13. *Ophthalmology* *123*, 9–18.

Smiley, S., Nickerson, P.E., Comanita, L., Daftarian, N., El-Sehemy, A., Tsai, E.L.S., Matan-Lithwick, S., Yan, K., Thurig, S., Touahri, Y., et al. (2016). Establishment of a cone photoreceptor transplantation platform based on a novel cone-GFP reporter mouse line. *Sci. Rep.* *6*.

Solovei, I., Kreysing, M., Lanctôt, C., Kösem, S., Peichl, L., Cremer, T., Guck, J., and Joffe, B. (2009). Nuclear Architecture of Rod Photoreceptor Cells Adapts to Vision in Mammalian Evolution. *Cell* *137*, 356–368.

Stadtfeld, M., Nagaya, M., Utikal, J., Weir, G., and Hochedlinger, K. (2008). Induced Pluripotent Stem Cells Generated Without Viral Integration. *Science* (80-.). *322*, 945–949.

Steinberg, R.H., Flannery, J.G., Naash, M., Oh, P., Matthes, M.T., Yasumura, D., Lau-Villacorta, C., Chen, J., and LaVail, M.M. (1996). Transgenic rat models of inherited retinal degeneration caused by mutant opsin genes. *Investig. Ophthalmol. Vis. Sci.* *37*.

Stern, J.H., Tian, Y., Funderburgh, J., Pellegrini, G., Zhang, K., Goldberg, J.L., Ali, R.R., Young, M., Xie, Y., and Temple, S. (2018). Regenerating Eye Tissues to Preserve and Restore Vision. *Cell Stem*

Cell 22, 834–849.

Stett, A., Egert, U., Guenther, E., Hofmann, F., Meyer, T., Nisch, W., and Haemmerle, H. (2003). Biological application of microelectrode arrays in drug discovery and basic research. *Anal. Bioanal. Chem.* 377, 486–495.

Stingl, K., Bartz-Schmidt, K.U., Besch, D., Braun, A., Bruckmann, A., Gekeler, F., Greppmaier, U., Hipp, S., Hördörfer, G., Kernstock, C., et al. (2013). Artificial vision with wirelessly powered subretinal electronic implant alpha-IMS. *Proc. Biol. Sci.* 280, 20130077.

Strauss, O. (2005). The Retinal Pigment Epithelium in Visual Function. *Physiol. Rev.* 85, 845–881.

Strettoi, E., Mears, A.J., and Swaroop, A. (2004). Recruitment of the Rod Pathway by Cones in the Absence of Rods. *J. Neurosci.* 24, 7576–7582.

Swaroop, A., Kim, D., and Forrest, D. (2010). Transcriptional regulation of photoreceptor development and homeostasis in the mammalian retina. *Nat. Rev. Neurosci.* 11, 563–576.

Swijnenburg, R.J., Schrepfer, S., Govaert, J.A., Cao, F., Ransohoff, K., Sheikh, A.Y., Haddad, M., Connolly, A.J., Davis, M.M., Robbins, R.C., et al. (2008). Immunosuppressive therapy mitigates immunological rejection of human embryonic stem cell xenografts. *Proc. Natl. Acad. Sci. U. S. A.* 105, 12991–12996.

Tachibana, M., Amato, P., Sparman, M., Gutierrez, N.M., Tippner-Hedges, R., Ma, H., Kang, E., Fulati, A., Lee, H.S., Sritanaudomchai, H., et al. (2013). Human embryonic stem cells derived by somatic cell nuclear transfer. *Cell* 153, 1228–1238.

Takahashi, K., and Yamanaka, S. (2006). Induction of Pluripotent Stem Cells from Mouse Embryonic and Adult Fibroblast Cultures by Defined Factors. *Cell* 126, 663–676.

Takahashi, K., Tanabe, K., Ohnuki, M., Narita, M., Ichisaka, T., Tomoda, K., and Yamanaka, S. (2007). Induction of Pluripotent Stem Cells from Adult Human Fibroblasts by Defined Factors. *Cell* 131, 861–872.

Takahashi, M., Palmer, T.D., Takahashi, J., and Gage, F.H. (1998). Widespread integration and survival of adult-derived neural progenitor cells in the developing optic retina. *Mol. Cell. Neurosci.* 12, 340–348.

Thiadens, A.A.H.J., den Hollander, A.I., Roosing, S., Nabuurs, S.B., Zekveld-Vroon, R.C., Collin, R.W.J., De Baere, E., Koenekoop, R.K., van Schooneveld, M.J., Strom, T.M., et al. (2009). Homozygosity mapping reveals PDE6C mutations in patients with early-onset cone photoreceptor disorders. *Am. J. Hum. Genet.* 85, 240–247.

Thomson, J.A. (1998). Embryonic Stem Cell Lines Derived from Human Blastocysts. *Science* (80-). 282, 1145–1147.

Tropepe, V., Coles, B.L., Chiasson, B.J., Horsford, D.J., Elia, A.J., McInnes, R.R., van der Kooy, D., and Tropepe V Chiasson BJ, Horsford DJ, Elia AJ, McInnes RR, van der Kooy D., C.B.L. (2000). Retinal stem cells in the adult mammalian eye. *Science* (80-). 287, 2032–2036.

Tsai, Y., Lu, B., Bakondi, B., Girman, S., Sahabian, A., Sareen, D., Svendsen, C.N., and Wang, S. (2015). Human iPSC-Derived Neural Progenitors Preserve Vision in an AMD-Like Model. *Stem Cells* 33, 2537–2549.

Tucker, B.A., Park, I.H., Qi, S.D., Klassen, H.J., Jiang, C., Yao, J., Redenti, S., Daley, G.Q., and Young, M.J. (2011a). Transplantation of adult mouse iPS cell-derived photoreceptor precursors restores retinal structure and function in degenerative mice. *PLoS One* 6.

Tucker, B.A., Scheetz, T.E., Mullins, R.F., DeLuca, A.P., Hoffmann, J.M., Johnston, R.M., Jacobson, S.G., Sheffield, V.C., and Stone, E.M. (2011b). Exome sequencing and analysis of induced pluripotent stem cells identify the cilia-related gene male germ cell-associated kinase (MAK) as a cause of retinitis pigmentosa. *Proc. Natl. Acad. Sci.* 108, E569–E576.

Tucker, B.A., Mullins, R.F., Streb, L.M., Anfanson, K., Eyestone, M.E., Kaalberg, E., Riker, M.J., Drack, A. V., Braun, T.A., and Stone, E.M. (2013). Patient-specific iPSC-derived photoreceptor precursor cells as a means to investigate retinitis pigmentosa. *Elife* 2013, 1–18.

- Turner, D.L., and Cepko, C.L. (1987). A common progenitor for neurons and glia persists in rat retina late in development. *Nature* *328*, 131–136.
- Veleri, S., Lazar, C.H., Chang, B., Sieving, P.A., Banin, E., and Swaroop, A. (2015). Biology and therapy of inherited retinal degenerative disease: insights from mouse models. *Dis. Model. Mech.* *8*, 109–129.
- Vergara, M.N., Flores-Bellver, M., Aparicio-Domingo, S., McNally, M., Wahlin, K.J., Saxena, M.T., Mumm, J.S., and Canto-Soler, M.V. (2017). Enabling quantitative screening in retinal organoids: 3D automated reporter quantification technology (3D-ARQ). *Development* *dev.146290*.
- Viczian, A.S., Solessio, E.C., Lyou, Y., and Zuber, M.E. (2009). Generation of functional eyes from pluripotent cells. *PLoS Biol.* *7*.
- Völkner, M., Zschätzsch, M., Rostovskaya, M., Overall, R.W., Buskamp, V., Anastassiadis, K., and Karl, M.O. (2016). Retinal Organoids from Pluripotent Stem Cells Efficiently Recapitulate Retinogenesis. *Stem Cell Reports* *6*, 525–538.
- Wahlin, K.J., Maruotti, J.A., Sripathi, S.R., Ball, J., Angueyra, J.M., Kim, C., Grebe, R., Li, W., Jones, B.W., and Zack, D.J. (2017). Photoreceptor Outer Segment-like Structures in Long-Term 3D Retinas from Human Pluripotent Stem Cells. *Sci. Rep.* *7*, 766.
- Waldron, P. V, Marco, F. Di, Kruczek, K., Ribeiro, J., Graca, A.B., Hippert, C., Aghaizu, N.D., Kalargyrou, A.A., Barber, A.C., Grimaldi, G., et al. (2017). Stem Cell Reports Transplanted Donor-or Stem Cell-Derived Cone Photoreceptors Can Both Integrate and Undergo Material Transfer in an Environment-Dependent Manner. *Stem Cell Reports* *10*, 1–16.
- Wang, X., Xiong, K., Lin, C., Lv, L., Chen, J., Xu, C., Wang, S., Gu, D., Zheng, H., Yu, H., et al. (2015). New medium used in the differentiation of human pluripotent stem cells to retinal cells is comparable to fetal human eye tissue. *Biomaterials* *53*, 40–49.
- Warren, L., Manos, P.D., Ahfeldt, T., Loh, Y.H., Li, H., Lau, F., Ebina, W., Mandal, P.K., Smith, Z.D., Meissner, A., et al. (2010). Highly efficient reprogramming to pluripotency and directed differentiation of human cells with synthetic modified mRNA. *Cell Stem Cell* *7*, 618–630.
- Wassle, H., Puller, C., Muller, F., and Haverkamp, S. (2009). Cone Contacts, Mosaics, and Territories of Bipolar Cells in the Mouse Retina. *J. Neurosci.* *29*, 106–117.
- Welby, E., Lakowski, J., Di Foggia, V., Budinger, D., Gonzalez-Cordero, A., Lun, A.T.L., Epstein, M., Patel, A., Cuevas, E., Kruczek, K., et al. (2017). Isolation and Comparative Transcriptome Analysis of Human Fetal and iPSC-Derived Cone Photoreceptor Cells. *Stem Cell Reports* *9*, 1898–1915.
- Wiley, L.A., Burnight, E.R., DeLuca, A.P., Anfinson, K.R., Cranston, C.M., Kaalberg, E.E., Penticoff, J.A., Affatigato, L.M., Mullins, R.F., Stone, E.M., et al. (2016a). cGMP production of patient-specific iPSCs and photoreceptor precursor cells to treat retinal degenerative blindness. *Sci. Rep.* *6*, 30742.
- Wiley, L.A., Burnight, E.R., Drack, A. V., Banach, B.B., Ochoa, D., Cranston, C.M., Madumba, R.A., East, J.S., Mullins, R.F., Stone, E.M., et al. (2016b). Using Patient-Specific Induced Pluripotent Stem Cells and Wild-Type Mice to Develop a Gene Augmentation-Based Strategy to Treat *CLN3* - Associated Retinal Degeneration. *Hum. Gene Ther.* *27*, 835–846.
- Williams, R.L., Hilton, D.J., Pease, S., Willson, T. a, Stewart, C.L., Gearing, D.P., Wagner, E.F., Metcalf, D., Nicola, N. a, and Gough, N.M. (1988). Myeloid leukaemia inhibitory factor maintains the developmental potential of embryonic stem cells. *Nature* *336*, 684–687.
- Won, J., Shi, L.Y., Hicks, W., Wang, J., Hurd, R., Naggert, J.K., Chang, B., and Nishina, P.M. (2011). Mouse Model Resources for Vision Research. *J. Ophthalmol.* *2011*.
- Wong, W.L., Su, X., Li, X., Cheung, C.M.G., Klein, R., Cheng, C.-Y., and Wong, T.Y. (2014). Global prevalence of age-related macular degeneration and disease burden projection for 2020 and 2040: a systematic review and meta-analysis. *Lancet Glob. Heal.* *2*, e106–e116.
- Worthington, K.S., Wiley, L.A., Kaalberg, E.E., Collins, M.M., Mullins, R.F., Stone, E.M., and Tucker, B.A. (2017). Two-photon polymerization for production of human iPSC-derived retinal cell grafts. *Acta Biomater.* *55*, 385–395.

- Wright, A.F., Chakarova, C.F., Abd El-Aziz, M.M., and Bhattacharya, S.S. (2010). Photoreceptor degeneration: Genetic and mechanistic dissection of a complex trait. *Nat. Rev. Genet.* *11*, 273–284.
- Xu, R.H., Chen, X., Li, D.S., Li, R., Addicks, G.C., Glennon, C., Zwaka, T.P., and Thomson, J.A. (2002). BMP4 initiates human embryonic stem cell differentiation to trophoblast. *Nat. Biotechnol.* *20*, 1261–1264.
- Yamada, M., Johannesson, B., Sagi, I., Burnett, L.C., Kort, D.H., Prosser, R.W., Paull, D., Nestor, M.W., Freeby, M., Greenberg, E., et al. (2014). Human oocytes reprogram adult somatic nuclei of a type 1 diabetic to diploid pluripotent stem cells. *Nature* *510*, 533–536.
- Yamanaka, S. (2012). Induced pluripotent stem cells: Past, present, and future. *Cell Stem Cell* *10*, 678–684.
- Yanai, A., Laver, C.R.J., Joe, A.W., Viringipurampeer, I. a, Wang, X., Gregory-Evans, C.Y., and Gregory-Evans, K. (2013). Differentiation of human embryonic stem cells using size-controlled embryoid bodies and negative cell selection in the production of photoreceptor precursor cells. *Tissue Eng. Part C. Methods* *19*, 755–764.
- Yang, Y., Mohand-Said, S., Léveillard, T., Fontaine, V., Simonutti, M., and Sahel, J.-A. (2010). Transplantation of Photoreceptor and Total Neural Retina Preserves Cone Function in P23H Rhodopsin Transgenic Rat. *PLoS One* *5*, e13469.
- Yang, Z., Chen, Y., Lillo, C., Chien, J., Yu, Z., Michaelides, M., Klein, M., Howes, K.A., Li, Y., Kaminoh, Y., et al. (2008). Mutant prominin 1 found in patients with macular degeneration disrupts photoreceptor disk morphogenesis in mice. *J. Clin. Invest.* *118*, 2908–2916.
- Ying, Q.L., Nichols, J., Chambers, I., and Smith, A. (2003). BMP induction of Id proteins suppresses differentiation and sustains embryonic stem cell self-renewal in collaboration with STAT3. *Cell* *115*, 281–292.
- Yoshida, T., Ozawa, Y., Suzuki, K., Yuki, K., Ohyama, M., Akamatsu, W., Matsuzaki, Y., Shimmura, S., Mitani, K., Tsubota, K., et al. (2014). The use of induced pluripotent stem cells to reveal pathogenic gene mutations and explore treatments for retinitis pigmentosa. *Mol. Brain* *7*, 45.
- Young, R.W. (1976). Visual cells and the concept of renewal. *Investig. Ophthalmology Vis. Sci.* *15*, 700–725.
- Young, R.W. (1985). Cell differentiation in the retina of the mouse. *Anat. Rec.* *212*, 199–205.
- Young, M.J., Ray, J., Whiteley, S.J.O., Klassen, H., and Gage, F.H. (2000). Neuronal differentiation and morphological integration of hippocampal progenitor cells transplanted to the retina of immature and mature dystrophic rats. *Mol. Cell. Neurosci.* *16*, 197–205.
- Yu, J., Vodyanik, M.A., Smuga-Otto, K., Antosiewicz-Bourget, J., Frane, J.L., Tian, S., Nie, J., Jonsdottir, G.A., Ruotti, V., Stewart, R., et al. (2007). Induced pluripotent stem cell lines derived from human somatic cells. *Science* *318*, 1917–1920.
- Yvon, C., Ramsden, C.M., Lane, A., Powner, M.B., da Cruz, L., Coffey, P.J., and Carr, A.-J.F. (2015). Using Stem Cells to Model Diseases of the Outer Retina. *Comput. Struct. Biotechnol. J.* *13*, 382–389.
- Zeitz, C., Robson, A.G., and Audo, I. (2015). Congenital stationary night blindness: an analysis and update of genotype-phenotype correlations and pathogenic mechanisms. *Prog. Retin. Eye Res.* *45*, 58–110.
- Zhao, X.Y., Li, W., Lv, Z., Liu, L., Tong, M., Hai, T., Hao, J., Guo, C.L., Ma, Q.W., Wang, L., et al. (2009). IPS cells produce viable mice through tetraploid complementation. *Nature* *461*, 86–90.
- Zhong, X., Gutierrez, C., Xue, T., Hampton, C., Vergara, M.N., Cao, L.-H., Peters, A., Park, T.S., Zambidis, E.T., Meyer, J.S., et al. (2014). Generation of three-dimensional retinal tissue with functional photoreceptors from human iPSCs. *Nat. Commun.* *5*, 1–14.
- Zhou, S., Flamier, A., Abdouh, M., Tetreault, N., Barabino, A., Wadhwa, S., and Bernier, G. (2015). Differentiation of human embryonic stem cells into cone photoreceptors through simultaneous inhibition of BMP, TGF and Wnt signaling. *Development* *142*, 3294–3306.

Zhu, J., Cifuentes, H., Reynolds, J., and Lamba, D.A. (2017a). Immunosuppression via Loss of IL2ry Enhances Long-Term Functional Integration of hESC-Derived Photoreceptors in the Mouse Retina. *Cell Stem Cell* *20*, 374–384.e5.

Zhu, J., Reynolds, J., Garcia, T., Cifuentes, H., Chew, S., Zeng, X., and Lamba, D.A. (2017b). Generation of Transplantable Retinal Photoreceptors from a Current Good Manufacture Practice-Manufactured Human Induced Pluripotent Stem Cell Line. *Stem Cells Transl. Med.*

Zhu, Y., Carido, M., Meinhardt, A., Kurth, T., Karl, M.O., Ader, M., and Tanaka, E.M. (2013). Three-Dimensional Neuroepithelial Culture from Human Embryonic Stem Cells and Its Use for Quantitative Conversion to Retinal Pigment Epithelium. *PLoS One* *8*.

Zuber, M.E. (2010). Eye field specification in *Xenopus laevis*. In *Current Topics in Developmental Biology*, T.A. Cagan, Ross L;Reh, ed. (Elsevier Inc.), pp. 29–60.